



Atmospheric degradation of VOCs: Isoprene and its ozonolysis products, a perfluoro-ketone and long chain ketones

Yangang Ren

► To cite this version:

Yangang Ren. Atmospheric degradation of VOCs: Isoprene and its ozonolysis products, a perfluoro-ketone and long chain ketones. Ocean, Atmosphere. Université d'Orléans (UO), Orléans, FRA., 2017. English. NNT : . tel-03581629

HAL Id: tel-03581629

<https://hal.science/tel-03581629v1>

Submitted on 20 Feb 2022

HAL is a multi-disciplinary open access archive for the deposit and dissemination of scientific research documents, whether they are published or not. The documents may come from teaching and research institutions in France or abroad, or from public or private research centers.

L'archive ouverte pluridisciplinaire **HAL**, est destinée au dépôt et à la diffusion de documents scientifiques de niveau recherche, publiés ou non, émanant des établissements d'enseignement et de recherche français ou étrangers, des laboratoires publics ou privés.

ÉCOLE DOCTORALE
(ENERGIE, MATERIAUX, SCIENCES DE LA TERRE ET DE L'UNIVERS)

ICARE-CNRS ORLEANS

THÈSE présentée par :
Yangang REN

soutenue le : **29 Mai 2017**

pour obtenir le grade de : **Docteur de l'université d'Orléans**

Discipline/ Spécialité : Chimie et Physique de l'Environnement

Atmospheric degradation of VOCs:
Isoprene and its ozonolysis products, a
perfluoro-ketone and long chain ketones

THÈSE dirigée par :

Abdelwahid MELLOUKI

Directeur de recherche au CNRS-ORLEANS

RAPPORTEURS :

Christian GEORGE

Directeur de recherche au CNRS-LYON

Alexandre TOMAS

Professeur à IMT Lille Douai

JURY:

Christian GEORGE

Alexandre TOMAS

Valéry CATOIRE

Jianmin CHEN

Véronique DAËLE

Abdelwahid MELLOUKI

Directeur de recherche - CNRS-IRCELYON

Professeur - IMT Lille Douai

Professeur - Université d'Orléans/CNRS-LPC2E

Professeur - Fudan University, Shanghai

Chargée de recherche (HDR) – CNRS-ICARE

Directeur de recherche - CNRS-ICARE

Rapporteur

Rapporteur

Examinateur

Examinateur

Co-Encadrante

Directeur de thèse

Table of Contents

Abstract.....	1
Chapter 1- Introduction	4
1-1- Composition of the atmosphere	4
1-1-1- Volatile organic compounds (VOCs).....	4
1-1-2- Reactive species	6
1-1-3- Atmospheric aerosol.....	9
1-2- Chemistry in the troposphere.....	10
1-2-1- Photo-oxidation	10
1-2-2- OH chemistry.....	10
1-2-3- O ₃ chemistry.....	12
1-2-4- Cl atom chemistry	13
1-2-5- NO ₃ chemistry	15
1-2-6- Formation of secondary organic aerosols (SOA).....	17
1-3- The Master Chemical Mechanism.....	18
1-4- Motivation.....	20
1-5- Outline of the thesis	21
References	23
Chapter 2- Experimental Methods & Instrumentation	32
2-1- UV-Visible absorption	32
2-2- Pulsed laser photolysis-laser induced fluorescence (PLP-LIF)	34
2-3- Atmospheric simulation chambers	35
2-3-1- Small indoor simulation chamber - 200 L.....	36
2-3-1-1- Introduction.....	36
2-3-1-2- Gas chromatography-flame ionization detector.....	37
2-3-2- Moveable simulation chamber - 3.4 m ³	38
2-3-2-1- Introduction.....	38

2-3-2-2- Fourier transform infrared spectroscopy 3 (FTIR3)	39
2-3-3- <i>Large indoor simulation chamber (CSA)-7.3 m³</i>	41
2-3-3-1- Introduction	41
2-3-3-2- Fourier transform infrared spectroscopy 2 (FTIR2)	43
2-3-3-3- Scanning Mobility Particle Sizers (SMPS)	44
2-3-4- <i>Large outdoor simulation chamber-90 m³ (HELIOS)</i>	47
2-3-4-1- Introduction	47
2-3-4-2- Fourier transform infrared spectroscopy 1 (FTIR1)	53
2-3-4-3- Automated Thermal Desorption-Gas chromatography/mass spectrometer (ATD-GC/MS)	53
2-3-4-4- Proton transfer reaction-time of flight-mass spectrometer (PTR-ToF-MS)	56
2-3-4-5- Ultra High Performance Liquid Chromatograph-Mass Spectrometry (UHPLC-MS)	58
2-3-4-6- Formaldehyde (HCHO) analyzer	60
2-3-4-7- Spectroradiometer	61
2-4- Instrumentation Conclusion	62
References	64
Chapter 3- Investigation of the reaction of ozone with isoprene, methacrolein and methyl vinyl ketone using the HELIOS Chamber	66
3-1- Introduction	67
3-2- Experimental and Material.....	69
3-2-1- <i>Experimental</i>	69
3-2-2- <i>Chemicals</i>	71
3-3- Results and discussion	71
3-3-1- <i>Kinetic measurements</i>	71
3-3-2- <i>Products measurements</i>	78
3-3-2-1- OH formation yields	78
3-3-2-2- Gas phase stable products formation yields.....	81
3-3-2-3- Secondary organic aerosol formation	90

3.4- Conclusions and future work.....	93
References	96
Chapter 4 - Photolysis studies: comparing and contrasting fluorinated and non-fluorinated 2-methyl-3-pentanone.....	103
4-1- Introduction	104
4-2- Experimental Section	105
4-2-1- <i>UV absorption spectra</i>	105
4-2-2- <i>Outdoor atmospheric simulation chambers</i>	106
4-2-2-1- HELIOS chamber	106
4-2-2-1- 3.4 m ³ outdoor chamber	107
4-2-3- <i>Photolysis experiments</i>	108
4-2-4- <i>Loss correction</i>	109
4-2-5- <i>Chemicals</i>	110
4-3- Results and Discussion	110
4-3-1- <i>UV absorption cross section</i>	110
4-3-2- <i>Photolysis rate of PF-2M3P</i>	114
4-3-3- <i>Photolysis products of PF-2M3P</i>	118
4-3-4- <i>Photolysis rate of 2-methyl-3-pentanone</i>	124
4-3-5- <i>Mechanism of the 2M3P photolysis</i>	125
4-3-6- <i>Comparison of photolysis mechanism between PF-2M3P and 2M3P</i>	131
4-3-7- <i>Kinetics of PF-2M3P and 2M3P reaction with O₃</i>	131
4-3-8- <i>The Global Warming Potential (GWP)</i>	134
4-3-8-1- Radiative Forcing (RF) and Radiative Efficiency (RE)	134
4-3-8-2- Infrared absorption cross section.....	135
4-4- Atmospheric Implication and Conclusion.....	136
References	139
Chapter 5 - Kinetic and Product studies of OH Reactions with a series of Ketones	144
5-1- Introduction	145
5-2- Experimental and Material.....	147

5-2-1- 200L Indoor Bag	147
5-2-2- PLP-LIF	149
5-2-3- 7.3 m ³ large indoor simulation chamber.....	150
5-2-4- Chemicals.....	151
5-3- Results.....	152
5-3-1- Rate constants of ketones + OH radical using RR method	152
5-3-2- Rate constant of ketones + OH radical using AR method.....	155
5-3-3- Products formation from the ketones + OH radical.....	158
5-3-3-1- 2M3P+OH.....	159
5-3-3-2- 3M2P+OH.....	163
5-3-3-3- 4M2P+OH.....	167
5-4- Discussion	171
5-4-1- Comparison of rate constant with literature data for ketone + OH reaction	171
5-4-2- Trends in the Ketones + OH Reaction Rate Constants.....	173
5-4-3- Temperature dependence of the ketone + OH radical reaction	174
5-4-4- Reaction mechanism of the OH radical + ketones reaction	175
5-4-4-1- 2M3P+OH.....	176
5-4-4-2- 3M2P+OH.....	182
5-4-4-3- 4M2P	188
5-5- Atmospheric implications	191
5-6- Conclusion	192
References	194
Chapter 6- Kinetic and Product studies of Cl atoms Reactions with a series of branched Ketones.....	200
6-1- Introduction	200
6-2- Experimental and Material.....	202
6-2-1- Kinetic measurement	202
6-2-2- Products analysis.....	204
6-2-3- Chemical	204

6-3- Results.....	204
6-3-1- Rate constant for ketones + Cl atoms using RR method	204
6-3-2- Products formation from the reactions of ketones + Cl atoms	208
6-3-2-1- 2M3P+Cl.....	208
6-3-2-2- 3M2P+Cl.....	211
6-3-2-2- 4M2P+Cl.....	214
6-4- Discussion	217
6-4-1- Comparison with literature of the rate coefficients for ketone + Cl reactions	217
6-4-2- Kinetic estimation based on the Structure-Reactivity Relationship (SAR)	218
6-4-3- Reaction mechanism of the reaction of Cl atoms + ketones.....	221
6-4-3-1- 2M3P+Cl.....	222
6-4-3-2- 3M2P+Cl.....	230
6-4-3-3- 4M2P+Cl.....	234
6-4-4- Reaction mechanism comparison between the studied reactions with Cl atoms	238
6-5- Atmospheric implications	239
6-6- Conclusion	241
References	243
Chapter 7- Conclusions and Perspectives.....	248
References	252
Acknowledges	254
Annex I: Uncertainty analysis.....	257
1- Linear least-squares fitting	257
2- Uncertainty analysis of Rate constant	258
2-1- Uncertainty analysis of decay rate k' (s ⁻¹)	258
2-2- Uncertainty analysis of Rate constant (AR method).....	259
2-3- Uncertainty analysis of Rate constant (RR method)	260
2-4- Uncertainty analysis of product formation yield.....	261

Annex II: IR absorption cross sections	262
References	272

Abstract

Volatile organic compounds (VOCs) constitute major gas pollutants emitted from both human and biogenic activities. They have a major influence on the chemistry of the troposphere impacting human health, air quality and global climate change. The atmospheric oxidation processes of VOCs that occur within the troposphere do so by the action of sunlight, by reactions with free radicals such as OH and NO₃ and by reactions with O₃, and Cl atoms. This can be studied both kinetically and mechanistically under predetermined and controlled conditions in atmospheric simulation chambers for example. Wide array of atmospheric simulation chambers enable the deep understanding of key issues surrounding the atmospheric behaviors and bridge the gaps between the field measurements and models.

In the present work, the newly built outdoor atmospheric simulation chamber-HELIOS at CNRS-ICARE (Orléans, France) is a 90 m³ Teflon-FEP chamber that allows a wide study of kinetics and mechanistic investigations under dark and natural irradiation conditions to be used. In addition, three other simulation chambers have been used to conduct different types of investigations: the 7.3 m³ indoor chamber-CSA, 3.4 m³ moveable chamber and 200 L indoor chamber at CNRS-ICARE (Orléans, France). These chambers allow kinetics and mechanistic investigations over a wide range of VOCs concentrations under dark and artificial irradiation. Two other complementary experimental methods available at ICARE laboratory have been deployed to investigate the atmospheric chemistry of the species of interest in this thesis (pulsed laser photolysis-laser induced fluorescence (PLP-LIF) and UV-Vis-absorption cell).

For the kinetic studies, absolute rate (AR) and relative rate (RR) methods were used to measure the rate constants of a number of reactions, e.g. ozonolysis of isoprene, MACR (methacrolein) and MVK (methyl vinyl ketone), OH and Cl reactions with three ketones: 2M3P (2-methyl-3-pentanone), 3M2P (3-methyl-2-pentanone) and 4M2P (4-methyl-2-pentanone). In addition, a pulsed laser photolysis-laser induced fluorescence (PLP-LIF) system was used to measure the first temperature dependence of the rate constants for the reactions of OH with 2M3P and

3M2P. In order to determine the photolysis rate of PF-2M3P and 2M3P, their absorption cross sections were measured using an absorption cell coupled with one UV-visible spectrophotometer then their photolysis were studied under solar light conditions.

The kinetic parameters obtained for the ozonolysis of isoprene, MACR and MVK have been found to be in good agreement with literature which enables to perfectly characterize the dark experiment conditions in HELIOS. The isoprene-O₃ reaction system was investigated to determine the OH radical and the SOA yields in presence and absence of OH scavenger. The photolysis rate of PF-2M3P under natural irradiation is in good agreement with the literature, and this work provides the first determination of photolysis rate of 2M3P under natural irradiation. For the photolysis of PF-2M3P and 2M3P, the inter-comparison of the photolysis schemes was performed. The kinetic determinations of OH radical and Cl atom reactions with 3M2P/4M2P are in agreement with the existing values and this work provides the first kinetic determination for 2M3P reaction with OH radical / Cl atom. The observed stable products yields are interpreted in terms of branching ratio for each channel within the postulated mechanism of reactions of OH radical and Cl atom with 2M3P, 3M2P and 4M2P. These results update the Structure Activity Relationship (SAR) for OH radical / Cl atom reactions with ketones and confirm that CH_x (1, 2, 3) reactivity in ketones depends on their position relative to C=O group and $k_{(-CH_3)} < k_{(-CH_2)} < k_{(-CH<)}$ in the β position of C=O group.

A wide range and complementary analytical tools have been used to conduct the present work including Fourier Transform Infrared Spectroscopy (FTIR), Gas Chromatograph-Mass spectrometer (GC-MS), Gas Chromatograph-Flame Ionization Detector (GC-FID), Proton Transfer Reaction-Time of Flight-Mass Spectrometer (PTR-ToF-MS), Ultra High speed Liquid Chromatograph-Mass Spectrometer (UHPLC-MS) for measuring VOC/OVOC, Scanning Mobility Particle Sizer-Condensation Particle Counter (SMPS-CPC) for measuring size distribution of SOA.

The results obtained are presented and discussed in terms of their atmospheric impacts.

Chapter 1.

Introduction

Chapter 1- Introduction	4
1-1- Composition of the atmosphere	4
1-1-1- Volatile organic compounds (VOCs).....	4
1-1-2- Reactive species	6
1-1-3- Atmospheric aerosol.....	9
1-2- Chemistry in the troposphere.....	10
1-2-1- Photo-oxidation	10
1-2-2- OH chemistry	10
1-2-3- O ₃ chemistry.....	12
1-2-4- Cl atom chemistry	13
1-2-5- NO ₃ chemistry.....	15
1-2-6- Formation of secondary organic aerosols (SOA).....	17
1-3- The Master Chemical Mechanism	18
1-4- Motivation.....	20
1-5- Outline of the thesis.....	21
References	23

Chapter 1- Introduction

In order to gain a full understanding of current atmospheric issues, such as air quality (local to global), climate change, ozone layer depletion, a comprehensive understanding of atmospheric chemistry processes is therefore imperative for elucidation of the atmospheric composition change at different scales. This introductory chapter provides basis and prospect of these themes, the investigation of atmospheric chemistry and its important role in the troposphere.

1-1- Composition of the atmosphere

1-1-1- Volatile organic compounds (VOCs)

The atmospheric chemistry of volatile organic compounds (VOCs) has been known to have significant influence on human health and global climate change. VOCs are major gas pollutants emitted into the atmosphere in large quantity by both anthropogenic and biogenic sources and have a major influence on the chemistry of the troposphere. The anthropogenic sources include the evaporation of solvents and fuels in the industrial processes, commercial operations or consumer products; some oxygenated VOCs (OVOCs) can also be emitted from incomplete fuel combustion and atmospheric oxidation of hydrocarbons present in the atmosphere. In the U.S., the Environmental Protection Agency (EPA, 2016) listed the major anthropogenic sources of VOCs that ultimately form OVOCs are emitted from the incomplete fuel use: solvent utilization (18.6%), highway vehicles (11.1%) and off-highway combustion engines (9.9%), petroleum related industry (20.3%), others like storage & transport and institutional & residential & commercial fuel combustion also add additional input of VOCs emissions. In Europe, European Environment Agency (EEA, 2014) listed the NMVOCs emission sources as: energy use & supply (29%), road transport (13%), industrial processes (7%), other transport (2%), agriculture (4%), waste (1%) and others (44%). The biogenic sources include ocean, soils, growing plants and plants debris. Guenther et al (1995) grouped the VOCs from terrestrial and ocean sources into four categories: isoprene, monoterpenes (α -pinene, β -pinene etc.), other reactive VOCs (2-methyl-3-buten-2-ol, etc.) and other unreactive VOCs (methanol

etc.). They estimated that the annual global VOCs flux is 1150 Tg C with their global model, composed of 44% isoprene, 22.5% other reactive VOCs, 22.5% other VOCs and 11% monoterpenes. The global annual emissions of some important VOCs are presented in Table 1-1. In addition, some examples of the structures of main VOCs in atmosphere are presented in Figure 1-1. Either the biogenic source or the anthropogenic source is of most interest to humans due to the direct impact on human, animal and plant health. This has led to the development of detailed VOC oxidation schemes explaining the degradation processes of these pollutants in the troposphere.

Table 1-1: Global annual emissions of some important VOCs

Terpene	Emission (Tg/year)
Isoprene	535
α -Pinene	66.1
β -Pinene	33
Sabinene	9
3-Carene	7.1
Limonene	11.4
α - and γ -terpinene	1.4
Myrcene	8.7
Alcools terpenoid	30
Ocimene	3
Sesquiterpene	14.5
Acetone	43.7
Acetaldehyde	20.7
146 VOC	1007

From Finlayson-Pitts et Pitts (2000), Guenther et al., (2012)

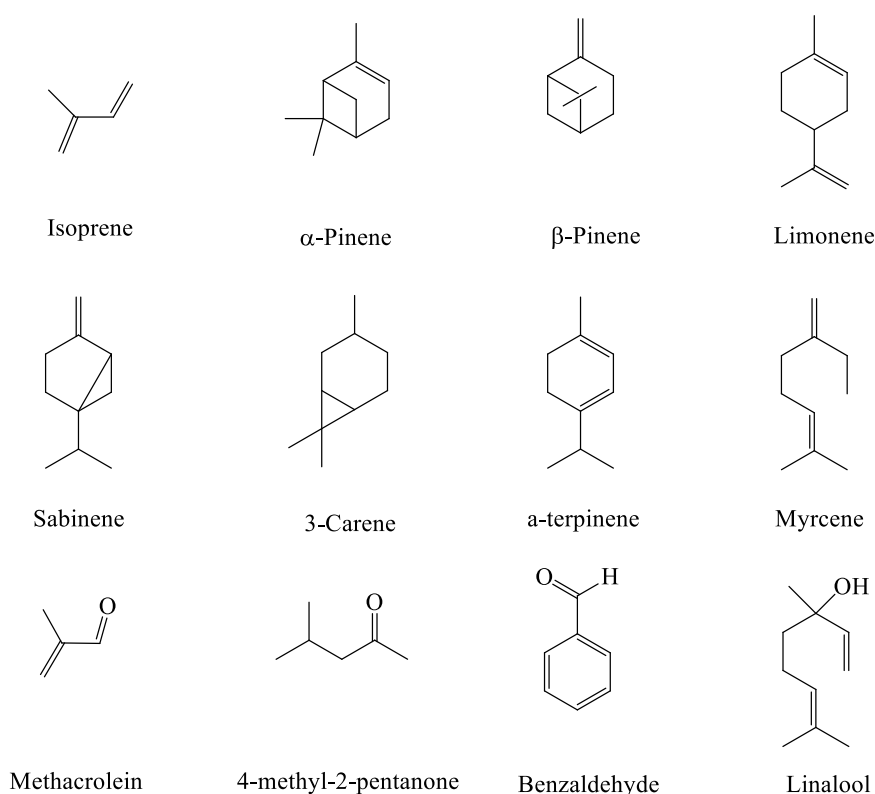


Figure 1-1: Examples of the structures of some VOCs in atmosphere.

1-1-2- Reactive species

When VOCs are released to the atmosphere, they are rapidly oxidized by the hydroxyl radical (OH), ozone (O₃), the nitrate radical (NO₃) during nighttime and occasionally chlorine atom (Cl), the average concentration of OH, O₃, NO₃ and Cl atom have been shown in Table 1-2. OH radical plays an essential role in atmospheric behavior and transformations of VOCs (Prinn et al., 2001;Eisele et al., 1997). For a wide range of VOCs, reaction with OH radical represents an important removal process from the atmosphere and is also a potential pathway for their transformation into more toxic compounds (Atkinson and Arey, 2003).

The nitrate radical, NO₃, is well known as a nighttime tropospheric oxidant, and is thought to be a key contributor to the oxidizing capacity in the lower atmosphere (Geyer et al., 2001;Brown et al., 2011). This has been demonstrated through investigations of NO₃ reactions with alkenes, organosulphur compounds, aldehydes and hydroxy-substituted aromatics (Carter et al., 1981;Platt et al., 1990). These reactions may have further impacts on tropospheric reactions through the generation of peroxy radicals.

Gas phase Cl atom, when present in the atmosphere, react by mechanisms analogous to those of the OH radical. However, the rate constants of the Cl initiated reactions are often much faster than the corresponding OH reactions. The effects of Cl atom on the atmosphere include the oxidation of VOCs and increases in O₃ production rates as well as possible formation of chlorinated VOCs. Although concentrations of Cl atom are typically lower compared to other reactive species, its reaction with most VOCs contributes to their removal from the atmosphere leading the formation of species that may alter air quality. This is particularly evident in the case of Cl atom-induced localized increasing in O₃ concentrations.

Tropospheric O₃ has a threefold importance, O₃ is a powerful greenhouse gas (GHG), producing an extra radiative forcing of 0.35 Wm⁻² (Monks et al., 2009). O₃ is also at the center of atmospheric tropospheric gas phase photochemistry, it acts as the main source of OH radical through its photolysis. Finally, surface O₃ is an oxidant that induces respiratory problems and is associated with premature human mortality (Bell et al., 2006), reduces photosynthesis and growth and therefore crop yields (Reich and Amundson, 1985).

Atmospheric chemistry usually includes complex reactions of VOCs, inorganic compounds, O₃, nitric oxide (NO), nitrogen dioxide (NO₂), OH radical, hydroperoxy radical (HO₂), NO₃ radical, Cl atom, photo-oxidation, and aerosol. Their complicated inter-reaction is depicted in Figure 1-2. In addition, the lifetime of VOCs depending on their reaction with NO₃, OH, O₃ and Cl atom ranging from minutes to days and shown in Table 1-3.

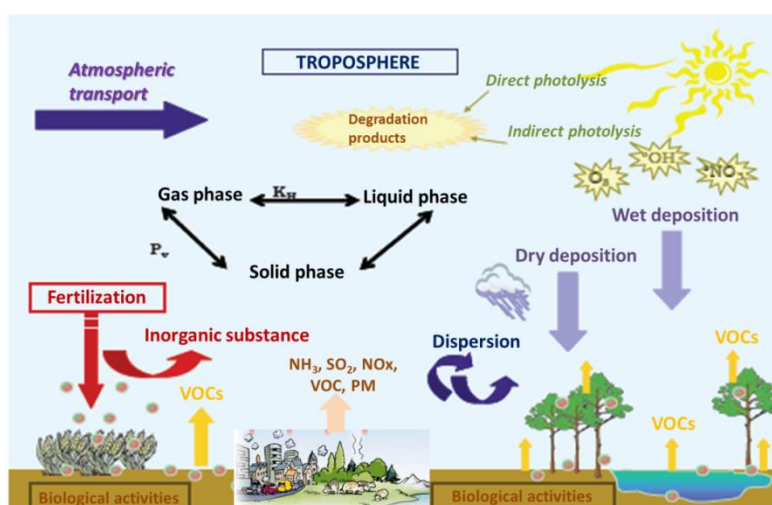


Figure 1-2: Behavior of reactive species includes VOCs, NH₃, NO_x, OH, NO₃ and O₃ in the atmosphere (adapted from thesis of Pflieger (2009))

Table 1-2: Typical concentration and dominant reactions of the oxidants.

Oxidant	Average Concentration (molecule cm ⁻³)	Reaction
OH	2×10 ⁶ ^a	Dominant day time in the troposphere. Reacts by H-abstraction and addition
Cl	10 ³ -10 ⁴ ^b (troposphere average), max ≈10 ⁵ atom cm ⁻³ ^c (over marine environment)	Mainly fast H-abstraction, but can also react by addition
NO ₃	5×10 ⁸ ^d	Dominant nighttime for the degradation of unsaturated compounds. Mainly slow H-abstraction but also addition
RO ₂	Other minor radical species (HO ₂ , RO ₂ , etc), HO ₂ ≈2×10 ⁸ ^e	Participate in tropospheric cycles
O ₃	7×10 ¹¹ ^f	Day and night: degradation of unsaturated compounds

^a OH concentration: a 12-h daytime average adapted from Hein et al., (1997)

^b Troposphere average Cl concentration adapted from Saiz-Lopez and von Glasow (2012)

^c max Cl concentration over marine environment adapted from Rudolph et al., (1996)

^d NO₃ concentration: a 12-h night time average adapted from Calvert et al., (2011)

^e troposphere average HO₂ concentration adapted from Finlayson-Pitts et al., (1986).

^f troposphere average O₃ concentration adapted from Monks et al.,(2009)

Table 1-3: Example of the atmospheric lifetime of VOCs derived from reactions with OH radical, O₃, NO₃ radical and photolysis

VOC	lifetime			
	OH	O ₃	NO ₃	Photolysis
α-Pinene	2.6 h	4.6 h	11 min	
β-Pinene	1.8 h	1.1 d	27 min	
Sabinene	1.2 h	4.8 h	7 min	
Limonene	49 min	2 h	5 min	
Myrcene	39 min	50 min	6 min	
Linalool	52 min	55 min	6 min	
β-caryophyllene	42 min	2 min	3 min	
α-Humulene	28 min	2 min	2 min	
3-Carene	1.6 h	10.7 h	3.7 min	
2-Carene	1.7 h	1.7 h	1.8 min	
Acetone	53 d	>11 yr		≈60 d
Formaldehyde	1.3 d	>4.5 yr	80 d	4 h
acetaldehyde	8.8 h	>4.5 yr	17 d	6 d
Benzene	9.4 d	>4 yr	>4.5 yr	
Toluene	1.9 d	1.9 yr	>4.5 yr	
m-Xylene	5.9 h	200 d	>4.5 yr	

adapted from Calvert et al., (2000), Atkinson et al., 1995, Atkinson (2000)

[OH] = 2×10⁶ molecule cm⁻³ (average of 12 hours)

[O₃] = 7×10¹¹ molecule cm⁻³ (average of 24 hours)

[NO₃] = 5×10⁸ molecule cm⁻³ (average of 12 hours)

1-1-3- Atmospheric aerosol

Atmospheric aerosols are derived from many different sources, their diameters can vary from nanometers to tens of micrometers and have complex chemical compositions. The fine particles (diameter $< 2.5 \mu\text{m}$) are mostly emitted from combustion processes or are formed in the atmosphere via gas-to-particle conversion, such as sulfates (H_2SO_4 , NH_4HSO_4 , and $(\text{NH}_4)_2\text{SO}_4$) and nitrates (NH_4NO_3) that are formed by the oxidation of SO_2 and NO_x to H_2SO_4 and HNO_3 followed by reaction with NH_3 , and organic components of oligomeric species and secondary organic aerosol (SOA), which are primarily formed via the atmospheric oxidation of (semi-volatile) VOCs emitted from anthropogenic sources such as vehicles and industry, and biogenic sources that are dominated by vegetation. The larger, coarse particles (diameter $> 2.5 \mu\text{m}$) are primarily formed by mechanical processes and consist mostly of materials such as soil dust, sea salt, and plant debris (Andreae and Rosenfeld, 2008; Seinfeld and Pandis, 1998). Often, aerosols are composite mixtures of a core refractory material (black carbon BC, dust, sea salt) with a coating of organics, sulfates, and nitrates.

One of the most visible impacts of aerosols is the brownish haze; its long-range atmospheric transport transforms haze into a regional-scale aerosol layer. Well-known examples are the Arctic haze, the Indo-Asian haze, the East Asian dust and haze traveling across the Pacific and the biomass burning and dust plumes from North Africa (Sahara and Sahel regions) that spread over most of the subtropical Atlantic. However, aerosol lifetimes are only a week or less, resulting in substantial spatial and temporal variations with peak concentrations near the source (Ramanathan et al., 2001). Furthermore, the size and composition of aerosols determines its properties such as phase, volatility, light scattering and absorption, hygroscopicity, cloud nucleating activity, and chemical reactivity, which in turn affect the transport and lifetimes of chemicals in the atmosphere, visibility, the hydrologic cycle, cloud formation, climate, and environmental and human health (Davidson et al., 2005; Ramanathan et al., 2001). Indeed, aerosols affect the climate system via the following physical mechanisms: First, they can scatter and absorb solar radiation. Second, they can scatter, absorb and emit thermal radiation. Third, aerosols act as cloud condensation nuclei (CCN) and ice nuclei (IN) (Lohmann and Feichter, 2005).

1-2- Chemistry in the troposphere

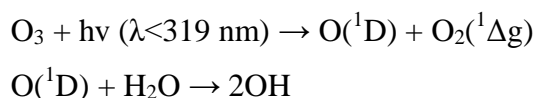
1-2-1- Photo-oxidation

Photo-oxidation induced by ultraviolet (UV) light from the sun is one of the most significant processes of changing the chemical nature of VOCs. The solar light wavelength range which initiates the photolysis action includes the ultraviolet (UV) region of solar radiation, consisting of 5% UV-B (280-315 nm) and 95% UV-A (315-400 nm). The UV-C (100-280 nm) and UV-B light are largely absorbed by the earth's atmosphere (Lee, 2003). The total amount of radiation reaching the earth's surface is called the global radiation. It consists of both direct solar radiation and diffuse radiation from light-scattering by the atmosphere and surroundings.

Hence, many important tropospheric radical reactions are initiated by photo-oxidation of a few trace gases in the atmosphere, for example, NO₂, O₃, HCHO, CH₃CHO, HONO, NO₃, and H₂O₂. Then the photo-dissociation of O₃, HONO, and H₂O₂ causes the formation of OH radicals, some reaction pathways for aldehydes primarily produce the HO₂ radical. In addition, the photolysis frequencies (J) could also depend on a more complex function of atmospheric conditions (temperature and pressure) and surface parameters including surface albedo, profiles of vertical O₃ density and turbidity or the amount and the type of cloud cover (Finlayson-Pitts and Pitts, 1986). Furthermore other properties of the troposphere like micro- and macro-scale cloud parameters become important if the vertical (and horizontal) profiles of J are modeled and compared with results of atmospheric chemical measurements. (Ruggaber et al., 1994).

1-2-2- OH chemistry

In the troposphere, OH radicals can be formed from a series of reactions initiated by the photolysis of ozone in the presence of water vapor (Krol et al., 1998):



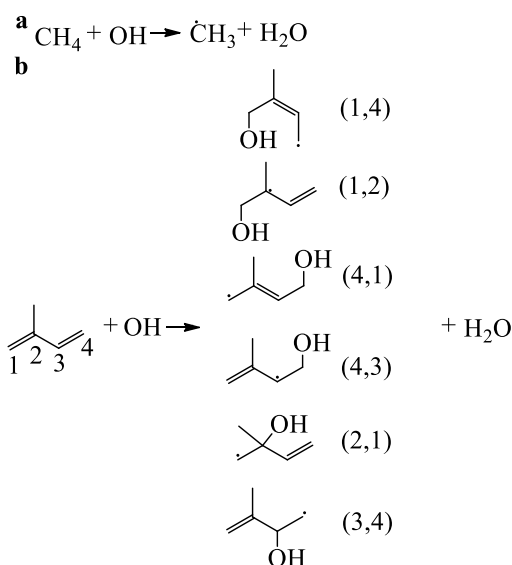
and from the photo-dissociation of HONO:



Other mechanisms involve the reaction of HO_2 with NO (Eisele et al., 1997), and photolysis of formaldehyde (Seinfeld and Pandis, 2016).

Due to the nature of its formation and reaction chemistry, OH radical concentration is dependent on temporal and meteorological factors including season, time of day, cloud cover, latitude, and relative humidity (RH) (Atkinson and Arey, 2007; Krol and Lelieveld, 2003), as well as concentration of O_3 (a key source) and NO_2 (a key sink reactant). For example, the highest OH concentration is expected in the tropics where UV light intensity levels and RH are the highest (Krol and Lelieveld, 2003).

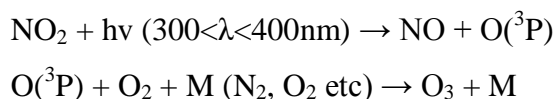
The reaction of VOCs with OH radicals can be initiated via two possible reaction pathways. These are illustrated for the CH_4 and isoprene in Scheme 1-1. The proposed pathways involve: (1) H-atom abstraction from C–H groups (Scheme 1-1(a)) of alkane, carbonyls, and alkyl nitrates and other saturated organics, or, (2) OH addition to the unsaturated $>\text{C}=\text{C}<$ and $-\text{C}\equiv\text{C}-$ bonds to form alkyl radical (Scheme 1-1(b)), like alkenes, alkynes, haloalkenes and oxygen-containing organics with $>\text{C}=\text{C}<$. Then alkyl radical further reacts with O_2 , to form RO_2 radical. Except of the structure of VOCs, the relative importance of these two proposed reaction pathways is dependent on the temperature and pressure. While the OH-addition mechanism is expected to dominate at room temperature, and H-atom abstraction from the C–H bonds will become of increasing importance at elevated temperatures (Atkinson and Arey, 2007).



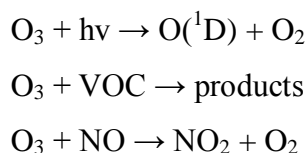
Scheme 1-1(a-b): Mechanism for the reaction of gas-phase VOCs with OH radicals; (a) H-atom abstraction; (b) OH addition

1-2-3- O₃ chemistry

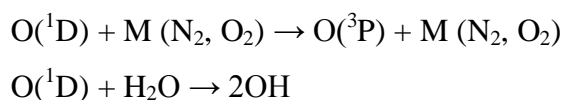
O₃ is a constituent of the natural troposphere due primarily to its production in the stratosphere (Warneck, 1999). A fraction of stratospheric O₃ passes to the troposphere (transported by folding events, for example). In addition, the photolysis of NO₂ is the major source of O(³P) and hence produce tropospheric O₃ through:



However, O₃ is lost through photochemistry and other reactions and it is deposited to the Earth's surface.



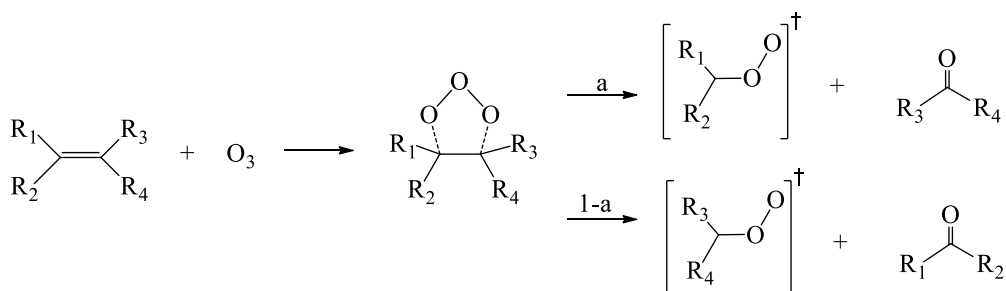
Although most of the O(¹D) are quenched to reform O(³P) to produce O₃ a fraction of the O(¹D) react with water vapor to form OH radical,



In remote regions, the overall tropospheric O₃ concentrations result from a balance between chemistry and transport of precursors from polluted regions and deposition. However, the changing balance between O₃ production and loss has changed during the 20th century, mainly owing to human activity (Volz and Kley, 1988). At a regional scale, like large cities, mean O₃ concentrations often have a positive trend in city centers owing to large amount of NO_x emission. Furthermore, the largest O₃ concentrations are found over continental (polluted) regions: eastern U.S., Europe and China (Monks et al., 2009).

From the literature (Calvert et al., 2002; Calvert et al., 2008; Calvert et al., 2011), O₃ does not react at measureable rates with alkanes ($k < 10^{-23} \text{ cm}^3 \text{ molecule}^{-1} \text{ s}^{-1}$ at 298 K) and other saturated VOCs ($k < 10^{-20} \text{ cm}^3 \text{ molecule}^{-1} \text{ s}^{-1}$ at 298 K) and aromatic hydrocarbons ($k < 10^{-20} \text{ cm}^3 \text{ molecule}^{-1} \text{ s}^{-1}$ at 298 K) and aliphatic amines. The dominant reaction of O₃ is with VOCs containing >C=C< bonds. The mechanism for

the reaction of O_3 with alkenes was first suggested by Criegee in the late 1940s in Scheme 1-2 (Criegee, 1975) and involves the addition of ozone to form a primary ozonide (POZ), which rapidly decomposes to form a vibrationally excited carbonyl oxide (Criegee intermediate) and carbonyl products. The Criegee intermediate can then either be collisionally stabilized by a third body (M), or undergo unimolecular decomposition to form products.

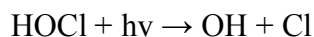


Scheme 1-2: A schematic representation of the oxidation of an alkene initiated by reaction with O_3

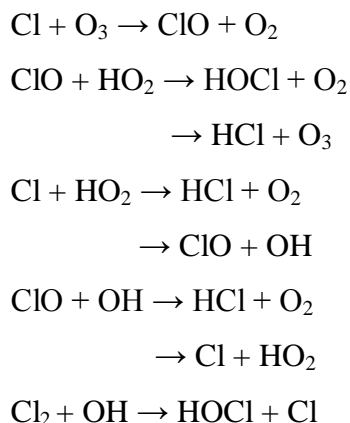
1-2-4- Cl atom chemistry

Although the global estimation of the Cl atom concentration in the northern hemisphere is only about $10^3 \text{ atom cm}^{-3}$ (Rudolph et al., 1996), it is significantly higher in conditions of the coastal regions, marine boundary layer (MBL), and also in arctic region, especially during sunrise, reaching a peak concentration of about $10^5 \text{ atom cm}^{-3}$ (Spicer et al., 1998). The generation of Cl atom from inorganic chlorides, like $ClNO_2$, $NaCl$, via heterogeneous reactions is attributed to be responsible for this high concentration in these areas. A recent field study (Thornton et al., 2010) found that Cl atom may be formed to a similar level, even in mid-continental regions, thousands of kilometers away from the coastal area, probably due to the presence of anthropogenic pollutants. In addition, one estimate (Chang and Allen, 2006) suggested that anthropogenic $HOCl$ and Cl_2 emissions in the Houston area are, 10^4 kg day^{-1} , coming from swimming pools, cooling towers and industrial point sources. In the troposphere, photo-dissociation of Cl_2 and $HOCl$ are expected to be two most important sources of Cl atom:

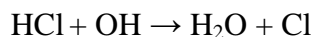




The presence of Cl atom can modify the HO_x levels and the HO₂/OH ratio in the atmosphere, this occurs from reactions resulting in the inter-conversion of OH and HO₂ (Atkinson et al., 2007), as

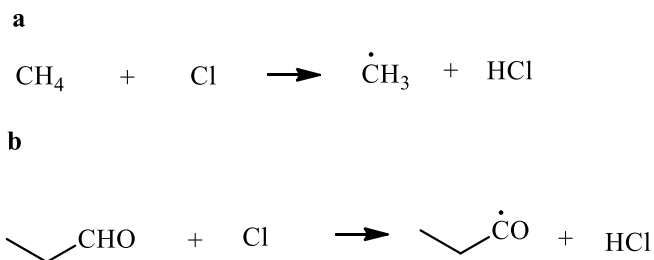


Not like OH, Cl atom is not regenerated during the oxidation cycle. However, Cl atom can be regenerated by heterogeneous cycling from chloride containing aerosols or by the volatilisation and oxidation of HCl as follow (Faxon and Allen, 2013).



However, the concentration of Cl atom in the atmosphere, even in the marine areas, is expected to be lower than the OH radical. The rate constants of Cl atom reacting with most of the VOCs are higher, by an order of magnitude or more, as compared to the OH radical. Hence, despite the lower concentration, the reaction of Cl atom contributes significantly to the atmospheric degradation of VOCs in the areas of prevalent in the MBL and highly polluted industrial and urban.

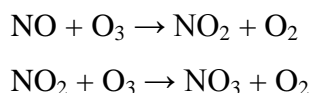
The reactivity of Cl atom towards most VOCs is similar to that of the OH radical, proceeding via H-abstraction from -CH group (Scheme 1-3(a), alkane, ketones) or -CHO group (Scheme 1-3(b), aldehyde) or addition to the >C=C< bond. Note that Cl atom addition to aromatic rings is very slow (Sokolov et al., 1998) and reactions of Cl atom with alkyl-benzenes proceeded by H-atom abstraction from the C-H bonds of the alkyl substituent groups (Wang et al., 2005). The reaction of Cl atom with CH₄ is especially important, which is not only very abundant and hence the main sink for Cl atom but it is also a very potent greenhouse gas. Cl atom can contribute 3–15% (Lawler et al., 2011) to the chemical sink of CH₄:



Scheme 1-3(a-b): Mechanism for the reaction of gas-phase VOCs with Cl atom: (a) H-atom abstraction from -CH group; (b) H-abstraction from -CHO group

1-2-5- NO₃ chemistry

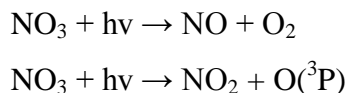
The levels of NO₃ concentration in the atmosphere are controlled by the complex interplay of the reactions that lead to its formation or removal. In the troposphere, NO₃ radical is formed via the sequential reactions of O₃ with NO₂ (Atkinson et al., 1990b):



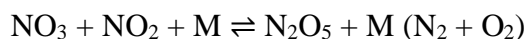
However, NO₃ reaction with NO will lead to its removal from the troposphere (Atkinson, 1990):



Photolysis of NO₃ radical by solar radiation can also contribute to its removal from the troposphere following the two pathways (Atkinson et al., 1986; Magnotta and Johnston, 1980):



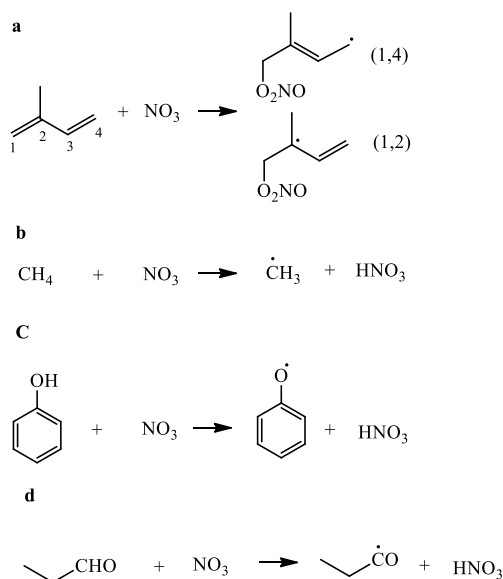
There is an equilibrium between reaction of NO₃ with NO₂ and subsequently thermally decomposition of N₂O₅. However, it is also suggested that N₂O₅ can be hydrolyzed to form HNO₃, which leads to the removal of NO₃ from the troposphere (Asaf et al., 2009; Atkinson and Lloyd, 1984; Malko and Troe, 1982):





Because of its reaction with NO and rapid photolysis, the concentrations of the NO₃ radical in the lower troposphere will be lower during daytime (Atkinson, 1986). Concentrations of NO₃ radical will therefore be present at significant levels only during night time when photolysis is absent and NO levels are low (Atkinson and Arey, 1994; Atkinson and Arey, 2007). Levels of NO₃ radical in the troposphere will therefore be subject to substantial temporal and spatial variability (Atkinson and Arey, 2007), ranging from $< 5 \times 10^7$ molecules cm⁻³ to 10^{10} molecules cm⁻³ (Atkinson, 1986). Atkinson (Atkinson, 1986) has suggested an average 12 h night time NO₃ radical concentration in the lower troposphere of $[\text{NO}_3] \approx 5 \times 10^8$ molecules cm⁻³ (≈ 20 pptV) over continental areas.

In the continental boundary layer, NO₃ radical can rapidly react with several VOCs, particularly, with alkenes like isoprene and monoterpenes, through the NO₃ addition to the $>\text{C}=\text{C}<$ bonds (Scheme 1-4(a)). For the saturated VOCs or aromatic alcohols or aldehydes, their reaction with NO₃ radical can either take place through H-abstraction from the C-H group (Scheme 1-4(b)) or -OH (Scheme 1-4(c)) or -CHO (Scheme 1-4(d)) group. Generally, the NO₃ addition to the $>\text{C}=\text{C}<$ bond is the dominant pathway. Atkinson et al (1992) suggested that the H-abstraction from -OH group accounts for at least $25 \pm 5\%$ of its overall reaction of NO₃ radical with phenol (Scheme 1-4(c)) in the presence of NO_x.



Scheme 1-4(a-d): Mechanism for the reaction of gas-phase VOCs with NO₃ radicals: (a) NO₃ addition; (b) H-atom abstraction from -CH group; (c) H-abstraction from -OH group; (d) H-abstraction from -CHO group

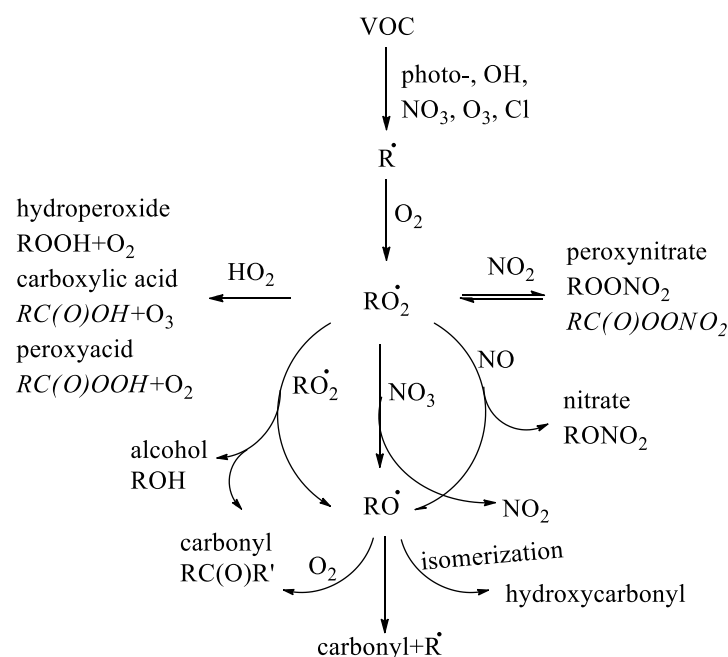
1-2-6- Formation of secondary organic aerosols (SOA)

SOA comprises a large fraction of atmospheric particle mass, which can have significant effects on atmospheric chemistry, human health, visibility and climate. SOA is expected to be formed in the atmosphere when VOCs emitted from biogenic and anthropogenic sources are oxidized by reactions with OH radicals (typically during daylight hours), NO₃ radicals (during evening and nighttime hours), O₃ or Cl atom (coastal and marine, and possibly also continental areas) to form less volatile VOCs that subsequently partition into aerosol particles. The literature (Ziemann and Atkinson, 2012) shows that the key VOC degradation intermediates (Scheme 1-5) are alkyl (or substituted alkyl), alkyl peroxy (RO₂) and alkoxy (RO) radicals, their reactions (with HO₂, NO, NO₂ or self-reaction) could lead to products (ROOH, RONO₂, ROONO₂, and carbonyls and alcohols) with different functional groups (Scheme 1-5), which all have significantly lower vapor pressures. The presence or absence of NO_x (NO, NO₂) and their concentrations could significantly affect the physical and chemical properties of these products and their propensity to form SOA.

In the following heterogeneous/multiphase series of reactions, the organic compounds contain carboxylic, carbonyl, peroxy-carboxyl, hydroxyl and hydroperoxy, groups that are most likely to play a role in SOA formation. Nitrate and ester groups are not expected to participate directly in such reactions (Ziemann and Atkinson, 2012), although the alcohols and carboxylic acids formed when they can hydrolyze (usually very slowly at typical atmospheric aerosol acidities (Darer et al., 2011; Hilal, 2006)). Like: (path 1) 1,4-Hydroxycarbonyl reactions to form cyclic hemiacetals and dihydrofurans; (path 2) Alcohol + carbonyl reactions to form hemiacetals and acetals; (path 3). Hydroperoxide + carbonyl reactions to form peroxyhemiacetals and peroxyacetals; (path 4) Peroxyacid + carbonyl reactions to form acyl peroxyhemiacetals and carboxylic acids; (path 5) Alcohol + carboxylic acid reactions to form esters; (path 6) Aldehyde reactions to form aldols. In addition, the heterogeneous/multiphase oligomer-forming reactions can occur on time scales and have sufficiently large equilibrium constants to significantly alter SOA composition and yields. In a relatively clean atmosphere, the case for particles containing weak and strong acids and low water content, which drives dehydration reactions toward oligomeric products and suggest that at equilibrium the most likely oligomers are peroxyhemiacetals (path 3) and carbonyls, and esters (path 5). In a polluted area,

where hydroperoxides and carboxylic acids are likely to be less abundant, one might expect the dominant oligomers to be hemiacetals (path 2) although esters have been shown to form from the reactions of isoprene under these conditions (Ziemann and Atkinson, 2012).

In the atmosphere, the major classes of SOA precursors are volatile and semi-volatile alkanes, alkenes, aromatic hydrocarbons, and oxygenated compounds (OVOCs) (Atkinson and Arey, 2003). Indeed, biogenic emissions contribute 90% of non-methane VOCs globally, with anthropogenic emissions being more important in urban areas (Guenther et al., 1995). The concentration of inorganic salt (NH_4HSO_4 , $(\text{NH}_4)_2\text{SO}_4$ and NH_4NO_3) could be important to the formation of SOA, which act as the seed in the atmosphere. In addition, the meteorological conditions, e.g. relative humidity, wind speed, temperature, also has important influence on the formation of SOA in the atmosphere.



Scheme 1-5: Reactions of alkyl peroxy (RO_2) radicals. The products in italics are formed from reactions of acyl peroxy (ROC(O)O_2) radicals (adapted from (Ziemann and Atkinson, 2012)).

1-3- The Master Chemical Mechanism

The degradation of emitted VOCs has a major influence on the chemistry of the troposphere, contributing to the formation of O_3 , secondary organic aerosol (SOA) and other secondary pollutants (Jenkin and Clemitshaw, 2000), which may have a

harmful impact on human health and on the environment. Over the past decades, the availability of kinetic and mechanistic data to help elucidate the degradation mechanisms of VOC has increased significantly, and various aspects of the tropospheric chemistry of VOCs have been reviewed extensively, especially for isoprene (Calvert et al., 2011; Jenkin et al., 2015). However, the detail mechanisms of oxidation of VOCs are still not clear due to the limited techniques. Then, the simulation models (like, master chemical mechanism, MCM; chemistry-transport model, CTMs, etc) could help to understand the reaction mechanisms, products formation and their influence on the local air quality.

The series of versions of the Master Chemical Mechanism (from MCMv1 to MCMv3.3) (Saunders et al., 2003; Jenkin et al., 2003; Jenkin et al., 2015; Jenkin et al., 1997; Bloss et al., 2005) provides detailed gas-phase chemical processes involved in the tropospheric degradation of a series of primary emitted VOCs. The philosophy behind the construction of the MCM is to use available information on the kinetics and products of elementary reactions relevant to VOC oxidation to build up a near-explicit representation of the degradation mechanisms. Indeed, it has been widely used by the atmospheric science community both directly, and as a benchmark representation against which to develop and optimize reduced chemical mechanisms for using in CTMs. The entire MCM treats the degradation of methane and 142 non-methane VOCs and considers photolysis and oxidation by OH radical, Cl atom, O₃ and NO₃ radical. Hence, the MCM is used where the kinetics and products of a large number of unstudied chemical reactions can be defined on the basis of the known reactions of a comparatively small number of similar chemical species, by analogy and with the use of Structure-Activity Relationship (SAR) correlations.

Practically, atmospheric simulation chambers are useful tools in obtaining data suitable for testing VOC oxidation models prior to compiling chemical mechanisms, to predict the major fates of VOC oxidation processes. In the simulation chambers, experiments can be carried out under controlled and well-characterized conditions. Then, the experimental results can later be compared with those predicted by models, like MCM, and used as an indicator on how well the chemistry is known. Furthermore, the development and application of MCM are important since the condition of potential interest for control strategies cannot be simulated experimentally. Consequently, the capacity of accurately describing both the chemical and physical aspects of atmospheric processes is critical in developing and assessing effective

control strategies.

1-4- Motivation

As discussed in the previous, summaries of the gas-phase kinetics of the alkanes, alkenes and OVOCs reactions with OH and NO₃ radicals and ozone and Cl atom, products of these reactions and the pathways leading to their formation can be found in several review articles and books, e.g. (Atkinson, 1991;Atkinson et al., 1990a;Calvert et al., 2008;Calvert et al., 2011;Calvert et al., 2002). VOC oxidation processes play an important role in the tropospheric chemistry, furthermore, the oxygenated organics formed from the oxidation of parent VOCs mainly play a fundamental role in the oxidation capacity of atmosphere and SOA formation. Ziemann and Atkinson et al., (2012) have summarized laboratory studies of SOA formation performed over the last decade. As a result of ever increasing information on the nature of the gas-phase products and the composition of the resulting aerosol from the oxidation of VOCs from the laboratory studies and field measurements (El Haddad et al., 2015;Ziemann and Atkinson, 2012;Abbatt et al., 2012), much effort is now being spent in developing combined gas-phase kinetics and aerosol partitioning models to represent SOA formation in ambient models (Griffin et al., 2005;Kamens and Jaoui, 2001). However, the transition of these results to the real atmospheric conditions still requires thorough interpretation and further analysis and understanding of the chemical mechanisms.

In addition, understanding VOC oxidation processes is essential in the predictions made on local air quality and global climate change and decisions made in setting emission limits as well as for interpreting their effects to human health of various pollutants, e.g. VOCs, NO_x, O₃, OH, Cl₂ etc (Ravishankara et al., 2012). Hence, a complete understanding of the gas phase reactions of VOCs with reactive species remains elusive, and the detailed product analyses necessary in conjunction with the experimental rate constants measurements are extremely challenging. Therefore the purposes of this study are:

Determination of SOA and radical (OH) yield from the ozonolysis of alkenes of biogenic and anthropogenic origin;

Measurement of the products formation and identification of the mechanism for the photolysis of ketone and fluorinated ketone;

Measurements of the products formation and identification of the mechanism for the reaction of ketones with OH radical / Cl atom.

These objectives have been achieved through a series of experiments using a series of atmospheric simulation chambers, in Orléans, France. A combination of several different instruments was used to perform comprehensive measurements of products formation from the studied reaction.

1-5- Outline of the thesis

This thesis is subdivided into subsequent chapters:

Chapter 1 has outlined the composition of the troposphere and the tropospheric chemistry included photolysis, reaction with OH radical, NO₃ radical, O₃ and Cl atom, and the hot issues of new particle formation. It is the fundament of the troposphere and influence the troposphere, and also the air quality and climate. Hence, this chapter showed our research direction.

A brief introduction into the atmospheric simulation chambers and instruments used in this thesis is given in chapter 2. The strengths and weaknesses of different simulation chambers are also discussed.

The kinetic and products formation of the ozonolysis of isoprene, methacrolein (MACR) and methyl vinyl ketone (MVK) were conducted under atmospheric condition, which is shown in chapter 3. The idea is to investigate their rate coefficients, OH radical formation and SOA formation with relative low concentration using the large simulation chamber HELIOS.

Photolysis of perfluoro-2-methyl-3-pentanone (PF-2M3P) and 2-methyl-3-pentanone (2M3P) under sunlight conditions is shown in chapter 4. The idea is to inter-compare their decomposition pathway by the natural irradiation using HELIOS.

Kinetics and products studies of OH reactions with a series of ketones are presented in chapter 5. The idea is to understand the influence of methyl branch and its position in the ketones to their reactivity toward OH radical. This was achieved by the kinetics (combining the absolute and relative rate methods) and products studies and SAR calculation.

Kinetics and products studies of Cl atom reactions with a series of ketones are given in chapter 6. The idea is to understand the reaction pathways of ketones with Cl

atom and define its similarities and differences compared with the reaction with OH radical.

Chapter 7 summarizes the results and gives an outlook into further possible research work.

References

- Abbatt, J. P. D., Lee, A. K. Y., and Thornton, J. A.: Quantifying trace gas uptake to tropospheric aerosol: recent advances and remaining challenges, *Chemical Society Reviews*, 41, 6555-6581, 10.1039/C2CS35052A, 2012.
- Andreae, M. O., and Rosenfeld, D.: Aerosol–cloud–precipitation interactions. Part 1. The nature and sources of cloud-active aerosols, *Earth-Science Reviews*, 89, 13-41, <http://dx.doi.org/10.1016/j.earscirev.2008.03.001>, 2008.
- Asaf, D., Pedersen, D., Matveev, V., Peleg, M., Kern, C., Zingler, J., Platt, U., and Luria, M.: Long-Term Measurements of NO₃ Radical at a Semiarid Urban Site: 1. Extreme Concentration Events and Their Oxidation Capacity, *Environmental Science & Technology*, 43, 9117-9123, 10.1021/es900798b, 2009.
- Atkinson, R., and Lloyd, A. C.: Evaluation of Kinetic and Mechanistic Data for Modeling of Photochemical Smog, *Journal of Physical and Chemical Reference Data*, 13, 315-444, doi:<http://dx.doi.org/10.1063/1.555710>, 1984.
- Atkinson, R.: Kinetics and mechanisms of the gas-phase reactions of the hydroxyl radical with organic compounds under atmospheric conditions, *Chemical Reviews*, 86, 69-201, 10.1021/cr00071a004, 1986.
- Atkinson, R., Winer, A. M., and Pitts, J. N.: Estimation of night-time N₂O₅ concentrations from ambient NO₂ and NO₃ radical concentrations and the role of N₂O₅ in night-time chemistry, *Atmospheric Environment* (1967), 20, 331-339, [http://dx.doi.org/10.1016/0004-6981\(86\)90035-1](http://dx.doi.org/10.1016/0004-6981(86)90035-1), 1986.
- Atkinson, R.: Gas-phase tropospheric chemistry of organic compounds: A review, *Atmospheric Environment. Part A. General Topics*, 24, 1-41, [http://dx.doi.org/10.1016/0960-1686\(90\)90438-S](http://dx.doi.org/10.1016/0960-1686(90)90438-S), 1990.
- Atkinson, R., Hasegawa, D., and Aschmann, S. M.: Rate constants for the gas-phase reactions of O₃ with a series of monoterpenes and related compounds at 296 ± 2 K, *International Journal of Chemical Kinetics*, 22, 871-887, 10.1002/kin.550220807, 1990a.
- Atkinson, R., Tuazon, E. C., and Arey, J.: Reactions of naphthalene in N₂O₅ NO₃ NO₂ air mixtures, *International Journal of Chemical Kinetics*, 22, 1071-1082, 10.1002/kin.550221006, 1990b.
- Atkinson, R.: Kinetics and Mechanisms of the Gas - Phase Reactions of the NO₃

- Radical with Organic Compounds, *Journal of Physical and Chemical Reference Data*, 20, 459-507, doi:<http://dx.doi.org/10.1063/1.555887>, 1991.
- Atkinson, R., Aschmann, S. M., and Arey, J.: Reactions of hydroxyl and nitrogen trioxide radicals with phenol, cresols, and 2-nitrophenol at 296 \pm 2 K, *Environmental Science & Technology*, 26, 1397-1403, 10.1021/es00031a018, 1992.
- Atkinson, R., and Arey, J.: Atmospheric chemistry of gas-phase polycyclic aromatic hydrocarbons: formation of atmospheric mutagens, *Environmental Health Perspectives*, 102, 117-126, 1994.
- Atkinson, R.: Atmospheric chemistry of VOCs and NO_x, *Atmospheric Environment*, 34, 2063-2101, [http://dx.doi.org/10.1016/S1352-2310\(99\)00460-4](http://dx.doi.org/10.1016/S1352-2310(99)00460-4), 2000.
- Atkinson, R., and Arey, J.: Atmospheric Degradation of Volatile Organic Compounds, *Chemical Reviews*, 103, 4605-4638, 10.1021/cr0206420, 2003.
- Atkinson, R., and Arey, J.: MECHANISMS OF THE GAS-PHASE REACTIONS OF AROMATIC HYDROCARBONS AND PAHS WITH OH AND NO₃ RADICALS, *Polycyclic Aromatic Compounds*, 27, 15-40, 10.1080/10406630601134243, 2007.
- Atkinson, R., Baulch, D. L., Cox, R. A., Crowley, J. N., Hampson, R. F., Hynes, R. G., Jenkin, M. E., Rossi, M. J., and Troe, J.: Evaluated kinetic and photochemical data for atmospheric chemistry: Volume III – gas phase reactions of inorganic halogens, *Atmos. Chem. Phys.*, 7, 981-1191, 10.5194/acp-7-981-2007, 2007.
- Bell, M. L., Peng, R. D., and Dominici, F.: The exposure-response curve for ozone and risk of mortality and the adequacy of current ozone regulations, *Environ Health Perspect*, 114, 532-536, 2006.
- Bloss, C., Wagner, V., Jenkin, M. E., Volkamer, R., Bloss, W. J., Lee, J. D., Heard, D. E., Wirtz, K., Martin-Reviejo, M., Rea, G., Wenger, J. C., and Pilling, M. J.: Development of a detailed chemical mechanism (MCMv3.1) for the atmospheric oxidation of aromatic hydrocarbons, *Atmospheric Chemistry and Physics*, 5, 641-664, 2005.
- Brown, S. S., Dubé, W. P., Peischl, J., Ryerson, T. B., Atlas, E., Warneke, C., de Gouw, J. A., de Lintel Hekkert, S., Brock, C. A., Flocke, F., Trainer, M., Parrish, D. D., Feshenfeld, F. C., and Ravishankara, A. R.: Budgets for nocturnal VOC oxidation by nitrate radicals aloft during the 2006 Texas Air Quality Study, *Journal of*

- Geophysical Research: Atmospheres, 116, n/a-n/a, 10.1029/2011JD016544, 2011.
- Calvert, J. G., Atkinson, R., Kerr, J. A., Madronich, S., Moortgat, G. K., Wallington, T. J., and G., Y.: The Mechanisms of Atmospheric Oxidation of the Alkenes, Oxford University Press, New York, 2000.
- Calvert, J. G., Atkinson, R., Becker, K. H., Kamens, R. M., Seinfeld, J. H., Wallington, T. J., and G., Y.: The Mechanisms of Atmospheric Oxidation of Aromatic Hydrocarbons, Oxford University Press, New York, 2002.
- Calvert, J. G., Derwent, R. G., Orlando, J. J., Tyndall, G. S., and J., W. T.: Mechanisms of Atmospheric Oxidation of the Alkanes, Oxford University Press, New York, 2008.
- Calvert, J. G., Mellouki, A., Orlando, J. J., Pilling, M. J., and J., W. T.: The Mechanisms of Atmospheric Oxidation of the Oxygenates, Oxford University Press, New York, 2011.
- Carter, W. P. L., Winer, A. M., and Pitts, J. N.: Major atmospheric sink for phenol and the cresols. Reaction with the nitrate radical, Environmental Science & Technology, 15, 829-831, 10.1021/es00089a009, 1981.
- Chang, S., and Allen, D. T.: Atmospheric Chlorine Chemistry in Southeast Texas: Impacts on Ozone Formation and Control, Environmental Science & Technology, 40, 251-262, 10.1021/es050787z, 2006.
- Criegee, R.: Mechanism of Ozonolysis, Angewandte Chemie International Edition in English, 14, 745-752, 10.1002/anie.197507451, 1975.
- Darer, A. I., Cole-Filipiak, N. C., O'Connor, A. E., and Elrod, M. J.: Formation and Stability of Atmospherically Relevant Isoprene-Derived Organosulfates and Organonitrates, Environmental Science & Technology, 45, 1895-1902, 10.1021/es103797z, 2011.
- Davidson, C. I., Phalen, R. F., and Solomon, P. A.: Airborne Particulate Matter and Human Health: A Review, Aerosol Science and Technology, 39, 737-749, 10.1080/02786820500191348, 2005.
- Eisele, F. L., Mount, G. H., Tanner, D., Jefferson, A., Shetter, R., Harder, J. W., and Williams, E. J.: Understanding the production and interconversion of the hydroxyl radical during the Tropospheric OH Photochemistry Experiment, Journal of Geophysical Research: Atmospheres, 102, 6457-6465, 10.1029/96JD02207, 1997.

- Faxon, C. B., and Allen, D. T.: Chlorine chemistry in urban atmospheres: a review, *Environmental Chemistry*, 10, 221-233, <http://dx.doi.org/10.1071/EN13026>, 2013.
- Finlayson-Pitts, B. J., and Pitts, J. N.: *Atmospheric Chemistry: Fundamentals and Experimental Techniques*, Wiley, New York, 1986.
- Finlayson-Pitts, B. J., and Pitts Jr, J. N.: Preface, in: *Chemistry of the Upper and Lower Atmosphere*, Academic Press, San Diego, xvii-xviii, 2000.
- Geyer, A., Alicke, B., Konrad, S., Schmitz, T., Stutz, J., and Platt, U.: Chemistry and oxidation capacity of the nitrate radical in the continental boundary layer near Berlin, *Journal of Geophysical Research: Atmospheres*, 106, 8013-8025, 10.1029/2000JD900681, 2001.
- Griffin, R. J., Dabdub, D., and Seinfeld, J. H.: Development and initial evaluation of a dynamic species-resolved model for gas phase chemistry and size-resolved gas/particle partitioning associated with secondary organic aerosol formation, *Journal of Geophysical Research: Atmospheres*, 110, n/a-n/a, 10.1029/2004JD005219, 2005.
- Guenther, A., Hewitt, C. N., Erickson, D., Fall, R., Geron, C., Graedel, T., Harley, P., Klinger, L., Lerdau, M., McKay, W. A., Pierce, T., Scholes, B., Steinbrecher, R., Tallamraju, R., Taylor, J., and Zimmerman, P.: A global model of natural volatile organic compound emissions, *Journal of Geophysical Research: Atmospheres*, 100, 8873-8892, 10.1029/94JD02950, 1995.
- Guenther, A. B., Jiang, X., Heald, C. L., Sakulyanontvittaya, T., Duhl, T., Emmons, L. K., and Wang, X.: The Model of Emissions of Gases and Aerosols from Nature version 2.1 (MEGAN2.1): an extended and updated framework for modeling biogenic emissions, *Geosci. Model Dev.*, 5, 1471-1492, 10.5194/gmd-5-1471-2012, 2012.
- Hein, R., Crutzen, P. J., and Heimann, M.: An inverse modeling approach to investigate the global atmospheric methane cycle, *Global Biogeochemical Cycles*, 11, 43-76, 10.1029/96GB03043, 1997.
- Hilal, S. H.: Estimation of hydrolysis rate constants of carboxylic acid ester and phosphate ester compounds in aqueous systems from molecular structure by SPARC [electronic resource] / By S. H. Hilal, Accessed from <http://nla.gov.au/nla.cat-vn4359151>, edited by: United States. Environmental Protection Agency. Office of, R., and Development, U.S. Environmental

- Protection Agency, Office of Research and Development, Washington, DC, 2006.
- Jenkin, M. E., Saunders, S. M., and Pilling, M. J.: The tropospheric degradation of volatile organic compounds: a protocol for mechanism development, *Atmospheric Environment*, 31, 81-104, [http://dx.doi.org/10.1016/S1352-2310\(96\)00105-7](http://dx.doi.org/10.1016/S1352-2310(96)00105-7), 1997.
- Jenkin, M. E., and Clemitshaw, K. C.: Ozone and other secondary photochemical pollutants: chemical processes governing their formation in the planetary boundary layer, *Atmospheric Environment*, 34, 2499-2527, [http://dx.doi.org/10.1016/S1352-2310\(99\)00478-1](http://dx.doi.org/10.1016/S1352-2310(99)00478-1), 2000.
- Jenkin, M. E., Saunders, S. M., Wagner, V., and Pilling, M. J.: Protocol for the development of the Master Chemical Mechanism, MCM v3 (Part B): tropospheric degradation of aromatic volatile organic compounds, *Atmos. Chem. Phys.*, 3, 181-193, 10.5194/acp-3-181-2003, 2003.
- Jenkin, M. E., Young, J. C., and Rickard, A. R.: The MCM v3.3.1 degradation scheme for isoprene, *Atmos. Chem. Phys.*, 15, 11433-11459, 10.5194/acp-15-11433-2015, 2015.
- Kamens, R. M., and Jaoui, M.: Modeling Aerosol Formation from α -Pinene + NO_x in the Presence of Natural Sunlight Using Gas-Phase Kinetics and Gas-Particle Partitioning Theory, *Environmental Science & Technology*, 35, 1394-1405, 10.1021/es001626s, 2001.
- Krol, M., van Leeuwen, P. J., and Lelieveld, J.: Global OH trend inferred from methylchloroform measurements, *Journal of Geophysical Research: Atmospheres*, 103, 10697-10711, 10.1029/98JD00459, 1998.
- Krol, M., and Lelieveld, J.: Can the variability in tropospheric OH be deduced from measurements of 1,1,1-trichloroethane (methyl chloroform)?, *Journal of Geophysical Research: Atmospheres*, 108, n/a-n/a, 10.1029/2002JD002423, 2003.
- Lawler, M. J., Sander, R., Carpenter, L. J., Lee, J. D., von Glasow, R., Sommariva, R., and Saltzman, E. S.: HOCl and Cl₂ observations in marine air, *Atmos. Chem. Phys.*, 11, 7617-7628, 10.5194/acp-11-7617-2011, 2011.
- Lee, R. F.: Photo-oxidation and Photo-toxicity of Crude and Refined Oils, *Science & Technology Bulletin*, 8, 157-162, [http://dx.doi.org/10.1016/S1353-2561\(03\)00015-X](http://dx.doi.org/10.1016/S1353-2561(03)00015-X), 2003.
- Lohmann, U., and Feichter, J.: Global indirect aerosol effects: a review, *Atmos. Chem.*

- Phys., 5, 715-737, 10.5194/acp-5-715-2005, 2005.
- Magnotta, F., and Johnston, H. S.: Photodissociation quantum yields for the NO₃ free radical, *Geophysical Research Letters*, 7, 769-772, 10.1029/GL007i010p00769, 1980.
- Malko, M. W., and Troe, J.: Analysis of the unimolecular reaction $\text{N}_2\text{O}_5 + \text{M} \rightleftharpoons \text{NO}_2 + \text{NO}_3 + \text{M}$, *International Journal of Chemical Kinetics*, 14, 399-416, 10.1002/kin.550140407, 1982.
- Monks, P. S., Granier, C., Fuzzi, S., Stohl, A., Williams, M. L., Akimoto, H., Amann, M., Baklanov, A., Baltensperger, U., Bey, I., Blake, N., Blake, R. S., Carslaw, K., Cooper, O. R., Dentener, F., Fowler, D., Fragkou, E., Frost, G. J., Generoso, S., Ginoux, P., Grewe, V., Guenther, A., Hansson, H. C., Henne, S., Hjorth, J., Hofzumahaus, A., Huntrieser, H., Isaksen, I. S. A., Jenkin, M. E., Kaiser, J., Kanakidou, M., Klimont, Z., Kulmala, M., Laj, P., Lawrence, M. G., Lee, J. D., Liousse, C., Maione, M., McFiggans, G., Metzger, A., Mieville, A., Moussiopoulos, N., Orlando, J. J., O'Dowd, C. D., Palmer, P. I., Parrish, D. D., Petzold, A., Platt, U., Pöschl, U., Prévôt, A. S. H., Reeves, C. E., Reimann, S., Rudich, Y., Sellegri, K., Steinbrecher, R., Simpson, D., ten Brink, H., Theloke, J., van der Werf, G. R., Vautard, R., Vestreng, V., Vlachokostas, C., and von Glasow, R.: Atmospheric composition change – global and regional air quality, *Atmospheric Environment*, 43, 5268-5350, <http://dx.doi.org/10.1016/j.atmosenv.2009.08.021>, 2009.
- Pflieger, M.: Heterogeneous degradation of pesticides adsorbed on atmospheric particles, *Université de Provence - Aix-Marseille I*, 2009.
- Platt, U., LeBras, G., Poulet, G., Burrows, J. P., and Moortgat, G.: Peroxy radicals from night-time reaction of NO₃ with organic compounds, *Nature*, 348, 147-149, 1990.
- Prinn, R. G., Huang, J., Weiss, R. F., Cunnold, D. M., Fraser, P. J., Simmonds, P. G., McCulloch, A., Harth, C., Salameh, P., O'Doherty, S., Wang, R. H. J., Porter, L., and Miller, B. R.: Evidence for Substantial Variations of Atmospheric Hydroxyl Radicals in the Past Two Decades, *Science*, 292, 1882-1888, 10.1126/science.1058673, 2001.
- Ramanathan, V., Crutzen, P. J., Kiehl, J. T., and Rosenfeld, D.: Aerosols, Climate, and the Hydrological Cycle, *Science*, 294, 2119-2124, 10.1126/science.1064034, 2001.

- Ravishankara, A. R., Dawson, J. P., and Winner, D. A.: New Directions: Adapting air quality management to climate change: A must for planning, *Atmospheric Environment*, 50, 387-389, <http://dx.doi.org/10.1016/j.atmosenv.2011.12.048>, 2012.
- Reich, P. B., and Amundson, R. G.: Ambient levels of ozone reduce net photosynthesis in tree and crop species, *Science*, 230, 566-570, 10.1126/science.230.4725.566, 1985.
- Rudolph, J., Koppmann, R., and Plass-Dülmer, C.: The budgets of ethane and tetrachloroethene: Is there evidence for an impact of reactions with chlorine atoms in the troposphere?, *Atmospheric Environment*, 30, 1887-1894, [http://dx.doi.org/10.1016/1352-2310\(95\)00385-1](http://dx.doi.org/10.1016/1352-2310(95)00385-1), 1996.
- Ruggaber, A., Dlugi, R., and Nakajima, T.: Modelling radiation quantities and photolysis frequencies in the troposphere, *Journal of Atmospheric Chemistry*, 18, 171-210, 10.1007/bf00696813, 1994.
- Saiz-Lopez, A., and von Glasow, R.: Reactive halogen chemistry in the troposphere, *Chemical Society Reviews*, 41, 6448-6472, 10.1039/C2CS35208G, 2012.
- Saunders, S. M., Jenkin, M. E., Derwent, R. G., and Pilling, M. J.: Protocol for the development of the Master Chemical Mechanism, MCM v3 (Part A): tropospheric degradation of non-aromatic volatile organic compounds, *Atmos. Chem. Phys.*, 3, 161-180, 10.5194/acp-3-161-2003, 2003.
- Seinfeld, J. H., and Pandis, S. N.: *Atmospheric Chemistry and Physics*, Wiley-Interscience, New York, 1998.
- Seinfeld, J. H., and Pandis, S. N.: *Atmospheric Chemistry and Physics: From Air Pollution to Climate Change*, 3rd Edition, John Wiley & Sons, Inc, 1232 pp., 2016.
- Sokolov, O., Hurley, M. D., Wallington, T. J., Kaiser, E. W., Platz, J., Nielsen, O. J., Berho, F., Rayez, M. T., and Lesclaux, R.: Kinetics and Mechanism of the Gas-Phase Reaction of Cl Atoms with Benzene, *The Journal of Physical Chemistry A*, 102, 10671-10681, 10.1021/jp9828080, 1998.
- Spicer, C. W., Chapman, E. G., Finlayson-Pitts, B. J., Plastring, R. A., Hubbe, J. M., Fast, J. D., and Berkowitz, C. M.: Unexpectedly high concentrations of molecular chlorine in coastal air, *Nature*, 394, 353-356, 1998.
- Thornton, J. A., Kercher, J. P., Riedel, T. P., Wagner, N. L., Cozic, J., Holloway, J. S., Dube, W. P., Wolfe, G. M., Quinn, P. K., Middlebrook, A. M., Alexander, B., and

- Brown, S. S.: A large atomic chlorine source inferred from mid-continental reactive nitrogen chemistry, *Nature*, 464, 271-274, 10.1038/nature08905, 2010.
- Volz, A., and Kley, D.: Evaluation of the Montsouris series of ozone measurements made in the nineteenth century, *Nature*, 332, 240-242, 1988.
- Wang, L., Arey, J., and Atkinson, R.: Reactions of Chlorine Atoms with a Series of Aromatic Hydrocarbons, *Environmental Science & Technology*, 39, 5302-5310, 10.1021/es0479437, 2005.
- Warneck, P.: *Chemistry of the Natural Atmosphere*, 2nd ed., Academic Press, San Diego, CA, USA, 1999.
- Ziemann, P. J., and Atkinson, R.: Kinetics, products, and mechanisms of secondary organic aerosol formation, *Chemical Society Reviews*, 41, 6582-6605, 10.1039/C2CS35122F, 2012.

Chapter 2.

Experimental Methods & Instrumentation

Chapter 2- Experimental Methods & Instrumentation	32
2-1- UV-Visible absorption	32
2-2- Pulsed laser photolysis-laser induced fluorescence (PLP-LIF).....	34
2-3- Atmospheric simulation chambers	35
2-3-1- Small indoor simulation chamber - 200 L	36
2-3-1-1- Introduction.....	36
2-3-1-2- Gas chromatography-flame ionization detector	37
2-3-2- Moveable simulation chamber - 3.4 m ³	38
2-3-2-1- Introduction.....	38
2-3-2-2- Fourier transform infrared spectroscopy 3 (FTIR3)	39
2-3-3- Large indoor simulation chamber (CSA)-7.3 m ³	41
2-3-3-1- Introduction.....	41
2-3-3-2- Fourier transform infrared spectroscopy 2 (FTIR2)	43
2-3-3-3- Scanning Mobility Particle Sizers (SMPS).....	44
2-3-4- Large outdoor simulation chamber-90 m ³ (HELIOS)	47
2-3-4-1- Introduction.....	47
2-3-4-2- Fourier transform infrared spectroscopy 1 (FTIR1)	53
2-3-4-3- Automated Thermal Desorption-Gas chromatography/mass spectrometer (ATD-GC/MS).....	53
2-3-4-4- Proton transfer reaction-time of flight-mass spectrometer (PTR-ToF-MS).....	56
2-3-4-5- Ultra High Performance Liquid Chromatograph-Mass Spectrometry (UHPLC-MS).....	58
2-3-4-6- Formaldehyde (HCHO) analyzer	60
2-3-4-7- Spectroradiometer	61
2-4- Instrumentation Conclusion	62
References	64

Chapter 2- Experimental Methods & Instrumentation

To gain insight into the atmospheric oxidation processes of VOCs in the atmosphere, laboratory studies at different scales as well as field measurements are conducted. The data obtained are used in atmospheric models describing the chemistry and evaluating the impacts on human health and different ecosystems. Since mechanism evaluation of VOCs oxidation requires studies over a range of conditions such as temperature, pressure, relative humidity..., the atmospheric simulation chambers are widely used. They allow the control of temperature, pressure, photolytic conditions, and the chemical composition of the studied systems which are important variables that affect the rates of reactions and mechanisms in atmospheric processes. Furthermore, several different simulation chambers: indoor and outdoor chamber, small and large chambers are used depending on the aim of investigation and control conditions. Complementary experimental techniques are also used to derive kinetic and spectroscopic parameters of atmospheric importance (pulsed laser photolysis-laser induced fluorescence, absorption spectroscopy ...). In the present thesis, we use a large variety of techniques dedicated to the atmospheric processes studies. The purpose of this chapter is to highlight the details of the different experimental techniques and analytical tools used to conduct the present work.

The experimental system dedicated to the UV-Visible absorption cross sections is first described, then the pulsed laser photolysis – laser induced fluorescence set-up used for the absolute OH reaction rate constants measurement as function of temperature is briefly described and different atmospheric simulation chambers used for kinetic and products studies. In addition, the analytical tools employed are also described in this chapter.

2-1- UV-Visible absorption

A UV-visible spectrophotometer (ACTON SP2300i) equipped with a 1200 grooves mm^{-1} grating, a 1024 element diode array detector (Princeton Instrument, Inc) and a CCD camera (Pixis, Roper Scientific) was used to measure the UV-Visible absorption spectra of some compounds studied in this work (Figure 2-1 and 2-2). In detail, the collimated output of a 30 W deuterium lamp passes through a 100 cm long

and 2.5 cm diameter Pyrex absorption cell equipped with quartz windows and focused onto the entrance slit of the spectrometer. The entrance slit is set to be 40 μm , providing a spectral resolution of 0.2 nm. The pressure in the absorption cell was measured with a 0–10 Torr capacitance manometer. The temperature is regulated by circulating heated-water or cooled ethanol through the cell jacket. Measurements were made over the wavelength region 220–400 nm by recording typically three overlapping regions of about 15 nm. Each measurement consisted of 8–13 scans of diode array. The wavelength scale was calibrated using the emission lines from low-pressure Hg (253.7, 313.2, and 365 nm) pen ray lamps. Absorption cross section, $\sigma(\lambda)$ (in $\text{cm}^2 \text{molecule}^{-1}$) is obtained using the Beer's law:

$$\sigma(\lambda) = \ln(-[I(\lambda)/I_0(\lambda)])/(C \times L)$$

where L is the path length of absorption cell (in cm), and C is the concentration of the considered compound in the gas phase (in molecule cm^{-3}). $I_0(\lambda)$ and $I(\lambda)$ are the light intensities in the absence and in the presence of the compound in the absorption cell, respectively.

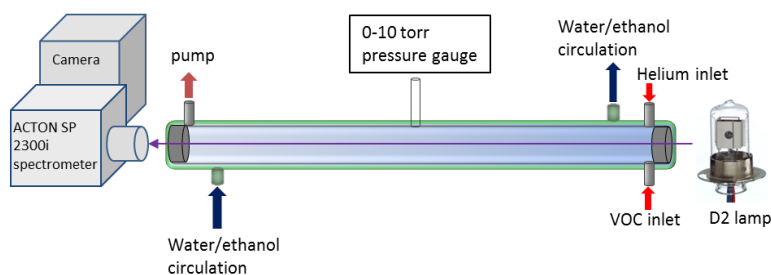


Figure 2-1: Schematic diagram of UV-Visible absorption equipment in ICARE, Orleans

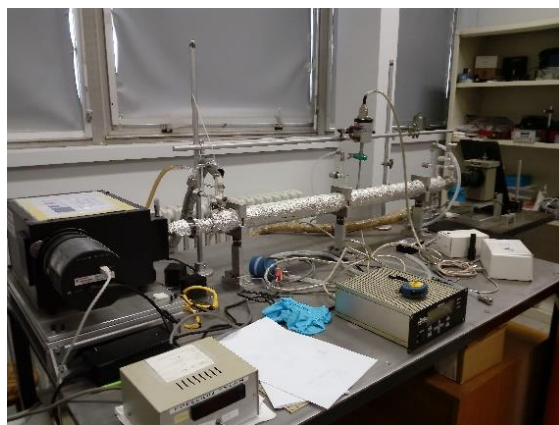


Figure 2-2: Picture of UV-Visible absorption equipment in ICARE, Orleans, France

2-2- Pulsed laser photolysis-laser induced fluorescence (PLP-LIF)

The pulsed laser photolysis–laser induced fluorescence (PLP-LIF) apparatus has been employed for OH radical kinetic studies, it is schematically shown in Figure 2-3. The OH radical precursor, H_2O_2 (70 wt. %), the investigated VOC, and the carrier gas, helium, are flowed vertically through the reaction cell mutually orthogonal to the photolysis and to the probe laser beams. The reaction cell is constructed of Pyrex and has an internal volume of about 200 cm^3 . The cell is jacketed, which allow water/ethanol circulate to regulate the temperature. The temperature in the cell is measured with a chromel-alumel thermocouple. By using the pulsed output of a KrF excimer laser ($2\text{--}15\text{ mJ cm}^{-2}$ in the cell), OH ($\text{X}^2\Pi$) radicals were generated by the photolysis of hydrogen peroxide (H_2O_2) at $\lambda=248\text{ nm}$. Detection of the concentration of OH radical at various reaction times ranging from ca. $10\text{ }\mu\text{s}$ to 10 ms was achieved by pulsed LIF using a delay time generator. A Nd:YAG-pumped frequency-doubled dye laser is triggered at a variable delay time after the photolysis pulse, which excites the (1,0) band of the OH ($\text{A}^2\Sigma\text{--X}^2\Pi$) system at $\lambda=282\text{ nm}$, and the fluorescence was detected by a photomultiplier tube, PMT, spectrally isolated with a 309 nm narrow band-pass filter. Both the photolysis and the probe lasers operate at a repetition rate of 10 Hz . The intersection of the lasers in the center of the cell defines the observation volume.

For the OH kinetics studies, the output pulse from the PMT was integrated for a preset period by a gated charge integrator. Typically, the averaged fluorescence signals from 100 probe laser shots for each delay time versus 10-15 different delay times to generate OH concentration-time profiles. In kinetic runs, typically 8 to 15 delays are sampled to map out an OH profile over at least three lifetimes. In addition, the ketone/ H_2O_2 mixtures in helium diluent were carried out under slow flow conditions, so that each photolysis/probe sequence integrated a fresh mixture and avoid the accumulation of reaction products in the cell. Furthermore, H_2O_2 is concentrated by bubbling helium through the solution for several days prior to use, to remove water.

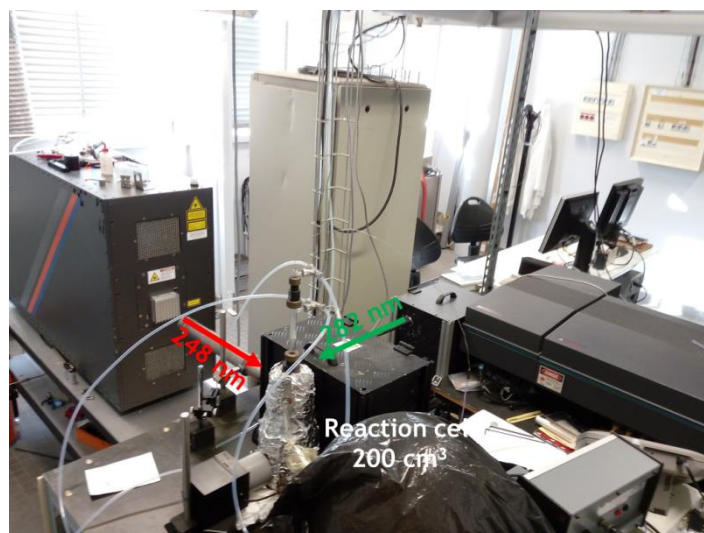
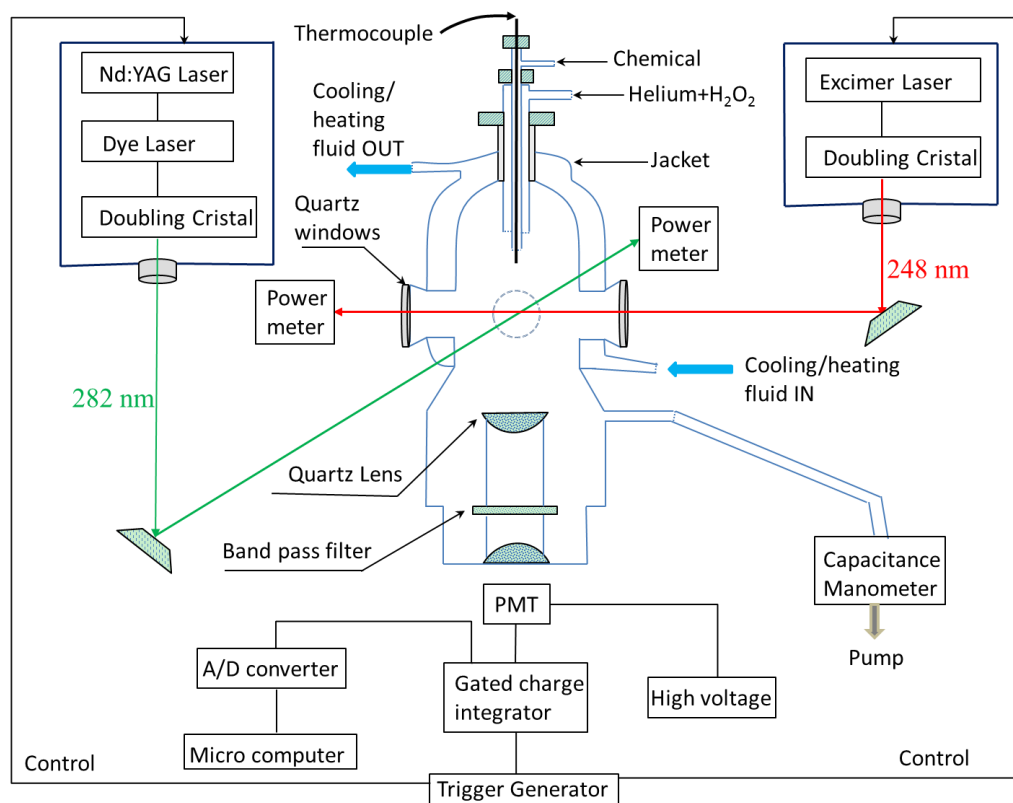


Figure 2-3: Schematic diagram and picture of the Pulsed laser photolysis-laser induced fluorescence (PLP-LIF) experimental set up

2-3- Atmospheric simulation chambers

Four different simulation chambers have been used in this work to investigate the photolysis, to measure the reactions rate constants and the products under different experimental conditions. The choice of the chamber used depends on the type of the experiment and the compound to investigate.

2-3-1- Small indoor simulation chamber - 200 L

2-3-1-1- Introduction

A 200 L FEP Teflon chamber (Indoor chamber, Figures 2-4 and 2-5) is suspended in a wooden protective housing with internal faces covered by aluminum foil and surrounded by six germicide lamps (Sylvania G30W) with irradiation wavelength at 254 nm and six black lamps (Philips, TL 20W/05) with irradiation wavelength at 365 nm. The aluminum foil can ensure that the light intensity is distributed evenly all over the chamber. For safety, the lamps can be turn on only when the protective housing was closed. The temperature was measured using a thermocouple sensor (Quick191AD) placed inside the housing. All experiments were performed in pure air (<2% relative humidity). Pure air was used to clean the chamber by purging it and filling and pumping.

Gaseous compounds were introduced into the chamber by streaming of pure air through a calibrated bulb (580 ml), e.g. chlorine (Cl_2) was used as the Cl atom source, vapor of studied ketones and reference compounds. Liquid compounds can be either injected with a known volume into a stream of pure air flowing directly into the chamber, e.g. hydrogen peroxide (H_2O_2) was used as OH radical source. Or liquid compounds were vaporized into a calibrated bulb (580 ml) with a known pressure, and introduced shortly after by flushing with pure air.

Gas phase chemical composition can be monitored at any time over the course of the experiment using the analytical equipment connected to the chamber: Gas Chromatography coupled to a Flame Ionization Detector (GC-FID, CP-3800, Varian) or FTIR, which will be described in the next section.

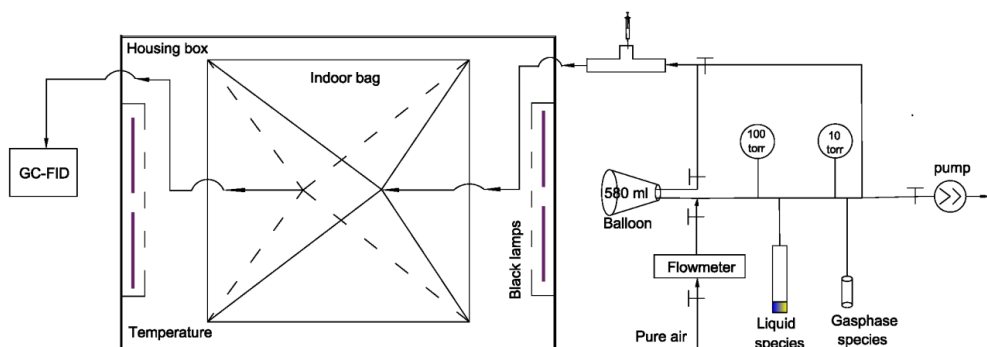


Figure 2-4: Schematic diagram of the 200 L indoor simulation chamber set up

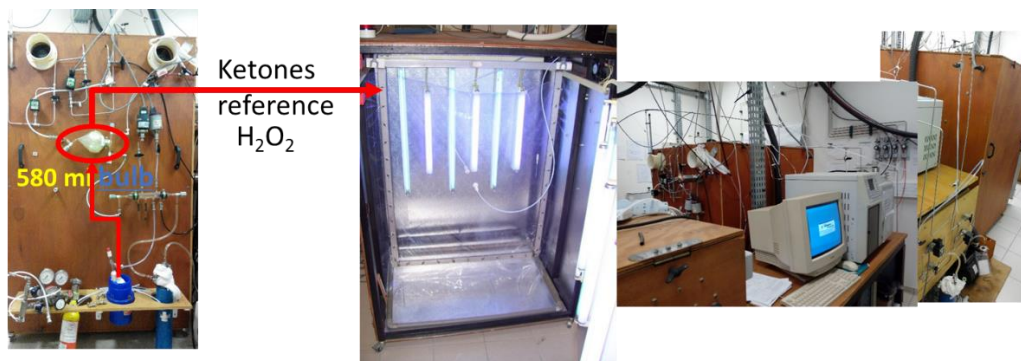


Figure 2-5: The 200 L indoor simulation chamber coupled with GC-FID

2-3-1-2- Gas chromatography-flame ionization detector

GC-FID is sensitive to a wide range of compounds but primarily to hydrocarbons. GC is a chemical analysis instrument for separating chemical compounds in a complex sample using a carrier gas flow with different rates depending on their various chemical and physical properties and their interaction with the column filling, called the stationary phase. As shown in Figure 2-6, the injector is a heated glass cylinder which serves to the introduction of the sample into the system. Temperature is fixed so that all components in the sample stay as vapor. Furthermore, GC column is the heart of the system. Column properties influencing the separation of a mixture are composition and thickness of the stationary phase, the diameter and the length of the column. In addition, an oven is used for optimizing the separation, using temperature to change interactions between column and analytes and best separations are usually observed for temperature gradients. As the analytes exit the end of the column in sequence, they are detected and identified electronically by dedicated detector. An FID typically uses a hydrogen/air flame into which carbon chained compounds are burned and produces cations and electrons. The ions are collected and produce an electrical signal which is then detected and computerized as “chromatograms”. As common with other GC techniques, a carrier gas, such as helium or nitrogen, is required with low water, hydrocarbons and O_2 impurities since they can interact with the stationary phase and cause high baseline noise.

In this work, GC-FID (CP-3800, Varian) coupled with 200 L simulation chamber is shown in Figure 2-5. The home-made auto sampling system is combined with a six-port switching valve. Upon switching, the contents in the sample loop are inserted into the carrier gas stream. DB-1 capillary column (J&W Scientific, 30 m, 0.32 mm, 5

μm film thickness) was used to perform the chromatographic separation. The column is located in an oven, where the temperature is precisely controlled electronically by the software.

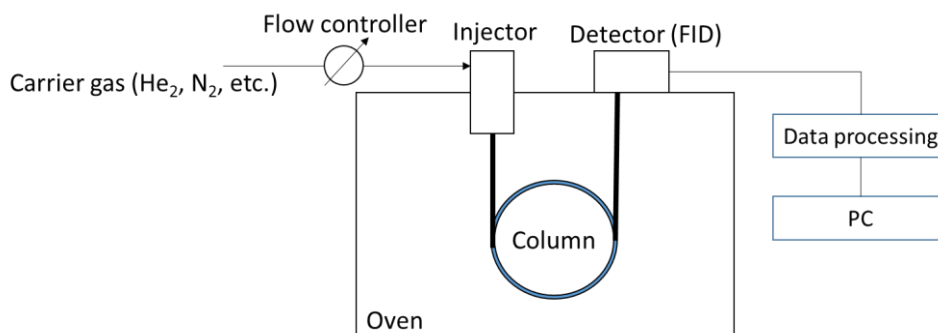


Figure 2-6: Overview over the components of a GC system

2-3-2- Moveable simulation chamber - 3.4 m³

2-3-2-1- Introduction

This cubic chamber is made of ethylene tetrafluoroethylene (ETFE) foil and has 3.4 m³ in volume (Figure 2-7 and 2-8). The transmission of the solar radiation is about 94-97% of total light for 380-780 nm wavelength range and 83-88% between 320 and 380 nm. During the photolysis experiments, the light intensity was continuously measured using a filter radiometer measuring the photolysis frequency of NO₂, J_{NO_2} (Meteorologie consult GmbH, Germany). The temperature and the relative humidity were continuously measured using a combined probe (Vaisala HMT330 series transmitters). A fan made of Teflon was also mounted into the chamber in order to ensure rapid mixing of reactants. The chamber was continuously filled with dry purified air flow ($\approx 1.2 \text{ L min}^{-1}$), in order to compensate leaks and sampling flows, leading to a constant and slight inner overpressure. Therefore, in order to estimate the dilution rate into the chamber, SF₆ was added to the gas mixture in all experiments. The liquid was introduced with purified air using a syringe. The concentration in the chamber was obtained by considering the volume of the liquid introduced, the pressure and the temperature, based on the ideal gas law.

The whole 3.4 m³ chamber is mounted to a support with four wheels and easy to move in or out of the laboratory. During dark experiments, the chamber is covered by a black and opaque rubber in order to protect the chamber from sunlight radiation. For

light experiment, the protection is easily removed leading to an immediate irradiation, starting the photolysis reaction.

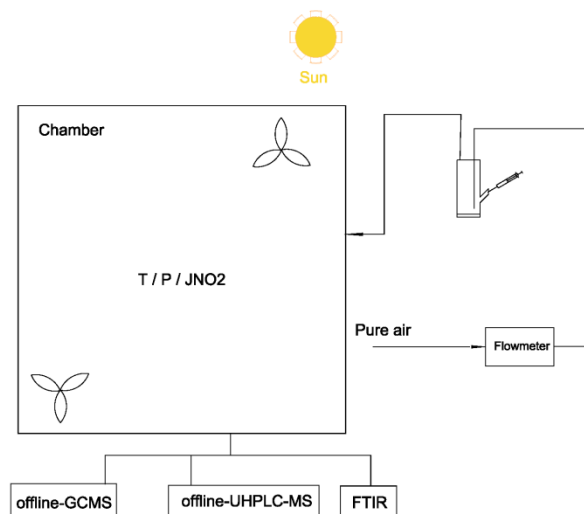


Figure 2-7: Schematic diagram of the 3.4 m³ moveable simulation chamber setup



Figure 2-8: The 3.4 m³ moveable simulation chamber in ICARE, Orleans, France

2-3-2-2- Fourier transform infrared spectroscopy 3 (FTIR3)

The infrared (IR) spectroscopy measures the infrared light that is absorbed by a substance, this absorption excites molecular vibrations and rotations (vibration theory), which have frequencies that are the same as those within the IR range of the electromagnetic spectrum. The IR can only be absorbed by a molecule if the dipole moment of the specific group of atoms changes during the vibration. The greater the change in dipole moment, the stronger the corresponding IR absorption band will be. In addition, the IR can be separated into mid-infrared (MIR), near-infrared (NIR) and far-infrared (FIR) as displayed in Figure 2-9. Fundamental vibrations are typically excited in MIR & overtone and combination vibrations are excited in NIR &

backbone vibrations of large molecules, as well as fundamental vibrations of molecules that include heavy atoms are excited. Today, almost every IR spectrometer used in MIR spectroscopy is of the Fourier transform type (FTIR).

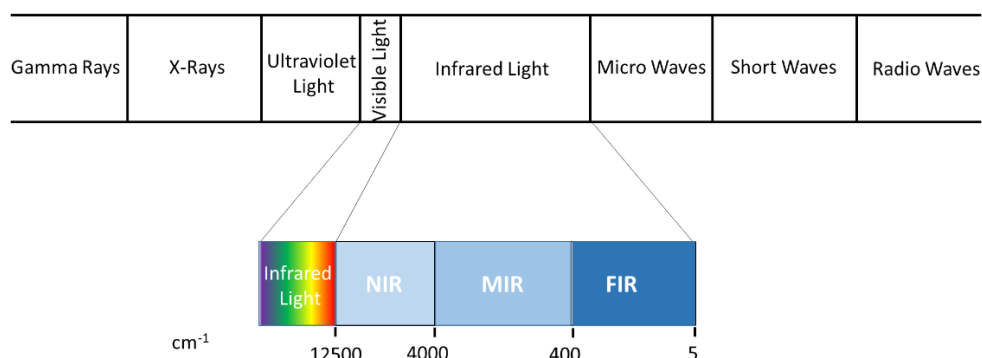


Figure 2-9: The electromagnetic spectrum of light

In typical FTIR systems, as shown in Figure 2-10, the IR light emitted from a source (e.g. SiC Globar) is directed into an interferometer, which modulates the light. The light passes through the same compartment (and also the sample) after the interferometer and then focused onto the detector. The signal measured by the detector is called the interferogram, which is the continuous sum, e.g. integral, of all the interference patterns produced by each wavelength. Then, data acquisition results in a digitized interferogram, which is converted into a spectrum by means of the mathematically called a Fourier Transform (FT).

For the experiments conducted using the 3400 L simulation chamber, chemical analysis of the gas mixture was characterized by an infrared spectrometer (Nicolet 550 Magna FTIR spectrometer, Figure 2-11) coupled to a White-type multi-pass mirror cell (2 L and optical path length 10 meters). IR spectra were recorded every 5 minutes by co-adding 130 interferograms at a resolution of 1 cm^{-1} and data treatment performed using the OMNIC software.

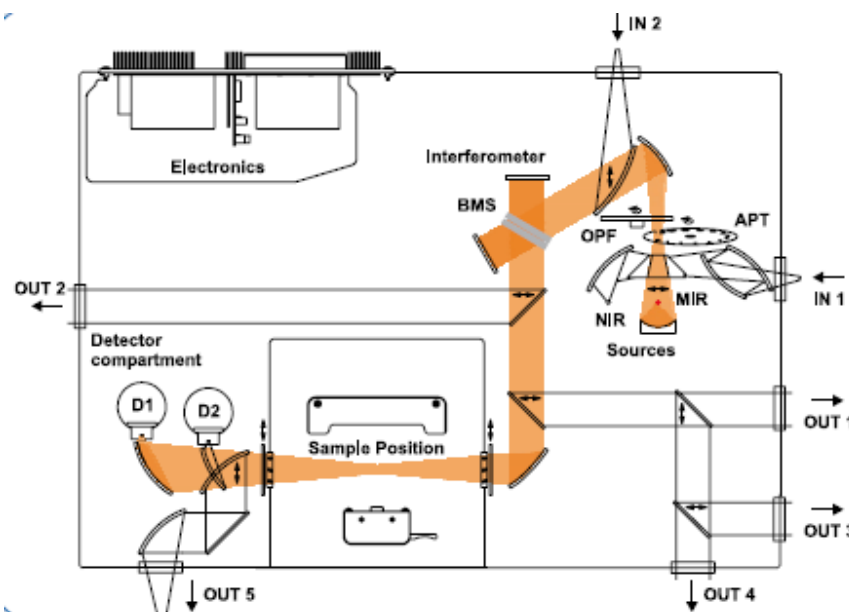


Figure 2-10: General FT-IR spectrometer layout



Figure 2-11: Nicolet 550 Magna FTIR3 spectrometer in ICARE, Orleans, France

2-3-3- Large indoor simulation chamber (CSA)-7.3 m³

2-3-3-1- Introduction

The cubic 7.3 m³ indoor simulation chamber (CSA, Figure 2-12 and 2-13) is made by Teflon foil and operated under the condition of room temperature and 760 Torr of purified air (<2% relative humidity). It is surrounded by protection panels with two roll-up doors, which makes it easier to perform the maintenance and dark reaction as shown in Figure 2-13. The chamber is equipped with 14 germicidal lamps (UV-A

T-40 L, 40W, Viber Lourmat) operating at 254 nm and 24 black lamps (UV-A T-40 L, Viber Lourmat) at 365 nm and 12 daylight lamps within the wavelength >300 nm (ORSAM ULTRA-VITALUX). Two fans made of Teflon were installed in the chamber and ensure the rapid mixing of reactants during the experiments. To introduce the liquid compounds (e.g. H_2O_2), a known volume of reactant is introduced into a homemade glass tube (gently heated when necessary) and further driven into the chamber with a stream of purified air, and the concentration is calculated by the ideal gas law. For the introduction of gaseous compounds (e.g. vapor of VOCs and other gas-phase compounds, e.g. NO , NO_2), certain quantity of gases is firstly introduced into a calibrated cylinder (0.9 L) connected to two pressure sensors (0–10 Torr and 0–100 Torr, MKS Baratron), then further driven into the chamber with a stream of purified air, and the concentration will be estimated by the ideal gas law. Temperature and relative humidity values were recorded by a combined sensor. In order to compensate sampling flows and leaks, a flow of purified air was added continuously during all experiments maintaining a slight inner overpressure, avoiding any contamination from outside air. SF_6 is introduced and used to determine the dilution of the gas volume in the chamber. After each experiment, the chamber is flushed with purified air (flow of around 250 L min^{-1}) in order to purge the remaining chemicals from the system.

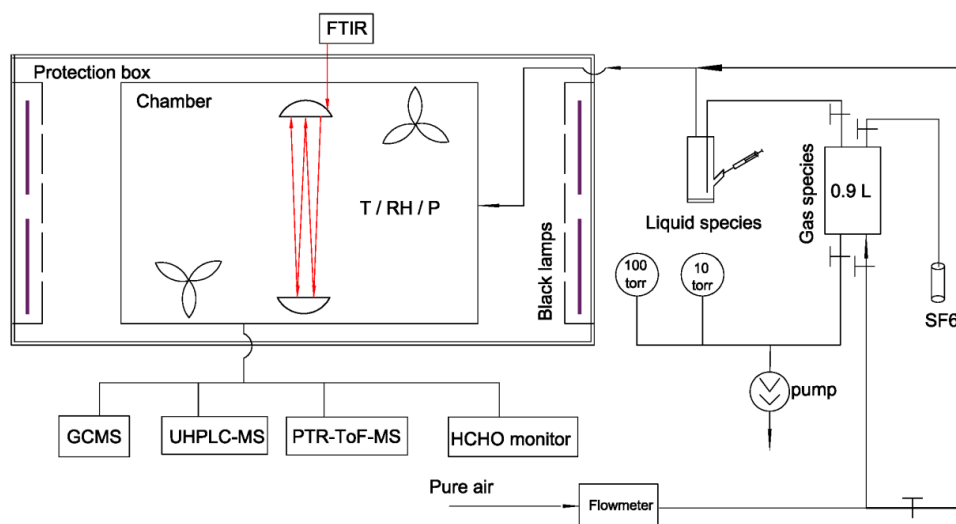


Figure 2-12: Schematic diagram of the 7.3 m^3 simulation chamber facility



Figure 2-13: 7.3 m³ indoor simulation chamber in ICARE, Orleans, France

2-3-3-2- Fourier transform infrared spectroscopy 2 (FTIR2)

The general principle of FTIR technique has been described in the previous section (Section 2-3-2-2-), only a brief description is presented here for FTIR2. Since the FTIR2 is an in-situ equipment coupled to the 7.3 m³ indoor simulation chamber, as shown in Figure 2-14, two symmetric transfer systems guide the collimated IR beam from the spectrometer to the White system and back to the spectrometer. In the chamber, the long-path absorption system is a White mirror arrangement. Due to its high reflectivity in the IR range, the mirrors are gold coated, and the adjustment screws allow an easy change of pathway length. In this work, the FTIR operates in the mid-IR region (4000-650 cm⁻¹) and with optical paths 148 m, the spectra were recorded by co-adding 130 interferograms within 5 min at a resolution of 1 cm⁻¹. Quantitative analysis of IR spectra was performed using OMNIC software.

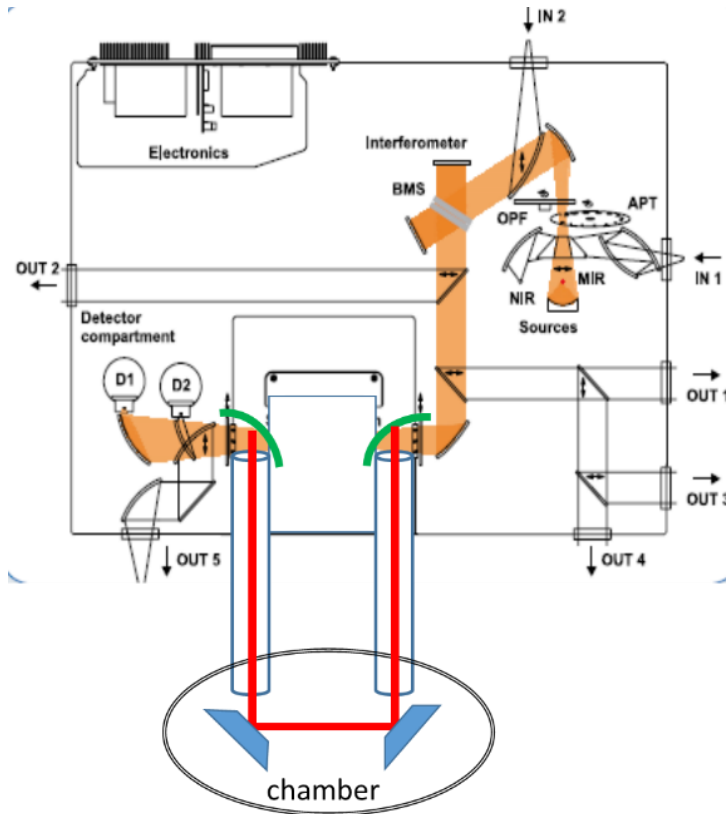


Figure 2-14: The in-situ FT-IR spectrometer layout coupled to 7.3 m³ simulation chamber

2-3-3-3- Scanning Mobility Particle Sizers (SMPS)

SMPS is an analytical instrument that combines an Electrostatic Classifier with either Long or Nano Differential Mobility Analyzer (DMA) and a Condensation Particle Counter (CPC), which can measure the size and number concentration of aerosol particles with diameter from 2.5 nm to 1000 nm. In principal, the polydisperse, submicrometer aerosol first enters an impactor, which removes particles above a known particle size by inertial impaction. Then, the polydisperse aerosols pass through a Kr-85 bipolar charger (or neutralizer), establishing a bipolar equilibrium charge level on the particles. The particles then enter the DMA and are separated according to their electrical mobility. The DMA contains two cylindrical electrodes made of polished stainless steel. The inner cylinder, the collector rod, is maintained at a controlled negative voltage, while the outer cylinder is electrically grounded. This creates an electric field between these two cylinders. As shown in Figure 2-15, since polydisperse aerosol and sheath air are introduced at the top of the Classifier and flow down the annular space between the cylinders, the electric field causes positive

particles (outer space between two cylinders) to be attracted through the sheath air to the negative collector rod. Depending on the electrical mobility, the classifier flow rate and the classifier geometry, the location of precipitated particles spread along the length of the collector rod. However, only particles within a narrow range of electrical mobility exit with monodisperse air flow through a small slit located at the bottom of the collector rod. They are then transferred to a particle sensor to determine their concentration.

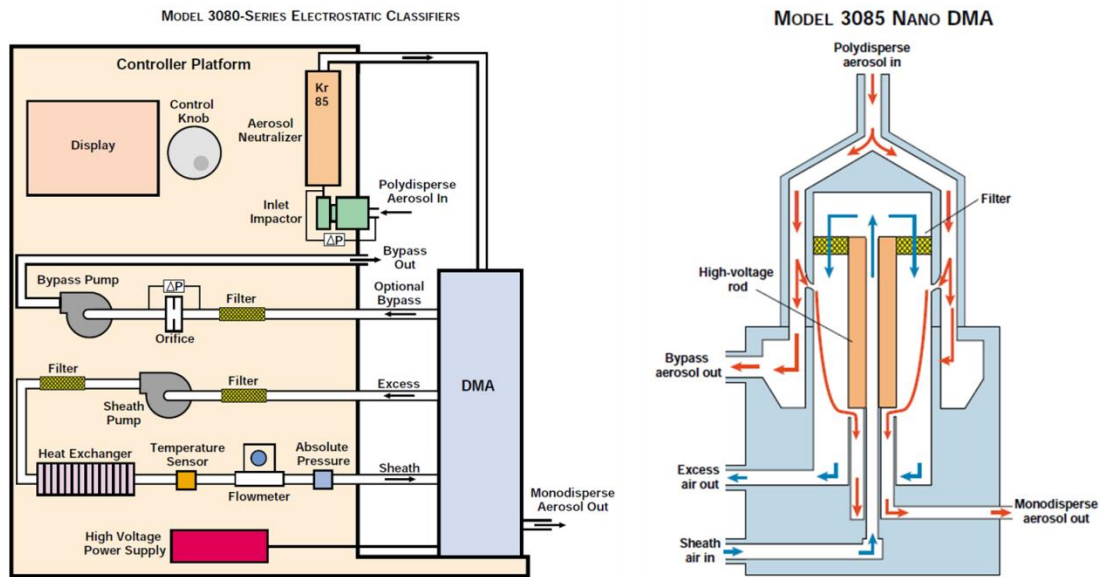


Figure 2-15: Flow schematic for the Electrostatic Classifier with Long DMA (TSI Inc.)

Monodisperse, submicrometer aerosol from Electrostatic Classifier then go through a Condensation Particle Counter (CPC) to measure the number concentration. As shown in Figure 2-16 (Mode 3788 CPC), in principal, the aerosol enters the saturator section (35 °C) and passes through a liquid-soaked wick, and the liquid evaporates and saturates the aerosol stream with vapor. The vapor-saturated aerosol then passes through a vertical, cooled vertical condenser tube (10 °C). Wherein the cooled, supersaturated vapor begins to condense on the particle nuclei to form larger droplets. The droplets then enter into the optical detector through a nozzle. In the optical detector, the combination of a laser diode, collimating lens and cylindrical lens form a horizontal ribbon of laser light above the aerosol exit nozzle measuring 10 μm by 2 mm. The collecting lenses then collect the light scattered by the droplets at 90 ° side-scatter and focus this light onto a low-noise photodiode. An analog-to-digital (A/D) converter is connected to a microprocessor and measures photodetector

voltages, which are then converted into electrical pulses.

In this work, the Mode 3080 Electrostatic Classifier, Mode 3081 Long DMA (or Mode 3085 Nano DMA) and Mode 3022 CPC (or Mode 3788 CPC) were combined and used to measure the particle concentration for diameter 2.5 nm to 500 nm. In addition, the liquid used in the saturator section are butanol and water for Mode 3022 CPC and Mode 3788 CPC, respectively. Compared to butanol, water is both more eco-friendly and easier to handle. Using water as a working fluid eliminates the potential for problems measuring high-humidity samples, which can occur in alcohol setups.

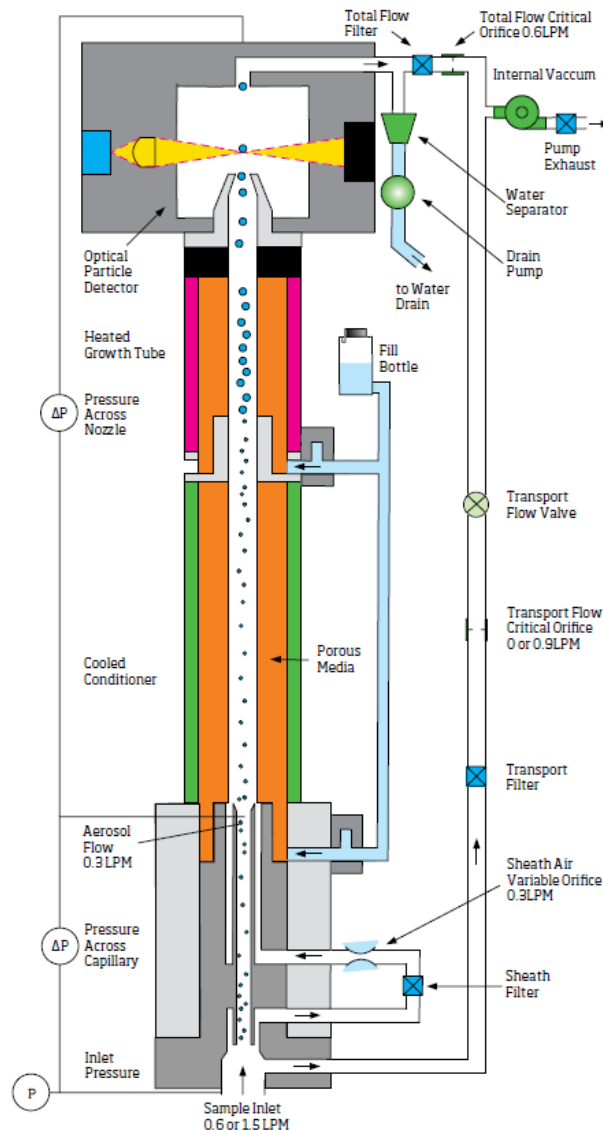


Figure 2-16: Flow schematic for the Mode 3788 CPC (TSI Inc.)

2-3-4- Large outdoor simulation chamber-90 m³ (HELIOS)

2-3-4-1- Introduction

(i) Body of Chamber

The HELIOS chamber is 90 m³ in volume, with a surface-to-volume ratio of 1.2 m⁻¹. Combined with a series of instruments, the main purpose of HELIOS is to determine how comparable the photochemical reactions are under artificial light and natural sunlight (Figure 2-17). For this purpose, HELIOS has been installed on the roof of ICARE (CNRS, Orléans, France, Figure 2-18). In the shape of a truncated hemisphere, the reactor is made of a fluorine-ethene-propene (FEP) foil, with a thickness of 250 µm (Vector Foiltec, GmBh, Bremen, Germany), transmitting 88% to 95% of the light in the entire solar spectrum. It is composed of 28 welded segments of the foil, suspended from a central point inside a frame of three half-arches. The reactor is inflated around a skeleton made with 12 epoxy parts. Reinforcing the chamber from the inside, the epoxy structure acts as a protection, since it can resist winds up to 25 km/h. Teflon tubes cover the skeleton to prevent friction between the reactor and the epoxy structure. At its top, the skeleton is fixed to a valve where the gases are blown out when the chamber is flushed.

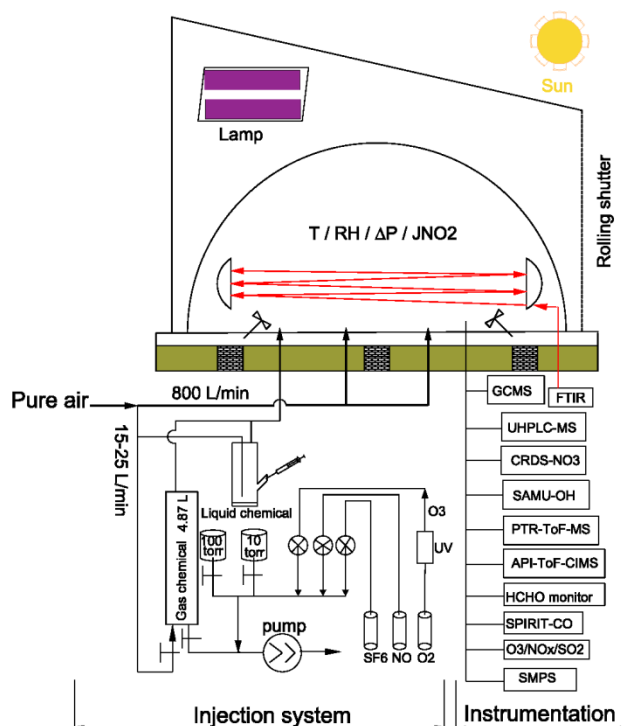


Figure 2-17: Schematic diagram of the HELIOS simulation chamber facility



Figure 2-18: Google earth screen shot of ICARE laboratory before installation of HELIOS (47°50'18.39N ; 1°56'40.03E)

(ii) Protection box of chamber

The chamber has been built in a structure supporting an 11 tons metallic box which can be moved along rails (Figure 2-19). Designed as the "Light Box", one of the main purposes of this movable protective housing is to protect the reactor from bad meteorological conditions, i.e. rain, snow and high winds. Xenon arc lamps will be installed inside the box, allowing the study of chemical reactions under artificial radiation. Finally, the Light Box allows maintenance operations on the chamber, up to its top, using a ladder and a bridge installed inside the box.

The protection box can be shifted in less than 2 minutes from one side of the roof to the other, thanks to two motors on rails. A silent block stops the vibrations, caused by the motion of the box, to be spread to the building. To prevent the vibration to be spread to the chamber, the ground of HELIOS has been raised by a few centimeters from the metallic assembly supporting the Light Box. The chamber is mounted on an anti-vibration structure, which is a superimposition of a special IPN structure, directly fixed on the building, of industrial grating and, on top, of wood conglomerate panels. The structure has been pierced in four different places, used to access the chamber from the laboratory located inside the building, beneath the reactor. The holes are plugged with movable INOX plates. Covered by a paper whose color is similar with the wood panel's, the plates are adapted to connect different instruments, located in the laboratory, to the chamber. A Teflon-FEP foil (500 μm thickness) covers the chamber floor, so the whole chamber has the same physicochemical properties.

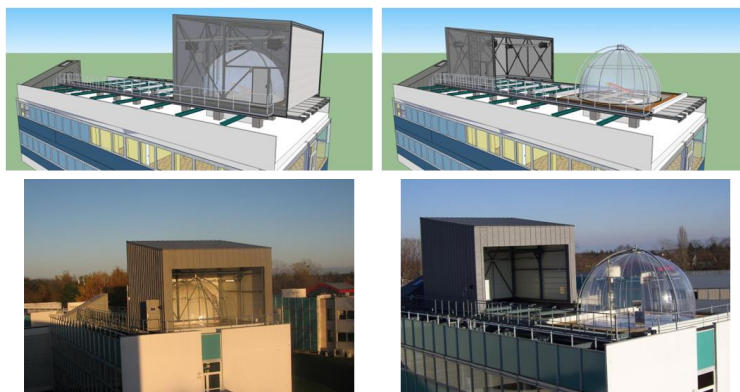


Figure 2-19: 3D view (top) and picture (bottom) of the roof of the building with the chamber when the Light Box is closed (left) and open (right)

(iii) Injection and mixing system

As shown in Figure 2-17, different methods are used to introduce compounds into the chamber, whether they are liquid, gaseous or solid. Liquid compound under ambient conditions are introduced into the chamber by placing a known volume in a glass-made bubbler using a syringe. Purified dry air is then blown through the bubbler, leading to the volatilization of the compounds and their transfer to the reactor. If needed, the bubbler is gently heated using a heat-gun to facilitate the volatilization of the compounds.

Gaseous compounds are introduced into HELIOS using a 4.87 L stainless steel cylinder: the cylinder is filled with a known pressure of the compounds and then flushed with pure dry air. To ensure a rapid mixing of the compounds, two fans are installed inside HELIOS. Opposite each other, their maximum rotation speed is 50 Hz (3,000 rpm). During the experiments, both fans were run at 20Hz giving an approximate mixing time less than 90s (calculated from SF₆, Figure 2-20). As a cleaning procedure, the chamber is flushed with purified dry air at a flow rate of 800 L min⁻¹, for an entire night prior to any experiment.

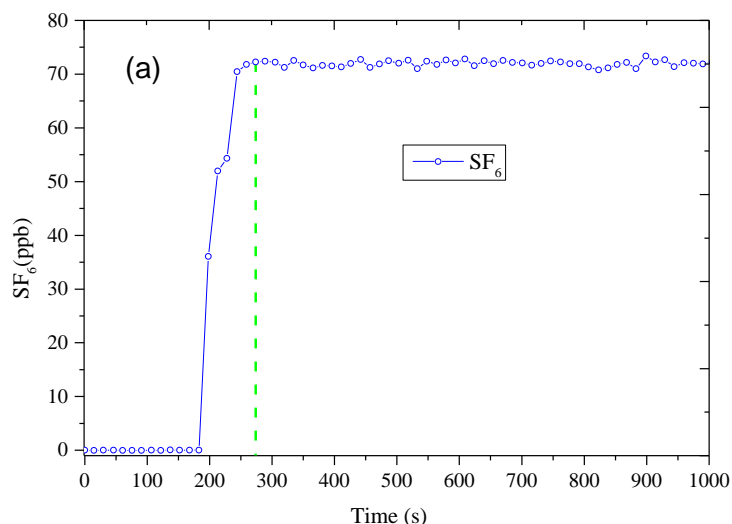


Figure 2-20: The mixing rate of compounds in the chamber (HELIOS), it was carried out in the dark chamber with SF_6 .

(iv) Air purification system

An air purification system has been installed to fill HELIOS with dry pure air. It is composed of an oil free compressor, an air dryer and an air purifier (Figure 2-21). Details of the equipment are given in Table 2-1. Briefly, approximately 390 m^3 of oil free air is obtained every hour from ambient air pressurization (at 10 bar) by the oil free compressor. The air is dried through a dryer (absorption without heat), with an air flow of $420 \text{ m}^3 \text{ h}^{-1}$. The air purifier eliminates all the contaminants: concentration of O_3 , SO_2 , H_2S , COS and NO_x is below 1 ppb; hydrocarbons, methane and carbon monoxide concentration reaches a maximum of 5 ppb in the dried air.

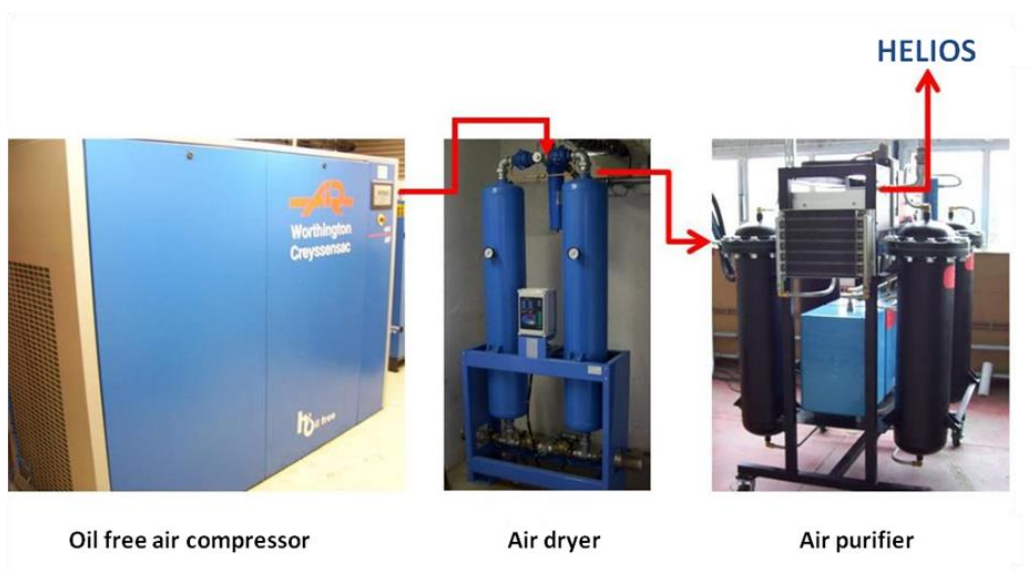


Figure 2-21: Air dryer and purifier system

Table 2-1: Technical characteristics of the elements composing the air purification system

Compressor	
Model with air cooling	Worthington Creyssensac WIS60 B
Service pressure	10 bar
Flow	389 m ³ h ⁻¹ (ISO 1217:1996)
Motor Power	45 kW /60 ch
Power supply	400 V triphased
Sound level	67 dB(A)
Installed Purged	Automatic BEKOMAT 32
Air drier	
Drier type	adsorption without heat
Flow	420 m ³ h ⁻¹
Inlet Flow	9.5 Bar
Temperature Air inlet	+40 °C
Dew point under pressure	-70 °C
Pressure losses	45 mbar
Half cycle time	5 minutes
Purification system	
Type	Aadco Aad 737-19C
Air flow	0 - 90 m ³ h ⁻¹
Pressure	0 - 7 bar
Air Purity level	< 1 ppb for Ozone, Methane, hydrocarbons, NO/NO _x , COS, SO ₂ , CO, CO ₂ , Fluorocarbons
Dew point	-51 °C or less
Oxygen concentration	20.8 % ±0.3% (constant)

(v) Loss of gas-phase species

The loss of gas-phase species contains dilution and wall loss. Dilution may occur due to the small leaks and high-volume sampling, which may vary with the number and type of instruments taking samples from the reactor. In each experiment, a low-reactive compound such as SF₆ was injected as a tracer for dilution. The SF₆ could be monitored by FTIR. Chamber wall effects include off-gassing reactive species like NO_x, chamber sourced radical like OH radical and species loss to the wall (Carter et al., 1982). They may have important impact on gas-phase reactivity and SOA formation.

In the HELIOS chamber, the loss rates (dilution + wall loss) of a series of species including isoprene, methacrolein (MACR), methyl vinyl ketone (MVK), cyclohexane, 2-methyl-3-pentanone, perfluoro-2-methyl-3-pentanone, cyclohexanone, formaldehyde and ozone were evaluated by injecting known concentrations of these species and

continuously monitoring their decay in the dark. The wall loss rates were obtained by subtracting the dilution rate of SF₆ from their loss rate as the following equation: $k_{\text{wall_loss}} = k'_{\text{loss}} - k'_{\text{SF}_6}$, the loss rate was treated as the first-order process in the chamber. The loss rates of studied species are shown in Table 2-2.

Table 2-2: Summary of loss rates (dilution + wall loss) of gas species in HELIOS chamber.

[organic] (×10 ¹² molecule cm ⁻³)	Air (L/min)	flow	Technique	k' _{loss} (×10 ⁻⁶ s ⁻¹)	k' _{SF₆} (×10 ⁻⁶ s ⁻¹)	k _{wall} (×10 ⁻⁶ s ⁻¹) _{loss}
Isoprene						
8.6	15		FTIR	7.2	6.5	0.8
8.9	15		FTIR	4.7	4.0	0.7
5.7	20		FTIR	5.8	5.0	0.7
4.1	25		FTIR	7.7	6.5	1.2
2.4	25		FTIR	9.2	8.1	1.1
6.7	15		PTR-ToF-MS	4.7	NA	NA
2.6	17		PTR-ToF-MS	5.0	NA	NA
Average						0.9±0.2
MACR						
0.6	25		PTR-ToF-MS	6.7	5.9	0.8
1.2	25		PTR-ToF-MS	7.1	6.0	1.1
1.3	25		PTR-ToF-MS	7.2	6.2	1.0
11.7	15		FTIR	6.6	4.7	1.9
0.6	25		GCMS	7.5	5.9	1.6
0.7	25		GCMS	9.1	6.8	2.3
1.3	25		GCMS	7.5	6.2	1.3
Average						1.4±0.5
MVK						
0.8	25		PTR-ToF-MS	6.0	5.0	1.0
4.9	25		PTR-ToF-MS	8.2	6.3	1.8
12.1	15		FTIR	5.8	4.4	1.4
10.7	25		FTIR	5.9	4.6	1.3
12.1	15		FTIR	6.0	4.3	1.7
2.5	17		GCMS	8.2	7.4	0.9
Average						1.4±0.4
cyclohexane						
165.6	17		FTIR	7.6	7.2	0.4
87.1	17		FTIR	7.4	6.7	0.8
94.2	20		FTIR	5.1	5.1	0.1
127.9	20		FTIR	6.5	5.7	0.8
223.8	25		FTIR	7.7	6.7	1.0
517.6	25		FTIR	8.7	7.7	1.0
121	17		FTIR	6.4	6.3	0.7
271.4	25		FTIR	9.8	8.7	1.1
304.3	25		FTIR	8.4	7.7	0.7
121	17		GCMS	7.0	6.3	0.7
Average						0.7±0.4
cyclohexanone (next page)						

0.9	25	PTR-ToF-MS	6.5		
1.3	17	FTIR	5.8	5.0	0.8
HCHO					
0.7	17	Aerolaser	5.2	5.1	0.1
2M3P					
33.2	15	FTIR	6.7	6.7	≈0
33.5	15	FTIR	5.2	5.5	≈0
34.3	15	FTIR	5.5	5.1	0.4
32.5	15	FTIR	5.3	5.4	≈0
33.8	15	FTIR	6.9	6.2	0.8
47.3	15	FTIR	6.5	6.7	≈0
Average					≈0.1
PF-2M3P					
36.4	15	FTIR	5.2	6.0	≈0
36.4	15	FTIR	5.6	4.9	0.7
7.5	15	FTIR	6.5	5.9	0.6
45.3	15	FTIR	6.5	5.9	0.6
Average					0.5±0.3
ozone					
25.3	15	Monitor	4.8	4.7	0.1
12.6	15	Monitor	4.9	5.2	≈0
20.3	25	Monitor	6.5	6.5	≈0
12.6	17	Monitor	5.5	5.8	≈0
39.5	15	FTIR	7.0	NA	NA
39.5	15	Monitor	6.4	NA	NA
15.5	15	FTIR	7.6	NA	NA
15.5	15	Monitor	7.3	NA	NA
Average					≈0

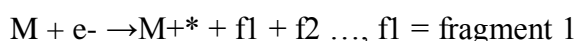
2-3-4-2- Fourier transform infrared spectroscopy 1 (FTIR1)

The technique of FTIR has been described in the previous Section 2-3-2-2- and Section 2-3-3-2-, hence only a simple description of FTIR1 was given here. FTIR1 is a Bruker Vertex 70 equipment, it is designed for data acquisition in the mid IR region (4000-700 cm⁻¹). Two gold coated mirrors are installed in the chamber. The adjustment screws of the gold coated mirror allow an easy change of pathway length. In this work, the optical paths of FTIR1 is 302.6 m, the spectra were recorded by coadding 250 interferograms within 3 min at a resolution of 1 cm⁻¹. Quantitative analysis of IR spectra was performed in OPUS (Bruker software).

2-3-4-3- Automated Thermal Desorption-Gas chromatography/mass spectrometer (ATD-GC/MS)

Gas chromatography/mass spectrometry (GC/MS) is commonly employed for

the separation and identification of species, using electron impact (EI) or chemical ionization (CI), which has been a “Gold standard” (Weinmann et al., 1999). As discussed in the previous Section 2-3-1-2-, GC utilizes a capillary column and whose parameter depending on the column's dimensions (length, film thickness, and diameter) as well as the phase properties (e.g. 5% phenyl polysiloxane). The different chemical properties of molecules in a mixture and their relative affinity for the stationary phase of the column will promote separation of these molecules as the sample travels the length of the column. Furthermore, the molecules are retained by the column and then eluted from the column at different times (retention time), and this allows the MS to ionize the molecules with different methods. In the Electron Impact method (Figure 2-22), the molecules are bombarded with free electrons emitted from a filament, forming the M^{+*} ions, in unique reproducible way to form a collection of fragment ions, which is called "hard ionization" technique comparing to the CI method, as follow:



The molecular fragmentation pattern depend on the electron energy applied to the system, typically 70 eV, and will not vary if this energy remains constant. These fragments are then separated depending on their masses m/z , typically by accelerating them and orienting them with the help of an electric or magnetic field. In a Quadrupole mass analyzer (Figure 2-23), oscillating electrical fields is used to selectively stabilize or destabilize the created fragments passing through a radio frequency (RF) Quadrupole field created between 4 parallel rods. Only certain m/z range of fragments is passed through the system. Finally, the charged fragments are detected by a photomultiplier detector, and the signal produced in the detector will create a mass spectrum. By far, EI is the most common and perhaps standard form of ionization. Since CI will be discussed in the previous Section 2-4-3 we only describe the EI in this section.

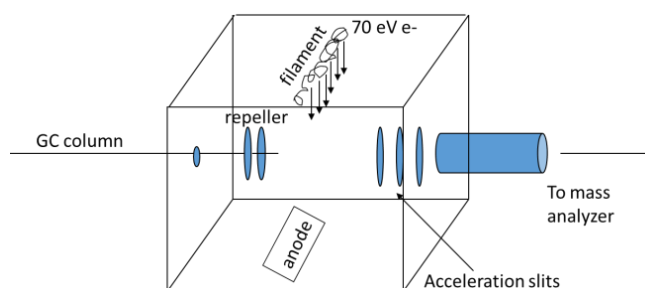
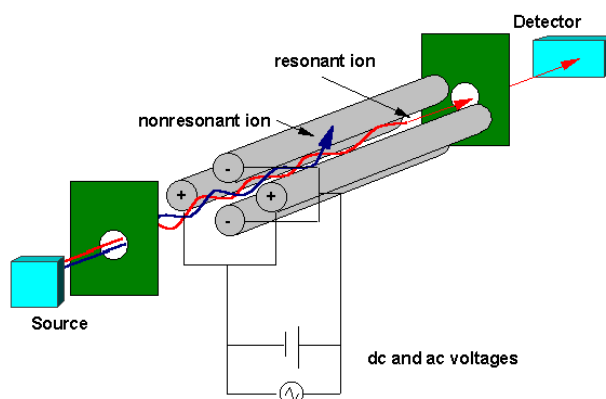
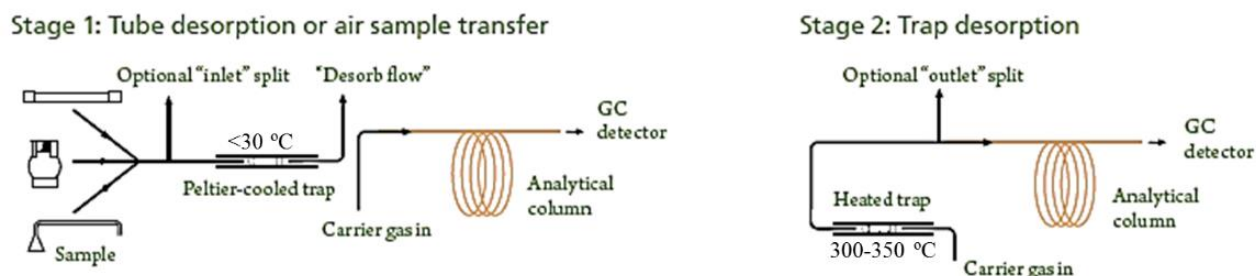


Figure 2-22: Schematic drawing of EI source**Figure 2-23:** Schematic drawing of Quadrupole mass analyzer

In this work, a GC/MS is attached to the HELIOS chamber, and combines a GC (Clarus 600C, Perkin Elmer) equipped with 60m Innowax PLOT column and Mass Spectrometer (Turbomass 600 MS, Perkin Elmer) with EI source and Quadrupole mass analyzer. In addition, a thermodesorber (TurboMatrix ATD150, Perkin Elmer) is used for online sampling or analyzing samples from Stainless Steel Airtoxics tubes. These tubes contain absorbent inside and can analyze C₂-C₁₆ volatile hydrocarbons. For superior resolution and sensitivity, PerkinElmer instruments feature a two-stage thermal desorption process that concentrates analytes before they are introduced into the GC. In detail, as shown in Figure 2-24, the samples desorbed from the tubes or from chamber (on-line sampling) are concentrated in a Peltier-cooled trap set at -30 °C. After the first desorption, this cold trap is flash-heated at a very high temperature (300-350 °C) and a carrier gas sends the analytes to the GC system for separation and detection.

**Figure 2-24:** Flow schematic of two-stage thermal desorption in TurboMatrix™ 150 ATD (PerkinElmer Inc.)

2-3-4-4- Proton transfer reaction-time of flight-mass spectrometer (PTR-ToF-MS)

PTR-ToF-MS is an instrument from Ionicon Analytik that is dedicated to VOCs analysis. We will here present the PTR-ToF-MS 8000 model, which is working with our HELIOS chamber. PTR-ToF-MS mainly contains four parts: ion source, PTR drift tube, Transfer Lens Systems and ToF-MS. Proton transfer reaction is one of soft CI chemical process, which is a technique used for creating ions of the interesting compound (analyte, M) by ion-molecule reactions from reagent ions that is generally present in a much greater abundance than the analyte and produced by electron ionization (EI) or radiation of the reagent gas (example in Figure 2-25). Compared with the traditional EI, the soft CI produces less fragmentation (or sometimes none), and usually give a simpler spectrum. The most common ion-molecule reactions in CI are proton transfer (which forms AH^+ or $[A-H]^+$ ions), charge or electron transfer (which forms A^{++} or A^{*-} ions), hydride transfer (which forms $[A-H]^+$ ions), and adduct formation or attachment (which forms $[A + R]^+$ or $[A + R]^-$ ions). CIMS is performed with both positively and negatively charged reactant ions. CI can be performed with any type of mass spectrometer, e.g. quadrupole, magnetic, ToF, Fourier transform ion cyclotron resonance (FTICR) and ion trap.

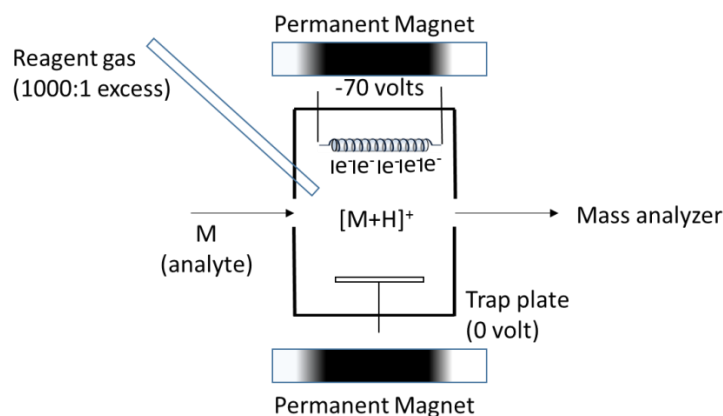
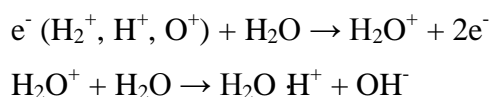


Figure 2-25: The simple diagram of ion-molecule reactions by chemical ionization

As shown in Figure 2-26, in sequence, H_3O^+ ions at high purity level (up to 98%) from water vapor is formed via a hollow cathode discharge, as:



Then, protonated water ($\text{H}_2\text{O H}^+$) is injected into the reaction chamber (PTR drift tube) via a Venturi-type inlet. The sample gas containing VOCs, which is continuously introduced, undergoes (mostly) non-dissociative proton transfer from $\text{H}_2\text{O H}^+$ during the collisions if the collision VOCs have a higher proton affinity, as:



Since O_2 , CO_2 , N_2 , Ar etc. have a lower proton affinity, $\text{H}_2\text{O H}^+$ ions do not react with any of these major components present in the clean air. Protonated VOCs are introduced into ToF-MS for mass analysis through a Transfer Lens System. The Transfer Lens System corrects the direction of VOCs H^+ into the ToF-MS.

ToF-MS is a mass spectrometry method in which the mass-to-charge ratio (m/z) is determined via a time and intensity measurement. Indeed, in an electric field (or magnetic field), the time for the ion to reach a detector at a known distance is measured. Because this time will depend on the velocity of the ion, and the velocity of the ion depends on the m/z , and therefore it is a measure of its m/z . In detail, as shown in Figure 2-26, the acceleration occurs in a region termed the ToF extractor, then ions travel to the opposite end of the flight chamber, where they enter a reflectron that reverses their trajectory and reflects them toward the detector (typically microchannel plate, MCP). Less energetic ions of the same m/z penetrate a shorter distance into the reflectron and, correspondingly, take a shorter path to the detector. Hence, the time elapsed between application of the impulse and collision with the detector is recorded. A point of simultaneous arrival of ions with same m/z but different energies is often referred as ToF focus. General signals include both intensity and time since the ion acceleration event are amplified and recorded by a computer. The continuous data array containing observed data signal intensities at all times of flight is called the ToF spectrum.

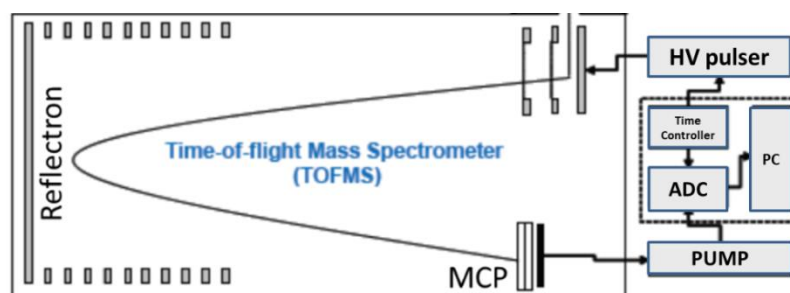


Figure 2-26: Schematic drawing of ToF-MS instrument (Aerodyne Research Inc.)

In PTR-ToF-MS, the ToF component gives the ability to analyze a whole mass spectrum in a split/second with a mass resolution of approximately 5000 $m/\Delta m$ (FWHM). Even isotopic species can therefore be distinguished with no instrumental mass range limitation. The mass spectrum obtained from the TofDAQ software can be either analyzed by a PTR-ToF data analyzer (designed by Markus Müller) or Tofwerk software (TOFWERK AG, Switzerland).

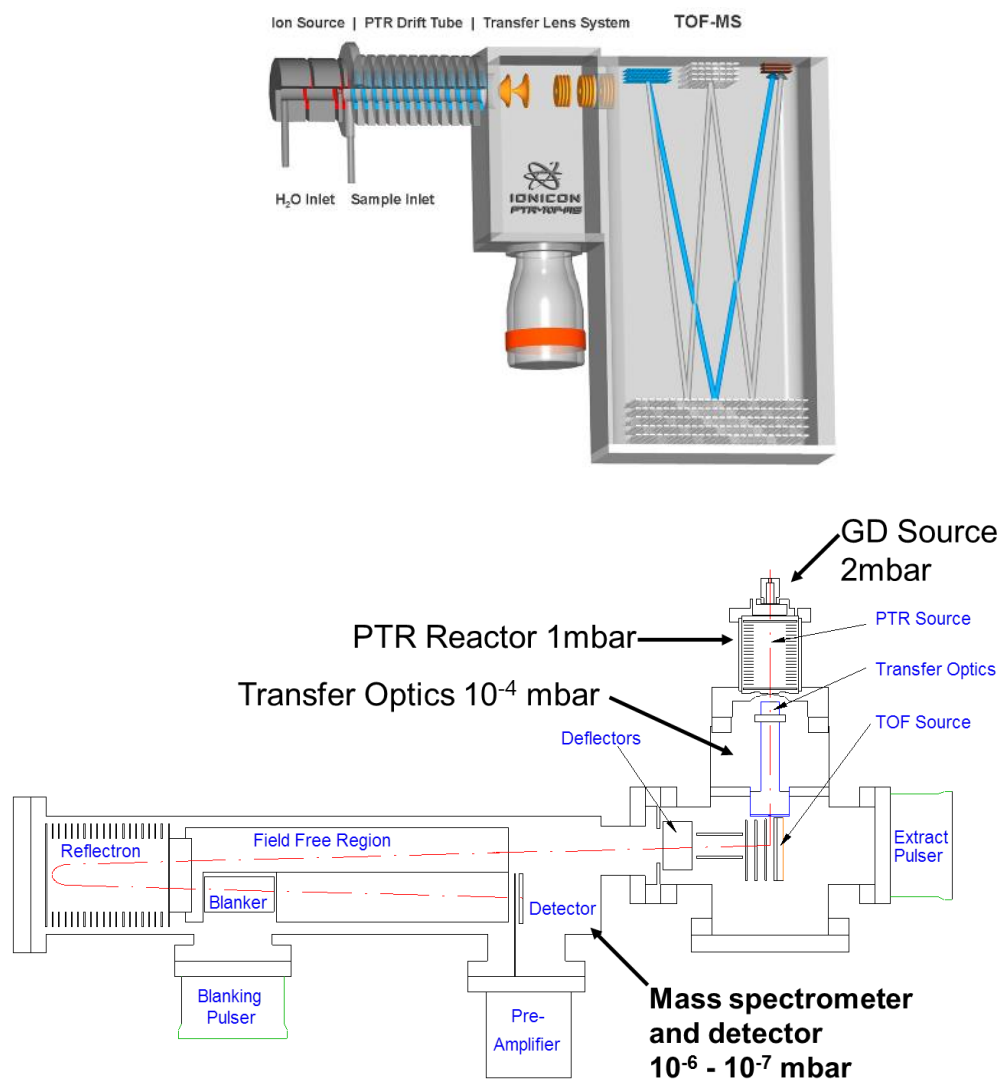


Figure 2-26: Schematic view of PTR-ToF-MS (Ionicon Analytik)

2-3-4-5- Ultra High Performance Liquid Chromatograph-Mass Spectrometry (UHPLC-MS)

In Helios, Ultra High Performance Liquid Chromatography (Nexera X2, Shimadzu) is used for fast separation performances compared to conventional HPLC. The system is also coupled with a Mass Spectrometer system (LCMS 2020,

Shimadzu). In the UHPLC system (Figure 2-27), acetonitrile and water are degassed and are sent to the mixer where the mobile phase is homogeneously mixed. Meanwhile, the auto-sampler automatically injects the samples into the flow lines. Then, the ultra-high pressure pumps bring the sample and mobile phase to the column. In the column, the components are separated by means of the mutual interactions of the mobile phase and the column packing. A column oven maintains the temperature of the column and flow lines at a constant temperature. Finally, the photodiode array continuously monitors the components eluted from the column by using of both a D2 (deuterium) lamp and W (tungsten) lamp as light sources and allow high sensitivity measurement of chromatograph and absorbance spectra over the entire wavelength range of 190-800 nm.

The LCMS-2020 is a Quadrupole mass spectrometer, which contains ionization sources (ESI or APCI), a Q-array, a skimmer, an Octapole and a Quadrupole system. For example, as shown in Figure 2-27, a sample separated by the UHPLC is sprayed and ionized by the atmospheric pressure ionization probe (e.g. electrospray ionization, ESI or atmospheric pressure chemical ionization, APCI probe, positive or negative mode). Indeed, as shown in Figure 2-28, the sample molecules are ionized by ion-molecular reactions (CI reactions) with the solvent ions. Nebulizer gas is used to spray the liquid in the same way as with ESI. Then the ionized sample is introduced into the first stage primary vacuum chamber through the sample introduction unit (DL), where it is efficiently focused at the tip of the skimmer by the Q-array. Passing through the skimmer, the multi-stage high frequency ion guides are arranged in the secondary vacuum chamber: Octapole. Subsequently, the ions are separated in accordance with their m/z by the Quadrupole mass filter with pre-rod, and the detection is performed by the electron multiplier with conversion dynode. Then the ion signals are amplified and then the analysis results processed by the LCMS data processing software are displayed.

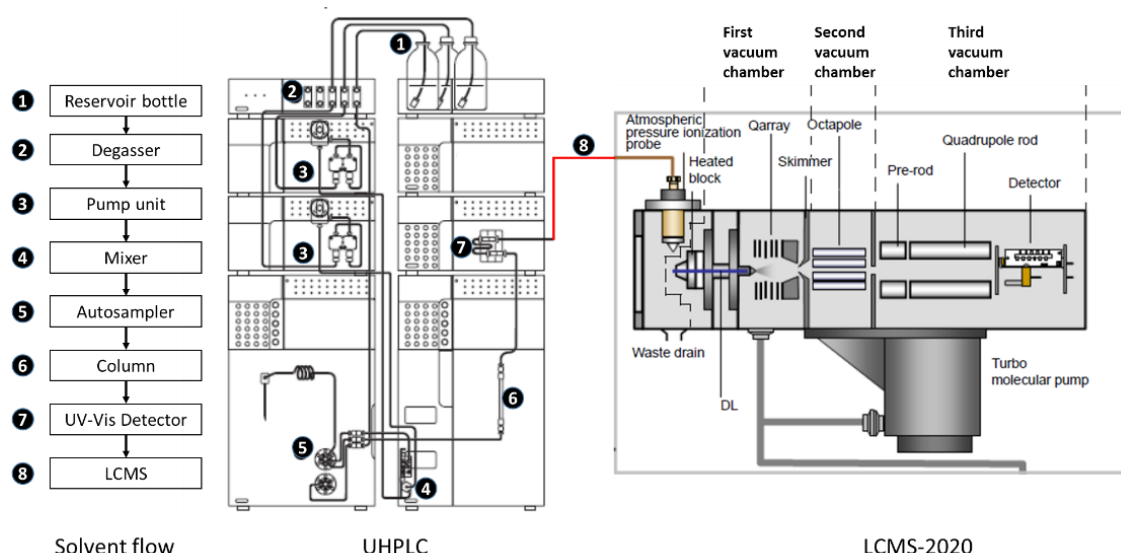


Figure 2-27: Configuration of the UHPLC-MS system (Shimadzu)

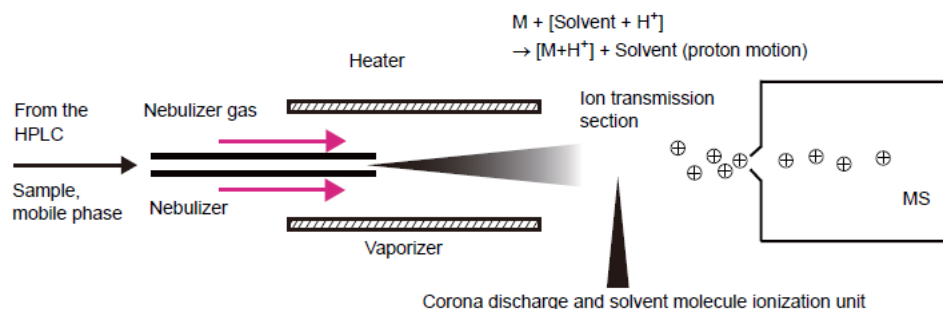
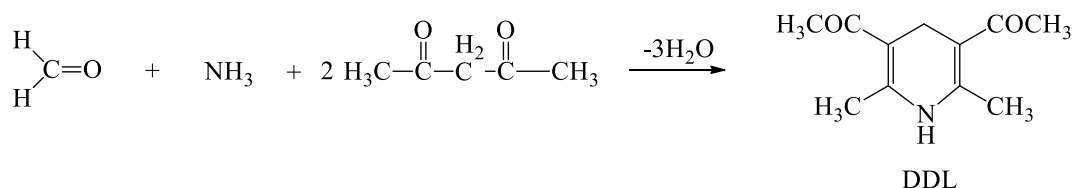


Figure 2-28: The simple diagram of ion-molecular reactions by atmospheric pressure chemical ionization (APCI, Shimadzu))

2-3-4-6- Formaldehyde (HCHO) analyzer

The AL4021 is a completely automated and continuously working formaldehyde (HCHO) analyzer for gaseous and liquid samples based on the Hantzsch reaction (acetyl acetone), as shown in Scheme 2-1, the liquid phase reaction of formaldehyde with acetyl-acetone (2,4-pentadione) and ammonia to produce 3,5-diacetyl-1,4-dihydrolutidine (DDL), which is absorbing light at 410 nm and shows a strong fluorescence around 510 nm. The complete chemical processing, including gas stripping, is integrated into the instrument. Since the Hantzsch reaction works in aqueous solution, gaseous formaldehyde needs to be trapped in aqueous solution first. As shown in Figure 2-29, the instrument samples ambient air with the help of an internal pump, and HCHO is dissolved into aqueous solution in a stripping coil where air and a stripping solution are brought into contact continuously at defined

flow rates and contact surfaces. The air and liquid streams are separated afterwards in a glass separator and the solution is then introduced into a heated reaction coil with a temperature of about 65 - 70 °C to initiate the Hantzsch reaction. After Hantzsch reaction and degassing, the solution flows into the fluorimeter cell, and the fluorescence light is measured by a photomultiplier. With this fluorimetric detection method, the instrument achieves an important selectivity, avoiding interferences of other chemical substances in the sample gas or liquid.



Scheme 2-1: mechanism of Hantzsch reaction

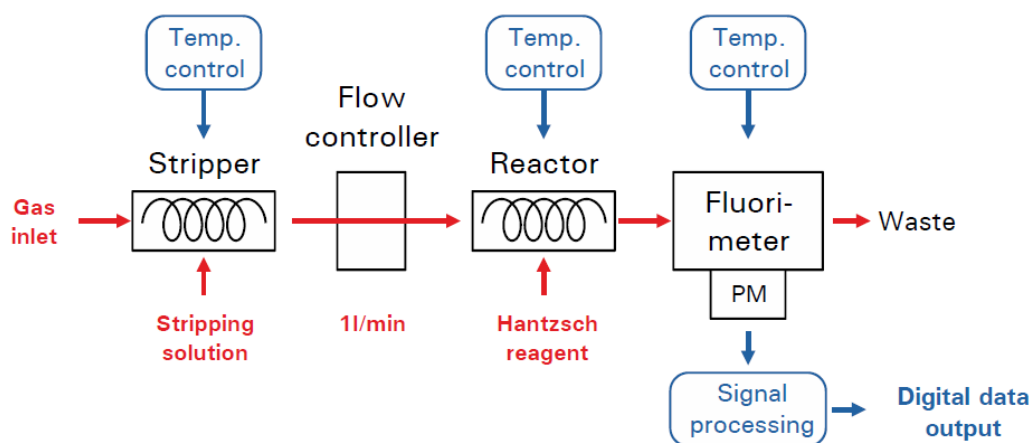


Figure 2-29: Simplified flow scheme of the AL4021 HCHO-analyzer (Aero-Laser GmbH)

2-3-4-7- Spectroradiometer

To perform the natural irradiation photolysis in HELIOS, the solar actinic flux (290-660 nm) and photolysis frequencies of H_2O_2 , HONO, HCHO, NO_3 , NO_2 and O1D were measured by a spectroradiometer (Meteorologie Consult GmbH 6007), which combines CCD-Detector-Spectrometer, optical receptor (2- π -actinic) and spectrometer via an optical fiber (Figure 2-30). This spectroradiometer is based on a monolithic monochromator, since it is made from ceramics/glass, which has

negligible sensitivity to temperature changes. This results in very stable wavelength settings. The spectrometer uses a 512 pixel CCD or diode array (PDA) detector with a spatial resolution of ca 0.85 nm (pixel distance) and an HWHF of ca. 2.4 nm. This spectrometer can determine O_3 photolysis rates with a time constant typically as low as 1 second, depending on the solar elevation. $J_{(\text{NO}_2)}$ is measured at frequencies up to > 5 Hz. The software supplied with the spectrometer records and stores spectral raw data as well as evaluates photolysis rates for e.g. $J_{(\text{O}^1\text{D})}$, $J_{(\text{HCHO})}$, $J_{(\text{NO}_2)}$, $J_{(\text{HONO})}$, $J_{(\text{NO}_3)}$... in real time.



Figure 2-30: Diode Array Spectrograph with actinic optics

2-4- Instrumentation Conclusion

In conclusion, atmospheric chambers enable the investigation under predetermined controlled conditions of complex atmospheric processes using a large range of instruments, the instrumentation and known detection limits and time resolutions of detectable stable and radical species are shown in Table 2-3. The activities enhance the application of the results obtained to the understanding of the real atmosphere. In addition, the researcher will utilize one appropriate simulation chamber depending on the aim of the experiment. Their use as test beds for field instruments as well as for inter-comparison of different measuring techniques has enhanced the importance of these instruments in the study of atmospheric chemistry. Furthermore, the discharge flow tube (like PLP-LIF) is one of other usual techniques for kinetic study, which allow for the performance of absolute method (two methods: absolute and relative exist for kinetic study) with high purity of studied compounds. Combining different simulation chambers and reactors and instruments, this resulted

in several breakthroughs in the knowledge of atmospheric trace species and aerosol chemistry.

Table 2-3: Instrumentation and known detection limits and time resolutions of detectable stable and radical species in this Thesis.

Instrument	Species detected	Detection limit	Time resolution
GCFID	VOCs	10-50 ppb	> 3 min
FTIR1	CO, O ₃ , SF ₆ , NO, NO ₂ , HNO ₃ ,	1 ppb	3 min
FTIR2	organic species (e.g.: hydrocarbons	5 ppb	5 min
FTIR3	and oxygenated compounds)	10 ppb	5 min
GCMS	SF ₆ , VOCs in gas-phase and aerosol (offline membrane sampling)	1 ppb	~20 min
API-ToF-CIMS	Aerosol (online), VOCs	4 ppt	few seconds for gas phase, 10 min for aerosol
PTR-ToF-MS	VOCs	10 ppt – 1000 ppb	few seconds
CRDS	NO ₃	0.1 ppt	few seconds
UHPLC-MS	carbonyl species (e.g. aldehyde, ketone etc.) in gas-phase and aerosol (offline membrane sampling)	1 ppb	~6 min
PLP-LIF	OH	10 ppt	microsecond
Aerolaser 4021	HCHO	100 ppt	90 s
SMPS-CPC	size distribution of particle	2-1000 nm and 7-9.9*10 ⁶ particles/cm ³	1 min
Spectroradiometer	actinic flux, J _{H2O2} , J _{HONO} , J _{HCHO} , J _{NO3} , J _{NO2} and J _{O1D}	1*10 ⁻⁴ W/m ² /nm for actinic flux; 1*10 ⁻⁷ s ⁻¹ for J value	1 s
UV-Visible absorption cell	cross section of all species	1*10 ⁻²⁰ cm ²	1 min
Commercial	NOx	1 ppb	1 min
Analyzers	O ₃	1 ppb	1 min

References

- Carter, W. P. L., Atkinson, R., Winer, A. M., and Pitts, J. N.: Experimental investigation of chamber-dependent radical sources, *International Journal of Chemical Kinetics*, 14, 1071-1103, 10.1002/kin.550141003, 1982.
- Weinmann, W., Wiedemann, A., Eppinger, B., Renz, M., and Svoboda, M.: Screening for drugs in serum by electrospray ionization/collision-induced dissociation and library searching, *Journal of the American Society for Mass Spectrometry*, 10, 1028-1037, [http://dx.doi.org/10.1016/S1044-0305\(99\)00070-7](http://dx.doi.org/10.1016/S1044-0305(99)00070-7), 1999.

Chapter 3.

**Investigation of the reaction of ozone
with isoprene, methacrolein and
methyl vinyl ketone using the
HELIOS Chamber**

Chapter 3- Investigation of the reaction of ozone with isoprene, methacrolein and methyl vinyl ketone using the HELIOS Chamber	66
3-1- Introduction.....	67
3-2- Experimental and Material	69
3-2-1- Experimental	69
3-2-2- Chemicals.....	71
3-3- Results and discussion.....	71
3-3-1- Kinetic measurements.....	71
3-3-2- Products measurements	78
3-3-2-1- OH formation yields	78
3-3-2-2- Gas phase stable products formation yields	81
3-3-2-3- Secondary organic aerosol formation	90
3.4- Conclusions and future work	93
References.....	96

Chapter 3- Investigation of the reaction of ozone with isoprene, methacrolein and methyl vinyl ketone using the HELIOS Chamber¹

Abstract:

The rate constants for the ozonolysis of isoprene (ISO), methacrolein (MACR) and methyl vinyl ketone (MVK) have been measured using the newly built large volume atmospheric simulation chamber at CNRS-Orleans (France), HELIOS (cHambrE de simuLation atmosphérique à Irradiation naturelle d'OrléanS). The OH radical yields from the ozonolysis of isoprene, MACR and MVK have been also determined as well as the gas phase stable products and their yields. The secondary organic aerosol yield for the ozonolysis of isoprene has been tentatively measured in presence and absence of OH radicals scavenger. The measurements have been performed under different experimental conditions with and without adding cyclohexane (cHX) as OH radical scavenger. All experiments have been conducted at 760 torr of purified dry air (RH < 1%) and ambient temperature (T = 281-295 K). The data obtained are discussed and compared with those from the literature. The use of the HELIOS facility and its associated analytical equipment enables to derive kinetic parameters as well as mechanistic information in near realistic atmospheric conditions.

¹ This work was published in Faraday Discussions: Yangang Ren, Benoit Grosselin, V éronique Da ðe and Abdelwahid Mellouki: Investigation of the reaction of ozone with isoprene, methacrolein and methyl vinyl ketone using the HELIOS Chamber, Faraday Discussions, 2017, Doi : 10.1039/C7FD00014F

3-1- Introduction

Atmospheric simulation chambers are among the most advanced tools for investigating the atmospheric processes to derive physico-chemical parameters which are required for air quality and climate models. Recently, the ICARE-CNRS at Orléans (France) has set up a new large outdoor simulation chamber, HELIOS (cHambrE de simuLation atmosphérique à Irradiation naturelle d'OrléanS). The new facility has been used to study the ozonolysis of isoprene (ISO), one of the most important volatile organic compounds in the atmosphere, and its major oxidation products, methacrolein (MACR) and methyl vinyl ketone (MVK). Isoprene is the most abundant emitted non-methane hydrocarbon (NMHC) into the atmosphere; it originates mainly from biogenic sources, primarily from terrestrial vegetation (Guenther et al., 2006; Zimmerman et al., 1988). Human activities may affect the lifecycle of these biogenic species and hence change their source capacity. Isoprene is sufficiently active to affect oxidant levels in the troposphere. It is removed from the atmosphere mainly through reaction with OH radicals during daytime and NO₃ radicals during nighttime. However, the reaction with ozone occurs throughout the day and night and hence could have a substantial contribution to the overall removal of isoprene from the atmosphere (Atkinson and Arey, 2003). The ozonolysis of isoprene has been the subject of large number of studies, in which the reaction rate constant value has been reported at room temperature, using both absolute (Sato et al., 2013; Karl et al., 2004; Neeb and Moortgat, 1999; Neeb et al., 1997; Klawatsch-Carrasco et al., 2004; Grosjean and Grosjean, 1996; Grosjean et al., 1993; Treacy et al., 1992; Kamens et al., 1982; Atkinson et al., 1982; Adeniji et al., 1981) and relative (Avzianova and Ariya, 2002; Khamaganov and Hites, 2001; Greene and Atkinson, 1992) methods. However, only a limited number of investigations have dealt with the temperature dependence near atmospheric conditions. The few mechanistic studies have indicated that the ozonolysis of isoprene ($\text{CH}_2\text{C}(\text{CH}_3)\text{CHCH}_2$) leads the formation of methacrolein ($\text{CH}_2\text{C}(\text{CH}_3)\text{CCHO}$), methyl vinyl ketone

(CH₂CHC(O)CH₃), and formaldehyde (HCHO) among the carbonyl products in addition to a series of intermediates including Criegee intermediates (CIs) which presently subject to high interest to the atmospheric scientific community (Nguyen et al., 2016; Sauer et al., 1999b; Gutbrod et al., 1997a; Niki et al., 1983; Kamens et al., 1982). Indeed, the CIs can react with a number of trace species in the atmosphere to form hydroperoxides, organic acids as well as aerosols (Sipila et al., 2014; Newland et al., 2015).

Using the new and well equipped HELIOS facility, we have initiated studies to investigate the chemistry of isoprene and its main oxidation products under conditions close to atmospheric ones. In this first work, we report the rate constants for the reactions of O₃ with isoprene, methacrolein and methyl vinyl ketone as well as the yields of the main products formed. The OH radicals yield from these reactions has been also determined as well as the secondary organic aerosol yield from the ozonolysis of isoprene. The data obtained are discussed and compared to the ones from previous studies. While several studies have been carried out earlier to investigate the reaction of ozone with isoprene, only a limited number have been performed under realistic atmospheric conditions and most of them have been conducted in flow tube system/small chamber using high reactant concentration. (e.g. high initial reactants concentrations) (Atkinson et al., 2006). The reaction of ozone with methacrolein and methyl vinyl ketone have been investigated only in a few studies (Atkinson et al., 2006). The present work provides new insight to the atmospheric importance of these two reactions. The chemistry of the Criegee intermediates and the subsequent reactions products are not discussed in the present paper, it is subject of an ongoing work in our laboratory.

3-2- Experimental and Material

3-2-1- Experimental

Experiments were carried out using the newly built large simulation chamber at CNRS-Orleans, HELIOS (cHambrE de simuLation atmosphérique à Irradiation naturelle d'OrléanS): The facility consists of 90 m³ hemispherical outdoor simulation chamber (47°50'18.39N; 1°56'40.03E) made of FEP Teflon film. Two fans installed in the chamber ensure a rapid mixing of reactants (within 90 seconds). Purified air is supplied by a pure air generation system (AADCO Instruments, Inc., 737 series). Pressure (P), relative humidity (RH) and temperature (T) were continuously measured by a three-axis Ultrasonic Anemometer (Delta Ohm, HD 2003) installed in the center of the chamber. In addition, six thermocouples (PT-100), spatially and equally placed in the chamber, were used to measure continuously the temperature distribution, they were found to be within ± 1 K. The chamber is protected from “severe” weather conditions such as rain and strong wind by a mobile protective housing which is also used to keep the chamber in full dark conditions in order to conduct ozonolysis experiments such as those reported in the present work. The chamber can be fully exposed to sunlight when needed within 30 s by automatically moving the protective housing.

Organic compounds were monitored by in situ Fourier transform infrared spectrometry (Bruker Vertex70 spectrometer) coupled to a White-type multipass cell (302.6 m optical path length). Infrared spectra were recorded every 3 minutes by co-adding 250 interferograms with a resolution of 0.4 cm⁻¹. Quantitative analysis of infrared spectra was performed either by subtraction or integration of the peak area using calibrated spectra. The gas phase mixtures were also analyzed using a gas chromatography coupled to a mass spectrometer (GC-MS, PekinElmer Clarus 600 C). Gas samples were collected from the chamber onto Air Toxics trap and analyzed through a thermal desorber (TurboMatrix™ 150 ATD), with split mode, followed by a thermal desorption at 300 °C (5 min) delivering the sample to a 60-m column

(GasPro diameter 0.320mm). The temperature of the GC oven was programmed as follows 25 °C min⁻¹ from 180 °C to 250 °C and held for 25 min. Ozone concentrations were measured continuously by a chemiluminescence analyzer (HORIBA, APOA 360). The organics were also monitored by PTR-ToF-MS (Proton Transfer Reaction - Time of Flight-Mass Spectrometer, IONICON 8000). PTR-ToF-MS spectra were analyzed by the PTR-ToF Data Analyzer (Müller et al., 2013). HCHO was monitored continuously by an Aerolaser A4021moniror using Hantzsch reaction (Aerolaser GMBH). The detection limits for the main species of interest (isoprene, MACR, MVK, HCHO, and cyclohexanone) were typically \approx 1-2 ppb by FTIR analysis, \approx 0.2-0.5 ppb by GCMS, and \approx 0.1-0.2 ppb by PTR-ToF-MS. The precisions were \leq 7%. The measurements of HCHO by the A4021moniror had a precision and detection limit of 2% and \approx 100 ppt, respectively. Ozone concentrations measurement the chemiluminescence analyzer (HORIBA, APOA 370) had a detection limit of 1 ppb.

Isoprene (ISO), methacrolein (MACR), methyl vinyl ketone (MVK) and cyclohexane (cHX) were introduced into the chamber by placing known volumes in a bubbler and flushed by a stream of purified air. Their concentrations were derived by considering the volume of the liquid introduced, the pressure and the temperature using the ideal gas law. O₃ was generated either through a Trailigaz® ozone generator or by using a Pen-Ray® Mercury Lamp radiation through a flow of O₂ prior to be introduced into the chamber. Gaseous reactants (i.e., SF₆) were injected into the chamber using a calibrated gas cylinder equipped with capacitance manometers. In order to compensate sampling flows and leaks, a slight flow of purified air (15-25 L/min) was added continuously during all experiments maintaining a slight overpressure in the chamber, avoiding any contamination from outside air. The dilution rate in the chamber was determined by monitoring the decay of introduced amount of SF₆ by FT-IR and was found to be typically $k_{\text{SF}_6} = (4.6 \pm 0.1) \times 10^{-6} \text{ s}^{-1}$.

Between each experiment, the chamber was cleaned by flushing pure air (800 L/min) for at least 12 hours. Background concentrations in the chamber were systematically checked and found to be below the detection limits of the available

analytical instruments (e.g., [NO_x] $<1.3\times10^{10}$, [O₃] $<1.3\times10^{10}$ and [VOC] $<1.3\times10^8$ molecule cm⁻³).

3-2-2- Chemicals.

The chemicals used in this work and their stated purities were: Isoprene (Aldrich, 99%), cHX (Aldrich, 99.5%), MACR (Aldrich, 95%), MVK (Aldrich, 98%), SF₆ (Mitry-Mory 99.95%) and O₂ (Alphagaz, 99.9999%).

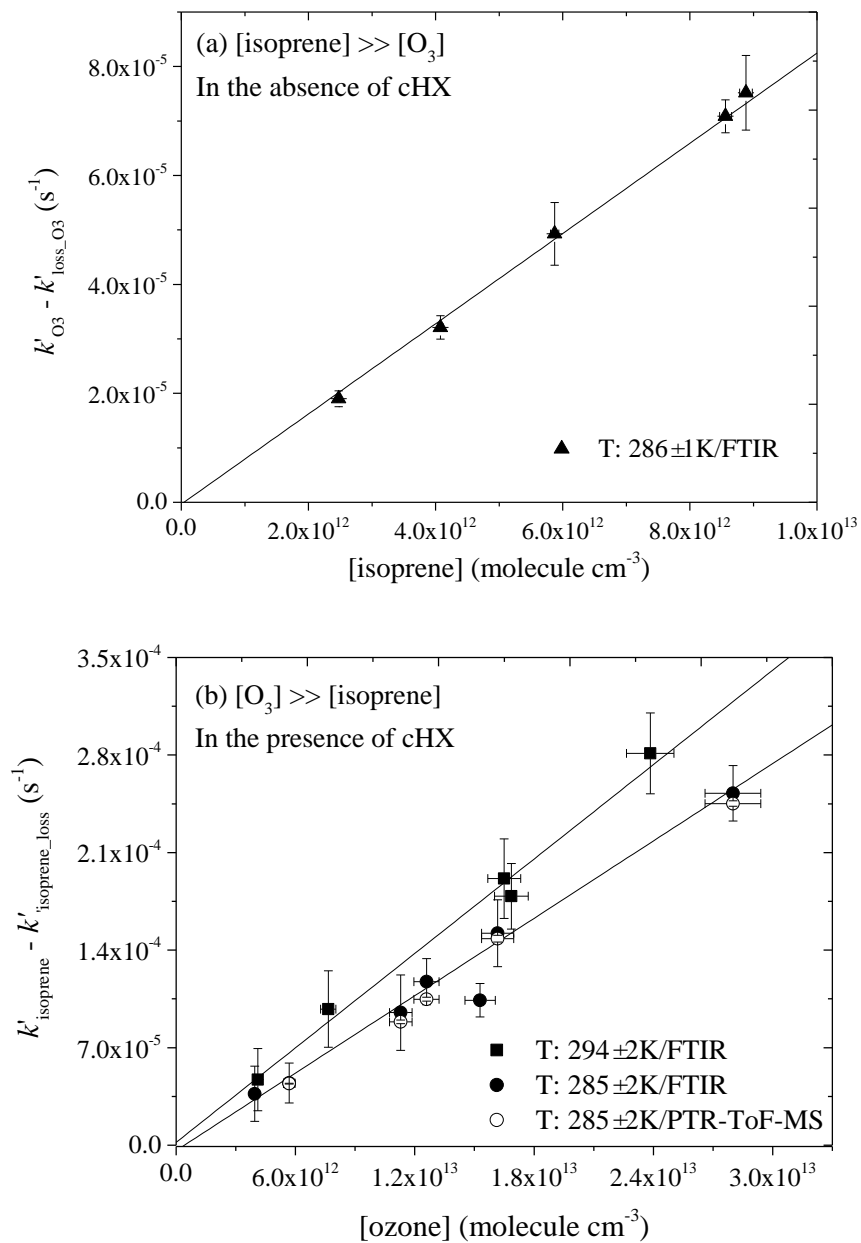
3-3- Results and discussion

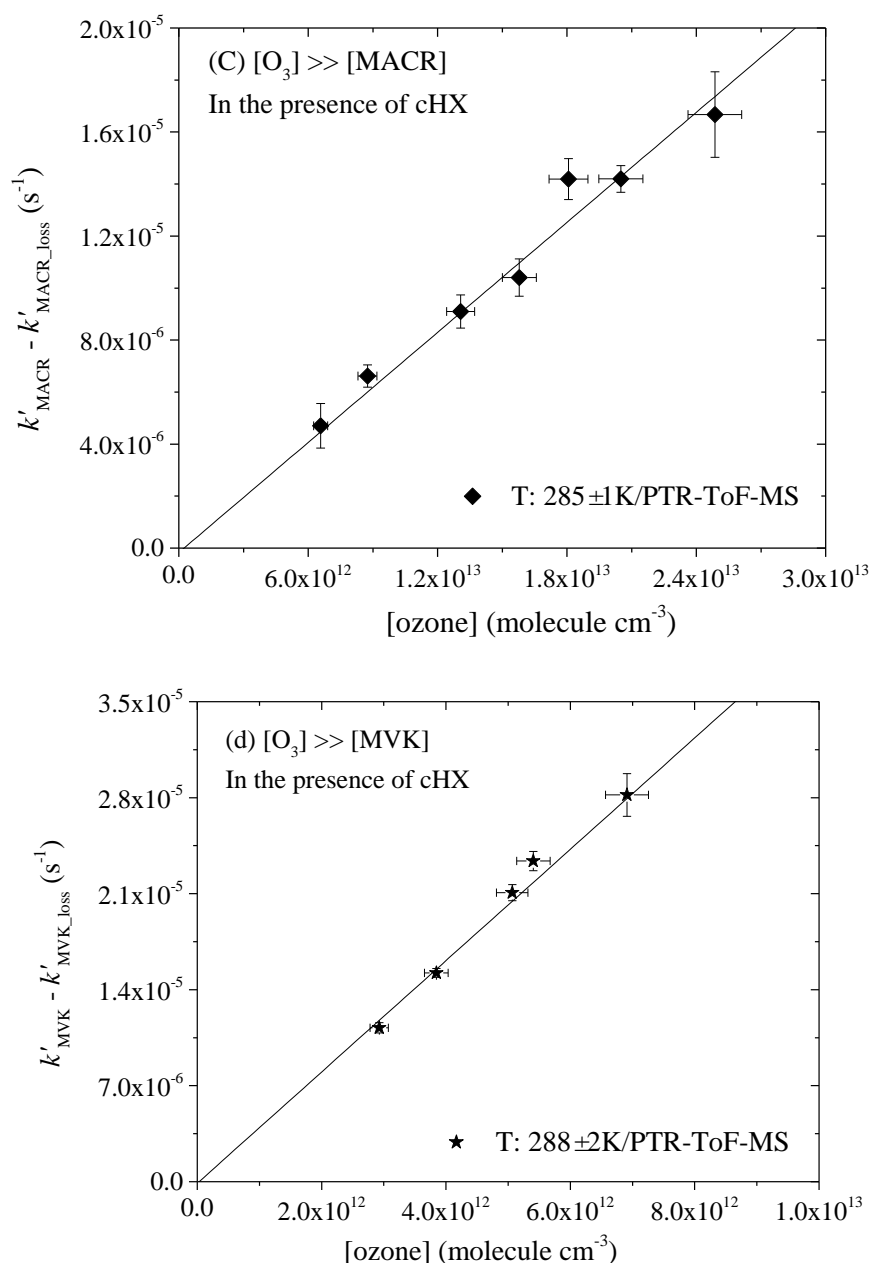
3-3-1- Kinetic measurements

It is well established that the ozonolysis of unsaturated organic compounds constitutes a potential non-photolytic source of OH radicals under atmospheric conditions (Schäfer et al., 1997; Chew and Atkinson, 1996; Alam et al., 2013). Hence, in order to take that into account during our measurements, we have conducted the experiments using three different strategies, (S1) [ISO] in excess over [O₃] in the absence of cHX; (S2): [O₃] in excess over [ISO/MACR/MVK] in the presence of cHX (used as OH scavenger) and (S3): [O₃] in excess over [ISO/MACR/MVK] in the absence of cHX. Typically, initial O₃ and ISO/MACR/MVK concentrations for the (S2) and (S3) strategies were in the range 110-1000 ppb and 9-90 ppb, respectively while initial O₃ and isoprene concentrations for (S1) were 13-35 ppb and 100-350 ppb, respectively. When added, cHX concentrations were in the range 1.5-17 ppm. Under (S2) and (S3) conditions, ISO/MACR/MVK were introduced into the chamber firstly to derive their losses in the absence of ozone which represent basically the wall loss and dilution. Under (S1) conditions, O₃ was introduced first into the chamber and its loss measured in the absence of organic reactants. Rate constants for the gas-phase reaction of O₃ with Organic (ISO/MACR/MVK) were determined by monitoring the enhanced decay rates of the O₃ or ORG (organic reactant) depending on the initial concentrations conditions. When the organic reactant is in excess, the decay of the

ozone concentration can be expressed as $[O_3]_t = [O_3]_0 \times \exp(-k't)$ where $k' = k \times [ORG]_0 + k'_0$, where k (in cm³ molecule⁻¹ s⁻¹) is the rate coefficient of the ozone reaction with organic, k'_0 (in s⁻¹) is the pseudo-first order decay rate of ozone in the absence of the organic reactant and $[ORG]_0$ is the initial concentration of organic. Similarly, when O₃ was in excess, the decay of the organic is expressed as $[ORG]_t = [ORG]_0 \times \exp(-k't)$ where $k' = k \times [O_3]_0 + k'_0$, where k'_0 is the pseudo-first order decay rate of organic in the absence of O₃ and $[O_3]_0$ is the initial concentration of ozone. In our experimental conditions, $k'_{0_ISO} = (4.9 \pm 0.7) \times 10^{-6}$, $k'_{0_MACR} = (6.0 \pm 1.0) \times 10^{-6}$, $k'_{0_MVK} = (5.7 \pm 1.0) \times 10^{-6}$ and $k'_{0_O_3} = (5.0 \pm 0.4) \times 10^{-6}$ s⁻¹. In excess of O₃ when CHX was not added to scavenge OH radicals, the loss of the organic due to the reaction with OH radicals was taken into account to correct the measured $k_{O_3 + ORG}$.

Figures 3-1(a-d) displays examples of the pseudo-first order rate constants versus the initial concentrations of the species in excess (O₃ or organic) obtained. The slopes of these plots were used to derive the reactions rate constants. The initial experimental conditions together with the measured rate constants for the reaction of O₃ with three organics (ISO/MACR/MVK) are listed in Tables 3-1, 3-2 and 3-3. The runs were performed under ambient temperatures, 280 to 295 K, which were the outdoor temperature during the experiments period. Consequently, the results have been assembled by averaging the values from different runs at the same temperature (± 3 K).





Figures 3-1(a-d): Plot of decay rate ($k' - k'_0$) as a function of [O₃]₀ or [Isoprene]₀, (a) [isoprene] in excess over [O₃] in the absence of cHX; (b) [O₃] in excess over [isoprene] in the presence of cHX; (c) [O₃] in excess over [MACR] in the presence of cHX; (d) [O₃] in excess over [MVK] in the presence of cHX.

In the experiments where isoprene concentrations were in excess over that of O₃, a rate constant value of $k_{\text{O}_3+\text{isoprene}} = (8.6 \pm 0.5) \times 10^{-18} \text{ cm}^3 \text{ molecule}^{-1} \text{ s}^{-1}$ at 285 ± 1 K was obtained. Under conditions where O₃ was in excess over the organic in the presence of cyclohexane as OH scavenger, several runs were performed at T = 294 ± 2 and 285 ± 2 K and a single run at 278 ± 1 K for the reaction of O₃ with isoprene. The

obtained values are: $k_{\text{O}_3+\text{isoprene}} = (11.3 \pm 1.7)$ and $(9.3 \pm 0.7) \times 10^{-18} \text{ cm}^3 \text{ molecule}^{-1} \text{ s}^{-1}$ at 294 ± 2 and $285 \pm 2 \text{ K}$, respectively, in excellent agreement with the IUPAC panel recommendations using the Arrhenius expression $k = 1.03 \times 10^{-14} \exp(-1995/T)$ in the range 240-360 K, $k_{\text{O}_3+\text{isoprene}} = 11.9$ and $9.4 \times 10^{-18} \text{ cm}^3 \text{ molecule}^{-1} \text{ s}^{-1}$. The rate constant value obtained in the single run at $278 \pm 1 \text{ K}$, $(6.7 \pm 0.9) \times 10^{-18} \text{ cm}^3 \text{ molecule}^{-1} \text{ s}^{-1}$, is $\approx 15 \%$ lower than the IUPAC recommendation $7.9 \times 10^{-18} \text{ cm}^3 \text{ molecule}^{-1} \text{ s}^{-1}$. In the absence of scavenger, the reaction rate constants values obtained at 284 ± 1 , 281 ± 1 , and $288 \pm 1 \text{ K}$ (a single run), respectively, $k_{\text{O}_3+\text{isoprene}} = (10.8 \pm 1.1)$, (9.7 ± 0.7) , and $(11.9 \pm 1.8) \times 10^{-18} \text{ cm}^3 \text{ molecule}^{-1} \text{ s}^{-1}$, have been found to be systematically $\approx 15 \%$ higher than those from the IUPAC recommendations 9.16×10^{-18} , 8.5×10^{-18} , and $10.9 \times 10^{-18} \text{ cm}^3 \text{ molecule}^{-1} \text{ s}^{-1}$. The reason for the observed differences is attributed to the contribution of the OH reaction to the consumption of isoprene when O₃ was in excess.

Table 3-1: Reaction of O₃ with isoprene: Initial experimental conditions and results from the kinetic studies

Experimental conditions	T (K)	[O ₃] ₀ (molecule cm ⁻³)	[Isoprene] ₀ (molecule cm ⁻³)	[Cyclohexane] ₀ (molecule cm ⁻³)	$k'-k'_0 (\pm I\delta)$ ($\times 10^{-5} \text{ s}^{-1}$)
Isoprene in excess, without OH scavenger	286 \pm 1	3.4×10^{12}	24.7×10^{11}	0	1.9 ± 0.1
	285 \pm 1	5.6×10^{12}	40.8×10^{11}	0	3.2 ± 0.2
	285 \pm 1	5.4×10^{12}	58.7×10^{11}	0	4.9 ± 0.6
	285 \pm 1	9.0×10^{12}	85.6×10^{11}	0	7.1 ± 0.3
	283 \pm 1	6.9×10^{12}	88.8×10^{11}	0	7.5 ± 0.7
	285 \pm 1	Average: $k = (8.6 \pm 0.5) \times 10^{-18} \text{ cm}^3 \text{ molecule}^{-1} \text{ s}^{-1}$			
	294 \pm 1	4.1×10^{12}	3.9×10^{11}	8.1×10^{13}	4.7 ± 2.2
O ₃ in excess, with OH scavenger	295 \pm 1	7.7×10^{12}	6.6×10^{11}	15.9×10^{13}	$9.8 \pm 2.7 / 9.5 \pm 0.1^a$
	295 \pm 1	16.5×10^{12}	14.4×10^{11}	18.4×10^{13}	$19.1 \pm 2.9 / 19.5 \pm 0.2^a$
	291 \pm 1	16.9×10^{12}	14.6×10^{11}	29.5×10^{13}	17.9 ± 2.4
	294 \pm 1	23.8×10^{12}	21.1×10^{11}	45.1×10^{13}	28.1 ± 2.9
	294 \pm 2	Average: $k = (11.3 \pm 1.7) \times 10^{-18} \text{ cm}^3 \text{ molecule}^{-1} \text{ s}^{-1}$			
	286 \pm 1	4.0×10^{12}	2.6×10^{11}	7.0×10^{13}	3.7 ± 2.0
	282 \pm 1	5.7×10^{12}	3.9×10^{11}	9.4×10^{13}	$4.5 \pm 1.4 / 4.4 \pm 0.1^a$
O ₃ in excess, with OH scavenger	284 \pm 1	11.3×10^{12}	5.6×10^{11}	12.8×10^{13}	$9.5 \pm 2.7 / 8.9 \pm 0.2^a$
	286 \pm 1	12.6×10^{12}	11.2×10^{11}	15.0×10^{13}	$11.7 \pm 1.7 / 10.5 \pm 0.3^a$
	284 \pm 1	16.2×10^{12}	8.4×10^{11}	22.4×10^{13}	$15.2 \pm 2.4 / 14.8 \pm 0.5^a$
	283 \pm 1	28.0×10^{12}	23.7×10^{11}	51.8×10^{13}	$25.2 \pm 2.0 / 24.5 \pm 0.5^a$
	285 \pm 2	Average: $k = (9.3 \pm 0.7) \times 10^{-18} \text{ cm}^3 \text{ molecule}^{-1} \text{ s}^{-1}$			
	278 \pm 1	15.3×10^{12}	13.8×10^{11}	24.7×10^{13}	$10.4 \pm 1.2 / 10.1 \pm 0.2^a$
		$k = (6.7 \pm 1.0) \times 10^{-18} \text{ cm}^3 \text{ molecule}^{-1} \text{ s}^{-1}$			

	283±1	3.3×10 ¹²	4.3×10 ¹¹	0	3.2±0.6
	283±1	4.0×10 ¹²	3.4×10 ¹¹	0	5.0±0.7
	285±1	11.9×10 ¹²	10.7×10 ¹¹	0	13.1±1.1
	283±1	12.8×10 ¹²	5.8×10 ¹¹	0	14.5±2.0/13.5±0.3 ^a
	285±1	15.8×10 ¹²	16.3×10 ¹¹	0	17.1±2.0/17.0±0.4 ^a
	284±1	Average: k=(10.8±1.1)×10 ⁻¹⁸ cm ³ molecule ⁻¹ s ⁻¹			
O ₃ in excess, without OH scavenger	280±1	10.7×10 ¹²	5.3×10 ¹¹	0	10.0±2.7/9.8±0.2 ^a
	282±1	12.6×10 ¹²	12.3×10 ¹¹	0	12.3±1.5
	279±1	14.2×10 ¹²	6.9×10 ¹¹	0	13.9±3.1
	281±1	20.3×10 ¹²	9.9×10 ¹¹	0	20.0±2.6/19.2±0.4 ^a
	281±1	25.3×10 ¹²	23.0×10 ¹¹	0	24.1±2.1
	281±1	Average: k=(9.7±0.7)×10 ⁻¹⁸ cm ³ molecule ⁻¹ s ⁻¹			
	288±1	21.3×10 ¹²	18.8×10 ¹¹	0	25.4±2.4/25.4±0.5 ^a
		k=(11.9±1.8)×10 ⁻¹⁸ cm ³ molecule ⁻¹ s ⁻¹			

^a value from PTR-ToF-MS

Regarding the O₃ reactions with MACR and MVK, experiments were conducted only in excess of O₃ in the presence and absence of OH scavenger. In the presence of scavenger, the rate constant values obtained at T=285±1 K for the reaction of O₃ with MACR is $k_{\text{O}_3+\text{MACR}} = (7.1 \pm 0.6) \times 10^{-19} \text{ cm}^3 \text{ molecule}^{-1} \text{ s}^{-1}$ which is slightly lower than the IUPAC recommended value ($k = 8.8 \times 10^{-19}$) using the expression $k = 1.4 \times 10^{-15} \exp(-2100/T) \text{ cm}^3 \text{ molecule}^{-1} \text{ s}^{-1}$ over the temperature range 240-330 K. The single run carried out at T=287±1 K leads to slightly lower value, $k=7.9 \times 10^{-19}$, compared to the recommendation, 9.3×10^{-19} . The runs performed in absence of scavenger led to higher values: $k_{282} = (12 \pm 1) \times 10^{-19}$ and $k_{289} = (15 \pm 2) \times 10^{-19}$ compared to those in the presence of scavenger and also to IUPAC recommendations which are $k_{282} = 8.2 \times 10^{-19}$ and $k_{289} = 8.8 \times 10^{-19} \text{ cm}^3 \text{ molecule}^{-1} \text{ s}^{-1}$.

Table 3-2: Reactions of O₃ with Methacrolein (MACR): Initial experimental conditions and results from the kinetic studies

	T (K)	[ozone] ₀ (molecule cm ⁻³)	[MACR] ₀ (molecule cm ⁻³)	[cyclohexane] ₀ (molecule cm ⁻³)	$k'-k'_{\text{loss}} (\pm 1\delta)$ (×10 ⁻⁶ s ⁻¹)
O ₃ in excess with OH scavenger	285±1	24.9×10 ¹²	9.8×10 ¹¹	18.9×10 ¹³	16.7±1
	284±1	15.8×10 ¹²	7.7×10 ¹¹	18.4×10 ¹³	10.4±0.7
	285±1	13.1×10 ¹²	5.3×10 ¹¹	17.3×10 ¹³	9.1±0.6
	285±1	20.5×10 ¹²	32.3×10 ¹¹	29.8×10 ¹³	14.2±0.5
	285±1	6.6×10 ¹²	2.8×10 ¹¹	27.1×10 ¹³	4.7±0.8

	285±1	8.8×10 ¹²	2.4×10 ¹¹	29.0×10 ¹³	6.6±0.4
	285±1	Average: k=(7.1±0.6)×10 ⁻¹⁹ cm ³ molecule ⁻¹ s ⁻¹			
	287±1	18.1×10 ¹²	10.4×10 ¹¹	28.5×10 ¹³	14.2±0.8
		k=(7.9±1.2)×10 ⁻¹⁹ cm ³ molecule ⁻¹ s ⁻¹			
O ₃ in excess without OH scavenger	280±1	7.1×10 ¹²	5.9×10 ¹¹	0	8.0±0.4
	280±1	5.1×10 ¹²	2.6×10 ¹¹	0	5.5±0.3
	284±1	8.2×10 ¹²	7.6×10 ¹¹	0	10.4±0.6
	282±1	3.8×10 ¹²	2.4×10 ¹¹	0	4.7±0.4
	283±1	24.7×10 ¹²	10.1×10 ¹¹	0	30.5±1.8
	282±2	Average: k=(1.2±0.1)×10 ⁻¹⁸ cm ³ molecule ⁻¹ s ⁻¹			
	290±1	15.4×10 ¹²	6.2×10 ¹¹	0	24.2±0.8
	289±1	17.4×10 ¹²	11.8×10 ¹¹	0	26.5±1.2
	289±1	11.2×10 ¹²	5.1×10 ¹¹	0	17.5±0.6
	289±1	14.1×10 ¹²	5.9×10 ¹¹	0	22.2±0.8
	288±1	20.0×10 ¹²	7.1×10 ¹¹	0	30.7±1.5
	289±1	Average: k=(1.5±0.2)×10 ⁻¹⁸ cm ³ molecule ⁻¹ s ⁻¹			

The O₃+MVK rate constant measured at T=289±3K in the presence of scavenger was found to be $k_{O_3+MVK} = (4.5 \pm 0.1) \times 10^{-18} \text{ cm}^3 \text{ molecule}^{-1} \text{ s}^{-1}$ in excellent agreement with the recommended value, $k_{O_3+MVK} = 4.4 \times 10^{-18}$, using the Arrhenius expression $k = 8.5 \times 10^{-16} \exp(-1520/T) \text{ cm}^3 \text{ molecule}^{-1} \text{ s}^{-1}$ over the temperature range 240-330 K. The experiment performed in absence of the scavenger at 287±2 K led to $k = (5.1 \pm 0.1) \times 10^{-18}$ which is $\approx 20 \%$ higher than the IUPAC preferred one, $k = 4.3 \times 10^{-18} \text{ cm}^3 \text{ molecule}^{-1} \text{ s}^{-1}$.

Table 3-3: Reactions of O₃ with Methyl vinyl ketone (MVK): Initial experimental conditions and results from the kinetic studies

	T (K)	[ozone] ₀ (molecule cm ⁻³)	[MVK] ₀ (molecule cm ⁻³)	[cyclohexane] ₀ (molecule cm ⁻³)	$k'-k'_{loss} (\pm 1\delta)$ (×10 ⁻⁵ s ⁻¹)
O ₃ in excess with OH scavenger	286±1	2.9×10 ¹²	2.3×10 ¹¹	3.9×10 ¹³	1.1±0.1
	288±1	5.1×10 ¹²	4.7×10 ¹¹	4.1×10 ¹³	2.1±0.1
	288±1	6.9×10 ¹²	5.5×10 ¹¹	5.9×10 ¹³	2.8±0.2
	290±1	3.8×10 ¹²	2.8×10 ¹¹	3.9×10 ¹³	1.5±0.1
	292±1	5.4×10 ¹²	4.9×10 ¹¹	5.8×10 ¹³	2.3±0.2
	289±3	Average: k=(4.5±0.1)×10 ⁻¹⁸ cm ³ molecule ⁻¹ s ⁻¹			
O ₃ in excess without OH scavenger	286±1	8.5×10 ¹²	7.6×10 ¹¹	0	4.2±0.2
	287±1	8.0×10 ¹²	7.0×10 ¹¹	0	4.0±0.5
	289±1	6.4×10 ¹²	6.3×10 ¹¹	0	3.1±0.4
	289±1	4.2×10 ¹²	3.0×10 ¹¹	0	2.0±0.1
	287±2	Average: k=(5.1±0.1)×10 ⁻¹⁸ cm ³ molecule ⁻¹ s ⁻¹			

3-3-2- Products measurements

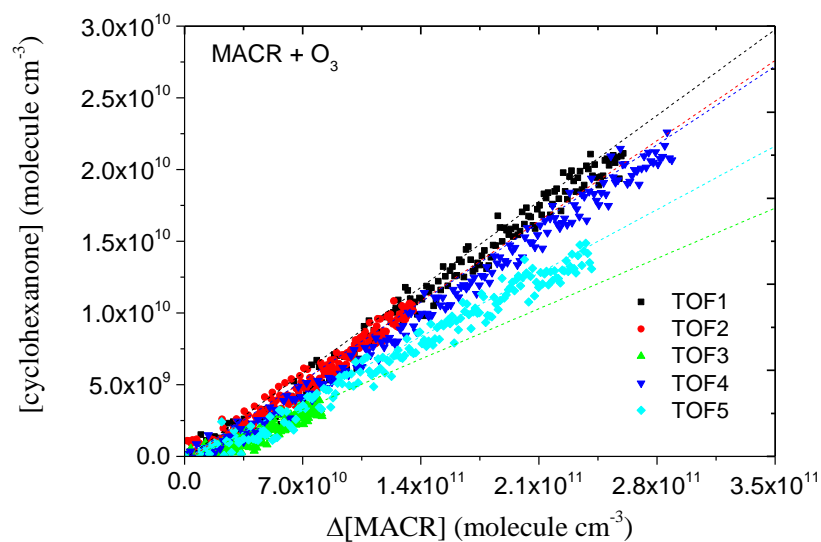
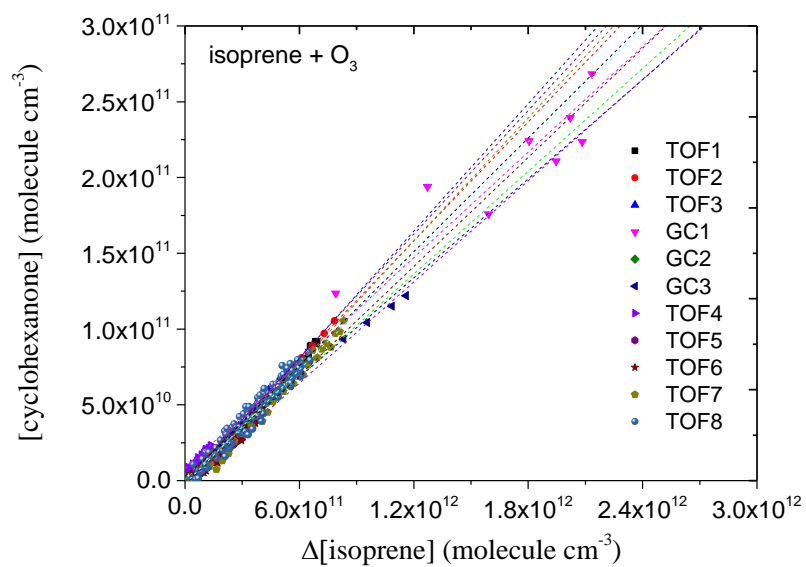
3-3-2-1- OH formation yields

Cyclohexane was used to scavenge OH radicals formed during the ozonolysis of ISO, MARC and MVK. The yield of cyclohexanone produced from the reaction of OH with cyclohexane enabled to derive the OH yields during the ozonolysis of the investigated organics. Cyclohexanone was monitored by GC-MS ($m/z=98$) and PTR-ToF-MS (measurement fragment as $m/z=81.0463$ and $C_6H_{10}O \cdot H^+$ as 99.0465). The OH yields were obtained from the equation:

$$Y_{OH} = \frac{[\text{cyclohexanone}]/\Delta[\text{organic}]}{[\text{cyclohexanone}]/\Delta[\text{cHX}]} = \frac{[\text{cyclohexanone}]/\Delta[\text{organic}]}{0.5}$$

in which cyclohexanone formation yield of $(50 \pm 7) \%$ from OH+cyclohexane reported by Atkinson and Aschmann (1993) was used.

Figure 3-2 shows the formation of cyclohexanone versus the consumed organics during the course of the experiments and Table 3-4 summarizes the experimental conditions and the obtained yield values. The results obtained are $Y_{OH} = 24.0 \pm 2.0$; 14.3 ± 3.5 and $13.4 \pm 4.1\%$ for the reactions of O₃ with isoprene, MACR and MVK, respectively. Y_{OH} from the reaction of O₃+isoprene is in excellent agreement with recent measurement by Malkin et al., (2010) and Nguyen et al., (2016) who reported 26 ± 2 and $28 \pm 5 \%$, respectively. It is also in excellent agreement with the IUPAC recommended value using the set of the literature data reported before 2005, $Y_{OH}=25 \%$ (Paulson et al., 1998; Neeb and Moortgat, 1999; Kroll et al., 2001; Atkinson et al., 2006). The obtained OH formation yields for O₃+MACR and O₃+MVK have been found to be similar, $Y_{OH} = 14\%$, in agreement with the only existing values from Aschmann et al., (1996) and Paulson et al., (1998).



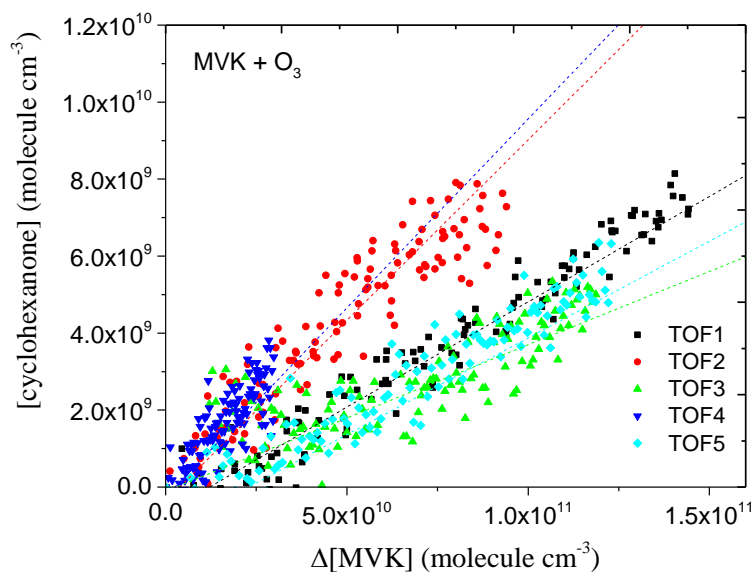


Figure 3-2: Plot of cyclohexanone concentration with respect to consumed isoprene, MACR and MVK (TOF, GC: data obtained using PTR-ToF-MS or GC-MS, respectively)

Table 3-4: The OH yields from the ozonolysis of isoprene, MACR and MVK: experimental conditions and results ^a

[cHX]/ [organic] ₀	[cyclohexanone]/ Δ[organic]	Y _{OH} (%)	Method	Reference
Isoprene+O ₃				
145	(12.49±0.21)×10 ⁻²	25.0±0.4	cHX as Scavenger	This work^b
130	(13.07±0.24)×10 ⁻²	26.1±0.5	PTR-ToF-MS	
240	(14.02±0.16)×10 ⁻²	28.0±0.3		
245	(13.60±0.29)×10 ⁻²	27.2±0.7		
245	(11.12±0.24)×10 ⁻²	22.2±0.5		
270	(11.99±0.20)×10 ⁻²	24.0±0.4		
220	(12.91±0.16)×10 ⁻²	25.8±0.3		
250	(12.53±0.21)×10 ⁻²	25.1±0.4		
200	(11.64±0.65)×10 ⁻²	23.3±1.3	cHX as Scavenger, GC-MS	
230	(11.31±1.21)×10 ⁻²	22.6±2.5		
180	(10.85±0.48)×10 ⁻²	21.7±0.9		
Average		24.0±2.0[*]	cHX as Scavenger	
		26±2	cHX as Scavenger, TMB tracer, FAGE	Malkin et al., 2010
		28±5	LIF and FAGE	Nguyen et al., 2016
		25	Recommendation	IUPAC
MACR+O ₃				
192	(8.56±0.66)×10 ⁻²	17.1±1.8	cHX as Scavenger	
240	(7.99±0.66)×10 ⁻²	16.0±1.9	PTR-ToF-MS	
330	(5.01±0.37)×10 ⁻²	10.0±1.0		

240	$(7.84 \pm 0.58) \times 10^{-2}$	15.6 ± 1.7		
270	$(6.33 \pm 0.51) \times 10^{-2}$	12.7 ± 1.4		
Average		14.3 ± 3.5	cHX as Scavenger	This work
		20^{+10}_{-13}	cHX as Scavenger GC-MS/GC-FID/GC-FTIR	Aschmann et al., 1986
MVK+O ₃				
82	$(5.47 \pm 0.66) \times 10^{-2}$	11.0 ± 1.9	cHX as Scavenger,	
86	$(9.39 \pm 1.08) \times 10^{-2}$	18.8 ± 2.2	PTR-ToF-MS	
107	$(3.8 \pm 0.70) \times 10^{-2}$	7.6 ± 1.6		
140	$(9.82 \pm 1.30) \times 10^{-2}$	19.6 ± 2.9		
119	$(5.03 \pm 1.18) \times 10^{-2}$	10.1 ± 1.1		
Average		13.4 ± 4.1	cHX as Scavenger	This work
		16 ± 8	cHX as Scavenger GC-MS/GC-FID/GC-FTIR	Aschmann et al., 1986
		16 ± 5	tracers, GC-FID	Paulson et al., 1998

^a Errors quoted are standard deviation (SD) obtained in the regression analysis combined with estimated overall uncertainties in the PTR-ToF-MS and GC-MS response factors for isoprene, MACR, MVK and cyclohexanone. ^b Average values determined by PTR-ToF-MS and GC-MS.

3-3-2-2- Gas phase stable products formation yields

Identified oxidation products and corresponding formation yields obtained with different analytical tools are listed in Table 3-5. Figures 3-3, 3-4, 3-5 display the typical IR spectra in the wavenumber region 750-4000 cm⁻¹ obtained during the experiments carried out. Isoprene, MACR, MVK and SF₆ have been monitored at 893.8, 2730, 998 and 948 cm⁻¹, respectively. Ozone was measured also by FTIR (at 1042 cm⁻¹) in addition to the measurement through the Horiba APOA monitor. Panels A show the spectra of organics/O₃/SF₆/ air mixtures at the start of the experiments (after typically ≈ 5 min of mixing the reactants). Panels B show the spectra after few hours of reactions while panels C display the spectra of the reaction products after subtraction of the initial organic reactants/O₃ and SF₆. Comparison of panels C with reference spectra of formaldehyde (HCHO), carbon monoxide (CO), formic acid (HCOOH) and methylglyoxal (CH₃C(O)C(O)H) in the remaining panels indicates the formation of these products. In a number of runs, the PTR-Tof-MS (C₅H₈•H⁺ at m/z 69.064, C₄H₆O•H⁺ at m/z 71.0442, C₆H₁₀•H⁺ at m/z 81.0463 and 99.0465) and GC-

MS (ISO at m/z 67, MACR/MVK at m/z 70, cyclohexanone at m/z 98) were also used to monitor the reactants and products.

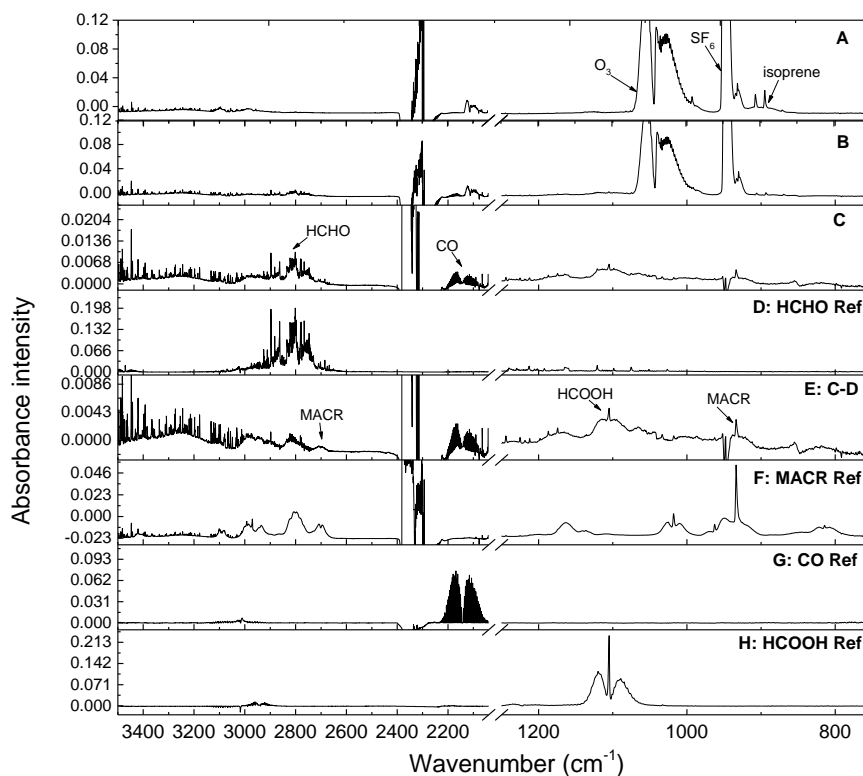


Figure 3-3: – O₃ + isoprene: FTIR spectra acquired after 5 minutes of reaction (A) and 2 hours (B), panel C = B-A (to identify the products), panel D = is the HCHO reference spectrum. Panel E shows the residual spectrum after subtraction of features attributable to formaldehyde. Reference spectra are shown for MACR (F), CO (G), and HCOOH (H).

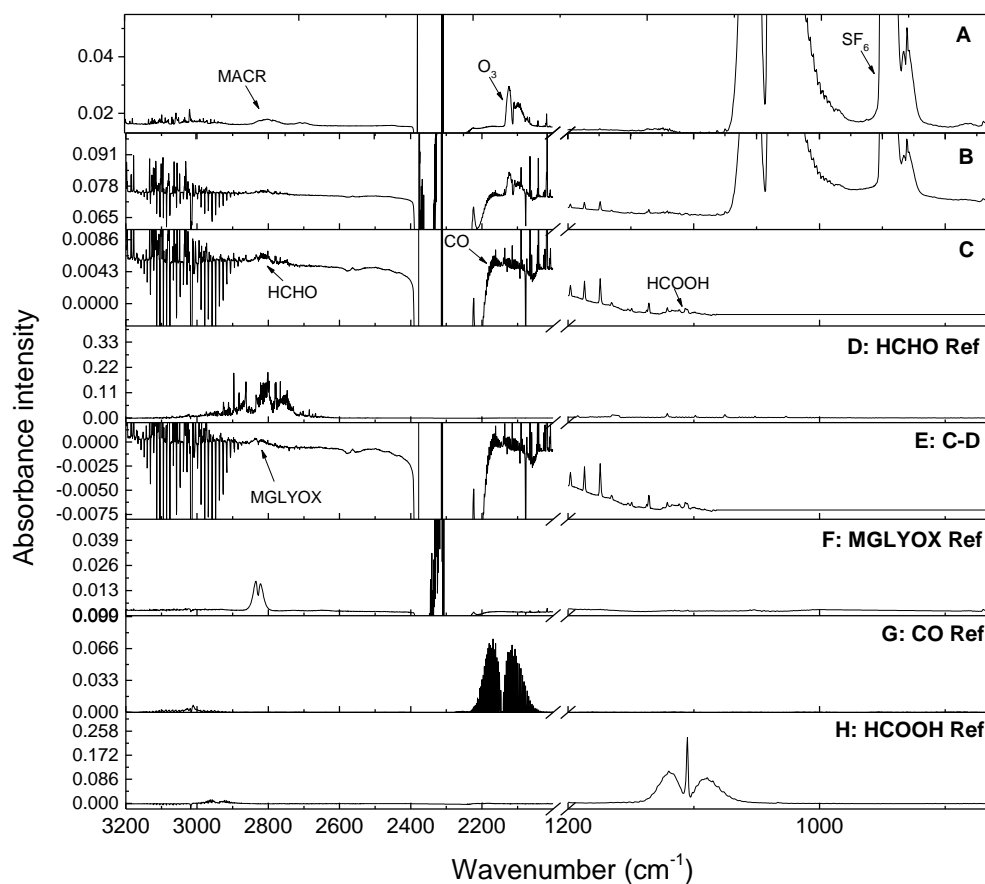


Figure 3-4: – O₃ + MACR: FTIR spectra acquired after 5 minutes of reaction (A) and 5 hours (B), panel C = B-A (to identify the products). Panel D is the HCHO reference spectrum. Panel E shows the residual spectrum after subtraction of features attributable to formaldehyde. Reference spectra are shown for methylglyoxal (F), CO (G), and HCOOH (H).

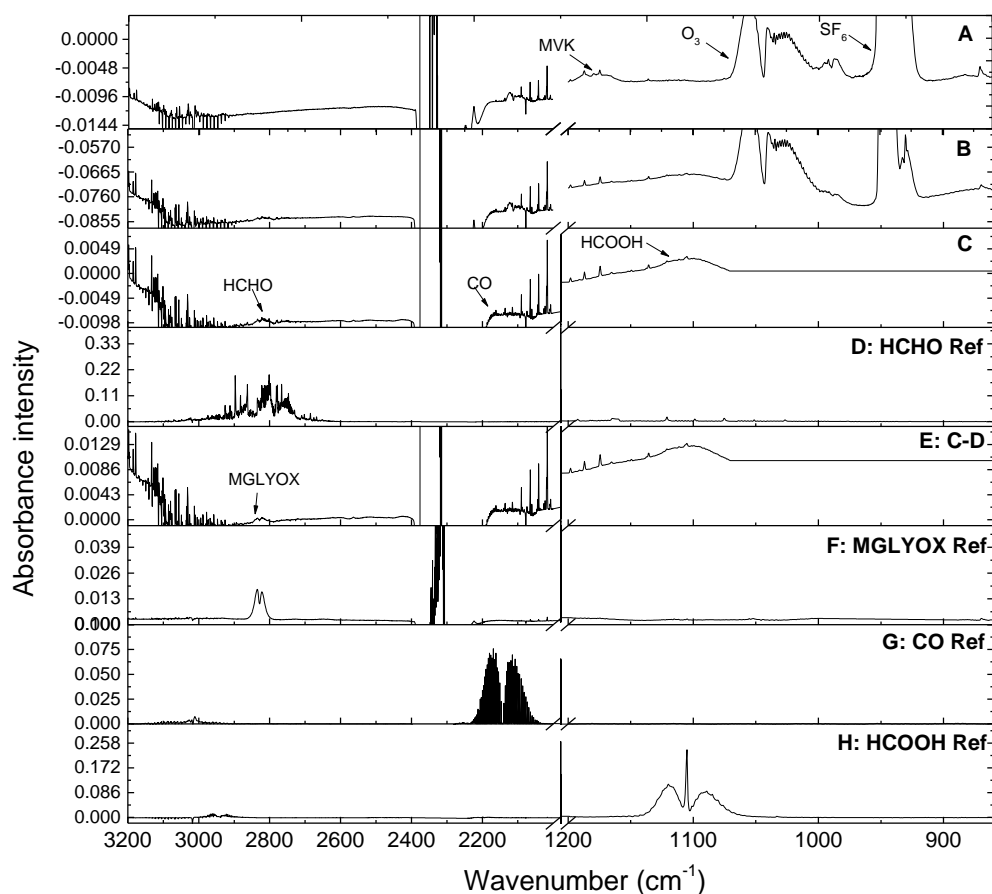


Figure 3-5: – O₃ + MVK: FTIR spectra acquired after 5 minutes of reaction (A) and 5 hours (B), panel C = B-A (to identify the products). Panel D is the HCHO reference spectrum. Panel E shows the residual spectrum after subtraction of features attributable to formaldehyde. Reference spectra are shown for methylglyoxal (F), CO (G), and HCOOH (H).

Figure 3-6(a-c) displays examples of the temporal profiles of the reactants and products from O₃+ISO, O₃+MACR and O₃+MVK obtained by FTIR, PTR-ToF-MS and HCHO-monitor. As shown, the experiments last typically for more than 20 hours each. Table 3-5 summarizes the experimental conditions and the obtained results along with the literature values. It has to be noted that the experiments presented in this work have been carried out at lower initial reactant concentrations compared to those reported in the previous studies. On the other hand, the experiments were performed in the temperature range 281-295 K while the literature data were mostly conducted in the range 293-298 K as shown in Table 3-5.

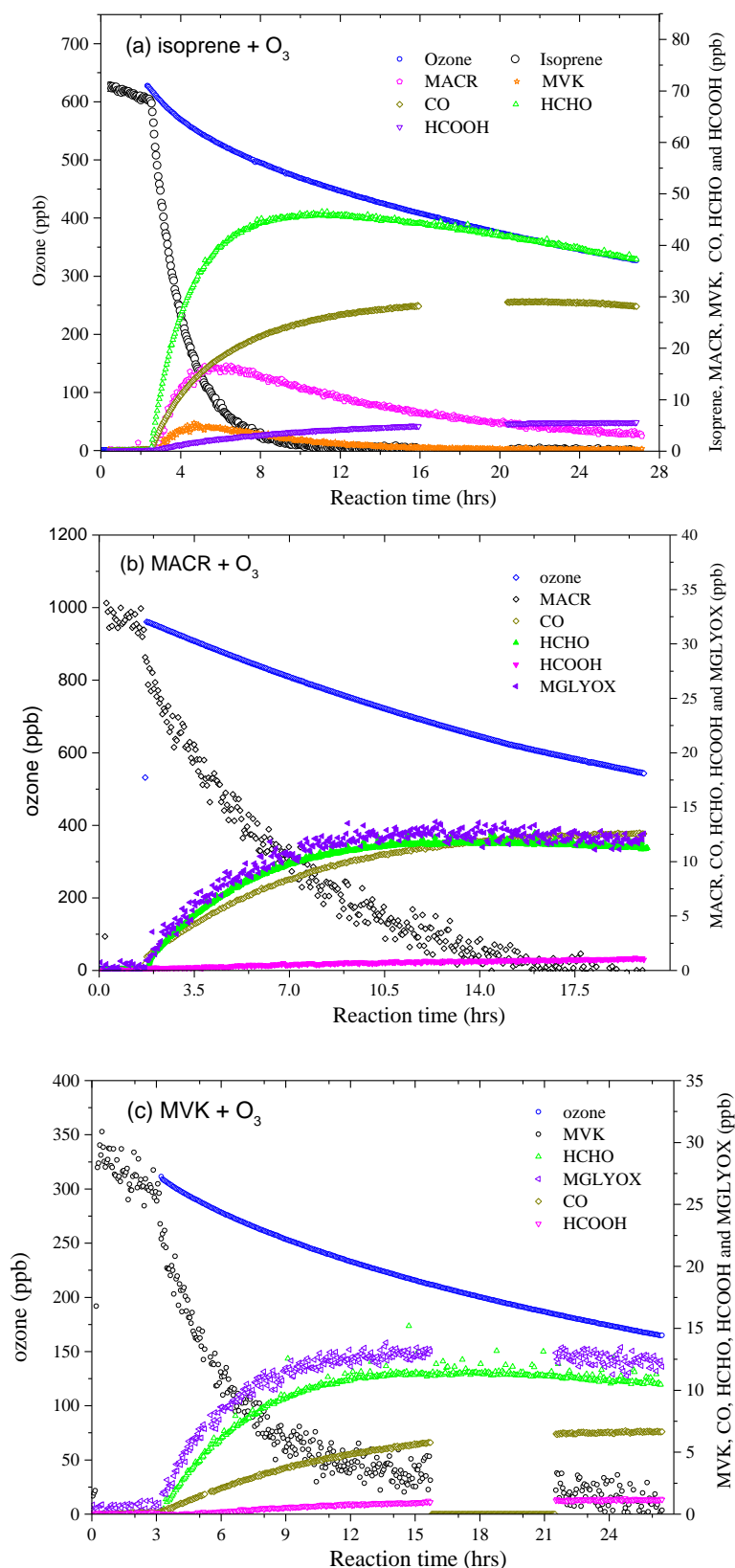


Figure 3-6(a-c): –Temporal profiles of reactants (isoprene/MACR/MVK, O₃) and observed products in the reactions of O₃-isoprene (a), O₃-MACR (b), O₃-MVK (c). Isoprene, O₃, CO, HCOOH and MGLYOX were monitored by FTIR, MACR and MVK were measured by PTR-ToF-MS, and HCHO was monitored by Aerolaser-4021.

For O₃+ISO, we have determined the formation yields for MACR, MVK, HCHO, CO and HCOOH. The measured MACR and MVK concentrations were corrected for reaction with O₃. The yields of MACR and MVK obtained under different experimental conditions (isoprene in excess or O₃ in excess with or without OH scavenger) are in general agreement with the literature values (Kamens et al., 1982; Niki et al., 1983; Paulson et al., 1992; Aschmann and Atkinson, 1994; Gutbrod et al., 1997b; Sauer et al., 1999a; Iannone et al., 2010; Nguyen et al., 2016) ranging from ≈ 30 to ≈ 40 % and ≈ 11 to ≈ 19 %, respectively, excluding the data from Paulson et al., (1992) in which higher values have been reported in absence of OH scavenger. Formaldehyde yield obtained in the present work was found to be between 45% and 90 % depending on the experimental conditions. $Y_{\text{HCHO}} = 45 \pm 9$ % in the runs with isoprene in excess over O₃ (in absence of cyclohexane), when O₃ was in excess $Y_{\text{HCHO}} = 69 \pm 10\%$ in the absence of cyclohexane and 90 ± 2 % in its presence. The observed difference might be an indication of the occurrence of additional sources/sinks to formaldehyde under such conditions. However, as shown in Table 3-5, the literature data (Nguyen et al., 2016; Sauer et al., 1999a; Gutbrod et al., 1997b; Niki et al., 1983; Kamens et al., 1982) report Y_{HCHO} ranging from 54 to 90 %. HCHO may be produced through different mechanisms involving Criegee intermediates as well as the chemistry of the OH radical scavengers, cyclohexane or methylcyclohexane used in different studies. Ongoing work in our laboratory is devoted to the understanding of the specific formation of formaldehyde through the investigated reactions. The CO formation yield measured in absence of OH scavenger and in excess of isoprene, $Y_{\text{CO}} = 21 \pm 3$ %, is in excellent agreement with the earlier work by Sauer et al., (1999a) under the same conditions who reported: 26 ± 1 %. The experiments conducted under excess of O₃ in the absence and presence of OH scavenger led to higher values: $Y_{\text{CO}} = 28 \pm 3$ and 41 ± 4 %, respectively. Formic acid yields, Y_{HCOOH} , under different experimental conditions were similar, $Y_{\text{HCOOH}} = 4 \pm 1$ %, which is in excellent agreement with

the measurements by Nguyen et al., (2016), Sauer et al., (1999a) and Neeb et al., (1997), $Y_{\text{HCOOH}} = 5 \pm 1\%$. Other products have been observed from the ozonolysis of isoprene but not mentioned here such as H₂O₂ and hydroxymethyl hydroperoxide (HMHP). This is a part of an ongoing work in our laboratory associated to the fate of the Criegee intermediates from a series of alkenes and dienes under atmospheric conditions using HELIOS chamber.

As for O₃+MACR and O₃+MVK reactions, the only studies reported so far are those from Grosjean et al., (1993) who conducted the experiments in excess of the organics in the presence of cyclohexane as the OH scavenger. They have reported yields for formaldehyde ($Y_{\text{HCHO}} = 12 \pm 3$ and 5 %) and methylglyoxal ($Y_{\text{MGLYOX}} = 58 \pm 6$ and 87 ± 5 %) for O₃+MACR and O₃+MVK, respectively. While a good agreement is observed between the present work and that from Grosjean et al., (1993) on the yields of methylglyoxal, a very large discrepancy exists in the formaldehyde yields as shown in Table 3-5.

Table 3-5: The product yields of the ozonolysis of isoprene, MACR and MVK under different experimental conditions.

Exp.	[organic]	[O ₃]	Y _{MACR} (%)	Y _{MVK} (%)	Y _{CO} (%)	Y _{HCOOH} (%)	Y _{HCHO} (%)	Y _{MGLYOX} (%)	T(K)	Reference
Isoprene+O ₃										
No Scavenger	2.5-8.9	0.3-0.9	29±6	10±1	21±3	3±1	45±9	-	283-286	This work*
No Scavenger	0.4-2.3	3.3-25.3	36±7	13±3	28±3	4±1	69±10	-	281-288	
w/ cHX	0.4-1.5	4.1-23.8	32±5	11±1	41±4	4±1	90±2	-	286-295	
w/ cHX	2.4	14.4	42±6	18±6	-	5	81±6	-	295	Nguyen et al., 2016
w/ CO	400	24	33.4±4.2	15.2±0.3	-	-	-	-	295	Iannone et al., 2010
No Scavenger	127	55.2	34±1	14±1	26±1	5±1	68±3	-	295±2	Sauer et al., 1999
No Scavenger	120	55			-	4	-	-		Neeb et al., 1997
w/ CO	504-576	200-230	30	20	-	-	55	-	298	Gutbrod et al., 1997
No Scavenger	504-576	200-230	28	21	-	-	54	-	298	Gutbrod et al., 1997
w/ cHX	45-48	5	38.7±3	15.9±1.3	-	-	-	-	296±2	Aschmann and
No Scavenger	45-48	5	33.9±2.6	19.1±1.5					296±2	Atkinson., 1994
w/ cHX	19.9	2.0	44±2	17±1			90±4	3	293±2	Grosjean et al., 1993
w/methyl-cHX	240-272	5760	37	17	-	-	-	-	298±8	Paulson et al., 1992
No Scavenger	312-408	5760	67±9	26±6					298±8	
No Scavenger	55	77	>33	>13	-	-	85	-		Niki et al., 1983
No Scavenger	22.3	16.9	41	18	-	-	90±5	-	295	Kamens et al., 1982
			39-44	16-17	-	-	90	-		IUPAC
MACR+O ₃										
No Scavenger	0.4-0.9	7.1-24.9			43±5	3±1	57±8	59±9	281-290	This work*
w/ cHX	0.3-0.8	8.7-24.9			44±6		66±4	-	285-288	
w/ cHX	21	1.4-2.1					12±3	58±6	293	
MVK+O ₃										
No Scavenger	0.7-0.8	6.4-8.5			22±2	4±1	38±6	71±6	286-289	This work*
w/ cHX	0.5-0.8	5.4-8.7			29±1	-	44±5	-	282-292	
w/ cHX	20	2.1			-	-	5	87±5	293	
										Grosjean et al., 1993

The units of [organic] and [O₃] in ×10¹² molecule cm⁻³, MGLYOX=methylglyoxal. * Average values determined from different experiments. Errors quoted are 1 standard deviation (SD) of different experiments.

As mentioned above, the ozonolysis of isoprene has been subject to numerous studies under different conditions (RH, presence or absence of OH scavengers). The general reaction scheme is similar to the ozonolysis of alkenes. The initial step involves the 1,3-dipolar addition of O₃ to C=C bond (cyclo-addition), which gives rise to the production of a 1,2,3-trioxolane (primary ozonide, POZ). The POZ is a short lived species that undergoes cycloreversion to form carbonyl oxides or Criegee intermediates (CIs) and carbonyls (aldehydes and ketones). Two reaction pathways exist for CIs, part of CIs have sufficient internal energy and are subjected to prompt unimolecular reaction to form a hydroperoxide intermediates through H migration which subsequently decomposes or isomerizes to give OH radical, carbonyls, CO₂ and other products, some of which are potential SOA precursors. The other part of CIs would go through collisional stabilization (SCI). SCI may undergo ring closure to form dioxirane that subsequently decomposes to HO₂ radical and other products via “hot acid intermediate”. Thermally stabilized SCI may also undergo bimolecular reactions with H₂O, HCHO and other species in the atmosphere. As isoprene is a conjugated diene, four possible product sets are formed due to two classes of cycloreversion pathway: methacrolein (MACR) and CH₂OO, formaldehyde (HCHO) and MACR oxide, methyl vinyl ketone (MVK) and CH₂OO, HCHO and MVK oxide following the formation of the two types of primary ozonides. MACR, MVK and HCHO are the dominant primary carbonyl products. The chemically activated MACR oxide and MVK oxide subsequently undergo decomposition and isomerization to form a number of products. The measured higher yield of MACR compared to MVK indicates that the O₃ reaction with isoprene occurs predominately through the attack on the CH₂=C(CH₃)- group.

The mechanisms of the ozonolysis of MACR and MVK have been subject to only one investigation each and from the same group, Grosjean et al., (1993). O₃+MACR leads to two channels, CH₃COCHO (methylglyoxal) + [CH₂COO]^{*} and HCHO + [CH₃COOCHO]^{*}, while O₃+MVK leads to CH₃COCHO (methylglyoxal) + [CH₂COO]^{*} and HCHO + [CH₃COCHOO]^{*}. In the present work, the experiments were performed in excess of O₃ over MACR and MVK. CO, HCHO, HCOOH and methylglyoxal have been observed from both reactions. The presence or absence of scavenger did not affect significantly the measured

yields of CO and HCHO but HCOOH and methylglyoxal were below the detection limit of our instrumentation in the experiments carried out in the presence of cyclohexane as OH scavenger. Formaldehyde formation yields were significantly higher than that reported from Grosjean et al (1993). Who conducted the experiments in excess of organics and added cyclohexane. Methylglyoxal yields obtained in the present work in absence of cyclohexane but using O₃ in excess are in agreement with those reported by Grosjean et al., (1993) conducted in the presence of cyclohexane under the organics in excess conditions. A large discrepancy is observed between the present measurements of the HCHO yields and those reported by Grosjean et al., (1993). Would this be due to some difficulties in analyzing HCHO in one of the two sets of experiments? Grosjean et al., (1993) have used HPLC analysis while we have used both in-situ FTIR and the sensitive and specific HCHO-AL4021 monitor based on Hantzsch reaction. Ongoing experiments in our laboratory are dedicated to check this possibility.

3-3-2-3- Secondary organic aerosol formation

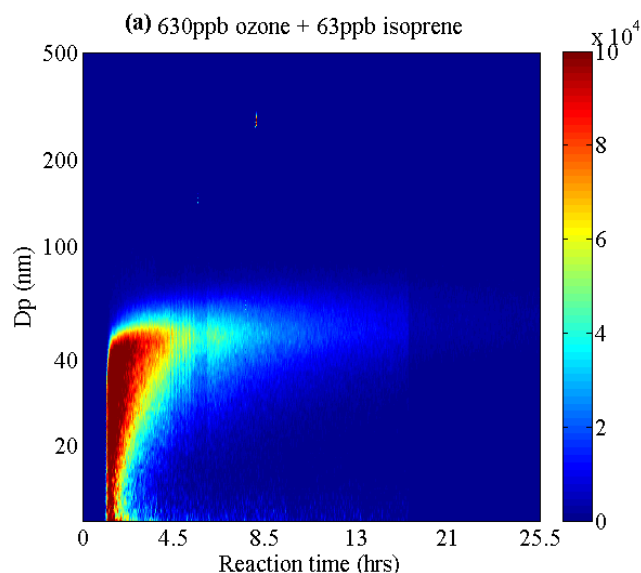
A limited number of runs were carried out to investigate the occurrence of secondary organic aerosol formation (SOA) during the ozonolysis of isoprene. The main aim of these runs was to check the capabilities of our new built chamber to study SOA formation. Experiments were conducted under the same experimental conditions as those used in the kinetic and products studies (excess of isoprene or O₃ and presence or absence of OH scavenger) in absence of added aerosol seeds. Particle size distributions from 10 to 490 nm were measured with a scanning mobility particle sizer (SMPS; Model 3934, TSI Inc.). Total particle number concentrations were monitored with condensation particle counter (CPC, TSI, Inc., 3022A) along with a differential mobility analyzer (TSI, Inc., 3081). Table 3-6 summarizes the experimental conditions and the aerosols yields obtained and Figure 3-7 displays examples of temporal profiles of SOA formation distribution under various experimental conditions (different initial concentrations of isoprene and O₃, with/without OH radical scavengers). The SOA yield (Y_{SOA}) was defined as the ratio of maximum SOA produced (ΔM_0 , $\mu\text{g}/\text{m}^3$) to the mass concentration

consumed ($\Delta[\text{isoprene}]$, $\mu\text{g}/\text{m}^3$), $Y_{\text{SOA}} = \Delta M_0 / (\Delta[\text{isoprene}])$ as Kleindienst et al., (2007). A density of $1 \text{ g}/\text{cm}^3$ was applied to convert the integrated SOA volume to mass concentration. The chamber wall loss of SOA was taken into account by applying a first order loss rate obtained from the decay of the particle volume concentration after reaching its maximum value for each individual experiment.

Table 3-6: Initial experimental conditions and results of secondary organic aerosol (SOA) mass concentration (ΔM_0) and SOA yield (Y_{SOA})^a.

Experimental conditions	[ISO] ₀ (ppb)	[O ₃] ₀ (ppb)	cHX (ppm)	[ISO] _{consumed} (ppb)	ΔM_0 (max) ($\mu\text{g}/\text{m}^3$)	Y_{SOA} (%)	T (K)
ISO in excess w/o cHX	354.6	27.4	-	29.0±1.6	2.9±0.15	3.3±0.3	283±1
	158.2	33.7	-	23.5±2.5	0.8±0.1	1.1±0.1	281±1
	220.6	42.5	-	35.1±3.6	6.4±0.5	6.1±1.0	281±1
O ₃ in excess w/o cHX	75.1	849.0	-	64.7±0.9	2.0±0.1	1.0±0.05	288±1
	64.6	627.5	-	54.6±1.1	1.9±0.2	1.1±0.2	285±1
	45.0	504.1	6.6	22.6±2.8	0.06±0.01	0.09±0.02	286±1
O ₃ in excess w/ cHX	58.6	670.9	7.5	31.4±4.5	0.25±0.01	0.26±0.04	295±1
	90.1	965.4	16.9	78.3±1.8	2.1±0.12	0.89±0.09	294±1
	58.4	672.5	11.8	32.6±2.9	0.52±0.05	0.53±0.07	291±1

^a Stated uncertainties were from scatter in particle volume measurements; ^b Assuming a density of $1.0 \text{ g}/\text{cm}^3$; ^c SOA yields were obtained from the maximum aerosol volume;



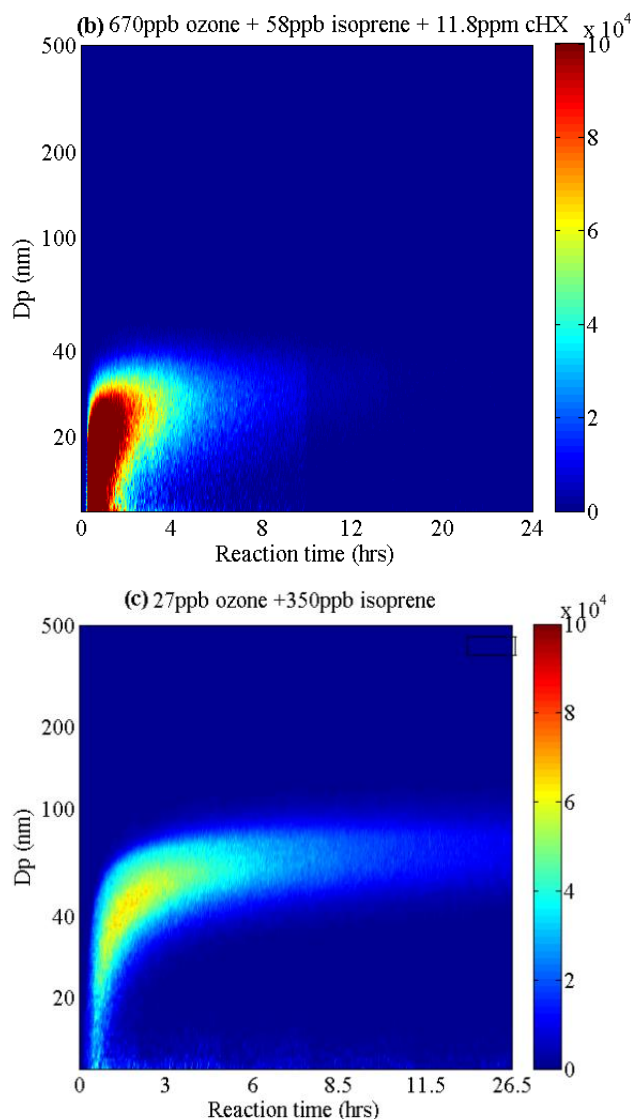


Figure 3-7(a-c): – Examples of temporal profiles of SOA formation (number concentration) under various experimental conditions including different initial concentrations of isoprene and O₃, with/without OH radical scavengers.

Figures 3-7(a-c) and 3-8 show, respectively, the prompt formation of SOA with the initiation of the reaction and their growth as function of the consumed isoprene under the three experimental conditions used in this study. The SOA yields obtained depend on the experimental conditions as shown in Table 3-6. In excess of isoprene and absence of cyclohexane, the SOA yield was $Y_{\text{SOA}} \approx 3.5 \pm 2.5 \%$, higher than that obtained during the experiments conducted in excess of ozone in both, without and with cyclohexane added, $Y_{\text{SOA}} \approx 1.0 \pm 0.2 \%$ and $< 1\%$, respectively. These data have to be considered as

preliminary and more experiments need to be carried out under wider experimental conditions in order to characterize more precisely the SOA yields. However, it has to be noted that the earlier studies conducted on the aerosol formation from the ozonolysis of isoprene have reported formation yields of $\approx 1\%$ (Kleindienst et al., (2007)) or less (e.g. Jang et al., (2002), Czoschke et al., (2003)) depending on the experimental conditions.

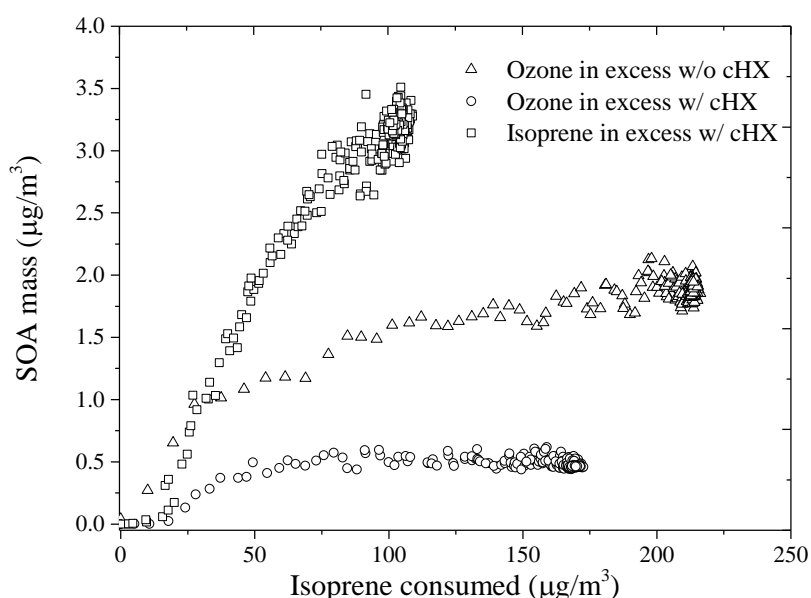


Figure 3-8: SOA growth as a function of consumed isoprene concentration under different experimental conditions.

3.4- Conclusions and future work

A series of experiments were carried out using the new built simulation chamber, HELIOS, to check its capacities in investigating complex gas phase processes. The characteristics of HELIOS enable us to conduct studies under ambient temperatures, typically around $\approx 10\text{ }^{\circ}\text{C}$ ($\approx 283\text{ K}$) from late autumn to early spring in the Orleans (France) area. The analytical equipment at the facility makes investigations under wide range concentrations of the reactants and products, from ppb to ppm levels, possible. In the current paper, we describe a first set of data obtained on the ozonolysis of isoprene, one of the most important VOCs in the atmosphere, and its main oxidation products, methacrolein and methyl vinyl ketone. Reactions rate constants for the reactions of ozone with the above organic species

have been measured in the ambient temperature range 281-295 K under different experimental conditions such as initial reactants concentrations, excess of O₃ over the organics and vis-versa in presence or absence of OH scavenger. The obtained values for $k_{O_3+organic}$ have been found in good agreement with the recommended values calculated using the Arrhenius expressions from IUPAC panel.

A section of the present work is dedicated to the OH radical and stable products formation from the investigated reactions. OH radical formation yield is reported for the three reactions, $Y_{OH} = 24 \pm 2\%$ from O₃+ISO, $14.3 \pm 3.5\%$ from O₃+MACR and $13.4 \pm 4.1\%$ from O₃+MVK. The OH formation yield has been subject to numerous studies (Paulson et al., 1992; Atkinson and Aschmann, 1993; Gutbrod et al., 1997b; Donahue et al., 1998; Paulson et al., 1998; Rickard et al., 1999; Neeb and Moortgat, 1999; Lewin et al., 2001; Iannone et al., 2010; Nguyen et al., 2016). Our measured value is in excellent agreement with the preferred value from IUPAC panel, $Y_{OH}=25\%$. The OH formation yield from O₃+MACR and O₃+MVK have been measured earlier in a very limited number of studies. The value obtained here for O₃+MACR reaction is in agreement with that from Aschmann et al., (1996), 20^{+10}_{-13} and that for O₃+MVK is in excellent agreement with the one measured by Aschmann et al., (1996), $18 \pm 8\%$ and by Paulson et al., (1998) $16 \pm 5\%$. Yields for series stable oxidation products are reported and compared to the literature data. We report here formation yields for MACR, MVK, HCHO, HCOOH and CO. The general trends of the obtained values are in line with the recommended IUPAC values for O₃ reaction with isoprene. The product yields obtained for the reactions of O₃ with MACR and MVK are also compared to those from the single available study on these reactions from Grosjean et al., (1993).

In addition to the gas phase product, a limited number of runs were performed to estimate the SOA formation yields from ozonolysis of isoprene which showed that the yields values depend on the initial experimental conditions. However, the experiments conducted in presence of OH scavenger ($\leq 1\%$) were lower than the ones in its absence (1-3.5%) which indicates a potential contribution of OH chemistry in the SOA production observed.

Work is ongoing in our laboratory to investigate the complete chemistry of the studied reactions by using wider set of analytical equipment for the analysis of unstable species as well as peroxides and hydroperoxydes. To this aim, new instrumentation such as API-ToF-CIMS and UHPLC-MS have been recently connected to the HELIOS chamber for the analysis of the missing organic fraction as well as characterizing the aerosol composition. The chamber is large enough to enable the collection of sufficient aerosol mass for chemical analysis. In addition, the CNRS-Orleans CIMS dedicated to the OH and HO₂ measurements will be used to conduct the ongoing work.

References

- Adeniji, S. A., Kerr, J. A., and Williams, M. R.: RATE CONSTANTS FOR OZONE-ALKENE REACTIONS UNDER ATMOSPHERIC CONDITIONS, *International Journal of Chemical Kinetics*, 13, 209-217, 10.1002/kin.550130210, 1981.
- Alam, M. S., Rickard, A. R., Camredon, M., Wyche, K. P., Carr, T., Hornsby, K. E., Monks, P. S., and Bloss, W. J.: Radical Product Yields from the Ozonolysis of Short Chain Alkenes under Atmospheric Boundary Layer Conditions, *The Journal of Physical Chemistry A*, 117, 12468-12483, 10.1021/jp408745h, 2013.
- Aschmann, S. M., and Atkinson, R.: Formation Yields of Methyl Vinyl Ketone and Methacrolein from the Gas-Phase Reaction of O₃ with Isoprene, *Environmental Science & Technology*, 28, 1539-1542, 10.1021/es00057a025, 1994.
- Aschmann, S. M., Arey, J., and Atkinson, R.: OH radical formation from the gas-phase reactions of O₃ with methacrolein and methyl vinyl ketone, *Atmospheric Environment*, 30, 2939-2943, [http://dx.doi.org/10.1016/1352-2310\(96\)00013-1](http://dx.doi.org/10.1016/1352-2310(96)00013-1), 1996.
- Atkinson, R., Winer, A. M., and Pitts Jr, J. N.: Rate constants for the gas phase reactions of O₃ with the natural hydrocarbons isoprene and α - and β -pinene, *Atmospheric Environment* (1967), 16, 1017-1020, [http://dx.doi.org/10.1016/0004-6981\(82\)90187-1](http://dx.doi.org/10.1016/0004-6981(82)90187-1), 1982.
- Atkinson, R., and Aschmann, S. M.: Hydroxyl radical production from the gas-phase reactions of ozone with a series of alkenes under atmospheric conditions, *Environmental Science & Technology*, 27, 1357-1363, 10.1021/es00044a010, 1993.
- Atkinson, R., and Arey, J.: Atmospheric degradation of volatile organic compounds, *Chemical reviews*, 103, 4605-4638, 10.1021/cr0206420, 2003.
- Atkinson, R., Baulch, D. L., Cox, R. A., Crowley, J. N., Hampson, R. F., Hynes, R. G., Jenkin, M. E., Rossi, M. J., Troe, J., and Subcommittee, I.: Evaluated kinetic and photochemical data for atmospheric chemistry: Volume II – gas phase reactions of organic species, *Atmos. Chem. Phys.*, 6, 3625-4055, 10.5194/acp-6-3625-2006, 2006.

- Avzianova, E. V., and Ariya, P. A.: Temperature-dependent kinetic study for ozonolysis of selected tropospheric alkenes, *International Journal of Chemical Kinetics*, 34, 678-684, 10.1002/kin.10093, 2002.
- Chew, A. A., and Atkinson, R.: OH radical formation yields from the gas-phase reactions of O₃ with alkenes and monoterpenes, *Journal of Geophysical Research: Atmospheres*, 101, 28649-28653, 10.1029/96JD02722, 1996.
- Czochke, N. M., Jang, M., and Kamens, R. M.: Effect of acidic seed on biogenic secondary organic aerosol growth, *Atmospheric Environment*, 37, 4287-4299, [http://dx.doi.org/10.1016/S1352-2310\(03\)00511-9](http://dx.doi.org/10.1016/S1352-2310(03)00511-9), 2003.
- Donahue, N. M., Kroll, J. H., Anderson, J. G., and Demerjian, K. L.: Direct observation of OH production from the ozonolysis of olefins, *Geophysical Research Letters*, 25, 59-62, 10.1029/97gl53560, 1998.
- Greene, C. R., and Atkinson, R.: RATE CONSTANTS FOR THE GAS-PHASE REACTIONS OF O₃ WITH A SERIES OF ALKENES AT 296-K \pm 2-K, *International Journal of Chemical Kinetics*, 24, 803-811, 10.1002/kin.550240905, 1992.
- Grosjean, D., Williams, E. L., and Grosjean, E.: Atmospheric chemistry of isoprene and of its carbonyl products, *Environmental Science & Technology*, 27, 830-840, 10.1021/es00042a004, 1993.
- Grosjean, E., and Grosjean, D.: Rate constants for the gas-phase reaction of ozone with 1,1-disubstituted alkenes, *International Journal of Chemical Kinetics*, 28, 911-918, 10.1002/(sici)1097-4601(1996)28:12<911::aid-kin8>3.0.co;2-q, 1996.
- Guenther, A., Karl, T., Harley, P., Wiedinmyer, C., Palmer, P. I., and Geron, C.: Estimates of global terrestrial isoprene emissions using MEGAN (Model of Emissions of Gases and Aerosols from Nature), *Atmos. Chem. Phys.*, 6, 3181-3210, 10.5194/acp-6-3181-2006, 2006.
- Gutbrod, R., Kraka, E., Schindler, R. N., and Cremer, D.: Kinetic and Theoretical Investigation of the Gas-Phase Ozonolysis of Isoprene: Carbonyl Oxides as an Important Source for OH Radicals in the Atmosphere, *Journal of the American Chemical Society*, 119, 7330-7342, 10.1021/ja970050c, 1997a.

- Gutbrod, R., Kraka, E., Schindler, R. N., and Cremer, D.: Kinetic and theoretical investigation of the gas-phase ozonolysis of isoprene: Carbonyl oxides as an important source for OH radicals in the atmosphere, *Journal of the American Chemical Society*, 119, 7330-7342, 10.1021/ja970050c, 1997b.
- Iannone, R., Koppmann, R., and Rudolph, J.: Stable carbon kinetic isotope effects for the production of methacrolein and methyl vinyl ketone from the gas-phase reactions of isoprene with ozone and hydroxyl radicals, *Atmospheric Environment*, 44, 4135-4141, <http://dx.doi.org/10.1016/j.atmosenv.2010.07.046>, 2010.
- Jang, M., Czoschke, N. M., Lee, S., and Kamens, R. M.: Heterogeneous Atmospheric Aerosol Production by Acid-Catalyzed Particle-Phase Reactions, *Science*, 298, 814-817, 10.1126/science.1075798, 2002.
- Kamens, R. M., Gery, M. W., Jeffries, H. E., Jackson, M., and Cole, E. I.: Ozone–isoprene reactions: Product formation and aerosol potential, *International Journal of Chemical Kinetics*, 14, 955-975, 10.1002/kin.550140902, 1982.
- Karl, M., Brauers, T., Dorn, H. P., Holland, F., Komenda, M., Poppe, D., Rohrer, F., Rupp, L., Schaub, A., and Wahner, A.: Kinetic Study of the OH-isoprene and O₃-isoprene reaction in the atmosphere simulation chamber, SAPHIR, *Geophysical Research Letters*, 31, L05117, 10.1029/2003GL019189, 2004.
- Khamaganov, V. G., and Hites, R. A.: Rate Constants for the Gas-Phase Reactions of Ozone with Isoprene, α - and β -Pinene, and Limonene as a Function of Temperature, *The Journal of Physical Chemistry A*, 105, 815-822, 10.1021/jp002730z, 2001.
- Klawatsch-Carrasco, N., Doussin, J. F., and Carlier, P.: Absolute rate constants for the gas-phase ozonolysis of isoprene and methylbutenol, *International Journal of Chemical Kinetics*, 36, 152-156, 10.1002/kin.10175, 2004.
- Kleindienst, T. E., Lewandowski, M., Offenberg, J. H., Jaoui, M., and Edney, E. O.: Ozone-isoprene reaction: Re-examination of the formation of secondary organic aerosol, *Geophysical Research Letters*, 34, L01805, 10.1029/2006GL027485, 2007.

- Kroll, J. H., Hanisco, T. F., Donahue, N. M., Demerjian, K. L., and Anderson, J. G.: Accurate, direct measurements of OH yields from gas-phase ozone-alkene reactions using an in situ LIF Instrument, *Geophysical Research Letters*, 28, 3863-3866, 10.1029/2001GL013406, 2001.
- Lewin, A. G., Johnson, D., Price, D. W., and Marston, G.: Aspects of the kinetics and mechanism of the gas-phase reactions of ozone with conjugated dienes, *Physical Chemistry Chemical Physics*, 3, 1253-1261, 10.1039/B010006O, 2001.
- Müller, M., Mikoviny, T., Jud, W., D'Anna, B., and Wisthaler, A.: A new software tool for the analysis of high resolution PTR-TOF mass spectra, *Chemometrics and Intelligent Laboratory Systems*, 127, 158-165, <http://dx.doi.org/10.1016/j.chemolab.2013.06.011>, 2013.
- Malkin, T. L., Goddard, A., Heard, D. E., and Seakins, P. W.: Measurements of OH and HO₂ yields from the gas phase ozonolysis of isoprene, *Atmos. Chem. Phys.*, 10, 1441-1459, 10.5194/acp-10-1441-2010, 2010.
- Neeb, P., Sauer, F., Horie, O., and Moortgat, G. K.: Formation of hydroxymethyl hydroperoxide and formic acid in alkene ozonolysis in the presence of water vapour, *Atmospheric Environment*, 31, 1417-1423, [http://dx.doi.org/10.1016/S1352-2310\(96\)00322-6](http://dx.doi.org/10.1016/S1352-2310(96)00322-6), 1997.
- Neeb, P., and Moortgat, G. K.: Formation of OH Radicals in the Gas-Phase Reaction of Propene, Isobutene, and Isoprene with O₃: Yields and Mechanistic Implications, *The Journal of Physical Chemistry A*, 103, 9003-9012, 10.1021/jp9903458, 1999.
- Newland, M. J., Rickard, A. R., Vereecken, L., Muñoz, A., Ródenas, M., and Bloss, W. J.: Atmospheric isoprene ozonolysis: impacts of stabilized Criegee intermediate reactions with SO₂, H₂O and dimethyl sulfide, *Atmos. Chem. Phys. Discuss.*, 15, 8839-8881, 10.5194/acpd-15-8839-2015, 2015.
- Nguyen, T. B., Tyndall, G. S., Crounse, J. D., Teng, A. P., Bates, K. H., Schwantes, R. H., Coggon, M. M., Zhang, L., Feiner, P., Milller, D. O., Skog, K. M., Rivera-Rios, J. C., Dorris, M., Olson, K. F., Koss, A., Wild, R. J., Brown, S. S., Goldstein, A. H., de Gouw, J. A., Brune, W. H., Keutsch, F. N., Seinfeld, J. H., and Wennberg, P. O.: Atmospheric fates of Criegee intermediates in the ozonolysis of isoprene, *Physical Chemistry Chemical Physics*, 18, 10241-10254, 10.1039/C6CP00053C, 2016.

- Niki, H., Maker, P. D., Savage, C. M., and Breitenbach, L. P.: Atmospheric ozone-olefin reactions, *Environmental Science & Technology*, 17, 312A-322A, 10.1021/es00113a720, 1983.
- Paulson, S. E., Flagan, R. C., and Seinfeld, J. H.: Atmospheric photooxidation of isoprene part II: The ozone-isoprene reaction, *International Journal of Chemical Kinetics*, 24, 103-125, 10.1002/kin.550240110, 1992.
- Paulson, S. E., Chung, M., Sen, A. D., and Orzechowska, G.: Measurement of OH radical formation from the reaction of ozone with several biogenic alkenes, *Journal of Geophysical Research*, 103, 25533, 10.1029/98jd01951, 1998.
- Rickard, A. R., Johnson, D., McGill, C. D., and Marston, G.: OH yields in the gas-phase reactions of ozone with alkenes, *Journal of Physical Chemistry A*, 103, 7656-7664, 10.1021/jp9916992, 1999.
- Sato, K., Inomata, S., Xing, J.-H., Imamura, T., Uchida, R., Fukuda, S., Nakagawa, K., Hirokawa, J., Okumura, M., and Tohno, S.: Effect of OH radical scavengers on secondary organic aerosol formation from reactions of isoprene with ozone, *Atmospheric Environment*, 79, 147-154, <http://dx.doi.org/10.1016/j.atmosenv.2013.06.036>, 2013.
- Sauer, F., Schäfer, C., Neeb, P., Horie, O., and Moortgat, G. K.: Formation of hydrogen peroxide in the ozonolysis of isoprene and simple alkenes under humid conditions, *Atmospheric Environment*, 33, 229-241, [http://dx.doi.org/10.1016/S1352-2310\(98\)00152-6](http://dx.doi.org/10.1016/S1352-2310(98)00152-6), 1999a.
- Sauer, F., Schafer, C., Neeb, P., Horie, O., and Moortgat, G. K.: Formation of hydrogen peroxide in the ozonolysis of isoprene and simple alkenes under humid conditions, *Atmospheric Environment*, 33, 229-241, 10.1016/s1352-2310(98)00152-6, 1999b.
- Schäfer, C., Horie, O., Crowley, J. N., and Moortgat, G. K.: Is the hydroxyl radical formed in the gas-phase ozonolysis of alkenes?, *Geophysical Research Letters*, 24, 1611-1614, 10.1029/97GL01545, 1997.
- Sipila, M., Jokinen, T., Berndt, T., Richters, S., Makkonen, R., Donahue, N. M., Mauldin, R. L., III, Kurten, T., Paasonen, P., Sarnela, N., Ehn, M., Junninen, H., Rissanen, M. P., Thornton, J., Stratmann, F., Herrmann, H., Worsnop, D. R., Kulmala, M., Kerminen, V. M., and Petaja, T.: Reactivity of stabilized Criegee intermediates (sCIs) from isoprene and monoterpene ozonolysis toward SO₂ and organic acids, *Atmospheric Chemistry and Physics*, 14, 12143-12153, 10.5194/acp-14-12143-2014, 2014.

Treacy, J., Elhag, M., Ofarrell, D., and Sidebottom, H.: REACTIONS OF OZONE WITH UNSATURATED ORGANIC-COMPOUNDS, *Berichte Der Bunsen-Gesellschaft-Physical Chemistry Chemical Physics*, 96, 422-427, 1992.

Zimmerman, P. R., Greenberg, J. P., and Westberg, C. E.: Measurements of atmospheric hydrocarbons and biogenic emission fluxes in the Amazon Boundary layer, *Journal of Geophysical Research: Atmospheres*, 93, 1407-1416, 10.1029/JD093iD02p01407, 1988.

Chapter 4.

Photolysis study: comparing and contrasting fluorinated and non-fluorinated 2-methyl-3-pentanone

Chapter 4 - Photolysis study: comparing and contrasting fluorinated and non-fluorinated 2-methyl-3-pentanone.....	103
4-1- Introduction.....	104
4-2- Experimental Section	105
4-2-1- UV absorption spectra	105
4-2-2- Outdoor atmospheric simulation chambers	106
4-2-2-1- HELIOS chamber	106
4-2-2-1- 3.4 m ³ outdoor chamber.....	107
4-2-3- Photolysis experiments	108
4-2-4- Loss correction.....	109
4-2-5- Chemicals	110
4-3- Results and Discussion.....	110
4-3-1- UV absorption cross section	110
4-3-2- Photolysis rate of PF-2M3P	114
4-3-3- Photolysis products of PF-2M3P	118
4-3-4- Photolysis rate of 2-methyl-3-pentanone.....	124
4-3-5- Mechanism of the 2M3P photolysis.....	125
4-3-6- Comparison of photolysis mechanism between PF-2M3P and 2M3P	131
4-3-7- Kinetics of PF-2M3P and 2M3P reaction with O ₃	131
4-3-8- The Global Warming Potential (GWP)	134
4-3-8-1- Radiative Forcing (RF) and Radiative Efficiency (RE)	134
4-3-8-2- Infrared absorption cross section	135
4-4- Atmospheric Implication and Conclusion	136
References	139

Chapter 4 - Photolysis study: comparing and contrasting fluorinated and non-fluorinated 2-methyl-3-pentanone

Abstract:

The UV-Vis absorption spectra and photolysis of *Perfluoro-2-methyl-3-pentanone* and *2-methyl-3-pentanone* by natural sunlight have been investigated at the large outdoor atmospheric simulation chamber (HELIOS) of CNRS-Orléans/France. The photolysis rate of PF-2M3P was obtained from HELIOS chamber (September, 2013) and 3.4 m³ chamber (July, 2010): (1.1-3.8) and (1.7-2.8)×10⁻⁶ s⁻¹, respectively. The photolysis rate of 2M3P equaled (1.9-3.4)×10⁻⁶ s⁻¹ by using HELIOS chamber in the period of October, 2013. The effective quantum yield of PF-2M3P and 2M3P were obtained under natural tropospheric sunlight conditions, of with 0.008-0.017 and 0.139-0.179, respectively. The photolysis of PF-2M3P gives CF₃C(O)F (74±1)%, COF₂ (191±8)% and CO (196±50)% with no quantified perfluoro-propionic acid (CF₃CF₂C(O)OH, PFPrA) and trifluoro-acetic acid (CF₃COOH, TFA) as the products. The photolysis of 2M3P gives CH₃CHO (80±9)%, HCHO (27±4)%, CH₃COCH₃ (90±6)% and CO (97±6)% as the products. By analogy to other (perfluoro)-ketone, the photolysis mechanism of PF-2M3P and 2M3P were proposed. Some different reaction pathways happen in the photolysis of 2M3P compared with PF-2M3P, and which need more investigation in experiment and modeling. The ozonolysis experiments were conducted in the HELIOS chamber, it indicated that both of the PF-2M3P and 2M3P do not react with O₃ and the upper limits for rate constants were established: $k_{\text{PF-2M3P}} < (2.2 \pm 0.2) \times 10^{-22}$ and $k_{\text{2M3P}} < (5.2 \pm 0.2) \times 10^{-22}$ cm³ molecule⁻¹ s⁻¹, respectively.

4-1- Introduction

Over the last decade, perfluorocarbons (PFCs) have been widely used for the cooling of power electronics. Along with hydrofluorocarbons (HFCs), perfluorocarbons (PFCs) are non-ozone depleting substances and therefore excluded from the Montreal Protocol (Forrest et al., 2013). However, HFCs and PFCs are greenhouse gases due to their long atmospheric lifetimes and their strong absorption in the infrared spectral region (Yao et al., 2012). Atmospheric concentrations of HFCs and PFCs have been growing rapidly over last decades and potentially continue to grow (Schaefer et al., 2006).

Perfluoro-2-methyl-3-pentanone (PF-2M3P, $\text{C}_2\text{F}_5\text{C}(\text{O})\text{CF}(\text{CF}_3)_2$, Novec 649/1230) is an advanced heat transfer perfluorocarbon with high dielectric strength. This fully fluorinated carbonyl compound may have an important climate impact if it lives for longtime once released into the atmosphere. Similarly to other fluorocarbons, PF-2M3P may be removed from the atmosphere through a number of physico-chemical processes such as photolysis by sunlight, chemical reactions with the main atmospheric oxidants, hydrolysis and deposition. The atmospheric fate of PF-2M3P has been subject to a limited number of investigations. Photolysis studies were based on the use of natural (Diaz-de-Mera et al., 2015; D'Anna et al., 2005) and artificial (Taniguchi et al., 2003) irradiations. The gas phase reactions with OH radicals and ozone have been proposed to have a minor contribution to the total removal of PF-2M3P from the atmosphere (Taniguchi et al., 2003). Hydrolysis of PF-2M3P was also suggested to be a minor pathway in the control of its atmospheric fate (Jackson et al., 2011).

The present work aims at evaluating the natural sunlight photolysis as removal process of PF-2M3P under atmospheric relevant conditions by using two different outdoor simulation chambers. In addition, experiments have been conducted under the same conditions on the photolysis of the non-halogenated analogue aliphatic ketone to perfluoro-2-methyl-3-pentanone: 2-Methyl-3-pentanone (2M3P, $\text{C}_2\text{H}_5\text{C}(\text{O})\text{CH}(\text{CH}_3)_2$). To the best of our knowledge, no experimental data on the photolysis of 2M3P under

natural condition have been reported so far. The UV-Visible absorption spectra of both ketones have been measured and their photolysis under sunlight condition investigated. In addition, limited runs were performed to derive the rate constants of O_3 with the compounds of interest. The data obtained are presented and discussed in terms of the photolysis pathways and atmospheric impact.

4-2- Experimental Section

4-2-1- UV absorption spectra

The apparatus used in this work has been described in previous studies (Mu and Mellouki, 2000) and is briefly presented here. The UV-Vis absorption spectra of PF-2M3P and 2M3P were measured by a spectrophotometer equipped with a 1200 grooves mm^{-1} grating and a CCD camera. The collimated output of a 30 W deuterium lamp passed through a 100 cm long and 2.5 cm diameter Pyrex absorption cell equipped with quartz windows and focused onto the entrance slit of the spectrometer. Measurements were made over the wavelength region 220–400 nm by recording typically three overlapping regions of about 15 nm. Each measurement consisted of 8-13 scans of diode array. The wavelength scale was calibrated using the emission lines from a low-pressure Hg pen ray lamps (253.7, 313.2, and 365 nm). Absorption cross sections, $\sigma(\lambda)$ (in $\text{cm}^2 \text{ molecule}^{-1}$) were obtained using the Beer's law:

$$\sigma(\lambda) = \frac{-[I(\lambda)/I_0(\lambda)]}{CL} \quad \text{Eq. (a)}$$

where L is the path length of absorption cell (in cm), and C is the concentration of the studied compound (in molecule cm^{-3}). $I_0(\lambda)$ and $I(\lambda)$ are the light intensities in the absence and in the presence of the compound in the absorption cell, respectively. The concentration of the species of interest in the absorption cell was obtained from the measured pressure in the cell using a 0-10 Torr capacitance manometer. Measurements of the PF-2M3P and 2M3P UV absorption spectra were performed at $T=(292 \pm 1) \text{ K}$ using the concentration ranges of $[\text{PF-2M3P}]_0 = (0.29 - 2.7) \times 10^{17}$ and

$$[2\text{M3P}]_0 = (0.43 - 2.9) \times 10^{17} \text{ molecule cm}^{-3}.$$

4-2-2- Outdoor atmospheric simulation chambers

Photolysis of both, PF-2M3P and 2M3P, have been conducted in HELIOS and a limited number of runs on the photolysis of PF-2M3P was performed in a smaller outdoor chamber.

4-2-2-1- HELIOS chamber

The facility consists of 90 m³ hemispherical outdoor simulation chamber (47°50'18.39N; 1°56'40.03E) made of FEP Teflon film. The light transmission ranges from 88 to 95% over the entire solar spectrum. Two fans installed in the chamber ensure a rapid mixing of reactants (within 90 seconds). Purified air is supplied by an AADCO (AADCO Instruments, Inc., 737 series) pure air generation system. Solar actinic flux (290-660 nm) and photolysis frequencies of H₂O₂, HONO, HCHO, NO₃, NO₂ and O¹D were measured by a spectroradiometer (Meteorologie Consult GmbH 6007). Pressure, relative humidity and temperature were continuously measured by a three-axis Ultrasonic Anemometer (Delta Ohm, HD 2003) installed in the center of the chamber. In addition, in order to measure the temperature distribution within the chamber, six thermocouples (PT-100) spatially and equally distributed were used. The chamber is protected from “severe” weather conditions such as rain and strong wind by a mobile protective housing which is also used to keep the chamber in full dark conditions. The chamber can be fully exposed to sunlight with 30 s by moving the protective housing. During the photolysis, the chamber was typically exposed to solar irradiation during 3 to 7 hours, in which the temperature typically increased by ≈ 10 °C.

Organic compounds were monitored by in situ Fourier transform infrared spectrometry (FT-IR, Bruker Vertex70 spectrometer) coupled to a White-type multipass cell (302.6 m optical path length). Infrared spectra were recorded every 3 minutes by co-adding 250 interferograms with a resolution of 0.4 cm⁻¹. Quantitative

analysis of infrared spectra was performed either by subtraction or integration of the peak area using calibrated spectra. The gas phase mixture was also analyzed using a gas chromatography coupled to a mass spectrometer (GC-MS, PekinElmer Clarus 600 C). Gas samples were collected from the chamber at low temperature (-30 °C) onto Air Toxics tubes and analyzed through a thermal desorber (TurboMatrix™ 150 ATD), with split mode, followed by a thermal desorption at 300 °C (5 min) delivering the sample to a 60-m column (GasPro diameter 0.320mm). The temperature of the GC oven was programmed as follows: for PF-2M3P: 100 °C held for 5 min, then 15 °C min⁻¹ to 250 °C; and for 2M3P: 150 °C held for 10 min, then 50 °C min⁻¹ to 300 °C and held for 12 min. The presence of ozone and NO-NO_x concentrations were checked continuously by UV absorption (HORIBA, APOA 370) and a chemiluminescence analyzer (HORIBA, APNA 360), respectively.

PF-2M3P and 2M3P were introduced into the chamber by placing known volumes in a bubbler and flushed by purified air. Their concentrations were derived by considering the volume of the liquid introduced, the pressure and the temperature using the ideal gas law. Gaseous reactants (i.e., SF₆) were injected into the chamber using a calibrated gas cylinder equipped with capacitance manometers. In order to compensate sampling flows and leaks, a flow of purified air (15-25 L/min) was added continuously during all experiments enabling to maintain a slight inner overpressure, avoiding any contamination from outside air. Dilution of the gas volume in the chamber was determined by monitoring the decay of introduced amount of SF₆ (monitored by FT-IR). This decay was found to be in the range of $(5 - 20) \times 10^{-6} \text{ s}^{-1}$. Between each experiment, the chamber was cleaned by flushing for at least 12 hours. Background concentrations in the chamber were systematically checked and found to be below the detection limits of analytical instruments (e.g., [NO_x] < 1.3 × 10¹⁰, [O₃] < 1.3 × 10¹⁰, [VOC] < 1.3 × 10⁸ molecule cm⁻³).

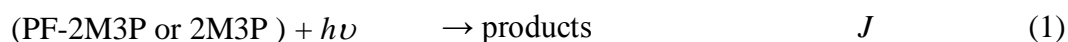
4-2-2-1- 3.4 m³ outdoor chamber

Studies of the photolysis of PF-2M3P were also performed in the 3.4 m³ ICARE

outdoor atmospheric simulation chamber made of ethylene tetrafluoroethylene (ETFE) foil. The light intensity was continuously measured using a filter radiometer measuring the photolysis frequency of NO₂, J_{NO_2} (Meteorologie consult gmbh, Germany). The temperature and the relative humidity were continuously measured using a combined probe (Vaisala HMT330 series transmitters). Chemical analysis of the gas mixture was characterised by an infrared spectrometer (Nicolet 550 Magna FT-IR spectrometer) coupled to a White-type multi-pass mirror cell (optical path length 10 meters). Infrared spectra were recorded every 5 minutes by co-adding 130 interferograms at a resolution of 1 cm⁻¹. A fan made of Teflon was also mounted into the chamber in order to ensure rapid mixing of reactant. Similarly the HELIOS experiment, the dilution rate was estimated by monitoring the loss of SF₆. IR reference spectrum of PF-2M3P was obtained by introducing a known volume of liquid in the chamber. During dark experiments, the chamber was covered by a black and opaque curtain in order to protect it from sunlight radiation which could be removed very quickly to expose to solar radiation to initiate the photolysis. Experiments were performed at 1013 mbar of purified air and in the temperature range 306 to 319 K. Initial concentrations were: [PF-2M3P]₀ = (0.89-2.7) × 10¹⁴ molecule cm⁻³. The gas mixture was exposed to solar irradiation for maximum of 4 hours.

4-2-3- Photolysis experiments

Under sunlight conditions, PF-2M3P and 2M3P may be removed by photolysis, dilution and wall processes following the reactions:



Where J is the photolysis rate of PF-2M3P or 2M3P while k_L is their decay rate under

the dark which includes dilution and wall loss, J and k_L are in s^{-1} . $k_{d,dark}$ and $k_{d,light}$ (in s^{-1}) are, respectively, the dilution decay rates obtained from SF_6 decay in the dark and during irradiation which could be slightly different depending on the wind conditions. Under irradiation, the total decays of PF-2M3P and 2M3P are obtained as follows:

$$\ln([Compound]_0/[Compound]_t) = k_{tot} \times t$$

with $[Compound]_0$ and $[Compound]_t$ are the concentration of PF-2M3P or 2M3P at times t_0 and t , respectively. k_{tot} (in s^{-1}), the total decay rate of the compound under irradiation, is expressed as:

$$k_{tot} = J_{meas} + k_{d,light} + (k_L - k_{d,dark})$$

The atmospheric photolysis rate coefficient can be also calculated, J_{calc} , and compared to the measured one, J_{mea} . J_{calc} is obtained from the measured cross sections:

$$J_{calc} = \int \sigma(\lambda)\Phi(\lambda)F(\lambda)d\lambda \quad (\lambda = 290-400 \text{ nm}) \quad \text{Eq. (b)}$$

where $\sigma(\lambda)$, $\Phi(\lambda)$ and $F(\lambda)$ are the absorption cross-section, the quantum yield of dissociation and the actinic flux over the absorption 290 to 400 nm. The actinic flux was directly measured by a GmbH 6007 spectroradiometer placed inside the chamber. Assuming the quantum yield for photodissociation is unity across the absorption region of PF-2M3P or 2M3P, the maximum photolytic rate coefficient can be calculated, $J_{max} = J_{cal}$ when $\Phi = 1$ for both compounds using Eq. (b). An effective photodissociation quantum yield can then be derived from the ratio:

$$\Phi_{eff} = J_{meas}/J_{max} \quad \text{Eq. (c)}$$

4-2-4- Loss correction

The concentration of each product formed from the photolysis of PF-2M3P and 2M3P was corrected to account for dilution and its possible photolysis under irradiation. $[Pro]_{corr}$ (in molecule cm^{-3}) was determined iteratively using the following recursive discrete time equation:

$$[Pro]_{i,corr} = [Pro]_{i-1,corr} + \Delta[Pro] + [Pro]_{i-1} \Delta t(k_{d,light} + J_{pro})$$

Where $[\text{Pro}]_{i,\text{corr}}$ (in molecule cm^{-3}) is the corrected concentration of the product at measured time i , $[\text{Pro}]_{i-1}$ (in molecule cm^{-3}) is the measured product concentration at time $i-1$, Δt (in s) is the time between measured i and $i-1$, $\Delta[\text{Pro}]$ (in molecule cm^{-3}) is the observed net change in $[\text{Pro}]$ that occurs over Δt , $k_{\text{d,light}}$ is the dilution decay rate obtained from SF_6 during irradiation (in s^{-1}), and J_{pro} is the photolysis rate constant of the product. In this study, the photolysis rate for CH_3CHO and CH_3COCH_3 were calculated by following Eq.(b), where the $\sigma(\lambda)$ and $\Phi(\lambda)$ are the recommended data by IUPAC, and the $F(\lambda)$ is same as described previously. The photolysis rate for HCHO was measured and calculated by our spectroradiometer as described above.

4-2-5- Chemicals

The sources of the chemicals used in this work and their stated purities were as follows: perfluoro-2-methyl-3-pentanone (99%, 3M Belgium N.V, Chemical Group-EBC), 2-Methyl-3-pentanone (97%, Sigma-Aldrich), SF_6 (99.9995%, Air Liquide) and O_2 (99.9995%, Air Liquide). PF-2M3P and 2M3P samples were further purified by using several freeze-pump-thaw cycles, the analysis by GC-MS did not show any observable impurities.

4-3- Results and Discussion

4-3-1- UV absorption cross section

In order to test the accuracy of the measurements, the UV absorption spectrum of acetone has been measured and compared to the recommended UV spectrum from NASA/JPL evaluation (Sander et al., 2011). As shown in Figure 4-1, the level of agreement between both measured and recommended spectra is high, within the measurement accuracy of the recommended UV-Vis absorption spectra (8%). This excellent agreement brings us more confidence in the reliability of the absorption cross section measurement conducted in this work.

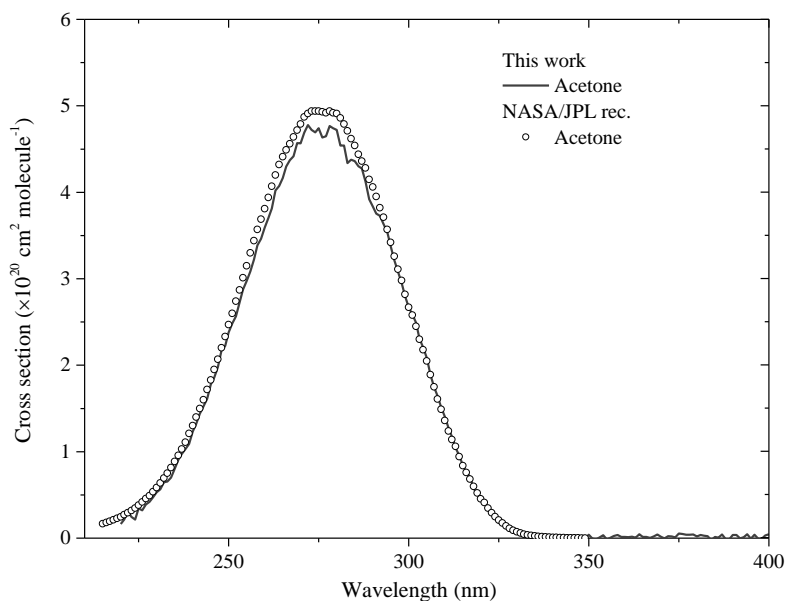


Figure 4-1: UV absorption spectra of acetone from this work and NASA/JPL (Sander et al., 2011)).

The measured UV-Vis absorption spectra of PF-2M3P and 2M3P between 220 and 400 nm at (300 ± 2) K are depicted in Figure 4-2 and the corresponding absorption cross section values are listed in Table 4-1 (5 nm intervals). Between 260 and 350 nm, the standard deviation of the measured absorption cross section was better than 5%. The absorption measurements satisfied Beer's law over a wide concentration range (an order of magnitude). The measured absorbance, A (base e) ranged from 0.2 to 1.7 for PF-2M3P, 0.3 to 2.0 for 2M3P. Graphical representations of Beer's law fits of the data measured in this work are given in Figure 4-3.

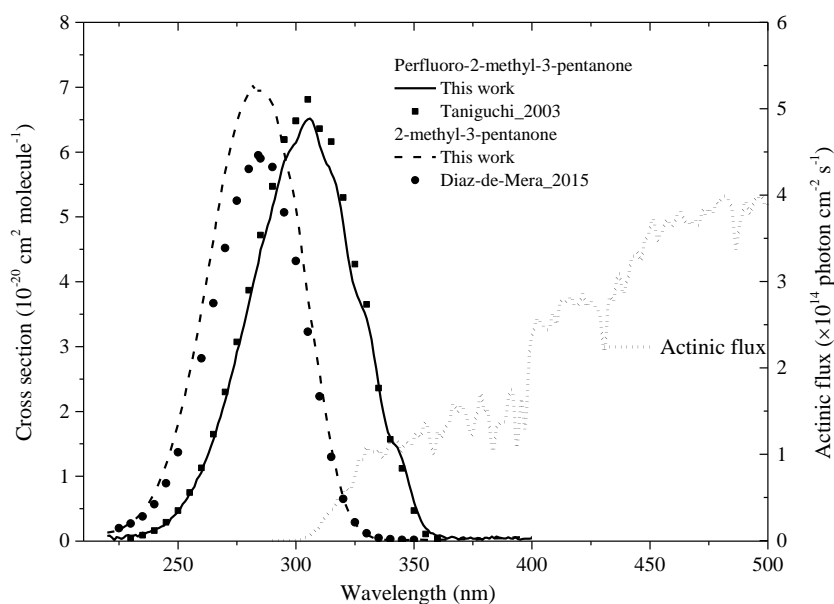


Figure 4-2: UV absorption spectra of Perfluoro-2-methyl-3-pentanone (from this work and Taniguchi et al., (2003)), 2-methyl-3-pentanone (this work and Diaz-de-Mera et al., (2015)). The actinic flux in the HELIOS chamber recorded at 13:00±5 min, 27 September, 2013 (Local Time) is also added.

Table 4-1: UV absorption cross sections (base e) of perfluoro-2-methyl-3-pentanone (PF-2M3P), 2-methyl-3-pentanone (2M3P) measured in this work.

Wavelength (nm)	Cross section ($10^{-20} \text{ cm}^2 \text{ molecule}^{-1}$)			Wavelength (nm)	Cross section ($10^{-20} \text{ cm}^2 \text{ molecule}^{-1}$)		
	Acetone	PF- 2M3P	2M3P		Acetone	PF- 2M3P	2M3P
220	0.16	0.08	0.13	310	1.40	6.11	2.59
225	0.34	0.05	0.20	315	0.84	5.68	1.45
230	0.53	0.04	0.29	320	0.47	4.89	0.68
235	0.80	0.13	0.45	325	0.18	3.89	0.27
240	1.23	0.17	0.74	330	0.09	3.43	0.10
245	1.78	0.29	1.19	335	0.02	2.41	0.04
250	2.38	0.45	1.80	340	0.03	1.60	0.01
255	2.98	0.74	2.61	345	0.02	1.27	0.01
260	3.59	1.06	3.58	350	0.04	0.60	0.02
265	4.16	1.57	4.64	355	0.01	0.20	0.02
270	4.57	2.16	5.70	360	0.01	0.08	0.02
275	4.74	2.92	6.46	365	0.01	0.05	0.03
280	4.72	3.66	6.91	370	0.02	0.05	0.03
284			6.99	375	0.05	0.04	0.04

285	4.36	4.49	6.96	380	0.02	0.05	0.03
290	3.83	5.16	6.75	385	0.02	0.07	0.05
295	3.38	5.86	5.99	390	0.04	0.06	0.04
300	2.67	6.15	5.14	395	0.03	0.02	0.06
305	2.08	6.50	3.76	400	0.04	0.05	0.06

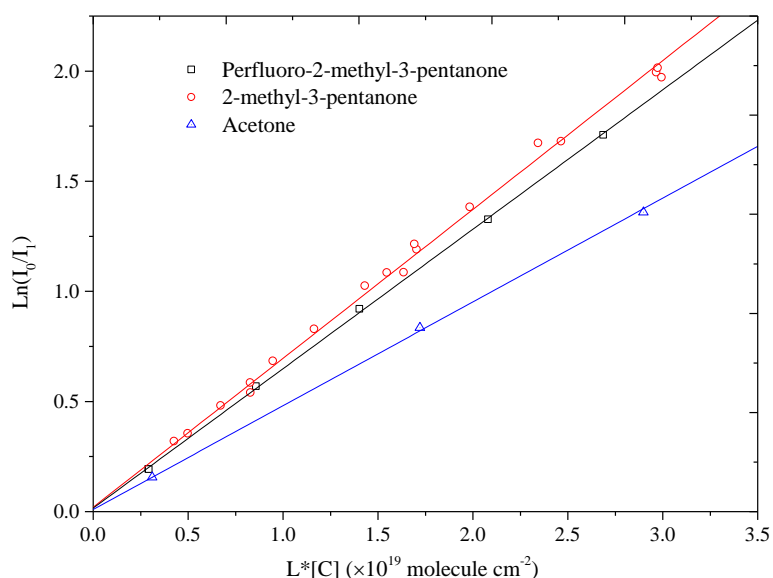


Figure 4-3: Beer's law fits for perfluoro-2-methyl-3-pentanone (PF-2M3P), 2-methyl-3-pentanone (2M3P) and acetone at their maximum absorption: 305 nm, 284 nm and 280 nm, respectively. L : the length of the absorption cell; $[C]$: concentration of the compound in the absorption cell, I_0 and I_1 are the light intensities in the absence and in the presence of compound in the absorption cell.

As shown in Figure 4-2, 2M3P has a maximum absorption at 284 nm ($\sigma_{(284 \text{ nm})} = (6.99 \pm 0.28) \times 10^{-20} \text{ cm}^2 \text{ molecule}^{-1}$) while PF-2M3P shows absorption features between 240 and 360 nm with a maximum around 305 nm ($\sigma_{(305 \text{ nm})} = (6.50 \pm 0.14) \times 10^{-20} \text{ cm}^2 \text{ molecule}^{-1}$). The quoted uncertainties on the measured absorption cross section data originate from one standard deviation (1σ) of the average of individual measurements.

The absorption spectra obtained in this work are compared with those reported in literature when possible and presented in Figure 4-2. The absorption spectrum of PF-2M3P is in agreement with the reported one by Taniguchi et al., (2003), within 5%. The UV absorption cross sections of 2M3P obtained in the present work are slightly

higher than those reported by Diaz-de-Mera et al., (2015), typically by 18% at the peak of the absorption spectrum.

The absorption band of ketones is caused by the dipole forbidden $n\text{-}\pi^*$ transition of the C=O group. For non-fluorinated ketones, the maximum absorption relies on the nature of the structure and the groups within the rest of the molecule (Mu and Mellouki, 2000). Furthermore, fluorination shifts the carbonyl absorption band to longer wavelength (Chiappero et al., 2006). As shown in Figure 4-2, the maximum absorption of PF-2M3P is red-shifted around 20 nm compared to 2M3P. These results are consistent with previous studies, reported for fluorinated ketones (Metcalf and Phillips, 1976) and aldehydes (Chiappero et al., 2006; Simpson et al., 2007).

The actinic flux in the chamber at $13:00 \pm 5$ min (local time) on 7th of September 2013 is also displayed on Figure 4-2. The integrated absorption cross section over the actinic flux region for PF-2M3P was estimated to $5.22 \times 10^{-18} \text{ cm}^2 \text{ molecule}^{-1}$ compared to that of 2M3P, which is $2.44 \times 10^{-18} \text{ cm}^2 \text{ molecule}^{-1}$. Uncertainty values are 1σ based on the propagation error technique, and estimated to 5%. This implies that the photolysis rates of PF-2M3P will be higher than that of 2M3P when exposed to natural irradiation.

4-3-2- Photolysis rate of PF-2M3P

The photolysis of PF-2M3P was investigated in two outdoor simulation chambers having quite different characteristics as described in the experimental section, a relatively small chamber (3.4 m^3) and the HELIOS chamber (90 m^3).

In the 3.4 m^3 chamber, experiments were conducted in June-July. First, temporal concentrations profiles of PF-2M3P and SF_6 were monitored under the dark for about 4 hours. No discernible loss other than dilution has been observed; the first order decay rates of PF-2M3P and SF_6 were in the order of $(6.6 - 8.1) \times 10^{-6} \text{ s}^{-1}$. The chamber was then exposed to solar radiation, thus starting the photolysis. The photolysis rate of PF-2M3P, $J_{\text{PF-2M3P}}$, was obtained by considering the total loss of PF-2M3P (k_{tot}) and that from dilution which was obtained from the loss rate of SF_6 (k_{d})

under irradiation. Experimental details and results derived from the four runs conducted are displayed in Table 4-2. For all experiments, the photolysis rates of NO_2 were in the range of $(4.4\text{-}5.5)\times 10^{-3} \text{ s}^{-1}$. The consumed fractions of PF-2M3P from photodissociation were between 2.1 and 3.7 % and the derived photolysis rates were $(1.7\text{-}2.8)\times 10^{-6} \text{ s}^{-1}$ under our experimental conditions ($J_{\text{NO}_2} = (4.4\text{-}5.5)\times 10^{-3} \text{ s}^{-1}$). The quoted error corresponds to 1σ obtained from the least square analysis applied on the experimental data and the estimated error on $J_{\text{PF-2M3P}}$ was in the range of 7-14 %.

Table 4-2: Experimental conditions and obtained results for the photolysis of Perfluoro-2-methyl-3-pentanone (PF-2M3P). The uncertainty is 1σ .

n	[PF-2M3P] ₀ (×10 ¹³ molecule cm ⁻³)	J _{NO2} (10 ⁻³ s ⁻¹)	J _{O(1D)} (10 ⁻⁶ s ⁻¹)	Photolysis loss (%)	Irradiation period (h:mm)	J _{PF-2M3P} (×10 ⁻⁶ s ⁻¹)	
						FT-IR	GC-MS
3.4 m ³ outdoor chamber							
1A	18	4.4±1.1	a	3.7	4:23	2.3±0.2	
2A	18	4.9±0.9	a	3.7	4:18	2.8±0.2	
3A	27	4.4±1.5	a	2.1	3:39	1.7±0.2	
4A	8.9	5.5±0.6	a	2.8	4:13	1.9±0.3	
HELIOS chamber							
1B	3.8	3.0±0.4	7.5±2.8	1.7	4:32	1.1±0.1	1.1±0.1
2B	3.0	5.3±1.0	11.0±4.0	7.7	5:01	3.8±0.3	3.5±0.5
3B	3.6	4.6±1.2	10.8±3.5	6.1	7:11	2.2±0.3	2.3±0.4
4B	3.5	5.6±0.7	14.5±1.5	7.4	7:08	3.7±0.5	3.6±0.5

[PF-2M3P]₀ is the initial concentration of PF-2M3P; J_{NO_2} is the NO_2 photolysis rate; $J_{\text{O}(\text{ID})}$ is the $\text{O}(\text{ID})$ production rate; ^a Not measured.

In Helios, the experiments were performed during September. Similarly to the small chamber runs, they were initiated by introducing known concentrations of SF_6 and PF-2M3P and monitoring continuously their concentrations, first under dark for typically 2 hours then after exposition to sunlight for typically 4 to 7 hours. PF-2M3P and SF_6 concentrations-time profiles were monitored by FT-IR and ATD-GC-MS. An example of the typical concentrations time profiles obtained is given in Figure 4-4. While SF_6 was lost only by dilution, PF-2M3P consumption was also due to photolysis. The loss rates of SF_6 and PF-2M3P were similar in the dark: $k_{\text{SF}_6} \approx k_{\text{PF-2M3P}} \approx (4.8\text{-}6.0)\times 10^{-6} \text{ s}^{-1}$. Both FT-IR and ATD-GC-MS analysis showed a slightly higher consumption of PF-2M3P than SF_6 under sunlight condition which may

indicate a possible photolysis of PF-2M3P under our experimental conditions. The photolysis rate of PF-2M3P was obtained from its total loss taking into account the contribution of the dilution (given by k_{SF_6} under irradiation) and was found to be $J_{\text{PF-2M3P}} = (1.1-3.8) \times 10^{-6}$ and $(1.1-3.6) \times 10^{-6} \text{ s}^{-1}$, obtained from FTIR and GC-MS measurements, respectively. Table 4-2 summarizes the full set of experimental conditions as well as the data obtained. The photolysis rate coefficient values of PF-2M3P obtained in HELIOS were 26-40% higher than those obtained using the 3.4 m³ chamber. The loss due to photolysis under our experimental conditions was estimated to 1.7-7.7 % in HELIOS chamber and 2.1-3.7 % in 3.4 m³ chamber experiments, respectively.

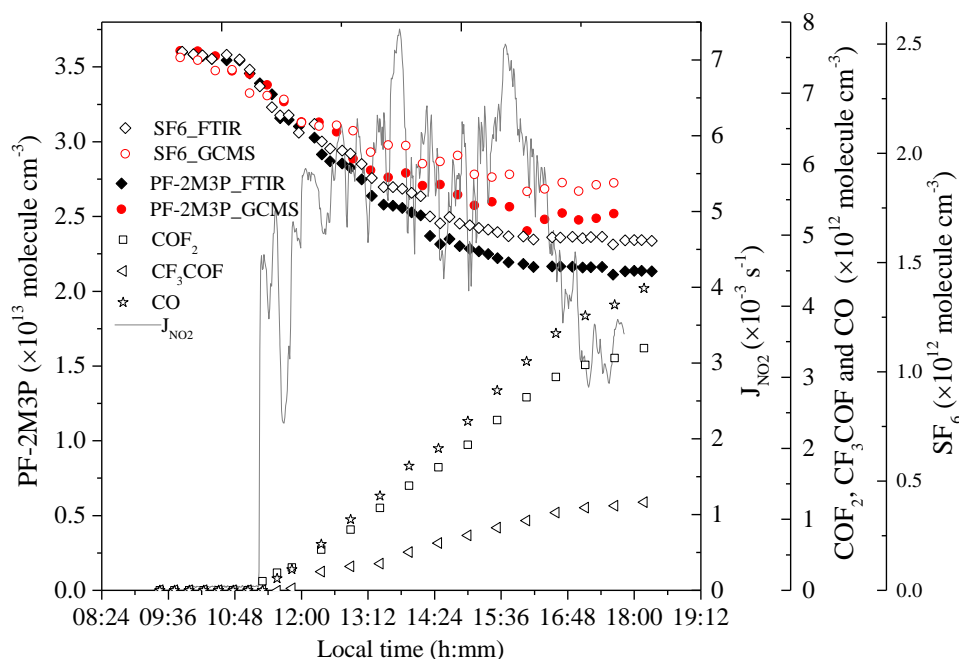


Figure 4-4: Time-concentration profiles of Perfluoro-2-methyl-3-pentanone (PF-2M3P) and the reaction products during the photolysis experiment (27 September, 2013).

In addition, the Tropospheric Ultraviolet-Visible (TUV) model was used to estimate the photolysis rate of PF-2M3P in Orleans for the different seasons. The parameters used and the data obtained are summarized in Table 4-3. In addition, the quantum yield was used as $\phi_{\text{eff}} = 0.017$ obtained in this work (in the below). Using 12 hours average (8am-8pm), the calculated annual photolysis rate ranges from (0.1 ± 0.08)

$\times 10^{-6}$ to $(0.9 \pm 0.5) \times 10^{-6} \text{ s}^{-1}$, and 3 hours average (12am-2pm) give an annual photolysis rate ranging from $(0.2 \pm 0.01) \times 10^{-6}$ to $(1.4 \pm 0.1) \times 10^{-6} \text{ s}^{-1}$. It shows that the photolysis of PF-2M3P mainly happen in the summer and the middle of the day (12am-2pm). In addition, the TUV mode values are in agreement with our chamber values.

Table 4-3: TUV model parameters and Photolysis rates of PF-2M3P based on the seasons of year from the TUV model using the quantum yield from this work.

47°N 1°E	Mar 22	Jun 22	Sept 22	Dec 22
O ₃ total vertical column (DU) ^a	370	340	278	302
Cloud total optical depth ^b	18	22	20	31
Altitude of Cloud base (km)			5	
Altitude of Cloud top (km)			7	
J _{PF-2M3P} ($\times 10^{-6} \text{ s}^{-1}$) 8am-8pm average	0.5 \pm 0.4	0.9 \pm 0.5	0.5 \pm 0.4	0.1 \pm 0.08
J _{PF-2M3P} ($\times 10^{-6} \text{ s}^{-1}$) 12am-2pm average	1.0 \pm 0.1	1.4 \pm 0.1	1.0 \pm 0.1	0.2 \pm 0.01
J _{2M3P} ($\times 10^{-6} \text{ s}^{-1}$) 8am-8pm average	0.7 \pm 0.5	1.0 \pm 0.6	0.6 \pm 0.5	0.1 \pm 0.08
J _{2M3P} ($\times 10^{-6} \text{ s}^{-1}$) 12am-2pm average	1.3 \pm 0.1	1.8 \pm 0.1	1.1 \pm 0.1	0.2 \pm 0.03

^a O₃ total vertical column data adapted from Veeffkind et al. (2006), ^b Cloud total optical depth adapted from NASA Earth Observations

Table 4-4 summarizes the photolysis rates of PF-2M3P obtained in this work and those reported earlier in the literature. The values from this work were lower than those reported earlier by D'Anna et al., (2005) and Diaz-de-Mera et al., (2015) who also conducted experiments under natural irradiation in Spain. The experiments conducted under artificial irradiation using black lamps or sunlamps led to lower photolysis rate values (Taniguchi et al., 2003). However, the TUV model values are in good agreement with the TUV values from the Jackson et al., (2011) and Diaz-de-Mera et al., (2015).

Table 4-4: Photolysis rate of perfluoro-2-methyl-3-pentanone (PF-2M3P) obtained in this work and compared to the reported data from the literature.

[PF-2M3P] ₀ ($\times 10^{13}$ molecule cm^{-3})	Nature of irradiation	$J_{\text{PF-2M3P}}$ (s^{-1})	J_{NO_2} (s^{-1})	Technique	T (K)	Reference
3.0-3.8	Solar irradiation - HELIOS chamber	$(1.1-3.8) \times 10^{-6}$ $(1.1-3.5) \times 10^{-6}$	$(3.0-5.6) \times 10^{-3}$ $(3.0-5.6) \times 10^{-3}$	FT-IR GC-MS	298-317	This work
8.9-27	Solar irradiation - 3.4 m ³ outdoor chamber	$(1.7-2.8) \times 10^{-6}$	$(4.4-5.5) \times 10^{-3}$	FT-IR	308-316	This work
8-64	Solar irradiation - Toledo, Spain	$(6.8 \pm 0.8) \times 10^{-6}$		GC-FID		Diaz-de-Mera et al., (2015)
2.5	Solar radiation - Euphore	$(6.4 \pm 0.3) \times 10^{-6}$	7.85×10^{-3}	FT-IR	301-309	D'Anna et al., (2005)
$(0.55-6.5) \times 10^3$	14 blacklamps 8 sunlamps	$(1.0 \pm 0.1) \times 10^{-7}$ $(6 \pm 2) \times 10^{-7}$		FT-IR	296	Taniguchi et al., (2003)
TUV model in 47 °N and 1 °E and times of year		$(0.2-1.4) \times 10^{-6}$				This work
TUV model in 39.9 °N and 4 °W and times of year		$(2.1 \pm 0.8) \times 10^{-6}$				Diaz-de-Mera et al., (2015)
TUV model in different latitude and times of year		$(0.82-3.1) \times 10^{-6}$				Jackson et al., (2011)

FT-IR: Fourier Transformed Infrared; ATD-GC-MS: Automated Thermal Desorption-Gas chromatography- Mass spectrometer; $J_{\text{PF-2M3P}}$ is the photolysis rate of PF-2M3P, and the error limits represents the standard deviation (1σ) from the average of individual experiments;

The maximum photolysis rate of PF-2M3P, $J_{\text{max-PF-2M3P}}$, was estimated using the absorption cross sections and the actinic flux measured in this work (Eq. b). It was found to be in the range $J_{\text{max-PF-2M3P}} = (1.4-2.3) \times 10^{-4} \text{ s}^{-1}$. Therefore, the observed photolysis rate corresponds to an effective quantum yield as $\phi_{\text{eff}} = 0.008-0.017$ which is 50-70% lower than that reported by D'Anna et al., (2005) and Diaz-de-Mera et al., (2015), 0.043 ± 0.011 and 0.044 ± 0.006 , respectively.

4-3-3- Photolysis products of PF-2M3P

Products from the photolysis of PF-2M3P were identified by FT-IR and ATD-GC-MS. Interpretations of IR spectra enabled us to identify CF_3COF , COF_2 and CO

as photolysis products. Figure 4-5 displays typical IR spectra obtained from the photolysis of PF-2M3P/SF₆/air mixture in HELIOS. Panels (A) and (B) show the IR spectra of PF-2M3P/SF₆/air mixture under the dark and after 4 hours of solar irradiation, respectively, while Panel (C) presents the residual spectrum of Panel (B) after subtraction of CF₃CF₂C(O)CF(CF₃)₂ and SF₆. The reference IR spectra of CF₃COF, COF₂ and CO are shown on Panels (D), (E) and (F), respectively. The residual spectrum resulting from the one in Panel (B) subtracted from which the reactants (PF-2M3P and SF₆) and identified products (CF₃COF, COF₂ and CO) have been shown in Panel G. In addition, perfluoro-propionic acid (CF₃CF₂C(O)OH, PFPrA) and trifluoro-acetic acid (CF₃COOH, TFA) have been tentatively identified ($m/z=69$), by aligning the acquired gas chromatograms in the NIST GCMS library (Figure 4-6). However, these two compounds have not been quantified.

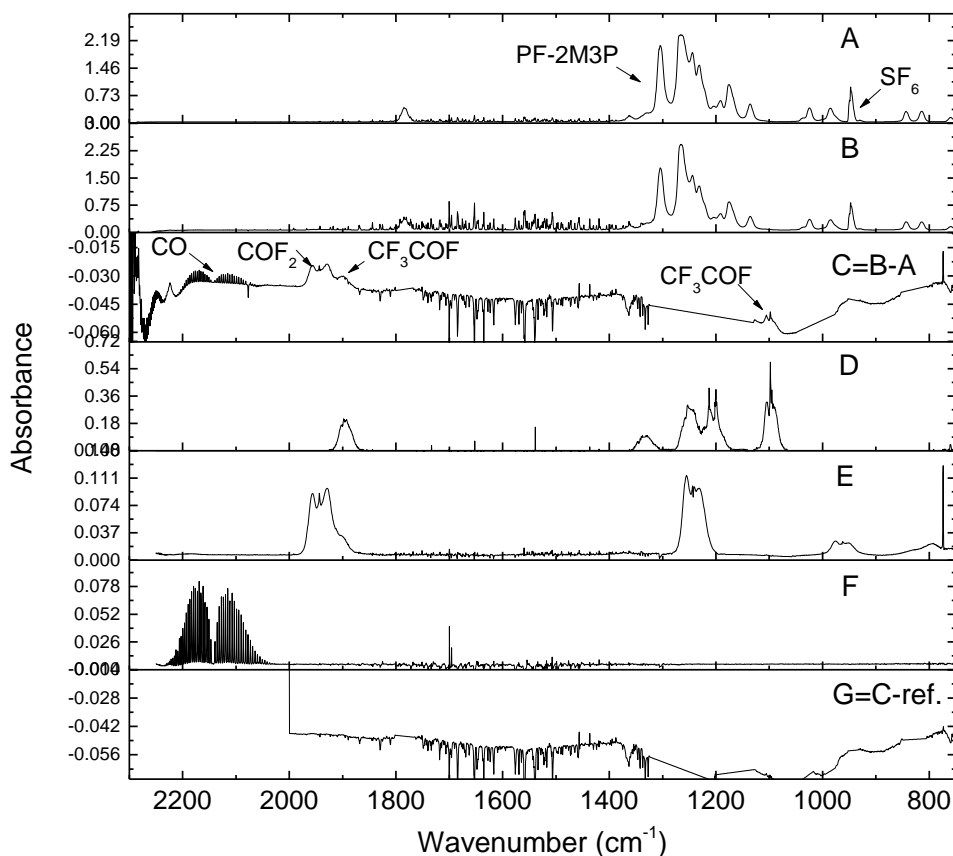


Figure 4-5: Photolysis of perfluoro-2-methyl-3-pentanone (PF-2M3P): FT-IR spectra recorded before (A) and after 4 hours exposure of PF-2M3P to sunlight (B). Panel C resulted from the subtraction of Panel B by Panel A. Reference spectra of CF₃C(O)F, COF₂ and CO are given in panel D, E and F, respectively. Residual spectrum subtracted from reactants and identified products are given in panel G (Experiments

conducted: on 19 September, 2013)

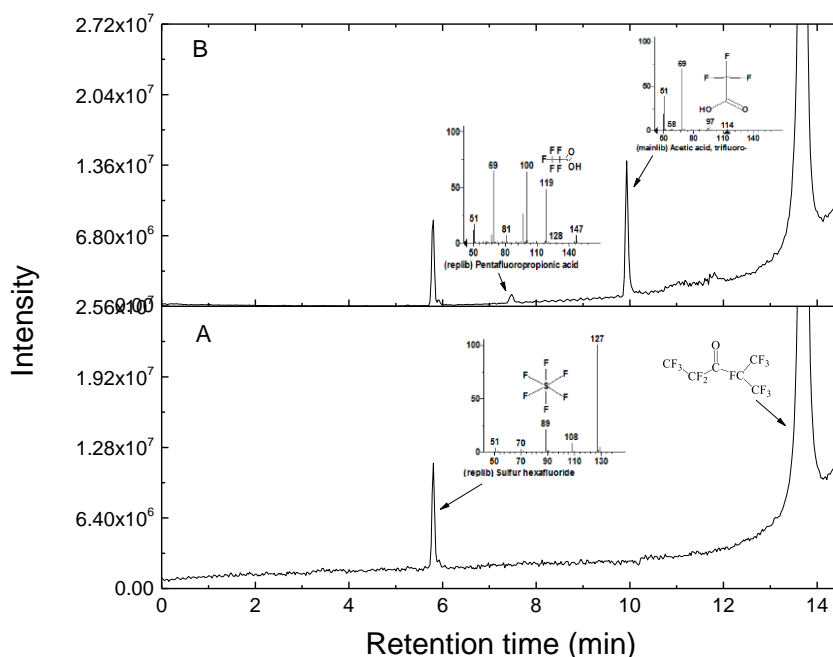


Figure 4-6: The Chromatogram and MS spectrum from GC-MS analysis: before (A) and after (B) 4 hours exposure of PF-2M3P to sunlight.

The products formation yields have been estimated at the first stage of the photolysis and obtained from a linear least-square fit of experimental data. Figure 4-7 displays the formation of COF_2 , CF_3COF and CO (corrected using the method described in section 4-2-4-) versus the consumed concentration of PF-2M3P obtained in HELIOS from the 4 runs conducted. The corresponding formation yields of the identified products for each individual run are shown in Table 4-5 leading average values of $(74 \pm 1)\%$, $(191 \pm 8)\%$, and $(196 \pm 50)\%$ for $\text{CF}_3\text{C}(\text{O})\text{F}$, COF_2 , and CO , respectively. Combining the products formation yields from HELIOS chamber and 3.4 m^3 outdoor chamber, the carbon and fluorine balance are estimated to be $(89 \pm 7)\%$ and $(57 \pm 2)\%$, respectively. The reported uncertainty is calculated using the standard deviation (1σ) from different runs.

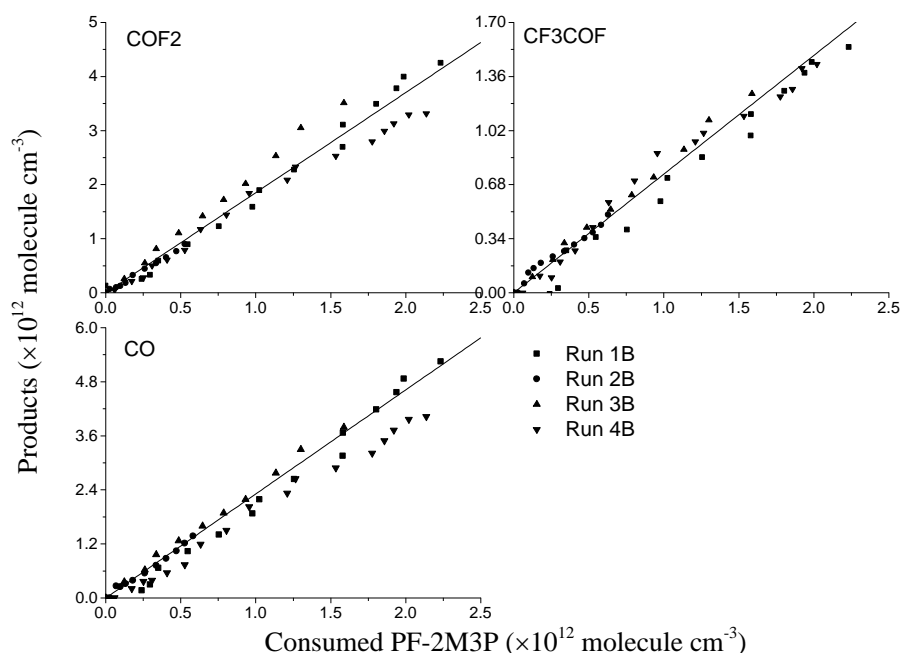


Figure 4-7: Photolysis of perfluoro-2-methyl-3-pentanone (PF-2M3P): formation of COF_2 , CF_3COF and CO versus the consumed concentration of PFMP obtained in the HELIOS chamber. The concentration of each product was corrected to account for dilution (k_{SF_6} under the irradiation condition). Solid lines represent linear least squares fit applied to the experimental data. Fits were not forced to zero intercept.

Table 4-5: Formation yield of identified products for each individual experiment obtained from the photolysis of perfluoro-2-methyl-3-pentanone (PF-2M3P).

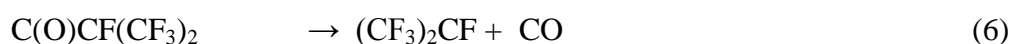
Run	COF_2 (%)	CF_3COF (%)	CO (%)	Fluorine balance (%)	Carbon balance (%)
3.4 m ³ outdoor chamber experiments					
1A	181 \pm 5	77 \pm 2	173 \pm 9	56 \pm 2	85 \pm 3
2A	247 \pm 13	81 \pm 4	176 \pm 7	68 \pm 4	98 \pm 5
3A	184 \pm 13	74 \pm 5	122 \pm 9	61 \pm 4	74 \pm 5
4A	173 \pm 8	63 \pm 3	170 \pm 9	50 \pm 2	78 \pm 4
Average \pm 1	196 \pm 34	74 \pm 8	160 \pm 26	59 \pm 8	84 \pm 11
HELIOS chamber experiments					
1B	165 \pm 5	76 \pm 3	264 \pm 8	53 \pm 1	97 \pm 2
2B	224 \pm 4	80 \pm 1	244 \pm 5	64 \pm 2	105 \pm 1
3B	164 \pm 4	74 \pm 3	190 \pm 4	52 \pm 2	84 \pm 1
4B	188 \pm 5	68 \pm 2	225 \pm 7	54 \pm 1	92 \pm 2
Average \pm 1	185 \pm 28	75 \pm 5	231 \pm 31	56 \pm 6	94 \pm 9
Rec. Average \pm 1	191 \pm 8	74 \pm 1	196 \pm 50	57 \pm 2	89 \pm 7

The uncertainty given in the formation yield of individual experiments originates from one-standard deviation (1σ) on linear least squares regression applied on the experimental data.

A proposed mechanism leading to the formation of the observed products from the solar irradiation photolysis of PF-2M3P is shown in Scheme 4-1. The photodissociation of PF-2M3P may occur through a C-C bond cleavage in the α position of the carbonyl group to generate perfluoroalkyl and perfluoroacetyl radicals:



Perfluoroacetyl radicals are expected to either decompose to give CO and perfluoroalkyl radical:



or react with O_2 leading to the corresponding peroxy radicals:



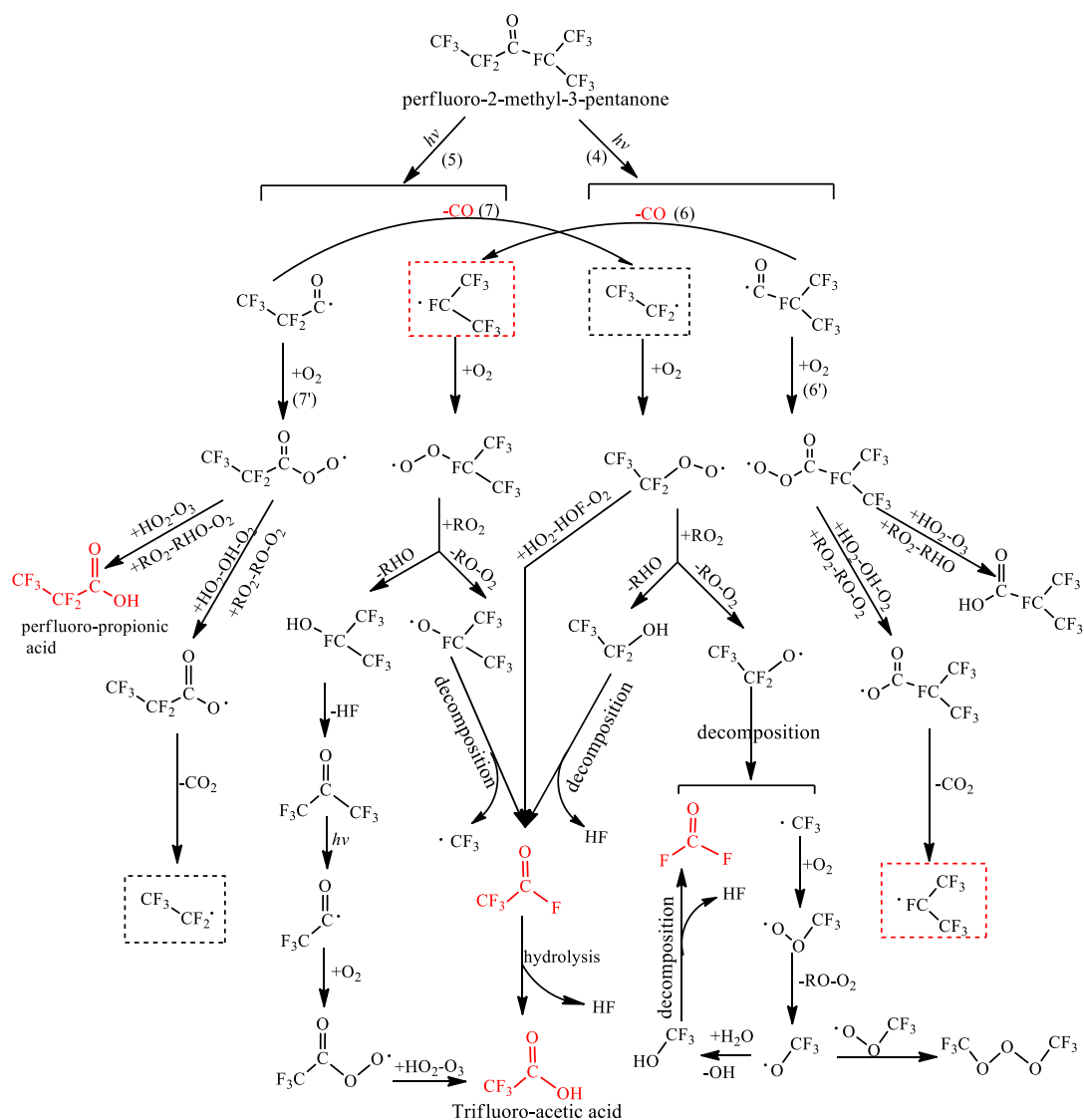
The high formation yield of CO (196 ± 50)% indicates that the thermal decomposition is an important pathway in the fate of perfluoroacetyl radical.

The perfluoroalkyl radical would only add O_2 leading to perfluoroalkyl peroxy radicals ($\text{CF}_3\text{CF}_2\text{O}_2$ and $\text{CF}(\text{CF}_3)_2\text{O}_2$). In addition to $\text{CF}_3\text{C}(\text{O})\text{F}$, COF_2 , and CO observed as stable products, PFPrA ($\text{CF}_3\text{CF}_2\text{C}(\text{O})\text{OH}$) was identified by GC-MS but could not be quantified. Its formation, if it really occurs in the chamber, may result from some “unknown” surface side reactions. Its formation during the GC-MS trap-analysis procedure is not excluded.

CF_3COF , identified among the photolysis products, could originate from the reactions of $\text{CF}_3\text{CF}_2\text{O}_2$ and $(\text{CF}_3)_2\text{CFCO}_2$ radicals with other alkylperoxy radicals present in the system leading to the corresponding RO radicals which further decompose to form CF_3COF , $\text{CF}(\text{CF}_3)_2\text{O}$ and $\text{CF}_3\text{CF}_2\text{O}$ radicals would thermally decompose to form CF_3 radicals and the corresponding fluorinated carbonyls $\text{CF}_3\text{C}(\text{O})\text{F}$ and COF_2 . In their study on the kinetics and mechanism of the self-reaction of $\text{CF}_3\text{CF}_2\text{O}_2$ radicals in the gas phase at 295 K, Sehested et al., (1993) assumed that

the decomposition $\text{CF}_3\text{CF}_2\text{O}$ radicals is the only loss process in the chamber. In this work, the formation yield of $\text{CF}_3\text{C}(\text{O})\text{F}$ was determined to be $(74 \pm 1)\%$.

Taniguchi et al., (2003) also identified $\text{CF}_3\text{O}_3\text{CF}_3$ and CF_3OH as products from the photolysis of PF-2M3P, which were not detected in this work. Indeed, $\text{CF}_3\text{O}_3\text{CF}_3$ and CF_3OH could be generated from the reaction of CF_3 radical (Scheme 4-1) via heterogeneous decomposition on the chamber wall. CF_3OH is also reported to transform rapidly into COF_2 (Wallington et al., 1993). In addition, COF_2 is expected to be formed through decomposition of $\text{CF}_3\text{CF}_2\text{O}$. The formation yield of COF_2 was determined to be $(196 \pm 50)\%$.



Scheme 4-1: Photolysis of perfluoro-2-methyl-3-pentanone (PF-2M3P): proposed mechanism leading to the formation of observed reaction products. Compounds in red represent products observed experimentally.

4-3-4- Photolysis rate of 2-methyl-3-pentanone

The study on the photolysis of 2-methyl-3-pentanone (2M3P) was conducted using the HELIOS simulation chamber. FTIR and GC-MS were used to monitor the concentration of 2M3P and the photolysis products. Control experiments of 2M3P/SF₆/air mixtures in the dark were conducted typically during 2 hours before exposing the mixture to the solar light. The loss rates of SF₆ and 2M3P were determined to be $(4.8-6.2) \times 10^{-6}$ and $(5.2-6.8) \times 10^{-6} \text{ s}^{-1}$ in the dark, respectively. The chemical mixture 2M3P/SF₆/air was then exposed to solar irradiation for typically 5-6 hours. From the decay of 2M3P, the effective photolysis rate, $J_{2\text{M3P}}$, was determined by correcting from the loss rate of SF₆ under irradiation ($k_{\text{d,light}}$) and wall loss ($k_{\text{L}} - k_{\text{d,dark}}$). Under our experimental conditions, the observed loss of 2M3P was ranging from 4 to 6.5%. The experimental conditions and the obtained values of $J_{2\text{M3P}}$ are summarized in Table 4-6. $J_{2\text{M3P}}$ were determined through FTIR and GC-MS measurements, yielding $J_{2\text{M3P}} = (1.9-3.4) \times 10^{-6}$ and $(2.0-3.3) \times 10^{-6} \text{ s}^{-1}$, respectively, where $J_{\text{NO}_2} = (2.2-5.6) \times 10^{-3} \text{ s}^{-1}$. The values of $J_{2\text{M3P}}$ obtained from FTIR and GC-MS agreed within (3-7) %.

Table 4-6: Experimental conditions and obtained results for the photolysis of 2-methyl-3-pentanone (2M3P). The uncertainty error is 1σ .

Run	[2M3P] ₀ (10 ¹³ molecule cm ⁻³)	J _{NO2} (10 ⁻³ s ⁻¹)	J _{O1D} (10 ⁻⁶ s ⁻¹)	Irradiation period (h:mm)	Photolysis loss (%)	J _{2M3P} (10 ⁻⁶ s ⁻¹)	
						FT-IR	GC-MS
I	3.3	2.9±1.2	7.6±3.1	6:00	5.7	2.3±0.7	2.3±0.4
II	3.4	2.2±0.3	4.1±1.5	5:49	3.9	1.9±0.2	2.0±0.4
III	3.4	2.4±1.1	6.8±2.4	6:14	3.9	2.2±0.2	2.4±0.3
IV	3.3	5.6±0.5	8.4±1.0	5:26	6.3	3.4±0.7	3.3±0.7
V	3.4	5.1±0.5	5.8±0.1	6:01	5.3	2.8±0.7	2.7±0.4
VI	3.4	5.1±0.7	6.2±1.3	4:58	4.8	2.7±0.6	2.7±0.4

[2M3P]₀ is the concentration of 2-methyl-3-pentanone; J_{NO2} is the NO₂ photolysis rate; J_{O(1D)} is the O(1D) production rate; Uncertainty represent the 1 σ presicion.

In addition, the Tropospheric Ultraviolet-Visible (TUV) model was used to estimate the photolysis rate of 2M3P in Orleans for the different seasons. Table 4-3 summarizes the conditions and the data obtained and the quantum yield was used as $\phi_{\text{eff}} = 0.179$ obtained in this work (in the below). Using 12 hours average (8am-8pm), the annual photolysis rate ranges from (0.1 ± 0.08) to $(1.0 \pm 0.6) \times 10^{-6} \text{ s}^{-1}$, and 3 hours average (12am-2pm) give an annual photolysis rate ranges from (0.2 ± 0.03) to $(1.8 \pm 0.1) \times 10^{-6} \text{ s}^{-1}$. It shows that the photolysis of 2M3P mainly happen in the summer and the middle of the day (12am-2pm). In addition, the TUV mode values are in agreement with our chamber values.

Finally, the maximum photolysis rate constant of 2M3P, $J_{\text{max-2M3P}}$, was estimated based on the integrated UV absorption spectrum over the actinic flux region and found to be $J_{\text{max-2M3P}} = (1.3-1.9) \times 10^{-5} \text{ s}^{-1}$. The measured photolysis rate led to an effective photolysis quantum yield estimated to $\phi_{\text{eff}} = 0.139-0.179$ under tropospheric sunlight conditions.

4-3-5- Mechanism of the 2M3P photolysis

Products were identified and quantified using FT-IR spectroscopy. The Figure 4-8 displays the typical spectra acquired before (panel A) and after (panel B) the photolysis of 2M3P, subtraction of IR features in panel A from panel B gives the residual spectrum (Panel C). Comparison with IR calibrated spectra shows the presence of CH_3CHO (panel D), CO (panel E), CH_3COCH_3 (panel F) and HCHO (panel G) among the oxidation products. Concentration-time profile is shown in Figure 4-9.

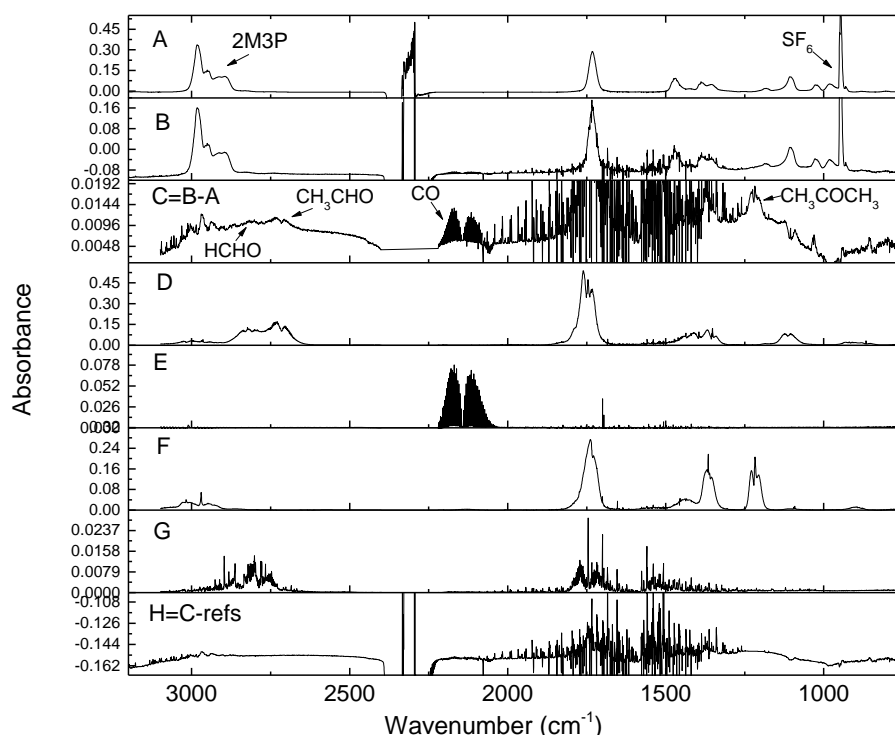


Figure 4-8: Photolysis of 2-methyl-3-pentanone (2M3P): FT-IR spectra recorded before (A) and after 6 hours exposure of MP to sunlight (B). Panel C shows the result of subtracting panel A from panel B. Reference spectra of CH_3CHO , CO , CH_3COCH_3 and HCHO are given in panel D, E, F and G. Residual spectrum subtracted from reactants and identified products is given in panel H.

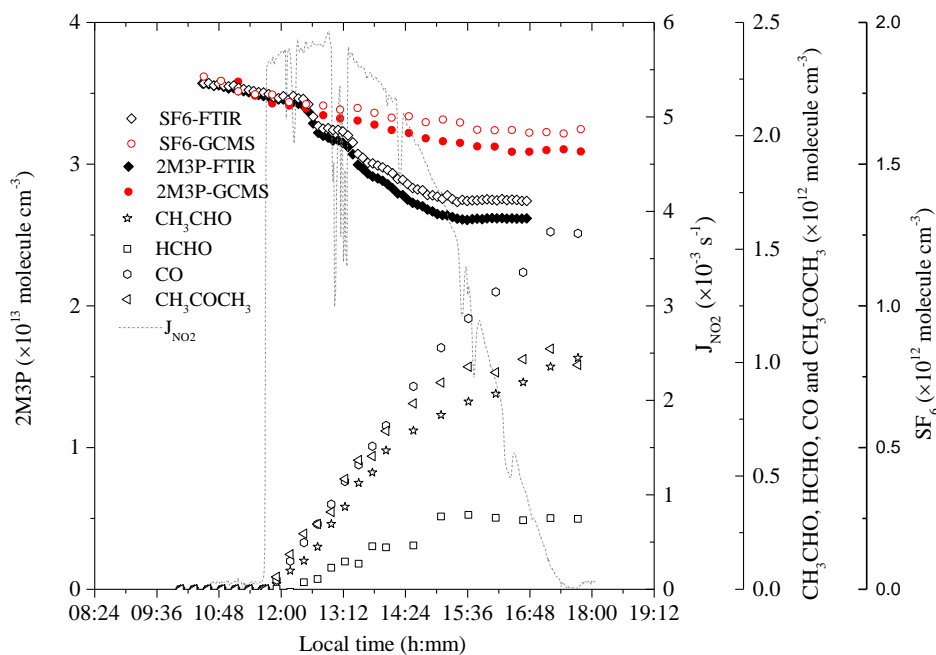


Figure 4-9: Photolysis of 2-methyl-3-pentanone (2M3P): Reactant and products profiles during the irradiation performed in the HELIOS chamber (Experiment conducted on 30 October, 2013).

Products formed from the photolysis of 2M3P were corrected to account for dilution and photolysis processes based on the method described in section 4-2-4, of CH_3CHO , HCHO , CH_3COCH_3 and CO are plotted as a function of consumed concentration of 2M3P (Figure 4-10). Not measured by the spectroradiometer, the photolysis rates for CH_3CHO and CH_3COCH_3 were calculated using the Eq.(b), where $\sigma(\lambda)$ and $\Phi(\lambda)$ were taken from IUPAC evaluation (2006). Linear least-square analysis was applied to the experimental dataset and the corresponding formation yields were extracted from the slope. The plots of CH_3CHO , HCHO , CH_3COCH_3 and CO versus consumed 2M3P at the beginning of the photolysis of 2M3P are linear, indicating that they were primary products.

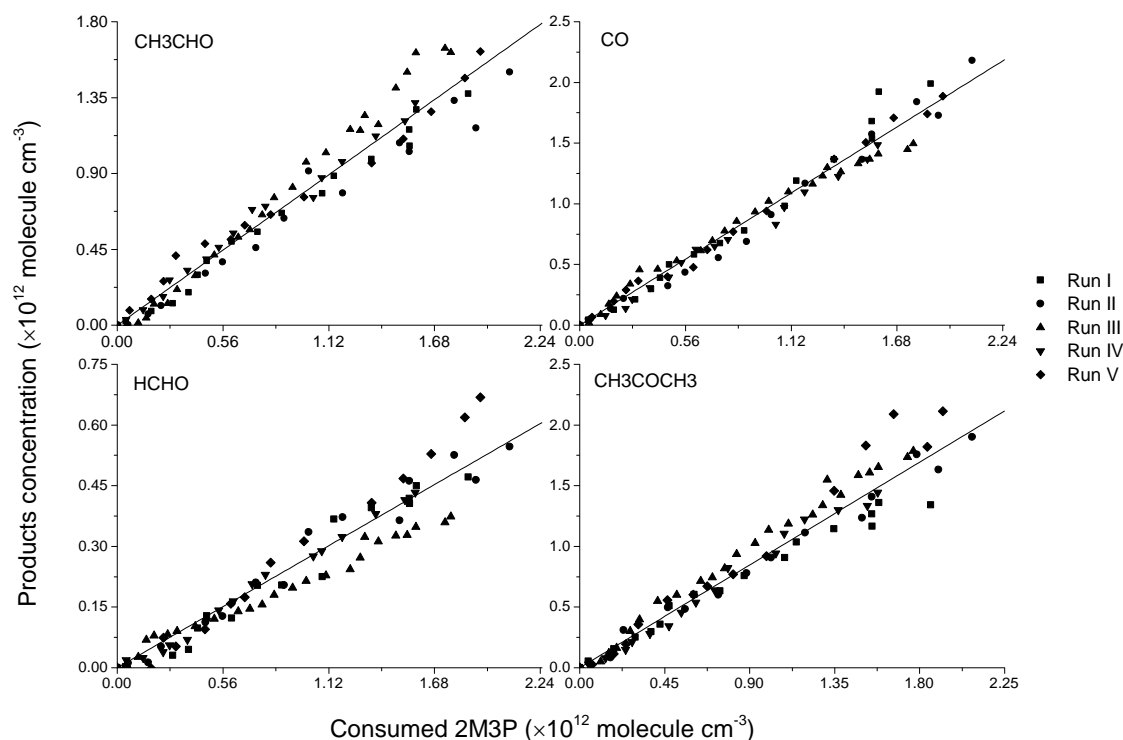


Figure 4-10: Photolysis of 2-methyl-3-pentanone (2M3P): formation of CH_3CHO , CO , HCHO and CH_3COCH_3 versus the consumed concentration of MP obtained in the HELIOS chamber from all the experiments. Solid lines represent linear least squares fit applied to the experimental data. Fits were not forced to zero intercept.

The formation yields of CH_3CHO , HCHO , CH_3COCH_3 and CO were estimated to be (80 ± 9) , (27 ± 4) , (90 ± 6) and (97 ± 6) %, respectively with a carbon balance

estimated to be (94 ± 6) %. Results are summarized in Table 4-7. The uncertainties on the formation yield originated from one standard deviation (1σ) on the average of individual runs.

Table 4-7: Formation yield of identified products for each individual experiment obtained from the photolysis of 2-methyl-3-pentanone (2M3P).

Run	CO	HCHO	CH ₃ CHO	CH ₃ COCH ₃	Carbon balance (%)
I	98 \pm 1	32 \pm 1	79 \pm 2	97 \pm 3	97 \pm 2
II	90 \pm 1	27 \pm 1	82 \pm 3	93 \pm 3	93 \pm 1
III	93 \pm 2	22 \pm 1	93 \pm 2	106 \pm 3	103 \pm 2
IV	102 \pm 4	28 \pm 2	70 \pm 3	90 \pm 3	90 \pm 2
V	104 \pm 2	26 \pm 3	74 \pm 3	84 \pm 2	88 \pm 2
VI *	79 \pm 1	22 \pm 1	66 \pm 3	79 \pm 2	78 \pm 2
Average \pmSD^a	97 \pm 6	27 \pm 4	80 \pm 9	90 \pm 6	94 \pm 6

The uncertainty given in the formation yield of individual experiments originate from one-standard deviation (1σ) on linear least squares regression applied on the experimental data.

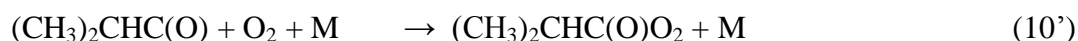
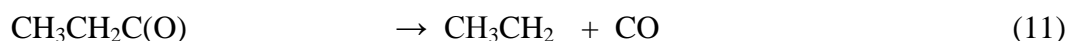
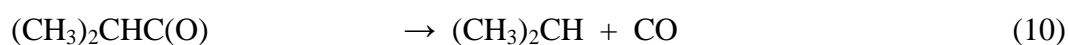
^a SD: the uncertainty associated to the average corresponds to one standard deviation (1σ).

* value (from VI) was not used in average because the formation yield is unexpected in large discrepancy with others (I-V)

Scheme 4-2 shows the proposed mechanistic pathways leading to the formation of the observed products during the photolysis of 2M3P. According to the product identification, the photolysis of 2M3P may occur via cleavage of a C-C bond associated with C=O group to form an alkyl and the corresponding acetyl radical:



CH₃CH₂C(O) and C(O)CH(CH₃)₂ radicals, are expected to either decompose to alkyl radicals (CH₃CH₂ and CH(CH₃)₂) leading to the elimination of carbon monoxide (CO) (reactions 10, 11) or react with O₂ to form the corresponding acetyl peroxy radicals ((CH₃)₂CHC(O)O and CH₃CH₂C(O)O₂) :





CO formation yield was estimated to (97±6)% indicating that this process is an important one.

The reaction of $\text{CH}_3\text{CH}_2\text{C}(\text{O})\text{O}_2$ with HO_2 radical has been reported to lead to the formation of $\text{CH}_3\text{CH}_2\text{C}(\text{O})\text{OH}$ and O_3 (Le Crâne et al., 2005) However the absence of the carboxylic acid and O_3 among the photolysis products indicated that the reaction of acetyl peroxy radicals with HO_2 was insignificant under our experimental conditions.

The acetyl peroxy radicals, e.g. $(\text{CH}_3)_2\text{CHC}(\text{O})\text{O}_2$ and $\text{CH}_3\text{CH}_2\text{C}(\text{O})\text{O}_2$ radicals may react mainly with RO_2 radicals (self-reaction or different $\text{R}'\text{O}_2$ radical). Since no carboxylic acids have been observed, it is speculated that these reactions could be not significant. The $\text{CH}_3\text{CH}_2\text{C}(\text{O})\text{O}$ and $(\text{CH}_3)_2\text{CHC}(\text{O})\text{O}$ radicals that could be formed at some stage of are expected to decompose and form CO_2 and the corresponding alkyl radicals, CH_3CH_2 and $(\text{CH}_3)_2\text{CH}$. The subsequent reaction of O_2 and further reactions with HO_2 radical (Tyndall et al., 2001) (reactions 12-13) or self-reaction lead to the formation of alkoxy radicals $\text{CH}_3\text{CH}_2\text{O}$ and $(\text{CH}_3)_2\text{CHO}$.



As concluded by Sander et al (2011), the self-reaction of $\text{CH}_3\text{CH}_2\text{O}_2$ radical would lead to the formation of $\text{CH}_3\text{CH}_2\text{O}$ radical (60%) and $\text{CH}_3\text{CHO} + \text{CH}_3\text{CH}_2\text{OH}$ (40%). In addition, the self-reaction of $(\text{CH}_3)_2\text{CHO}_2$ radical would lead to the formation of $\text{CH}_3\text{C}(\text{O})\text{CH}_3 + (\text{CH}_3)_2\text{CHO}$ radical (40%).

$\text{CH}_3\text{CH}_2\text{O}$ and $(\text{CH}_3)_2\text{CHO}$ alkoxy radicals are expected to react with O_2 (reactions 14,15) to form formaldehyde (HCHO), acetaldehyde (CH_3CHO) and acetone ($\text{CH}_3\text{C}(\text{O})\text{CH}_3$). The formation yields of CH_3CHO and CH_3COCH_3 were determined to be (80±9) % and (90±6) %, respectively.



4-3-6- Comparison of photolysis mechanism between PF-2M3P and 2M3P

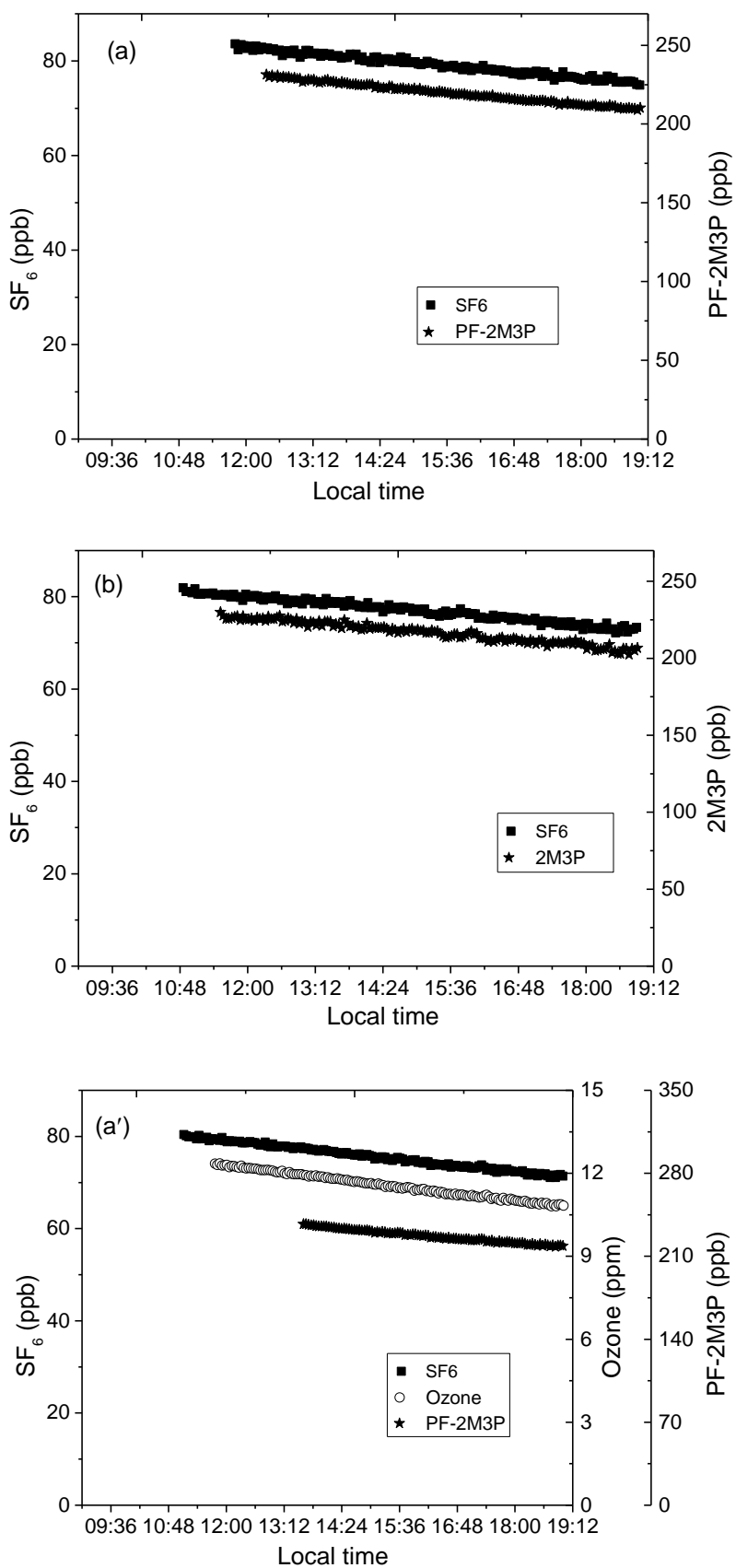
While both PF-2M3P and 2M3P show similar absorption spectra with that of 2M3P more shifted to the blue, the experiments conducted in the present work indicate that both species have similar photolysis rates under atmospheric conditions ($J_{\text{PF-2M3P}} = (1.1\text{-}3.8) \times 10^{-6} \text{ s}^{-1}$ and $J_{\text{2M3P}} = (1.9\text{-}3.4) \times 10^{-6} \text{ s}^{-1}$). Hence, the measured photolysis rates lead to different photolysis effective quantum yields, $\phi_{\text{eff_2M3P}} = 0.139\text{-}0.179$ and $\phi_{\text{eff_PF-2M3P}} = 0.008\text{-}0.017$.

By comparing the photolysis mechanisms suggested for PF-2M3P and 2M3P, the same pathways seem to occur. The photolysis of both species, proceed via a cleavage of the C-C bond associated with C=O group. Then the formed (perfluoro)acetyl radical may either eliminate CO to give the corresponding (perfluoro)alkyl radical or add O_2 to give (perfluoro)alkyl acetyl peroxy radicals. The only fate for (perfluoro)alkyl radicals is to add O_2 and lead to (perfluoro)alkyl peroxy radicals. Both, the (perfluoro)acetyl peroxy and (perfluoro)alkyl peroxy radicals can react with RO_2 and may produce the (perfluoro)acid, (perfluoro)alcohol, or (perfluoro)acetoxy and (perfluoro)alkoxy radicals. Then the (perfluoro)acetoxy radical will eliminate CO_2 to form the corresponding alkyl radical. The (perfluoro)alkoxy radical will eliminate the (perfluoro)methyl radical to give corresponding (perfluoro)aldehyde.

4-3-7- Kinetics of PF-2M3P and 2M3P reaction with O_3

Four and three runs were conducted for PF-2M3P and 2M3P, respectively. During the experiments, the initial O_3 concentration were $(2.7\text{-}9.9) \times 10^{14}$ and $(2.2\text{-}2.9) \times 10^{14} \text{ molecule cm}^{-3}$ for PF-2M3P $(5.7\text{-}5.9 \times 10^{12} \text{ molecule cm}^{-3})$ and 2M3P $(3.1\text{-}5.9 \times 10^{12} \text{ molecule cm}^{-3})$, respectively. The temporal behavior of the studied VOCs (PF-2M3P or 2M3P) was studied for 2 hours. Then ozone was introduced into the chamber starting the ozone reaction under ambient temperature (284-291 K) and pressure (744-760 torr). After 5 hours of reaction, the loss of PF-2M3P or 2M3P the

presence of O_3 did not differ from the loss in the absence of ozone as shown in Figure 4-11.



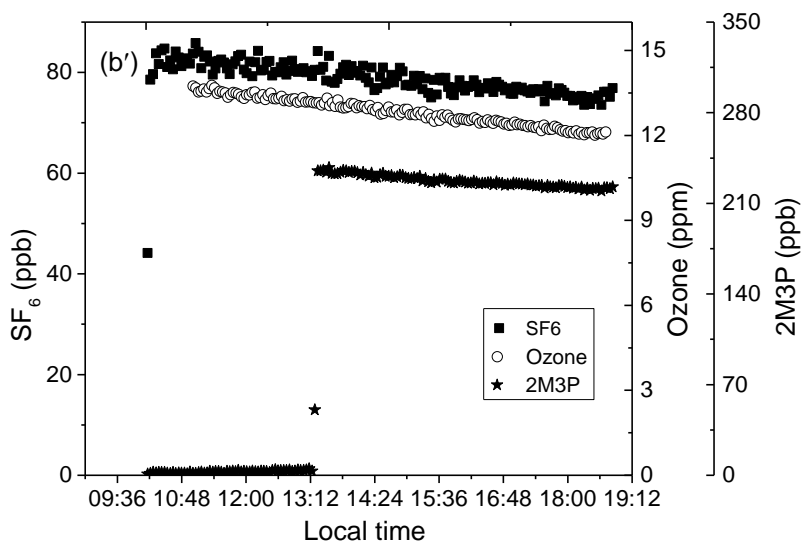


Figure 4-11: Time-concentration profiles of PF-2M3P (a) and 2M3P (b) in the absence of O_3 as well as PF-2M3P (a') and 2M3P (b') in the presence of O_3

Therefore, as shown in Table 4-8 the upper limit for the ozone rate coefficients of PF-2M3P and 2M3P determined to be: $k_{PF-2M3P} < 2.5 \times 10^{-22}$ and $k_{2M3P} < 5 \times 10^{-22} \text{ cm}^3 \text{ molecule}^{-1} \text{ s}^{-1}$, respectively. The upper limit found for the rate coefficient for the reaction of ozone with PF-2M3P is in agreement with the reported value by (Taniguchi et al., 2003), which was found to be $k_{PF-2M3P} < 4 \times 10^{-22} \text{ cm}^3 \text{ molecule}^{-1} \text{ s}^{-1}$ at 296 K.

Table 4-8: Initial experimental conditions and results of the experiments of O_3 reaction with studied VOCs as PF-2M3P and 2M3P.

Run	T (K)	VOCs ($\times 10^{12}$ molecule cm^{-3})	[Ozone] ₀ ($\times 10^{14}$ molecule cm^{-3})	k'_{SF6} ($\times 10^{-6}$ s^{-1})	k'_{VOC} ($\times 10^{-6}$ s^{-1})	k_{VOC} ($\times 10^{-8}$ s^{-1})
PF-2M3P + O_3						
1	288 \pm 1	5.8	2.8	5.6 \pm 0.1	5.7 \pm 0.1	6.5 \pm 0.4
2	289 \pm 1	5.7	2.7	5.8 \pm 0.2	5.9 \pm 0.1	6.0 \pm 0.4
3	285 \pm 1	5.9	2.8	4.2 \pm 0.1	4.3 \pm 0.1	5.3 \pm 0.5
4	284 \pm 1	5.9	9.9	3.9 \pm 0.1	4.1 \pm 0.1	21.9 \pm 0.8
$k_{(PF-2M3P+O_3)} < 2.5 \times 10^{-22} \text{ cm}^3 \text{ molecule}^{-1}$						
2M3P + O_3						
	291 \pm 1	3.1	2.2	6.6 \pm 0.3	6.7 \pm 0.1	8.0 \pm 0.8
	292 \pm 1	5.7	2.7	2.9 \pm 0.2	3.1 \pm 0.4	11.6 \pm 2.2
	290 \pm 1	5.9	2.9	3.7 \pm 0.3	3.8 \pm 0.2	15.0 \pm 2.9
$k_{(2M3P+O_3)} < 5 \times 10^{-22} \text{ cm}^3 \text{ molecule}^{-1}$						

Note: $k_{VOC} = k'_{VOC} - k'_{SF6}$

4-3-8- The Global Warming Potential (GWP)

The GWP is the time-integrated Radiative Forcing (RF) due to a *pulse emission* of a unit mass of gas, calculated relative to reference gas, normally CO₂. Because GWP includes the lifetime, it offers a better measure of the relative greenhouse impacts of different species than does RF alone (Brown et al., 1990). Thus, the GWP is defined as:

$$GWP_i(H) = \frac{\int_0^H RF_i(t)dt}{\int_0^H RF_{CO_2}(t)dt} = \frac{AGWP_i(H)}{AGWP_{CO_2}(H)}$$

Where H is the time horizon over which the integration is performed (IPCC presented GWP as 20, 100 and 500 years horizon and Kyoto Protocol has adapted GWP as 100 years horizon), $AGWP_i$ is an absolute GWP for gas i (usually in Watts m⁻² kg⁻¹ year), the integrated RF up to H is given by:

$$AGWP_i(H) = RE_i * \tau * (1 - \exp(-\frac{H}{\tau}))$$

Where RE_i is Radiative Efficiency for a species i , τ is the lifetime and assumed its removal from the atmosphere by exponential decay. Indeed, the $AGWP$ for CO₂ is more complicated because of its atmospheric lifetime of a perturbation cannot be represented by a simple exponential decay. In this work, the $AGWP$ for CO₂ was extracted from the review of Hodnebrog et al., (2013), they updated the $AGWP_{CO_2}$ value (based on the new impulse response function (IRF) and RE of CO₂) to be as 2.495, 9.171 and 32.17 ×10⁻¹⁴ W m⁻² yr(kCO₂)⁻¹ for the time horizons of 20, 100 and 500 years, respectively.

4-3-8-1- Radiative Forcing (RF) and Radiative Efficiency (RE)

In general, RF (in units of W m⁻²) refers to the effect of a species (a specified change in the concentration) to the radiation budget of the atmosphere, often over some given time period. Referred from Hodnebrog et al., (2013), the present

investigation also worked on the RF per unit change in halocarbon mixing ratio as RE ($\text{W m}^{-2} \text{ ppb}^{-1}$), which assumes the RF is linear in mixing ratio (normally appropriate in the case of small perturbations in mixing ratio about current concentrations and low background concentrations). Not using the complicate model like Reading Narrow Band Model (NBM) and Oslo Line-by-Line model (LBL), the RE calculations carried out here are based on the simple method outlined by Pinnock et al. (1995), in which RE was easily estimated as following:

$$\text{RE} = \sum_{\theta=1}^n (10 \text{ or } 1) \sigma_{av}^{\theta} F_{\sigma}^{\theta}$$

Where F_{σ}^{θ} [$\text{W m}^{-2} \text{ cm} (10^{-18} \text{ cm}^2 \text{ molecule}^{-1})^{-1}$] is the RE per unit cross section in band θ , σ_{av}^{θ} ($\text{cm}^2 \text{ molecule}^{-1}$) is the cross section averaged over each 10 or 1 cm^{-1} band.

Pinnock et al., (1995) showed that results from this simple method agreed to within 0.3% different with results from NBM, they also firstly proposed the instantaneous, cloud-sky, F_{σ} as a function of wavenumber (10 cm^{-1} wavenumber band) for global-annual mean atmosphere (GAM) using NBM, then Hodnebrog et al., (2013) updated it (10 and 1 cm^{-1} wavenumber band) using both NBM and LBL on incorporating a more GAM and three atmospheres representing the tropics and extra-tropics. This work used the curve of F_{σ} as a function of wavenumber (1 cm^{-1} wavenumber band of) from Hodnebrog et al., (2013) to calculate RE.

4-3-8-2- Infrared absorption cross section

In principle, the absorption cross section (σ) of a compound is determined via laboratory measurements using FT-IR. In this work, a Bruker Vertex70 spectrometer (described in previous section) has been used to obtain the spectra. Then, the absorption cross section ($\text{cm}^2 \text{ molecule}^{-1}$) of a compound at a specific wavenumber $\tilde{\nu}$ is given by:

$$\sigma(\tilde{\nu}) = \frac{A}{n \cdot l} = \frac{1}{n \cdot l} * \ln\left(\frac{I_0}{I_{tr}}\right)$$

where A is the nepierian absorbance from the nepierian logarithm of I_0 vs I_{tr} , in which I_0 and I_{tr} are the spectral intensity incoming and transmitted through the sample, respectively. n is the molecule concentration (molecule cm^{-3}) and l is the sample optical path length (cm).

Then the integrated absorption cross section, S ($\text{cm}^2 \text{ molecule}^{-1} \text{ cm}^{-1}$), is given as the integral of $\sigma(\tilde{\nu})$ over the wavenumber range $\tilde{\nu}_1$ to $\tilde{\nu}_2$.

$$S = \int_{\tilde{\nu}_1}^{\tilde{\nu}_2} \sigma(\tilde{\nu}) d\tilde{\nu}$$

In this work, the IR absorption cross section of PF-2M3P and 2M3P as a band of 1 cm^{-1} were shown in the Annex II. Finally, the GWP of PF-2M3P and 2M3P over 100 years horizon were calculated to be 0.18 and 1.2×10^{-6} , respectively, showed in Table 4-9. The GWP of PF-2M3P over 100 years horizon was in good agreement with the results from Hodnebrog et al., (2013) and Diaz-de-Mera et al., (2015), who reported a GWP of PF-2M3P over 100 years horizon to be <1 and 0.2, respectively.

Table 4-9: Lifetime, Radiative Efficiencies (RE) and GWPs (100 years) for PF-2M3P and 2M3P.

	Lifetime (days)	RE ($\text{W m}^{-2} \text{ ppb}^{-1}$)	GWP 100 year	refs
PF-2M3P	14	0.024	0.18	This work
	7	0.03	<1	Hodnebrog et al., (2013)
	5.5	0.39	0.2	Diaz-de-Mera et al., (2015)
2M3P	10	7.3×10^{-8}	1.2×10^{-6}	This work

4-4- Atmospheric Implication and Conclusion

The fate of PF-2M3P depending on the photolysis and ozonolysis were investigated in this work. The photolysis rate of PF-2M3P was obtained from HELIOS chamber (September, 2013) and 3.4 m^3 chamber (July, 2010): (1.1-3.8) and $(1.7\text{-}2.8) \times 10^{-6} \text{ s}^{-1}$, respectively, this corresponds to a lifetime of 73-277 hours under ambient temperature and pressure with J_{NO_2} was $(3.3\text{-}5.6) \times 10^{-3} \text{ s}^{-1}$. The low rate constant $(2.2 \pm 0.2) \times 10^{-22} \text{ cm}^3 \text{ molecule}^{-1} \text{ s}^{-1}$) for the reaction of PF-2M3P with O_3

indicated that the reaction of O_3 with PF-2M3P is minor pathway in the atmosphere. While the rate constant for hydrolysis of PF-2M3P was measured by Jackson et al., (2011) to be: $(3.1 \pm 0.3) \times 10^{-5} \text{ s}^{-1}$ at pH 8.5 to $(1.9 \pm 0.1) \times 10^{-5} \text{ s}^{-1}$ at pH 5.6, respectively. This shows that the hydrolysis is 10 times faster than the photolysis of PF-2M3P. Because the levels of liquid water are usually very low in the troposphere (per ml cloud only contain 10^{-6} - 10^{-7} ml liquid water and the global tropospheric volume only contain 15% cloud (Lelieveld and Crutzen, 1991)), so it suggests that the hydrolysis is a less important fate for PF-2M3P compared to photolysis.

The photolysis and ozonolysis of 2M3P were also investigated in this work. The photolysis rate of 2M3P was obtained from HELIOS chamber (October, 2013) to be $(1.9\text{-}3.4) \times 10^{-6} \text{ s}^{-1}$, which correspond to a range of atmospheric lifetime of 81-142 hours under ambient temperature and pressure with J_{NO_2} was $(2.2\text{-}5.6) \times 10^{-3} \text{ s}^{-1}$. In advance, some literatures (Tyndall et al., 2002; Vasvari et al., 2001) discussed the significant fraction of the reaction of OH radical with ketones proceeds. Because no OH scavenger was added during the experiments of the photolysis of 2M3P, the J_{2M3P} could be overestimated in this work. The low rate constant $((5.2 \pm 0.2) \times 10^{-22} \text{ cm}^3 \text{ molecule}^{-1} \text{ s}^{-1})$ for the reaction of 2M3P with O_3 indicated that the reaction of O_3 with 2M3P is minor pathway in the atmosphere. The photolysis process is an important removal process in the atmosphere.

In addition, the Tropospheric Ultraviolet-Visible (TUV) model was used to estimate the photolysis rate of PF-2M3P and 2M3P in Orleans in the different seasons, using 3 hours average (12am-2pm), annual photolysis rate obtained range from (0.2 ± 0.01) to $(1.4 \pm 0.1) \times 10^{-6} \text{ s}^{-1}$ and (0.2 ± 0.03) to $(1.8 \pm 0.1) \times 10^{-6} \text{ s}^{-1}$, respectively. The TUV model shows that the photolysis of PF-2M3P and 2M3P mainly happen in the summer, especially the middle of the day (12am-2pm).

In Orleans, the day-length was estimated to be 16 hours and 12.3 hours for July and September, respectively, by considering the sunrise and sunset time. Hence, the atmospheric lifetime of PF-2M3P with respect to the photolysis was $\tau_{\text{Phot}} \approx 6\text{-}21$ days. In agreement with the reported data from literatures (Taniguchi et al., 2003; D'Anna et al., 2005; Jackson et al., 2011), which have estimated that the lifetime was around 4-14

days from laboratory studies employing sunlamp and natural sunlight. In addition, the 11 hours of day-length was used to estimate the atmospheric lifetime of 2M3P. Hence, the atmospheric lifetime of 2M3P with respect to the photolysis was determined to be $\tau_{\text{Phot}} \approx 7.5\text{-}13$ days.

In this work, $\text{CF}_3\text{C}(\text{O})\text{F}$, COF_2 , TFA, PFPrA, and CO were identified from the photolysis of PF-2M3P. In the atmosphere, $\text{CF}_3\text{C}(\text{O})\text{F}$ will mainly hydrolyze and produce trifluoroacetic acid (TFA, $\text{CF}_3\text{C}(\text{O})\text{OH}$) (Francisco 1992). TFA and PFPrA are two perfluorinated carboxylic acid, which are ubiquitous in biotic and abiotic system (Yamashita et al., 2005; Houde et al., 2006). In the lower atmosphere, COF_2 would be lost through hydrolysis (Houde et al., 2006; Hanson and Ravishankara, 1991). Under stratospheric conditions, the major atmospheric fate of COF_2 is the photolysis (Nolle et al., 1999).

Photolysis of 2M3P in the troposphere will lead to the formation of $\text{CH}_3\text{C}(\text{O})\text{CH}_3$, CH_3CHO , HCHO and CO. The major atmospheric loss of $\text{CH}_3\text{C}(\text{O})\text{CH}_3$, CH_3CHO and HCHO is controlled by photolysis and reaction with OH radicals. In the upper troposphere, the photolysis can provide primary HO_x radical source (Jaegle et al., 2001).

The GWP over 100 years horizon of PF-2M3P and 2M3P have been calculated to be 0.18 and 1.2×10^{-6} , respectively. GWP of PF-2M3P has also been calculated to be < 1 over a 100 year time horizon (Hodnebrog et al., 2013).

References

- Atkinson, R., Baulch, D. L., Cox, R. A., Crowley, J. N., Hampson, R. F., Hynes, R. G., Jenkin, M. E., Rossi, M. J., Troe, J., and Subcommittee, I.: Evaluated kinetic and photochemical data for atmospheric chemistry: Volume II – gas phase reactions of organic species, *Atmos. Chem. Phys.*, 6, 3625-4055, 10.5194/acp-6-3625-2006, 2006.
- Brown, A. C., Canosa-Mas, C. E., Douglas Parr, A., and Wayne, R. P.: Laboratory studies of some halogenated ethanes and ethers: Measurements of rates of reaction with OH and of infrared absorption cross-sections, *Atmospheric Environment. Part A. General Topics*, 24, 2499-2511, [http://dx.doi.org/10.1016/0960-1686\(90\)90341-J](http://dx.doi.org/10.1016/0960-1686(90)90341-J), 1990.
- Chiappero, M. S., Malanca, F. E., Argüello, G. A., Wooldridge, S. T., Hurley, M. D., Ball, J. C., Wallington, T. J., Waterland, R. L., and Buck, R. C.: Atmospheric Chemistry of Perfluoroaldehydes ($C_xF_{2x+1}CHO$) and Fluorotelomer Aldehydes ($C_xF_{2x+1}CH_2CHO$): Quantification of the Important Role of Photolysis, *The Journal of Physical Chemistry A*, 110, 11944-11953, 10.1021/jp064262k, 2006.
- D'Anna, B., Sellevåg, S. R., Wirtz, K., and Nielsen, C. J.: Photolysis Study of Perfluoro-2-methyl-3-pentanone under Natural Sunlight Conditions, *Environmental Science & Technology*, 39, 8708-8711, 10.1021/es048088u, 2005.
- Diaz-de-Mera, Y., Aranda, A., Notario, A., Rodriguez, A., Rodriguez, D., and Bravo, I.: Photolysis study of fluorinated ketones under natural sunlight conditions, *Physical Chemistry Chemical Physics*, 17, 22991-22998, 10.1039/C5CP03527A, 2015.
- Forrest, E. C., Hu, L.-W., Buongiorno, J., and McKrell, T. J.: Pool Boiling Heat Transfer Performance of a Dielectric Fluid With Low Global Warming Potential, *Heat Transfer Engineering*, 34, 1262-1277, 10.1080/01457632.2013.793103, 2013.
- Hanson, D. R., and Ravishankara, A. R.: THE LOSS OF CF_2O ON ICE, NAT, AND SULFURIC-ACID-SOLUTIONS, *Geophysical Research Letters*, 18, 1699-1701, 10.1029/91gl02093, 1991.
- Hodnebrog, Ø., Etminan, M., Fuglestad, J. S., Marston, G., Myhre, G., Nielsen, C. J., Shine, K. P., and Wallington, T. J.: Global warming potentials and radiative efficiencies of

- halocarbons and related compounds: A comprehensive review, *Reviews of Geophysics*, 51, 300-378, 10.1002/rog.20013, 2013.
- Houde, M., Martin, J. W., Letcher, R. J., Solomon, K. R., and Muir, D. C. G.: Biological Monitoring of Polyfluoroalkyl Substances: A Review, *Environmental Science & Technology*, 40, 3463-3473, 10.1021/es052580b, 2006.
- Jackson, D. A., Young, C. J., Hurley, M. D., Wallington, T. J., and Mabury, S. A.: Atmospheric Degradation of Perfluoro-2-methyl-3-pentanone: Photolysis, Hydrolysis and Hydration, *Environmental Science & Technology*, 45, 8030-8036, 10.1021/es104362g, 2011.
- Jaegle, L., Jacob, D. J., Brune, W. H., and Wennberg, P. O.: Chemistry of HO_x radicals in the upper troposphere, *Atmospheric Environment*, 35, 469-489, 10.1016/s1352-2310(00)00376-9, 2001.
- Le Crâne, J.-P., Villenave, E., Hurley, M. D., Wallington, T. J., and Ball, J. C.: Atmospheric Chemistry of Propionaldehyde: Kinetics and Mechanisms of Reactions with OH Radicals and Cl Atoms, UV Spectrum, and Self-Reaction Kinetics of CH₃CH₂C(O)O₂ Radicals at 298 K, *The Journal of Physical Chemistry A*, 109, 11837-11850, 10.1021/jp0519868, 2005.
- Lelieveld, J., and Crutzen, P. J.: The role of clouds in tropospheric photochemistry, *J Atmos Chem*, 12, 229-267, 10.1007/bf00048075, 1991.
- Metcalf, J., and Phillips, D.: Photophysical processes in fluorinated acetones, *Journal of the Chemical Society, Faraday Transactions 2: Molecular and Chemical Physics*, 72, 1574-1583, 10.1039/F29767201574, 1976.
- Mu, Y. J., and Mellouki, A.: The near-UV absorption cross sections for several ketones, *Journal of Photochemistry and Photobiology a-Chemistry*, 134, 31-36, 2000.
- Nolle, A., Krumscheid, C., and Heydtmann, H.: Determination of quantum yields in the UV photolysis of COF₂ and COFCl, *Chemical Physics Letters*, 299, 561-565, 10.1016/s0009-2614(98)01257-3, 1999.
- NASA Earth Observations: <https://neo.sci.gsfc.nasa.gov/about/>.
- Pinnock, S., Hurley, M. D., Shine, K. P., Wallington, T. J., and Smyth, T. J.: Radiative forcing of climate by hydrochlorofluorocarbons and hydrofluorocarbons, *Journal of*

- Geophysical Research: Atmospheres, 100, 23227-23238, 10.1029/95JD02323, 1995.
- Sander, S. P., J. Abbatt, J. R., Barker, J. B., Burkholder, R. R., Friedl, D. M., Golden, R. E., Huie, C. E., Kolb, M. J., Kurylo, G., and K. Moortgat, V. L. O. a. P. H. W.: Chemical Kinetics and Photochemical Data for Use in Atmospheric Studies, Evaluation No. 17, JPL Publication 10-6, Jet Propulsion Laboratory, Pasadena, 2011 <http://jpldataeval.jpl.nasa.gov>, 2011.
- Schaefer, D. O., Godwin, D., and Harnisch, J.: Estimating future emissions and potential reductions of HFCs, PFCs, and SF6, Energy Journal, 63-88, 2006.
- Sehested, J., Ellermann, T., Nielsen, O. J., Wallington, T. J., and Hurley, M. D.: UV Absorption Spectrum, and Kinetics and Mechanism of the Self Reaction of CF₃CF₂O₂ Radicals in the Gas Phase at 295 K, International Journal of Chemical Kinetics, 25, 701-717, 10.1002/kin.550250903, 1993.
- Simpson, W. R., von Glasow, R., Riedel, K., Anderson, P., Ariya, P., Bottenheim, J., Burrows, J., Carpenter, L. J., Frieß, U., Goodsite, M. E., Heard, D., Hutterli, M., Jacobi, H. W., Kaleschke, L., Neff, B., Plane, J., Platt, U., Richter, A., Roscoe, H., Sander, R., Shepson, P., Sodeau, J., Steffen, A., Wagner, T., and Wolff, E.: Halogens and their role in polar boundary-layer ozone depletion, Atmos. Chem. Phys., 7, 4375-4418, 10.5194/acp-7-4375-2007, 2007.
- Taniguchi, N., Wallington, T. J., Hurley, M. D., Guschin, A. G., Molina, L. T., and Molina, M. J.: Atmospheric Chemistry of C₂F₅C(O)CF(CF₃)₂: Photolysis and Reaction with Cl Atoms, OH Radicals, and Ozone, The Journal of Physical Chemistry A, 107, 2674-2679, 10.1021/jp0220332, 2003.
- Tyndall, G. S., Cox, R. A., Granier, C., Lesclaux, R., Moortgat, G. K., Pilling, M. J., Ravishankara, A. R., and Wallington, T. J.: Atmospheric chemistry of small organic peroxy radicals, Journal of Geophysical Research: Atmospheres, 106, 12157-12182, 10.1029/2000JD900746, 2001.
- Tyndall, G. S., Orlando, J. J., Wallington, T. J., Hurley, M. D., Goto, M., and Kawasaki, M.: Mechanism of the reaction of OH radicals with acetone and acetaldehyde at 251 and 296 K, Physical Chemistry Chemical Physics, 4, 2189-2193, 10.1039/B111195G, 2002.
- Vasvari, G., Szilagyi, I., Bencsura, A., Dobe, S., Berces, T., Henon, E., Canneaux, S., and

- Bohr, F.: Reaction and complex formation between OH radical and acetone, *Physical Chemistry Chemical Physics*, 3, 551-555, 10.1039/B009601F, 2001.
- Veefkind, J. P., Haan, J. F. d., Brinksma, E. J., Kroon, M., and Levelt, P. F.: Total ozone from the ozone monitoring instrument (OMI) using the DOAS technique, *IEEE Transactions on Geoscience and Remote Sensing*, 44, 1239-1244, 10.1109/TGRS.2006.871204, 2006.
- Wallington, T. J., Hurley, M. D., Schneider, W. F., Sehested, J., and Nielsen, O. J.: Atmospheric chemistry of trifluoromethoxy radicals: reaction with water, *The Journal of Physical Chemistry*, 97, 7606-7611, 10.1021/j100131a033, 1993.
- Yamashita, N., Kannan, K., Taniyasu, S., Horii, Y., Petrick, G., and Gamo, T.: A global survey of perfluorinated acids in oceans, *Marine Pollution Bulletin*, 51, 658-668, 10.1016/j.marpolbul.2005.04.026, 2005.
- Yao, B., Vollmer, M. K., Zhou, L. X., Henne, S., Reimann, S., Li, P. C., Wenger, A., and Hill, M.: In-situ measurements of atmospheric hydrofluorocarbons (HFCs) and perfluorocarbons (PFCs) at the Shangdianzi regional background station, China, *Atmospheric Chemistry and Physics*, 12, 10181-10193, 10.5194/acp-12-10181-2012, 2012.

Chapter 5.

Kinetic and Product studies of OH Reactions with a series of Ketones

Chapter 5 - Kinetic and Product studies of OH Reactions with a series of Ketones .	144
5-1- Introduction.....	145
5-2- Experimental and Material	147
5-2-1- 200L Indoor simulation chamber	147
5-2-2- PLP-LIF.....	149
5-2-3- 7.3 m ³ large indoor simulation chamber.....	150
5-2-4- Chemicals	151
5-3- Results	152
5-3-1- Rate constants of ketones + OH radical using RR method	152
5-3-2- Rate constant of ketones + OH radical using AR method	155
5-3-3- Products formation from the ketones + OH radical	158
5-3-3-1- 2M3P+OH.....	159
5-3-3-2- 3M2P+OH.....	163
5-3-3-3- 4M2P+OH.....	167
5-4- Discussion.....	171
5-4-1- Comparison of rate constant with literature data for ketone + OH reaction.....	171
5-4-2- Trends in the Ketones + OH Reaction Rate Constants.....	173
5-4-3- Temperature dependence of the ketone + OH radical reaction.....	174
5-4-4- Reaction mechanism of the OH radical + ketones reaction.....	175
5-4-4-1- 2M3P+OH.....	176
5-4-4-2- 3M2P+OH.....	182
5-4-4-3- 4M2P	188
5-5- Atmospheric implications	191
5-6- Conclusion	192
References	194

Chapter 5 - Kinetic and Product studies of OH Reactions with a series of Ketones

Abstract:

The kinetic and products of reaction of OH radical with 2-methyl-3-pentanone (2M3P, $\text{CH}_3\text{CH}_2\text{C}(\text{O})\text{CH}(\text{CH}_3)_2$), 3-methyl-2-pentanone (3M2P, $\text{CH}_3\text{COCH}(\text{CH}_3)\text{CH}_2\text{CH}_3$) and 4-methyl-2-pentanone (4M2P, $\text{CH}_3\text{COCH}_2\text{CH}(\text{CH}_3)_2$), three widely used compounds in the industry, were investigated using two complementary techniques: Pulsed laser photolysis-laser-induced fluorescence (PLP-LIF) and continuous photolysis simulation chamber. Kinetic studies were investigated using absolute rate (AR) and relative rate (RR) method. The obtained results are: In a 200 L simulation chamber, RR method with four reference compounds at 293 ± 1 K led to (in $10^{-12} \text{ cm}^3 \text{ molecule}^{-1} \text{ s}^{-1}$): $k_{(\text{OH}+2\text{M3P})} = 3.40 \pm 0.45$, $k_{(\text{OH}+3\text{M2P})} = 6.0 \pm 0.14$ and $k_{(\text{OH}+4\text{M2P})} = 11.02 \pm 0.42$. Combining the PLP-LIF technique and RR result, $k_{(\text{OH}+2\text{M3P})} = (1.93 \pm 0.08) \times 10^{-12} \exp((183.2 \pm 23.9)/T) \text{ cm}^3 \text{ molecule}^{-1} \text{ s}^{-1}$ and $k_{(\text{OH}+3\text{M2P})} = (1.64 \pm 0.09) \times 10^{-12} \exp((387 \pm 31)/T) \text{ cm}^3 \text{ molecule}^{-1} \text{ s}^{-1}$ in the temperature range 253-376 K. Products studies were conducted in a 7.3 m³ simulation chamber using PTR-Tof-MS, UHPLC-MS and GC-MS. In the presence of NO_x, the acetone and acetaldehyde formation yields were determined to be 79.8 ± 3.0 % and 104.3 ± 10.0 %, respectively, from 2M3P reaction with OH; 2-butanone and acetaldehyde and 2,3-butanedione formation yields were determined to be 39.8 ± 1.9 % and 109.2 ± 6.1 % and 2.5 ± 1.8 %, respectively, from 3M2P reaction with OH; acetone and 2-methylpropanal formation yields were determined to be 87.4 ± 7.0 % and 10.7 ± 4.8 %, respectively, from 4M2P reaction with OH. The possible reaction mechanisms are discussed, and it provides direct evidence that the H-atom abstraction rate and branching ratio depend on the CH_x position relative to the >C=O group.

5-1- Introduction

Oxygenated volatile organic compounds (OVOCs) e.g. ethers, alcohols, aldehydes and ketones, are widely used as reagent in the industry; hence, a substantial proportion of these substances can be released into the atmosphere. Ketones are used as solvents and are also formed as intermediates during the oxidation of other hydrocarbons. Significant amounts of ketones are emitted into the atmosphere and thus considered as ubiquitous air pollutants, where they become available for photochemical transformation. The atmospheric degradation of ketones is mainly initiated by their photolysis and reaction with OH radical. However, photolysis is more important at high altitudes while the reaction with OH radical is predominant at the surface. In the atmosphere, ketones, depending on their chemical structure, constitute a potential source of free radicals, organic acids and nitrates, secondary organic aerosols, as well as O₃ formation.

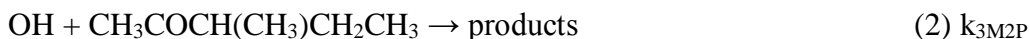
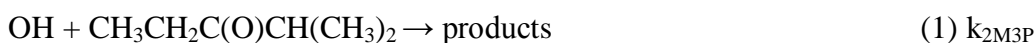
Hydroxyl radical (OH) is the most important reactive radical and the major tropospheric oxidant for a large series of organic compounds. Most ketones react in the gas-phase with OH radical, which is widely considered as the major oxidation route for these molecules in the atmosphere (Mellouki et al., 2015). By analogy with alkanes, the reactions of saturated ketones proceed through H-abstraction from CH_x groups leading to alkyl radicals (R) which react with O₂ to form alkyl peroxy radicals (RO₂) which in turn form alkoxy radicals (RO) following reaction with NO when present or self-reactions or with other RO₂ and HO₂. This later process may also lead to the formation of organic acids and hydroperoxides. Formation of organic nitrates and nitrites may occur depending on the conditions and environments in terms of NO_x concentrations, irradiation etc. (Calvert; et al., 2011). Various experimental studies have shown that the H-abstraction may depend on the position of CH_x group relative to the C=O (Kwok and Atkinson, 1995; Frank et al., 1998; Le Crâne et al., 2005). Furthermore, alkoxy radicals can react by three routes under atmospheric conditions: unimolecular decomposition via β -scission; unimolecular isomerization via a 1,5-H shift if a δ -hydrogen is present; reaction with O₂ if an α -hydrogen is

present (Davis and Francisco, 2011;Orlando et al., 2003;Somnitz and Zellner, 2000). The major uncertainty in the degradation of ketones is the relative importance of the fate of the intermediate radicals which may also go through thermal decomposition, isomerization or reaction with O₂. Indeed, these processes do affect the products formed.

Previous studies have mostly focused on the investigation of the reactions of OH with small and straight-chained ketones, e.g. acetone and 2-butanone, 2-pentanone, 3-pentanone, 2-hexanone and 3-hexanone (Calvert; et al., 2011). However, the rate constants for the reactions of OH with some branched ketones have also been investigated, such as 3-methyl-butanone, 4-methyl-2-pentanone and 5-methyl-2-hexanone (Cuevas et al., 2004;Le Calvé et al., 1998). The existing database shows that the reactivity of OH with numbers of ketones is well correlated by structure activity relationship (SAR) (Calvert; et al., 2011;Farrugia et al., 2015). Furthermore, Le Calvé et al., (1998) confirmed the activating effect of carbonyl group on the CH_x (x=1, 2, 3) groups in the β position, firstly observed by Atkinson et al., (1982), with the following reactivity trend CH > CH₂ > CH₃. The existing data enables also to derive the contribution of the alkyl groups from each side of the carbonyl groups to the total reactivity of the ketones (RC(O)R') with OH radicals (e.g. Wallington et al.,(1987), Le Calvé et al., (1998), Cuevas et al., (2004)). Overall, while a large set of data exists for the rate constants for OH with ketones, it is worth noting that the mechanistic investigations requires more work to be conducted. Indeed, only a limited number of studies have been performed so far on the OH-initiated oxidation of the higher chain ketones (Atkinson et al., 2000;Atkinson and Aschmann, 1995).

In light of the importance of ketones in the atmospheric chemistry, it is of importance to further investigate the degradation processes of ketones having different chemical structures. The current work is dedicated to an investigation of the reactions of OH radicals with three branched ketones: 2-methyl-3-pentanone (2M3P, CH₃CH₂C(O)CH(CH₃)₂), 3-methyl-2-pentanone (3M2P, CH₃COCH(CH₃)CH₂CH₃) and 4-methyl-2-pentanone (4M2P, CH₃COCH₂CH(CH₃)₂), which are widely used as solvents or as intermediates in the chemical industry. We report the rate constant

values and the products formed from the reactions of 2M3P, 3M2P, 4M2P with OH radical:



This work provides the first determination of the rate constant of OH reaction with 2M3P and the second one for that with 3M2P. In addition, we report the first measurement of the temperature dependence for reaction (1) and (2). The OH-initiated oxidation mechanism of 2M3P and 3M2P have not been investigated earlier, hence, we present in this work the first mechanism studies of (1) and (2). In addition to the experimental studies, our work aimed at better defining the reactivity and atmospheric fate of studied ketones toward the OH radical.

5-2- Experimental and Material

The experiments have been performed using two complementary systems (i) pulsed laser photolysis–laser induced fluorescence (PLP-LIF) and (ii) two atmospheric simulation chambers (200 L and 7.3 m³) at ICARE (CNRS - Orléans, France). The rate coefficients for the reaction of OH with 2M3P have been measured using both absolute rate (AR) and relative rate (RR) methods by employing, respectively, the PLP-LIF and the 200 L simulation chamber. The reaction rate coefficients of OH with the two other ketones (4M2P and 3M2P) have been determined only by the relative method. The OH-initiated oxidation mechanisms of the three ketones have been investigated in the 7.3 m³ ICARE simulation chamber.

5-2-1- 200L Indoor simulation chamber

Experiments were performed at ambient temperature ($T \approx 291$ K) and pressure ($P \approx 760$ Torr). The 200L ICARE chamber, made of FEP Teflon, has been previously described elsewhere (Bernard, 2009; Bernard et al., 2012) and is briefly presented in

Chapter 2.

RR method: the rate constant was determined by following the parallel decays of the ketones and reference compounds from the reaction with OH radical and loss (photolysis, leak and sampling):



$k_{\text{ketone_RR}}$ ($k_{2\text{M3P_RR}}$, $k_{4\text{M2P_RR}}$, $k_{3\text{M2P_RR}}$) and k_{ref} are the rate constants for the reaction of OH with ketones (2M3P, 4M2P, 3M2P) and reference compounds, respectively. $k_{\text{L-ketone}}$ and $k_{\text{L-ref}}$, the loss rate of ketones (2M3P, 4M2P, 3M2P) and reference compound.

The typical experimental procedure consisted in: (1) Prior to reaction initiation, a series of tests has been conducted: (i) only studied ketones without lamps on for 1 hour to check the possible wall loss; (ii) studied ketones with lamps on (2-4 254 nm lamps) for 1 hour to check possible photolysis decomposition; (iii) studied ketones with H_2O_2 without lamps on for 1 hour to verify possible dark reactions. The same tests have also been done for the reference compounds. Finally, no significant wall losses or dark reactions and photolysis have been observed for the ketones and reference compounds employed in this 200L ICARE chamber. (2) OH radical was generated via photolysis of H_2O_2 using 2-4 of 254 nm lamps, the reaction of studied ketones with OH radical was initiated.

Assuming that the ketone and reference compounds are lost only by reaction with OH radical, it can be shown that:

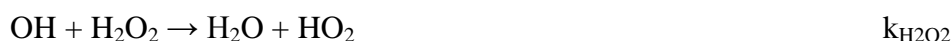
$$\ln\left(\frac{[\text{ketone}]_0}{[\text{ketone}]_t}\right) = \frac{k_{\text{ketone_RR}}}{k_{\text{ref}}} * \ln\left(\frac{[\text{reference}]_0}{[\text{reference}]_t}\right)$$

where $[\text{ketone}]_0$, $[\text{ketone}]_t$ and $[\text{reference}]_0$, $[\text{reference}]_t$ are the corresponding concentrations of ketone and reference compounds at initial time and t. Hence, plots of $\ln\left(\frac{[\text{keto}]_0}{[\text{ketone}]_t}\right)$ against $\ln\left(\frac{[\text{reference}]_0}{[\text{reference}]_t}\right)$ should be straight lines of slope $\frac{k_{\text{ketone_RR}}}{k_{\text{ref}}}$ and zero intercept.

5-2-2- PLP-LIF

The apparatus employed in this work has been described in detail previously in a number of publications and thesis from our group (Le Calvé et al., 1998; Mellouki et al., 1995) and also in Chapter 2 of this thesis.

AR method: The decay rate of OH in the reaction cell was governed by its reactions with the ketone and H₂O₂ and its removal from the detection zone due to diffusion:



$k_{\text{ketone_LIF}}$, $k_{\text{H}_2\text{O}_2}$, k_{diff} are the rate constants of the reactions of OH radical with ketone, H₂O₂ and the diffusional loss, respectively. All experiments were carried out under pseudo-first-order conditions, maintaining $[\text{ketone}] \gg [\text{OH}]$. According to the above reaction scheme, the decay of OH concentration should follow the pseudo-first order rate law:

$$[\text{OH}]_t = [\text{OH}]_0 \exp(-k't)$$

Where k' is the pseudo-first order rate constant that combines all OH loss processes:

$$k' = k_{\text{ketone_LIF}} [\text{ketone}] + k_0'$$

$$k_0' = k_{\text{H}_2\text{O}_2} [\text{H}_2\text{O}_2] + k_{\text{diff}}$$

The OH concentration at various reaction times (delay between the photolysis pulses and the probe pulses) were determined by the LIF signal at each decay time. The value of k' and k_0' were extracted from the linear least-square analysis of OH LIF signal plotted vs. decay time in the presence and absence of ketone. The linear least-squares fit of the data $k'-k_0'$ vs. various ketone concentration gives the second-order rate constant $k_{\text{ketone_LIF}}$.

The studied ketone (2M3P, 3M2P) was premixed in a 10 L glass light-tight bulb with helium to form 1.8% mixtures. All the gases (mixture of ketone with helium,

photolytic precursor, H_2O_2 , and the bath gas) were introduced by Teflon tubing and flowed through the reaction cell. The experiments were performed at a total pressure $P \approx 100$ torr of helium in the temperature range $T = (253\text{--}376)$ K. The ketones concentrations were calculated from their mass flow, pressure and temperature in the reaction cell. The mass flow was measured with a mass flow-controller calibrated by measuring the increasing rate of pressure in a known volume. Pressure inside the reaction cell was measured with a capacitive manometer connected in the entrance of the cell.

5-2-3- 7.3 m³ large indoor simulation chamber

The product experiments for the reactions of 2M3P, 4M2P and 3M2P with OH radical were conducted in the 7.3 m³ ICARE chamber, which was made by Teflon foil and operated in the condition of room temperature and 760 Torr of purified air (RH <2%). The 7.3 m³ ICARE chamber has been previously described elsewhere (Bernard et al., 2012; Bernard, 2009) and Chapter 2 of this thesis.

Chemical analysis was performed with an in-situ Fourier Transform Infrared Spectrometer (FTIR, Nicolet 5700 Magna), online PTR-ToF-MS (Proton Transfer Reaction - Time of Flight- Mass Spectrometer, IONICON 8000), offline analysis by ATD-GC-MS (Perkin Elmer GC/MS Clarus 600 C) and Ultra-High Performance Liquid Chromatograph-Mass Spectrometry (UHPLC/MS, Shimadzu LCMS-2020 Nexera X2). The FTIR is coupled to a White-type multi-path absorption cell system (optical path of 148 m), which was operated in the mid-IR region ($4000\text{--}650\text{ cm}^{-1}$) and the spectra were recorded by co - adding 130 interferograms within 5 min with a 1 cm^{-1} resolution. Quantitative analysis of infrared spectra was performed by subtraction using reference infrared spectra. PTR-ToF-MS spectra were analyzed by the PTR-ToF Data Analyzer (Müller et al., 2013).

The STS25 autosampler (PerkinElmer) was also used for VOC sampling with a time period of 1 hour per tube. After collection, compounds in the stainless steel tubes (AirToxics, PerkinElmer) were desorbed using a thermal desorber (TurboMatrix™

150 ATD) at a temperature of 330 °C and transferred under ultra-high purity helium flow into the second stage trap (AirToxics, PerkinElmer), which was cooled at -30 °C, using an inlet split of 30 mL/min. This second trap was heated to 300 °C to inject the sample in a 60-m PLOT column (Agilent GS-GasPro, diameter 0.320 mm), using an outlet split of 30 mL/min. This process would reduce the background water level and improve the chromatograph peak shape. Then the temperature of the GC oven was programmed as follows: 150 °C held for 10 min, then 50 °C min⁻¹ to 300 °C and held for 20 min. The chromatograms were analyzed with the help of NIST software.

Carbonyl compounds were also collected with 2,4-dinitro-phenylhydrazine (DNPH)-coated cartridges using a homemade offline auto-sampler. Then the derivatives created in the DNPH-coated cartridges were extracted using acetonitrile into vial and analyzed by UHPLC/MS with UV detector. The carbonyl compounds were separated with a Shimadzu column Shim-pack XR-ODS III C18 (2.2 μm x 50 mm (l) x 3 mm (i.d)) under 40 °C and ionized simultaneously with the help of the DUIS interface (Shimadzu) using two ionization methods: electrospray ionization (ESI), which is suitable for high polarity compounds, and atmospheric pressure chemical ionization (APCI), which is suitable for low-to-medium polarity compounds. With the UHPLC/MS, the measurements could be performed while switching alternately between positive and negative ionization modes. Then the mass to charge (m/z) was achieved in MS scanning using Quadrupole and qualitative plus quantitative analyzed in LabSolutions software from Shimadzu.

5-2-4- Chemicals

Helium carrier gas (Alphagaz 2, UHP certified >99.9999%) was used directly without further purification. H₂O₂ (50 wt%) solution was obtained from Prolabo and concentrated by bubbling helium through it to reduce the water content for several days prior to use. For PLP-LIF, H₂O₂ was continually concentrated during the course of the experiments and introduced into the reaction cell by passing a small flow of helium through a glass bubbler containing it. The used chemicals are high purity and

commercial possible, for example, 2M3P ($\approx 97\%$, Aldrich), 4M2P (99.5%, Aldrich), 3M2P (99%, Aldrich), propane (99.95%, Air liquid company), n-butane (99.5%, Air liquid company), hexane ($\geq 97\%$, Aldrich) and cyclohexane ($\geq 99.9\%$, Aldrich). All the liquid compounds in this study were further purified by repeating freeze, pump, thaw cycles and fractional distillation before use.

5-3- Results

5-3-1- Rate constants of ketones + OH radical using RR method

The rate constants for 2M3P (6.8-28.4 ppm), 4M2P (4.1-27.0 ppm) and 3M2P (3.7-28.1 ppm) have been obtained in a 200 L ICARE chamber using the reference compounds: propane (2.3-29.9 ppm), n-butane (3.6-29.1 ppm), n-hexane (4.1-29.3 ppm) and cyclohexane (3.0-28.4 ppm). The recommended rate constants of reference compounds reaction with OH are: $k_{(\text{propane}+\text{OH})}=(1.01\pm 0.15)\times 10^{-12}$ (Atkinson et al., 2006), $k_{(\text{n-butane}+\text{OH})}=(2.30\pm 0.35)\times 10^{-12}$ (Atkinson et al., 2006), $k_{(\text{n-hexane}+\text{OH})}=(5.07\pm 1.00)\times 10^{-12}$ (Atkinson, 2003) and $k_{(\text{cyclohexane}+\text{OH})}=(6.84\pm 1.36)\times 10^{-12}$ (Atkinson, 2003), unit in $\text{cm}^3 \text{ molecule}^{-1} \text{ s}^{-1}$, $T = 291\text{-}293 \text{ K}$.

Figures 5-1(a-c) show straight lines of $\ln\left(\frac{[\text{ketone}]_0}{[\text{ketone}]_t}\right)$ against $\ln\left(\frac{[\text{reference}]_0}{[\text{reference}]_t}\right)$ with zero intercept. For each plot, in consequence, all data points were gathered in common and the linear regression takes into account errors x and y values. This calculation was carried out based on the program developed by Brauers and Finlayson-Pitts (1997) leading to straight line slope $\frac{k_{\text{ketone_RR}}}{k_{\text{ref}}}$. The relative rate ratios, $\frac{k_{\text{ketone_RR}}}{k_{\text{ref}}}$, obtained for all the studied ketones are shown in Table 5-1 as well as the rate constants values, $k_{\text{ketone_RR}}$, obtained using the rate constant values of different references. The error for each $k_{\text{ketone_RR}}$ is a combination, in propagation of uncertainty, of the error in $\frac{k_{\text{ketone_RR}}}{k_{\text{ref}}}$ and the error of $k_{(\text{ref.}+\text{OH})}$. Table 5-1 shows a good agreement for the rate constant values $k_{\text{ketone_RR}}$ using different reference compounds. The final rate constants of studied ketones (2M3P, 4M2P and 3M2P) were obtained from the

weighted average of k_{ketone_RR} relative to the different references (k_{av} in Table 5-1).

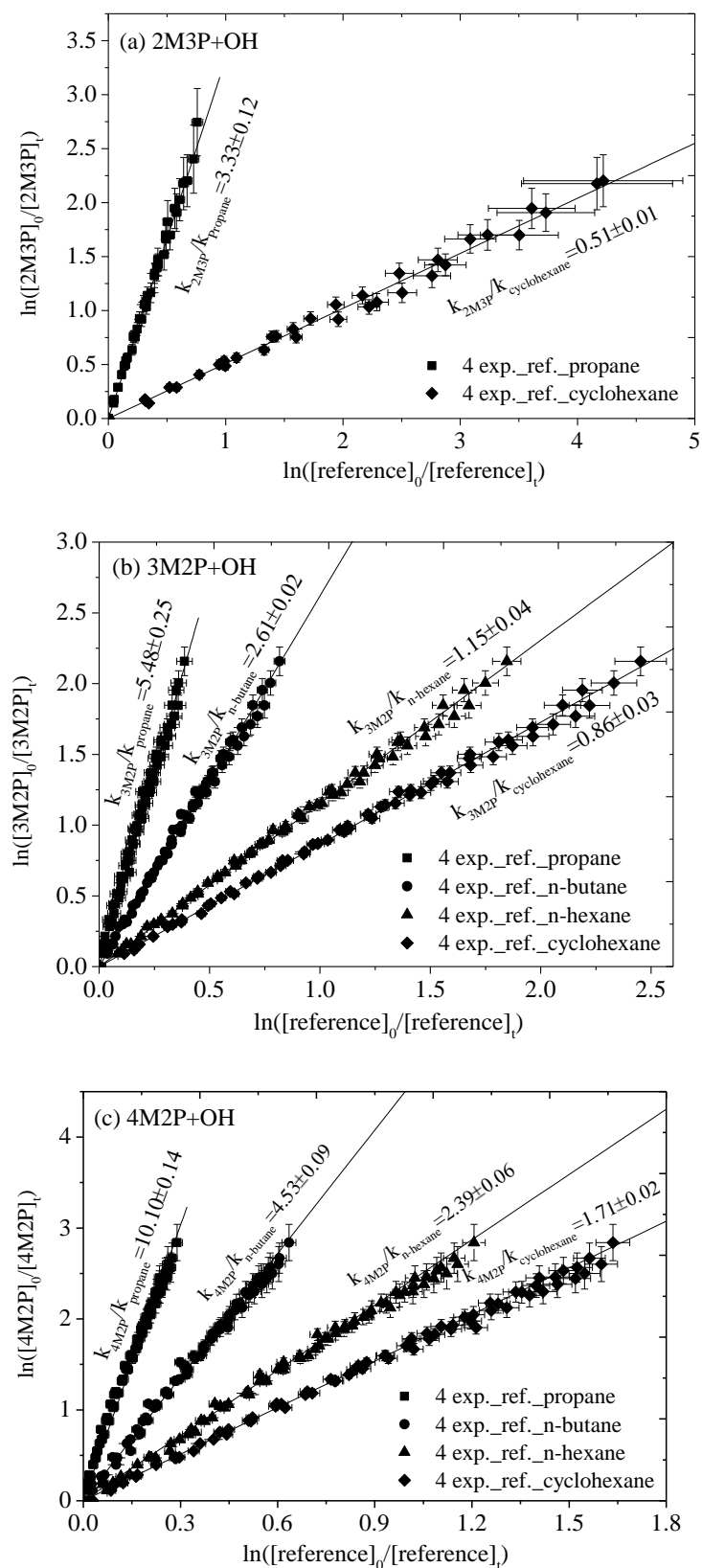
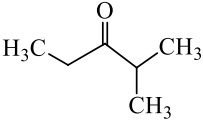
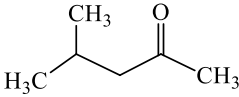
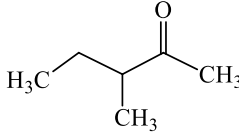


Figure 5-1(a-c): Plots of relative kinetic data from the reaction of 2M3P (a), 3M2P (b) and 4M2P (c) with OH radical using the propane, n-butane, n-hexane and cyclohexane as the references. 4 exp.= 4 experiments. ref.= reference

Table 5-1: Experimental conditions and rate constants of ketone+OH using RR method.

ketone	Structure	ref.	exp. T (K)	$\frac{k_{ketone_RR}^a}{k_{ref}}$	$k_{ketone_RR}^b (10^{-12} \text{ cm}^3 \text{ molecule}^{-1} \text{ s}^{-1})$	k_{av}^c
2M3P		propane	1	3.25±0.25	3.39±0.38	3.40±0.45
			2	3.35±0.24		
			3	3.30±0.24		
			4	3.41±0.24		
		cyclohexane	1	0.48±0.02	3.42±0.42	
			2	0.53±0.02		
			3	0.48±0.02		
			4	0.53±0.02		
4M2P		propane	1		10.44±0.74	11.02±0.42
			2	9.94±0.44		
			3	10.17±0.44		
			4	10.20±0.42		
		n-butane	1	4.49±0.17	10.41±0.63	
			2	4.58±0.12		
			3	4.63±0.12		
			4	4.42±0.10		
		n-hexane	1	2.47±0.06	11.99±0.78	
			2	2.36±0.04		
			3	2.38±0.04		
			4	2.35±0.04		
		cyclohexane	1	1.70±0.04	11.60±0.76	
			2	1.73±0.03		
			3	1.72±0.03		
			4	1.68±0.03		
3M2P		propane	1	5.92±0.75	5.78±0.51	5.90±0.36
			2	5.62±0.54		
			3	5.52±0.47		
			4	5.42±0.57		
		n-butane	1	2.75±0.09	6.05±0.48	
			2	2.62±0.05		
			3	2.68±0.07		
			4	2.50±0.05		
		n-hexane	1	1.19±0.03	5.90±0.45	
			2	1.18±0.02		
			3	1.16±0.02		
			4	1.12±0.02		
		cyclohexane	1	0.88±0.02	5.86±0.54	
			2	0.88±0.01		
			3	0.87±0.01		
			4	0.84±0.01		

- ^a The uncertainties for $k_{\text{ketone_RR}}/k_{\text{ref}}$ are 1σ of least-squares of $\ln\left(\frac{[\text{ketone}]_0}{[\text{ketone}]_t}\right)$ vs $\ln\left(\frac{[\text{reference}]_0}{[\text{reference}]_t}\right)$.
- ^b The uncertainties for $k_{\text{ketone_RR}}$ were estimated by combining the uncertainty of $k_{\text{ketone_RR}}/k_{\text{ref}}$ with the uncertainty of references using method in Annex I.
- ^c Weighted average $k_{\text{av}} = (w_{\text{ref1}}k_{\text{ketone_ref1}} + w_{\text{ref2}}k_{\text{ketone_ref2}} + \dots) / (w_{\text{ref1}} + w_{\text{ref2}} + \dots)$, where $w_{\text{ref1}} = 1/\sigma_{\text{ref1}}$, etc. The error, σ_{av} , is given by: $\sigma_{\text{av}} = (1/\sigma_{\text{ref1}} + 1/\sigma_{\text{ref2}} + \dots)^{-0.5}$ (ref. = reference, exp. = experiment)

5-3-2- Rate constant of ketones + OH radical using AR method

For the PLP-LIF kinetic studies, by using a high range (100-10000) of $[\text{ketone}]/[\text{OH}]$ ratios, the possible contributions to the measured rate constant from secondary OH reaction with the radicals produced in reactions of ketone+OH were negligible. Figure 5-2 shows the plot of $k' - k_0'$ vs. 2M3P and 3M2P concentration, respectively, obtained at room temperature from where $k_{2\text{M3P_LIF}}$ and $k_{3\text{M2P_LIF}}$ were derived from the linear least-square fit. The quoted errors for $k_{2\text{M3P_LIF}}$ and $k_{3\text{M2P_LIF}}$ include the statistical errors (2σ from the linear least-square analysis) and estimated systematic error (5% from due to the uncertainties in the measured concentration).

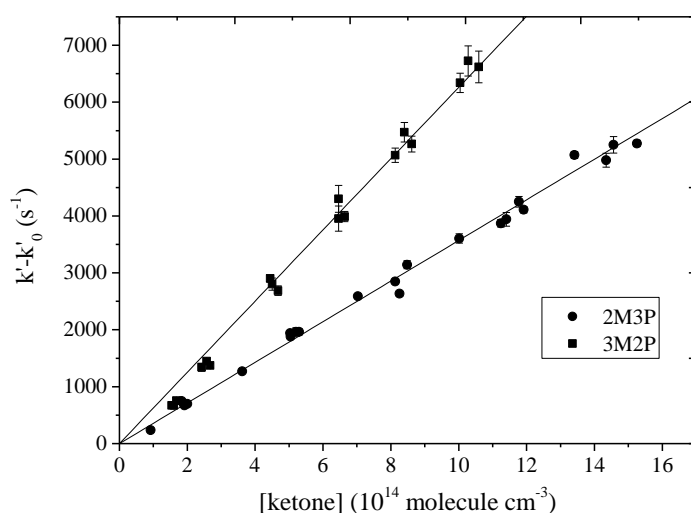


Figure 5-2: Plot of $(k' - k_0')$ vs 2M3P and 3M2P concentration at room temperature (296-303 K). The line represents the linear least-squares fitting. Note: $k' = k_{\text{ketone}} \times [\text{ketone}] + k_0'$, k_{ketone} is the rate constant of OH radical reaction with ketones. $k_0' = k_{\text{H}_2\text{O}_2} \times [\text{H}_2\text{O}_2] + k_{\text{diff}}$, $k_{\text{H}_2\text{O}_2}$ is the rate constant of OH radical reaction with H_2O_2 and k_{diff} is the decay rate of OH radical due to the diffusional loss.

Table 5-2 and Table 5-3 summarizes the PLP-LIF experimental conditions and the pseudo-first order rate constants over the temperature range 253-376 K for 2M3P+OH and 3M2P+OH, respectively, and plot in Figure 5-3. Combining the results obtained from both AR and RR method, we derived the following Arrhenius expression in the temperature range $T = 253\text{-}376\text{ K}$:

$$k_{(\text{OH}+2\text{M3P})} = (2.33 \pm 0.06) \times 10^{-12} \exp((127.4 \pm 18.6)/T) \text{ cm}^3 \text{ molecule}^{-1} \text{ s}^{-1}$$

$$k_{(\text{OH}+3\text{M2P})} = (1.64 \pm 0.09) \times 10^{-12} \exp((387 \pm 31)/T) \text{ cm}^3 \text{ molecule}^{-1} \text{ s}^{-1}$$

Then, the Arrhenius parameters for $k_{2\text{M3P_LIF}}$ and $k_{3\text{M2P_LIF}}$ are given in Table 5-2 and Table 5-3, respectively.

Table 5-2: Experimental conditions and the measured rate constants for the reaction of 2M3P+OH with PLP-LIF.

T (K)	[2M3P] (10^{14} molecule cm^{-3})	k'_0 (s^{-1}) ^b	k' (s^{-1}) ^a	$k'-k'_0$ (s^{-1})	$k_{2\text{M3P_LIF}} \pm 2\sigma$ (10^{-12} $\text{cm}^3 \text{ molecule}^{-1} \text{ s}^{-1}$)
253	2.3-17.8	111-115	958-6680	845-6567	3.43 ± 0.05
253	2.4-17.9	115-116	1000-7019	884-6904	3.31 ± 0.02
253	2.2-16.8	112-143	1021-6989	908-6875	3.46 ± 0.07
263	2.1-16.1	113-282	940-6382	826-6100	3.30 ± 0.07
263	2.2-17.0	139-145	987-6180	845-6038	3.35 ± 0.09
263	2.3-16.9	128	1051-6036	923-5908	3.49 ± 0.05
273	2.0-15.7	107-113	767-5451	657-5341	3.68 ± 0.06
273	2.1-16.4	124-126	857-5738	732-5613	3.61 ± 0.05
296	2.0-15.3	83-135	320-5357	236-5274	3.97 ± 0.06
297	1.8-14.3	127-142	872-5105	745-4978	4.13 ± 0.09
297	1.9-14.6	112-113	813-5363	701-5250	3.63 ± 0.01
303	1.9-13.4	120-122	793-5193	672-5072	3.56 ± 0.08
325	1.7-13.3	120	784-4349	667-4233	3.26 ± 0.08
327	0.8-13.4	108-142	218-4613	109-4478	3.41 ± 0.09
327	1.7-14.3	117	699-4836	582-4719	3.34 ± 0.02
348	1.6-12.5	111-112	633-3932	522-3820	3.60 ± 0.06
352	0.9-8.7	107-130	423-3147	297-3026	3.73 ± 0.07
352	1.7-13.2	110-113	605-4474	493-4363	3.75 ± 0.09
376	1.1-12.1	124-108	421-4183	305-4067	3.85 ± 0.14

376	1.5-11.7	122-124	643-3842	520-3701	3.88±0.10
298	3.57±0.05				
253-376 ^e	A ^c (10 ¹² cm ³ molecule ⁻¹ s ⁻¹): 1.64±0.09			E/R ^d (K): (127.4±18.6)	

^a $k' = k_{\text{ketone}} \times [\text{ketone}] + k_0'$; k_{ketone} is the rate constant of OH radical reaction with ketones

^b $k_0' = k_{\text{H}_2\text{O}_2} \times [\text{H}_2\text{O}_2] + k_{\text{diff}}$; $k_{\text{H}_2\text{O}_2}$ is the rate constant of OH radical reaction with H₂O₂; k_{diff} is the decay rate of OH radical due to the diffusional loss.

^c The uncertainties for A is $\Delta A = 2A\sigma \ln A$ for the Arrhenius form.;

^d The uncertainties for E/R is $\Delta E/R = 2\sigma E/R$ for the Arrhenius form.

^e Arrhenius expression using all data from AR and RR method.

Table 5-3: Experimental conditions and the measured rate constants for the reaction of 3M2P+OH with PLP-LIF.

T (K)	[3M2P] (10 ¹⁴ molecule cm ⁻³)	k' ₀ (s ⁻¹) ^b	k' (s ⁻¹) ^a	k'-k' ₀ (s ⁻¹)	k _{3M2P_LIF} ±2σ (10 ⁻¹² cm ³ molecule ⁻¹ s ⁻¹)
299	1.5-10.1	114-150	818-6484	670-6339	6.2±0.2
299	1.7-10.6	239-287	949-6895	756-6618	6.1±0.3
323	1.5-9.3	191-211	737-5366	600-5162	5.4±0.2
323	1.4-9.1	207-239	890-5218	741-4987	5.4±0.2
348	1.4-8.8	206-219	717-4700	568-4483	4.8±0.4
348	1.4-8.7	122-225	714-4613	585-4439	5.0±0.4
373	1.3-8.3	135-193	646-4001	500-3823	4.6±0.3
373	1.3-8.1	134-233	619-4095	485-3909	4.7±0.5
299	6.13±0.11				
253-376 ^e	A ^c (10 ¹² cm ³ molecule ⁻¹ s ⁻¹): 1.93±0.08			E/R ^d (K): (387±31)	

^a $k' = k_{\text{ketone}} \times [\text{ketone}] + k_0'$; k_{ketone} is the rate constant of OH radical reaction with ketones

^b $k_0' = k_{\text{H}_2\text{O}_2} \times [\text{H}_2\text{O}_2] + k_{\text{diff}}$; $k_{\text{H}_2\text{O}_2}$ is the rate constant of OH radical reaction with H₂O₂; k_{diff} is the decay rate of OH radical due to the diffusional loss.

^c The uncertainties for A is $\Delta A = 2A\sigma \ln A$ for the Arrhenius form.;

^d The uncertainties for E/R is $\Delta E/R = 2\sigma E/R$ for the Arrhenius form.

^e Arrhenius expression using all data from AR and RR method.

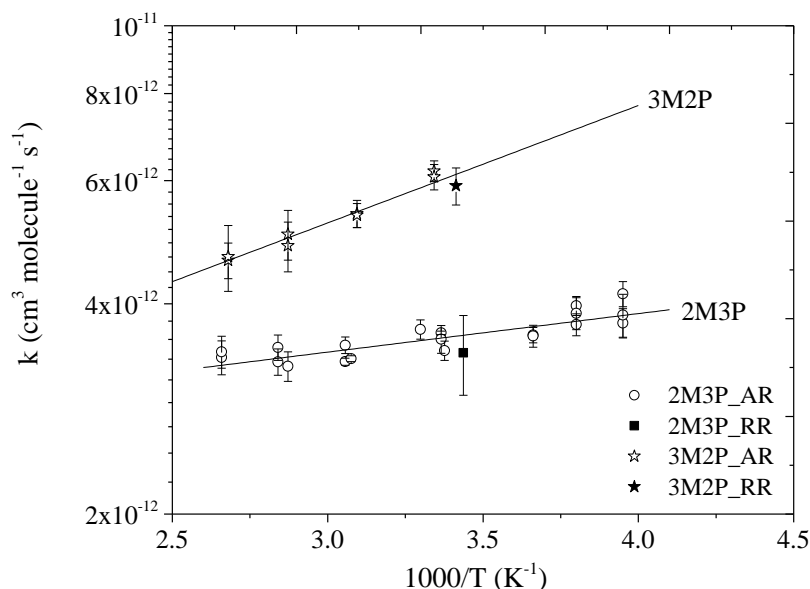


Figure 5-3: Plots of k_{2M3P} and k_{3M2P} vs $1/T$. The solid line represents the Arrhenius parameter least-squares fit to the individual data points at different temperatures combining all the data of AR and RR. The uncertainty of each point is 2σ .

5-3-3- Product formation from the ketones + OH radical

A series of experiments with H_2O_2 -NO-2M3P/3M2P/4M2P-air mixtures with irradiations at 254 nm were carried out in the 7.3 m³ ICARE chamber along with the analytical techniques (FTIR, UHPLC-MS, GC-MS, PTR-ToF-MS and HCHO monitor). The typical experimental procedure consisted in: (1) only studied ketones without lamps on for 1 hour to check the possible wall loss; (2) studied ketones with lamps on (7 of 254 nm lamps) for 1 hour to check possible photolysis decomposition; (3) studied ketones with H_2O_2 and NO without lamps on for 1 hour to verify possible dark reactions. (4) OH radical was generated via photolysis of H_2O_2 using 7 of 254 nm lamps, the reaction of studied ketones with OH radical was initiated. Finally, no significant wall losses (compared with the dilution of SF_6) or dark reactions have been observed for the studied ketones, however the photolysis of 2M3P/3M2P/4M2P was supposed to happen when the 254 nm lamps on without H_2O_2 and NO in the chamber. The photolysis rate constants and the products formed from the photolysis of 2M3P/3M2P/4M2P are shown in Table 5-4, which were used to correct the

2M3P/3M2P/4M2P consumption and products formation from the reaction of OH radical with 2M3P/3M2P/4M2P.

Table 5-4: The photolysis rate constants of 2M3P, 3M2P, 4M2P, HCHO, Ethanal, acetone, 2-butanone, 2,3-butanedione and 2-methylpropanal using 14 lamps (254 nm) in the ICARE 7.3 m³ chamber and the products yields from the photolysis of 2M3P, 3M2P and 4M2P.

VOC	J (10 ⁻⁵ s ⁻¹)	HCHO (%)	Acetone (%)	Ethanal (%)	2B (%)	2,3-BD (%)	2MP (%)
2M3P	8.0±0.2	20.0±0.5	64.6±1.2	50.9±6.7			
3M2P	4.5±0.1	59.8±0.8		62.4±9.8	43.4±0.6	8.2±0.1	
4M2P	5.3±0.1	87.7±2.3	59.2±1.7				115.3±6.0
HCHO	3.9±0.1						
Acetone	6.8±0.2						
Ethanal	6.5±0.3						
2B	10.7±0.2						
2,3-BD	5.2±0.1						
2MP	274.4±1						

The uncertainties are 1σ of the repeat experiments.

(Acetaldehyde = Ethanal, 2B: 2-butanone, 2,3-BD: 2,3-butanedione, 2MP: 2-methylpropanal)

5-3-3-1- 2M3P+OH

UHPLC-MS analysis showed the formation of acetone (CH3C(O)CH3), formaldehyde (HCHO), acetaldehyde (CH3CHO), propanal (CH3CH2CHO) and m/z=239 (Figure 5-4). As shown in Figures 5-5, the impurity was supposed to be the 4-hexen-3-one and represented less than 1% (not detected by UHPLC-MS) in liquid of 2M3P. This supposed that the impurity could be ignored. Additional analysis by GC-MS showed the presence of acetone, 2,3-dimethyl-2-nitro-butane and nitro-methane as reaction products (Figure 5-5). HCHO, CO, HCOOH were also detected by FTIR (Figure 5-6). In addition, HCHO was confirmed and quantified by an Aerolaser 4021 monitor using Hantzsch reaction (Aerolaser GMBH), acetone and acetaldehyde were quantified using PTR-ToF-MS.

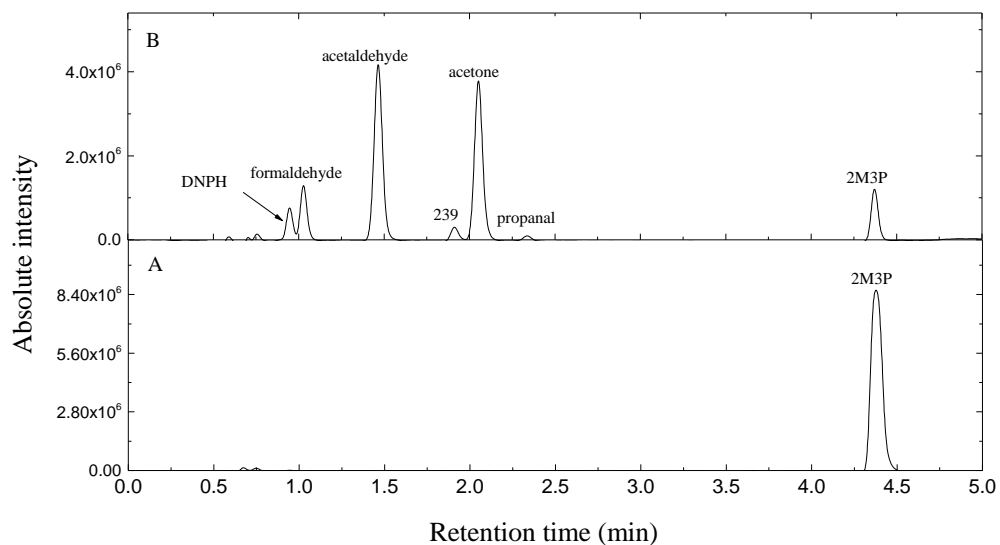


Figure 5-4: The Chromatogram from UHPLC-MS analysis: (A) before and (B) after 1 hour reaction of 2M3P with OH radical;

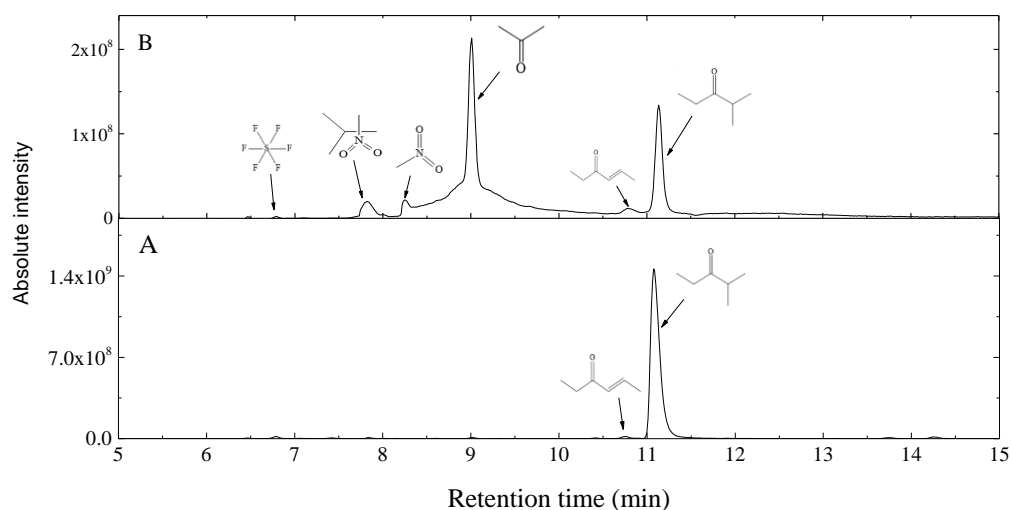


Figure 5-5: The Chromatogram spectra from GC-MS analysis: (A) before and (B) after 1 hour reaction of 2M3P with OH radical;

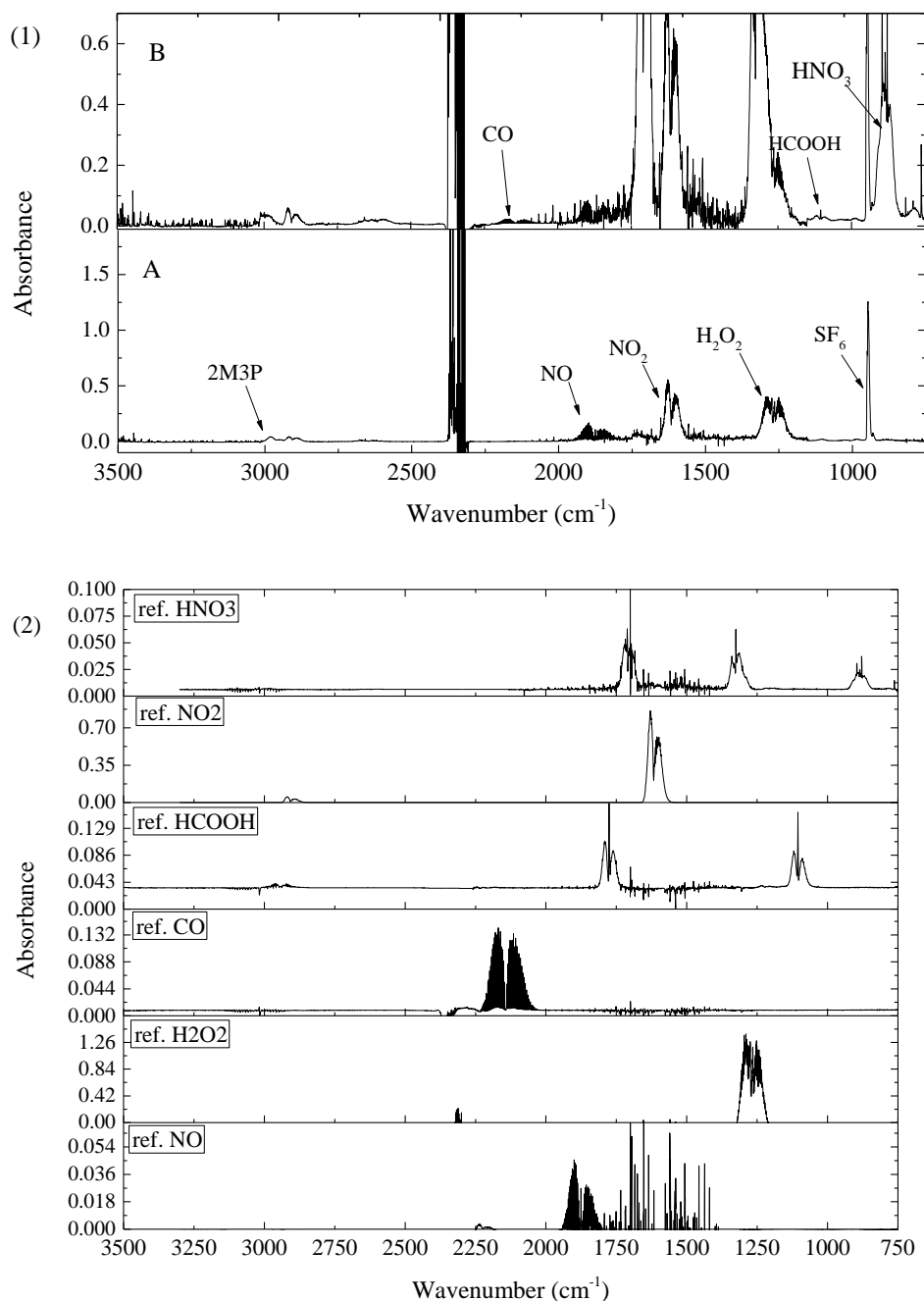


Figure 5-6: The FTIR spectra of the experiments (1) and references (2): (A) before and (B) after 4 hours reaction of 2M3P with OH radical; (ref. = references)

To obtain the formation yield of acetone, acetaldehyde and HCHO from 2M3P reaction of OH radical, the products formation from the photolysis of 2M3P (Table 5-4), products loss due to the photolysis (Table 5-4) and reaction with OH radical (referred from (Atkinson et al., 2006; Calvert; et al., 2008)) and dilution (decay of SF_6)

were corrected. The amounts of product formed versus the consumption of the 2M3P are plotted in Figure 5-7. The least-squares analyses lead to the formation yields given in Table 5-5. e.g. HCHO $34.0 \pm 6.0\%$, acetone $79.8 \pm 3.0\%$, acetaldehyde $104.3 \pm 10\%$.

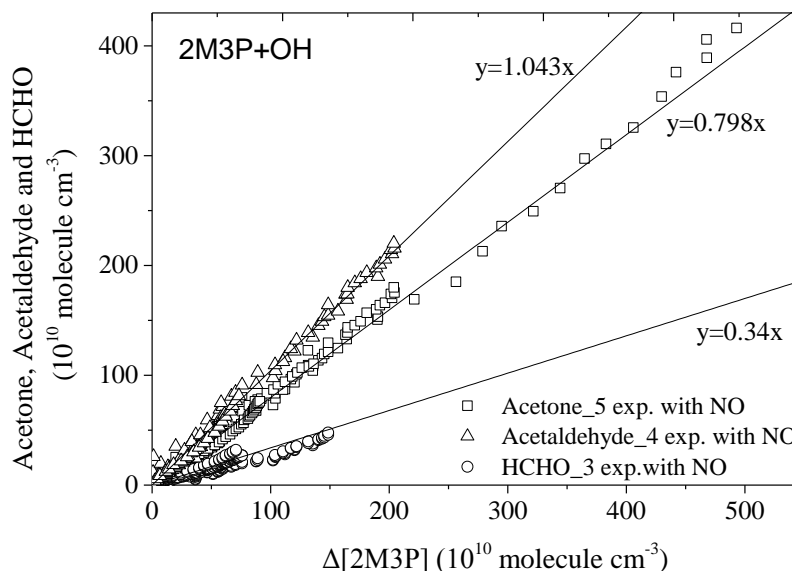


Figure 5-7: Plots of the amounts of product formed vs the consumed 2M3P. The concentration of products are corrected following the method described in the text. (The acetone and acetaldehyde were monitored by PTR-ToF-MS and HCHO was followed by the Aerolaser 4021 monitor. exp. = experiment)

Table 5-5: Experimental conditions and product formation for the reaction of 2M3P with OH radical under ambient temperature (296 ± 2 K) and pressure (≈ 760 torr).

	Exp.	[ketone] (ppb)	[NO] (ppb)	HCHO (%)	Acetone (%)	acetaldehyde (%)
2M3P	1	1094	1833		83.1 \pm 1.2	
	2	514	5629	28.1 \pm 0.1	81.9 \pm 0.6	101.7 \pm 5.7
	3	161	9204	33.3 \pm 0.1	75.9 \pm 0.9	105.3 \pm 1.4
	4	206			80.5 \pm 0.1	107.4 \pm 3.8
	5	93	5761	40.6 \pm 0.5	77.7 \pm 1.0	102.9 \pm 7.2
	Average			34.0 \pm 6.0	79.8 \pm 3.0	104.3 \pm 10
	Carbon budget (%)			80.4 \pm 0.7		

Indicated errors are 1σ standard deviations combined with estimated overall uncertainties of instruments and statistic errors of repeat experiments.

An example of the concentration-time profiles of 2M3P and the reaction products is shown in the Figure 5-8. Because CO and HCOOH could also be

secondary products (photolysis of primary products and their reactions with OH), we are not able to conclude on the formation yield for these species.

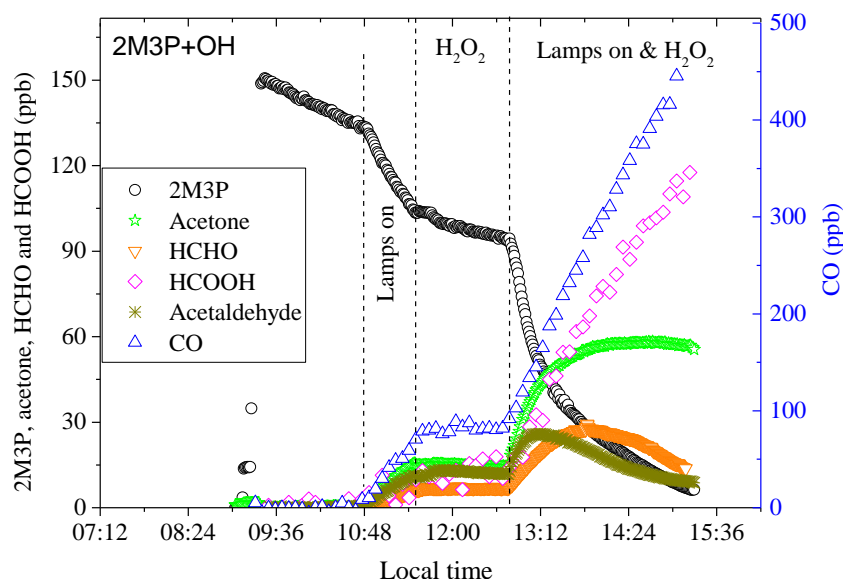


Figure 5-8: Concentration-time profiles of 2M3P and the products formed during the investigation of 2M3P reaction with OH radical.

5-3-3-2- 3M2P+OH

As shown in Figure 5-10, less than 1% impurity as 4-methyl-3-penten-2-one and 3-methyl-3-penten-2-one were present in 3M2P liquid sample used in this study (estimated from the GC-MS), which was confirmed by UHPLC-MS ($m/z=277$, Figure 5-9). In the reaction of 3M2P with OH radical, acetone, 2,3-dimethyl-2-nitro-butane and 2-butanone were found to be the products using GC-MS (Figure 5-10). 2-butanone was also detected by UHPLC-MS, as HCHO, acetaldehyde, propanal and $m/z=253$ (Figure 5-9). HCHO, CO, HCOOH were also detected by FTIR (Figure 5-11). In addition, HCHO was quantified by an Aerolaser A4021 monitor, 2-butanone, 2,3-butanedione and acetaldehyde were quantified using PTR-ToF-MS.

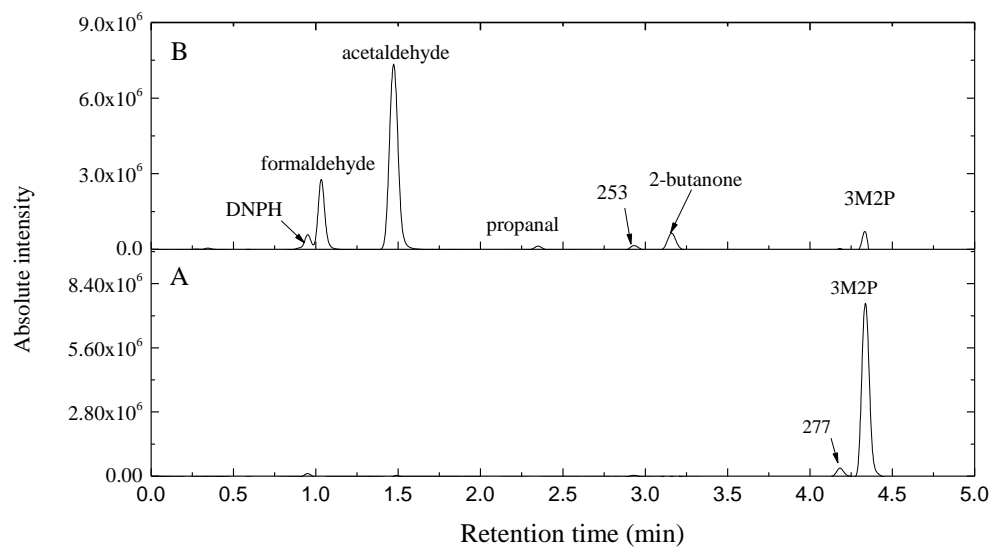


Figure 5-9: The Chromatogram from UHPLC-MS analysis: (A) before and (B) after 1 hour reaction of 3M2P with OH radical;

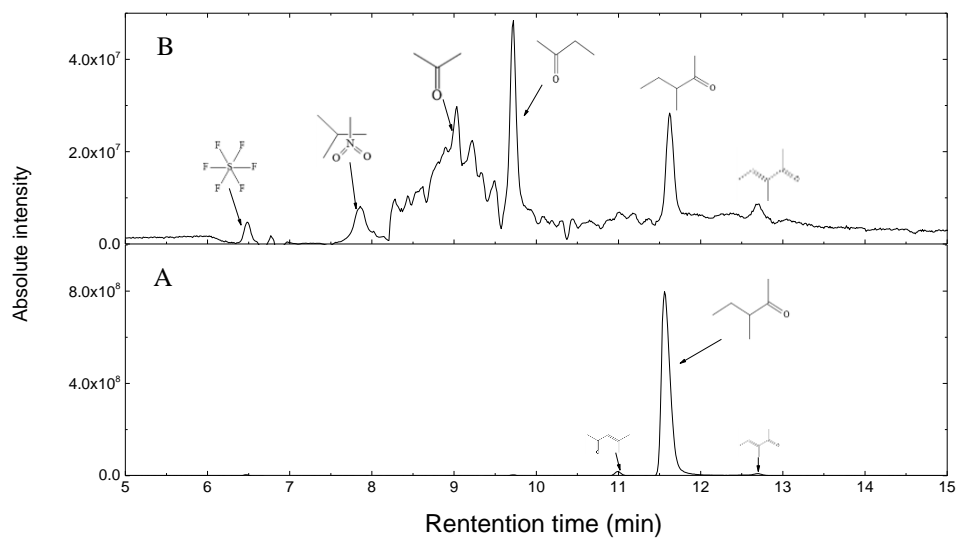


Figure 5-10: The Chromatogram from GCMS analysis: (A) before and (B) after 1 hour reaction of 3M2P with OH radical;

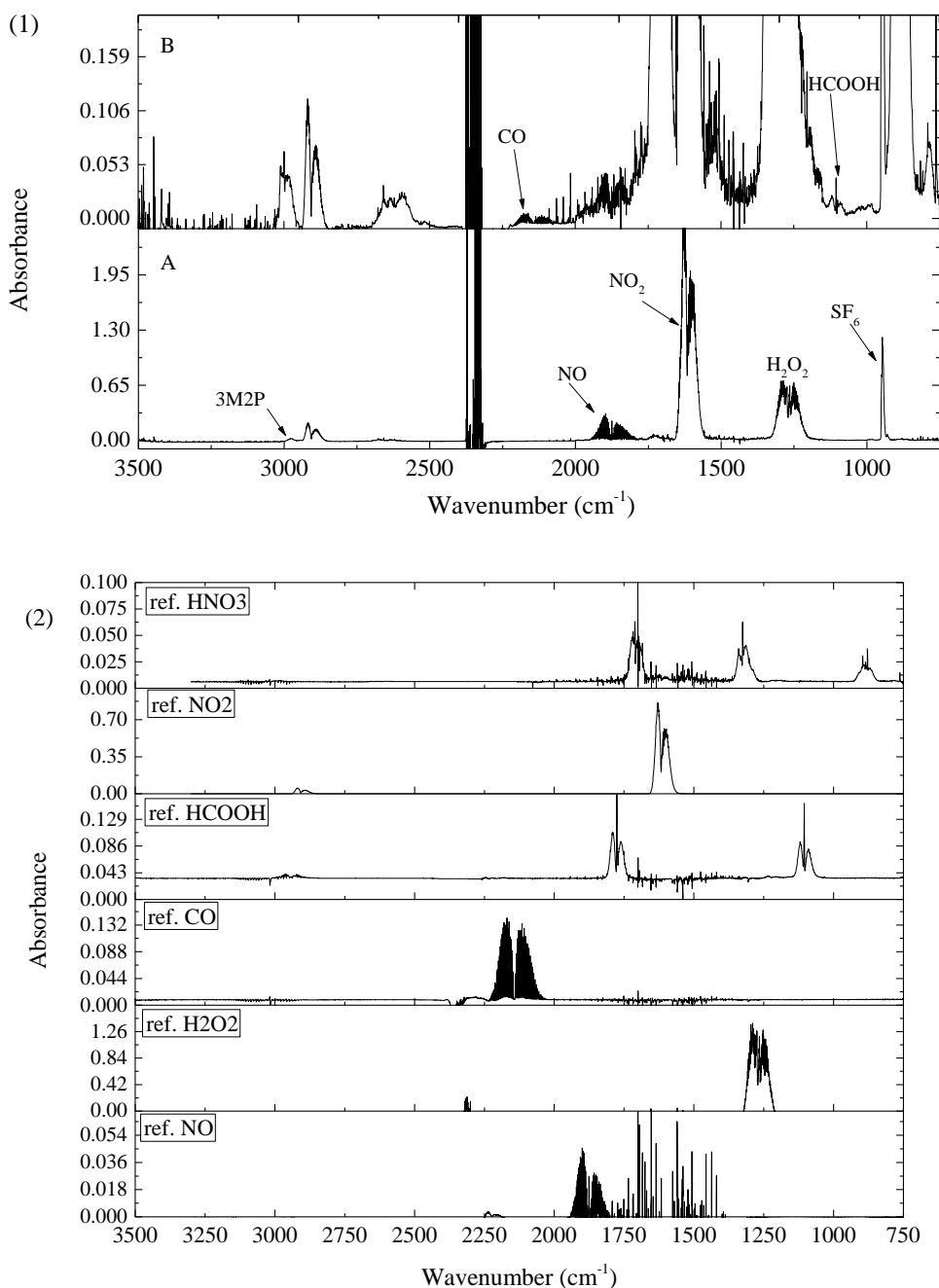


Figure 5-11: The FTIR spectra of the experiments (1) and references (2): (A) before and (B) after 4 hours reaction of 3M2P with OH radical; (ref. = references)

To obtain the formation yields of 2-butanone, acetaldehyde, 2,3-butanedione and HCHO from 3M2P reaction of OH radical, the products formation from the photolysis of 3M2P (Table 5-4), product loss due to the photolysis (Table 5-4) and reaction with OH radical (referred from (Atkinson et al., 2006; Calvert; et al., 2008)) and dilution (decay of SF₆) were corrected. The amounts of formed products versus the

consumption of the 3M2P are plotted in Figure 5-12. The least-squares analyses lead to the formation yields given in Table 5-6 e.g. HCHO $35.4 \pm 1.1\%$, 2-butanone $39.8 \pm 1.9\%$, 2,3-butanedione $2.5 \pm 1.8\%$, acetaldehyde $109.2 \pm 6.1\%$.

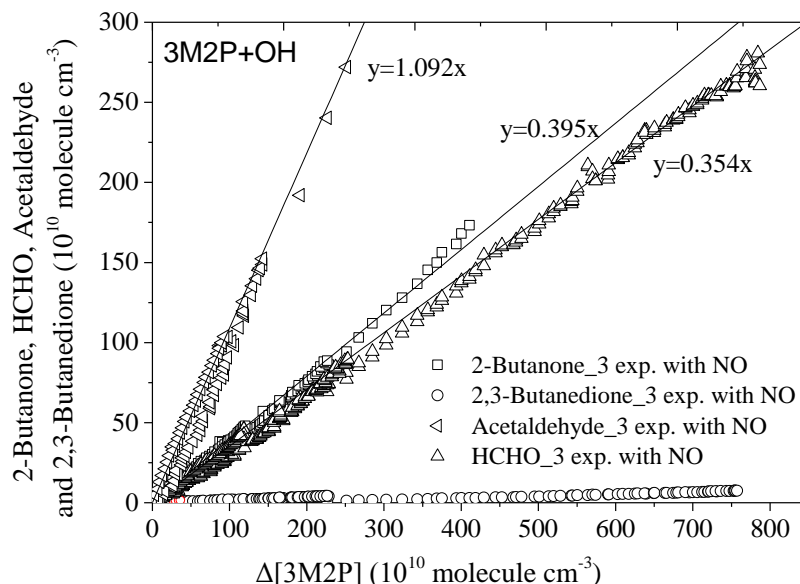


Figure 5-12: Plots of the amounts of formed products vs the consumed 3M2P. The concentrations of products were corrected following the method described in the text. (The 2-butanone, acetaldehyde and 2,3-butanedione were monitored by PTR-ToF-MS and HCHO was followed by the Aerolaser 4021 monitor. exp. = experiment)

Table 5-6: Experimental conditions and products formation for the reaction of 3M2P with OH radical under ambient temperature (296 ± 2 K) and pressure (≈ 760 torr).

	Exp.	[ketone] (ppb)	[NO] (ppb)	HCHO (%)	2B ^a (%)	2,3-BD ^b	acetaldehyde (%)
3M2P	1	523	4234	34.5 ± 0.1	40.9 ± 0.4	1.2 ± 0.1	104.4 ± 1.6
	2	389	10625	35.2 ± 1.1	39.3 ± 1.8	1.8 ± 0.5	115.7 ± 2.1
	3	92	4262	36.6 ± 1.2	39.1 ± 0.6	4.5 ± 0.7	107.4 ± 5.5
	Average			35.4 ± 1.1	39.8 ± 1.9	2.5 ± 1.8	109.2 ± 6.1
	Carbon budget (%)			70.5 ± 1.7			

^a 2B= 2-butanone

^b 2,3-BD= 2,3-butanedione;

product yield (%) = linear least-square fit of formed products concentration vs consumed studied ketones.

Indicated errors are 1σ standard deviations combined with estimated overall uncertainties of instruments and statistic errors of repeated experiments.

The concentration-reaction time profiles of 3M2P and the products are shown in

the Figure 5-13. Because of CO and HCOOH could also be formed as secondary products (photolysis of primary products and its reaction with OH), we are not capable to derive the formation yields for these species.

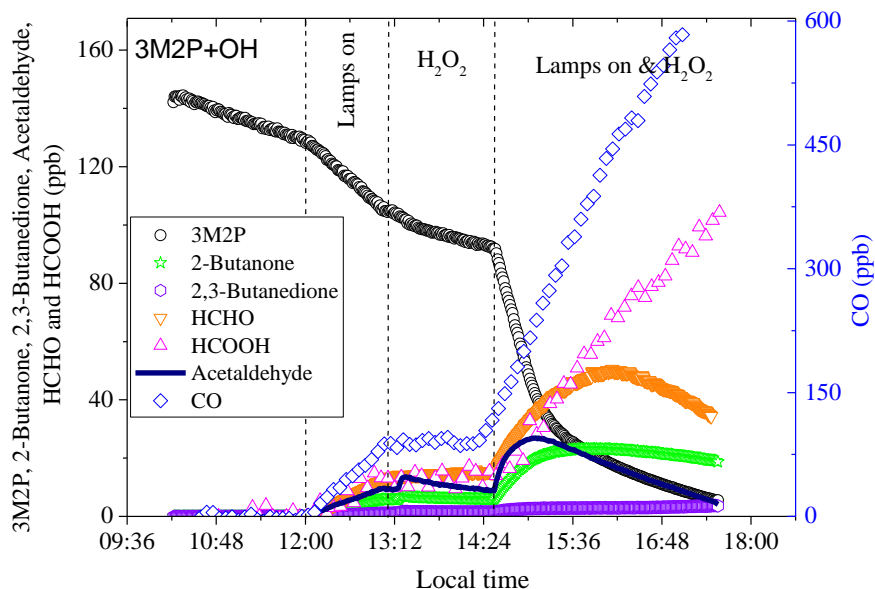


Figure 5-13: Concentration-time profiles of 3M2P and the products formed during the investigation of 3M2P reaction with OH radical.

5-3-3-3- 4M2P+OH

As shown in Figure 5-15, the impurity was supposed to be the 4-methyl-3-penten-2-one and represented less than 1% (estimated from the GC-MS), which was confirmed by UHPLC/MS measurement ($m/z=277$, Figure 5-14). For this reaction, acetone, 2-methylpropanal and 2,3-dimethyl-2-nitro-butane were detected as products using GC-MS (Figure 5-15). The presence of acetone was confirmed by the UHPLC-MS, and also the HCHO and acetaldehyde (Figure 5-14). HCHO, CO, HCOOH were also detected by FTIR (Figure 5-16). In addition, HCHO was quantified by an Aerolaser 4021 monitor, acetone, 2-methylpropanal and acetaldehyde were quantified using PTR-ToF-MS.

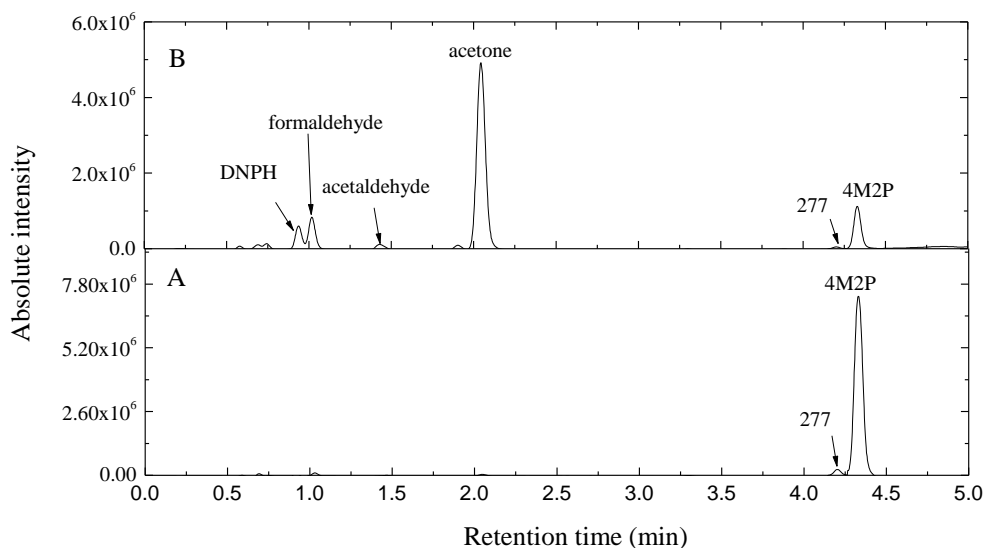


Figure 5-14: The Chromatogram spectra from UHPLC-MS analysis: (A) before and (B) after 1 hour reaction of 4M2P with OH radical;

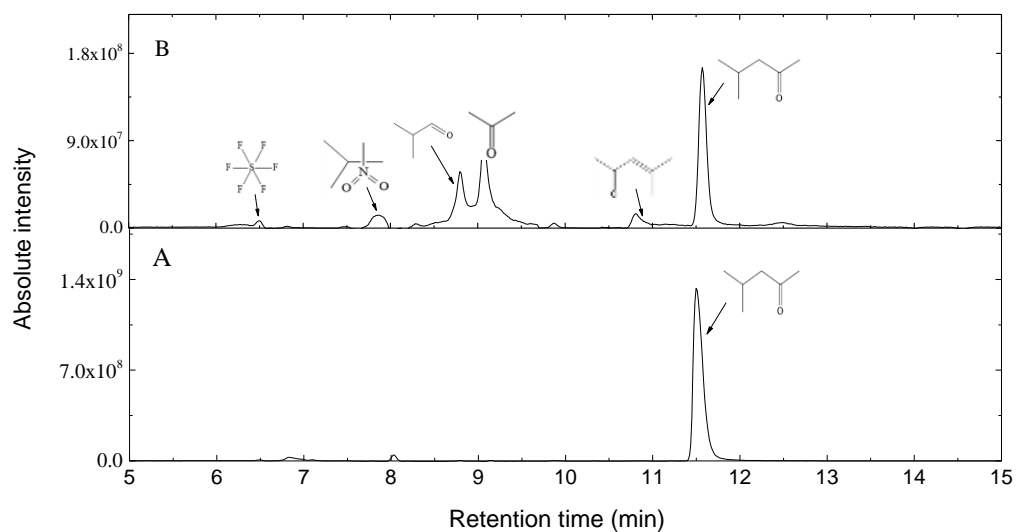


Figure 5-15: The Chromatogram spectra from GCMS analysis: (A) before and (B) after 1 hour reaction of 4M2P with OH radical;

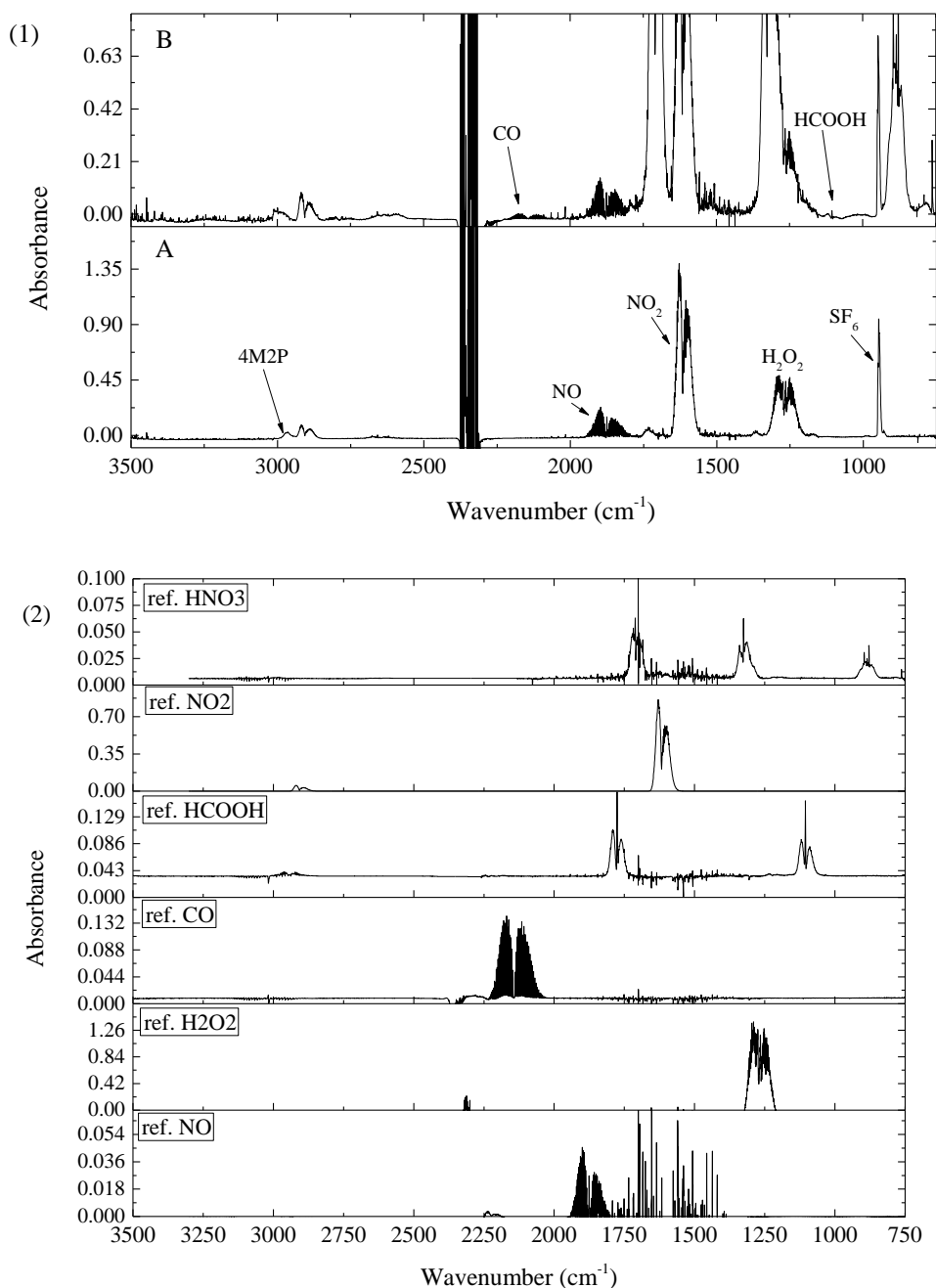


Figure 5-16: The FTIR spectra of the experiments (1) and references (2): (A) before and (B) after 4 hours reaction of 4M2P with OH radical; (ref. = references)

To obtain the formation yields of acetone, 2-methylpropanal and HCHO from 4M2P reaction of OH radical, the products formation from the photolysis of 4M2P (Table 5-4), product loss due to the photolysis (Table 5-4) and reaction with OH radical (referred from (Atkinson et al., 2006; Calvert; et al., 2008)) and dilution (decay of SF_6) were corrected. Finally, the amounts of formed products versus the

consumption of the 4M2P are plotted in Figure 5-17. The least-squares analyses lead to the formation yields given in Table 5-7 e.g. HCHO 51.9 \pm 3.5%, acetone 87.4 \pm 2.2%, 2-methylpropanal 10.7 \pm 4.8%.

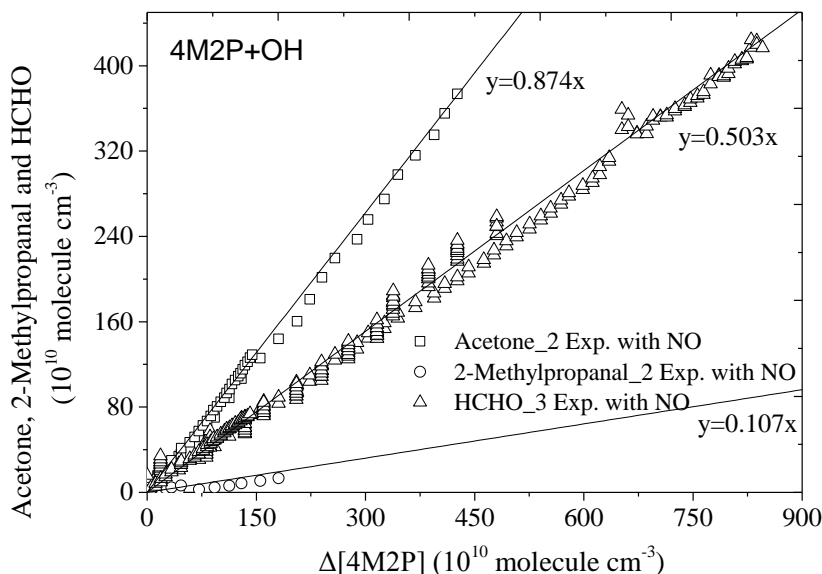


Figure 5-17: Plots of the amounts of formed products vs the consumed 4M2P. The concentrations of products were corrected following the method described in the text. (The acetone and 2-methylpropanal were monitored by PTR-ToF-MS and HCHO was followed by the Aerolaser 4021 monitor. exp. = experiment)

Table 5-7: Experimental conditions and products formation for the reaction of 4M2P with OH radical under ambient temperature (296 \pm 2 K) and pressure (\approx 760 torr).

	Exp.	[ketone] (ppb)	[NO] (ppb)	HCHO (%)	Acetone (%)	2MP ^a (%)
	1	580	6705	52.6 \pm 0.2	87.3 \pm 1.8	7.3 \pm 0.2
	2	630	8588	51.9 \pm 0.3		
4M2P	3	100	5650	51.3 \pm 3.5	87.5 \pm 1.3	14.1 \pm 0.4
	Average			51.9\pm3.5	87.4\pm2.2	10.7\pm4.8
	Carbon budget (%)			59.5 \pm 3.1		

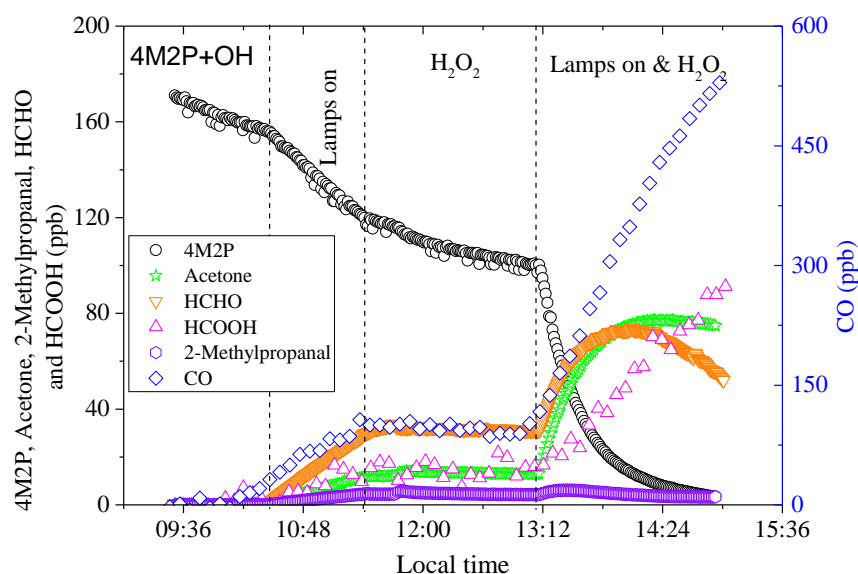
^a 2MP= 2-methylpropanal;

product yield (%) = linear least-square fit of formed products concentration vs consumed studied ketones.

Indicated errors are 1 σ standard deviations combined with estimated overall uncertainties of instruments and statistic errors of repeat experiments.

The profiles of the reactants 4M2P and possible products along with the experiments are shown in the Figure 5-18. Because CO and HCOOH could also be

acted as the secondary products (primary products photolysis and reaction with OH), we would not give the formation yield for these species.



Figures 5-18: Concentration- reaction time profiles of 4M2P and the products formed during the investigation of 4M2P reaction with OH radical.

5-4- Discussion

5-4-1- Comparison of rate constant with literature data for ketone + OH reaction

The present rate constant values for the reactions of studied ketones (2M3P, 4M2P and 3M2P) with OH are compared (Table 5-8) with the literature data for k_{3M2P} and k_{4M2P} , whereas this is the first determination reported for k_{2M3P} .

To improve the accuracy of the results, additional investigations were performed for k_{2M3P} and k_{3M2P} by using two different techniques: AR method with PLP-LIF and RR method with Simulation Chamber-GC/FID. The reaction of 4M2P with OH has been already investigated in a previous study in our laboratory using PLP-LIF technique (Le Calvé et al., 1998). Table 5-8 shows a good agreement between the two techniques used for k_{2M3P} , k_{3M2P} and k_{4M2P} . In addition, the value of k_{3M2P} in this work is in good agreement with the only existing previous relative measurement (Tuazon et

al., 2003). There are several studies on k_{4M2P} for the reaction of 4M2P with OH radical (Winer et al., 1976; Cox et al., 1980; Atkinson et al., 1982; O'Rji and Stone, 1992; Le Calvé et al., 1998). The value of k_{4M2P} in this work is in excellent agreement with the value from (Cox et al., 1980) where ethene was used as reference ($k_{(ethene+OH)}=7.9 \times 10^{-12} \text{ cm}^3 \text{ molecule}^{-1} \text{ s}^{-1}$). Calvert et al. (2008) recommended the Arrhenius expression $k=8.0 \times 10^{-13} \times \exp(828/T) \text{ cm}^3 \text{ molecule}^{-1} \text{ s}^{-1}$ and a rate constant at 298K of $k=12.8 \times 10^{-11} \text{ cm}^3 \text{ molecule}^{-1} \text{ s}^{-1}$ (uncertainty was estimated to be $\pm 15\%$). The excellent agreement of k_{4M2P} between our work and these of Calvert et al., (2008) would improve the reliability for k_{2M3P} and k_{3M2P} in this work.

Table 5-8: Summary of the rate constants for the reaction of OH radical with the studied ketones obtained in this work and in previous studies.

ketone	k_{SAR}	k	T (K)	Technique	Reference
2M3P	3.0 ^a	3.40 \pm 0.45	291 \pm 1	RR-GCFID	This work*
	3.7 ^b	3.57 \pm 0.05	297 \pm 1	PLP-LIF	This work*
	3.8 ^c				
3M2P	3.4 ^a	6.2 \pm 0.3	298	RR-GCFID	Tuazon et al., 2003
	6.2 ^c	5.90 \pm 0.36	293 \pm 1	RR-GCFID	This work*
		6.13 \pm 0.11	299 \pm 1	PLP-LIF	This work*
4M2P	8.9 ^a	9 \pm 3	305 \pm 2	RR-GCFID	Winer et al., 1976
	13.8 ^b	12.0 \pm 0.3	296	RR-GCFID	Cox et al., 1980
	14.0 ^c	14.5 \pm 0.7	299 \pm 2	RR-GCFID	Atkinson et al., 1982
		14.0 \pm 0.07	297 \pm 2	RR-GCFID	O'rji and Stone 1992
		12.1 \pm 0.5	298	PLP-LIF	Le Calve et al., 1998
		11.02 \pm 0.42	293 \pm 1	RR-GCFID	This work*

Unit of k_{SAR} and k is $10^{-12} \text{ cm}^3 \text{ molecule}^{-1} \text{ s}^{-1}$

^a Values calculated using SAR is based on the estimation of $-\text{CH}_3$, $-\text{CH}_2-$ and $-\text{CH}<$ group rate constant ($k_{(\text{CH}_x)}$) and which depend only on the identity of substituents attached to these groups.

^b Values calculated using SAR is based on the reactivity of R and R' group on either side of C=O group for OH reaction with ketones as $k_{\text{RC(O)R}'}=k_{(\text{R})}+k_{(\text{R}')}$

^c Values calculated using SAR is based on the rate constants for each CH_x ($x=1, 2, 3$) group of ketones depend on their position relative to C=O. e.g. $k_1=k_{\beta(-\text{CH}_3)}+k_{\alpha(-\text{CH}_2-)}+k_{\alpha(-\text{CH}-)}+k_{\beta(-\text{CH}_3)} \times 2$.

PLP-LIF= Pulsed Laser Photolysis-Laser Induced Fluorescence; RR-GCFID= Relative Rate method-Gas Chromatography Flame Ionization Detection.

5-4-2- Trends in the Ketones + OH Reaction Rate Constants

The obtained rate constants of studied ketones at 298 K can be also compared with the calculated ones using three structure-reactivity relationship (SAR) methods:

(1), SAR calculation of H abstraction is based on the estimation of $-\text{CH}<$, $-\text{CH}_2-$ and $-\text{CH}_3$ group rate constants. Assuming these group rate constants depend only on the identity of substituents attached to these groups, then:

$$k_{(\text{CH}_3-\text{X})}=k_{\text{prim}}F_{(\text{X})},$$

$$k_{(\text{X}-\text{CH}_2-\text{Y})}=k_{\text{sec}}F_{(\text{X})}F_{(\text{Y})},$$

$$k_{(\text{X}-\text{CH}-\text{Y})(\text{Z})}=k_{\text{tert}}F_{(\text{X})}F_{(\text{Y})}F_{(\text{Z})}.$$

At 298 K, the following parameters (Kwok and Atkinson, 1995) were used to calculate $k_{2\text{M3P}}$, $k_{3\text{M2P}}$ and $k_{4\text{M2P}}$: $k_{\text{prim}}=0.136$, $k_{\text{sec}}=0.934$, $k_{\text{tert}}=1.94$ (units in $10^{-12} \text{ cm}^3 \text{ molecule}^{-1} \text{ s}^{-1}$). $F_{(-\text{CH}_3)}=1$, $F_{(-\text{CH}_2-)}=F_{(-\text{CH}<)}=F_{(>\text{C}<)}=1.23$, $F_{(>\text{CO})}=0.75$, $F_{(-\text{CH}_2\text{C}(\text{O})\text{R})}=3.9$.

The calculated values for $k_{2\text{M3P}}$, $k_{3\text{M2P}}$ and $k_{4\text{M2P}}$ are: $k_{2\text{M3P}}=3.02$, $k_{3\text{M2P}}=3.38$ and $k_{4\text{M2P}}=8.86$, units in $10^{-12} \text{ cm}^3 \text{ molecule}^{-1} \text{ s}^{-1}$, indicates that $k_{4\text{M2P}} > k_{3\text{M2P}} > k_{2\text{M3P}}$. Since, the experimental values are: $k_{2\text{M3P}}=3.49 \pm 0.5$ (AR and RR), $k_{3\text{M2P}}=6.02 \pm 0.14$ (AR and RR) and $k_{4\text{M2P}}=11.02 \pm 0.42$, units in $10^{-12} \text{ cm}^3 \text{ molecule}^{-1} \text{ s}^{-1}$, respectively. It indicates that the SAR values and experimental values are close. And, this further confirm $k_{(-\text{CH}<)} > k_{(-\text{CH}_2-)} > k_{(-\text{CH}_3)}$ in the β position relative to $\text{C}=\text{O}$ group.

(2), $k_{\text{R_group}}$ ($\text{RC}(\text{O})\text{R}'$) additivity method: the rate constants for OH reaction with ketones $\text{RC}(\text{O})\text{R}'$ can also be calculated by assuming that the reactivity of the R (alkyl group) and R' groups on either side of the $\text{C}=\text{O}$ are independent and additive (Wallington and Kurylo, 1987). Thus $k_{\text{RC}(\text{O})\text{R}'}=k_{(\text{R})}+k_{(\text{R}')}$. Using $k_{(\text{R})}$ calculated previously in our group (Le Calvé et al., 1998) as shown in Table 5-9: $k_{(\text{n-C}_2\text{H}_5)}=1.0$, $k_{(\text{iso-C}_3\text{H}_7)}=2.7$, $k_{(\text{n-CH}_3)}=0.1$ and $k_{(\text{iso-C}_4\text{H}_9)}=13.7 \times 10^{-12} \text{ cm}^3 \text{ molecule}^{-1} \text{ s}^{-1}$, the $k_{2\text{M3P}}$ and $k_{4\text{M2P}}$ can be calculated as 3.7×10^{-12} and $13.8 \times 10^{-12} \text{ cm}^3 \text{ molecule}^{-1} \text{ s}^{-1}$, respectively, values in excellent agreement with the experimental data (Table 5-8). The value of $k_{3\text{M2P}}$ reported in this work provides the following new $k_{(\text{R})}$ at 298 K: $k_{(\text{sec-C}_4\text{H}_9)}=6.3 \times 10^{-12} \text{ cm}^3 \text{ molecule}^{-1} \text{ s}^{-1}$, see Table 5-8.

Table 5-9: Reactivity of Alkyl groups R or R' in ketones (RC(O)R') for ketone + OH reaction at 298 K from Le Calv é et al., (1998).

alkyl group R (R')	$10^{12} \times k_{(R)} \text{ cm}^3 \text{ molecule}^{-1} \text{ s}^{-1}$
CH ₃ -	0.1
n-C ₂ H ₅ -	1
n-C ₃ H ₇ -	3.9
iso-C ₃ H ₇ -	2.7
n-C ₄ H ₉ -	9
sec-C ₄ H ₉ -	6.3 ^a
iso-C ₄ H ₉ -	13.7
tert-C ₄ H ₉ -	1.1
n-C ₅ H ₁₁ -	8.8
iso-C ₅ H ₁₁ -	10.2

^a Value was recommended from the experimental data k_3 in this work.

(3) $k_{(\text{CH}_x)}$ additivity method: the rate constants for the reaction of OH with studied ketones (2M3P, 4M2P and 3M2P) can also be calculated from $k_{(\text{CH}_x)}$ ($x=1, 2, 3$) depending on their relative position to C=O group, e.g. $k_1 = k_{\beta(-\text{CH}_3)} + k_{\alpha(-\text{CH}_2-)} + k_{\alpha(-\text{CH}-)} + k_{\beta(-\text{CH}_3)} \times 2$. Calvert et al., (2011) has recommended the $k_{(\text{CH}_x)}$ for reaction of OH with ketones, see Table 5-10. Hence, the calculated $k_{2\text{M3P}}$, $k_{3\text{M2P}}$ and $k_{4\text{M2P}}$ could be 3.8 , 6.2 and $14.0 \times 10^{-12} \text{ cm}^3 \text{ molecule}^{-1} \text{ s}^{-1}$, respectively, are in excellent agreement with the experimental values (Table 5-8).

Table 5-10: CH_x ($x=1, 2, 3$) group rate coefficients $k_{(\text{CH}_x)}$ for reaction of OH radical with ketones at 298 K from Calvert et al., (2011)(units are $10^{-12} \text{ cm}^3 \text{ molecule}^{-1} \text{ s}^{-1}$)

CH _x group	α -position	β -position	γ -position	$>\delta$ -position
-CH ₃	0.1	0.37	0.27	0.12
-CH ₂ -	0.7	3.5	2.4	1.2
>CH-	2.0	12.7	7.8	2.9

5-4-3- Temperature dependence of the ketone + OH radical reaction

This work reports the first temperature dependence measurements for $k_{2\text{M3P}}$ and $k_{3\text{M2P}}$; the temperature dependence of $k_{4\text{M2P}}$ has been already reported using the same technique from our laboratory (Le Calv é et al., 1998). As displayed in Figure 5-19, it

shows the temperature dependence of k_{3M2P} is significantly negative, whereas k_{4M2P} presents the most negative temperature dependence, however the temperature dependence for k_{2M3P} is near zero. From the previous studies in our laboratory, Le Calvé et al., (1998) found the temperature dependence of 2-butanone and 3-methyl-2-butanone are near zero (Figure 5-19), which is explained by the fact that they only contain the deactivated $-\text{CH}<$ or $-\text{CH}_2-$ group in the α position relative to $\text{C}=\text{O}$ group and without the CH_x ($x=1,2$) group in the β position relative to $\text{C}=\text{O}$ group. Since 2M3P contain no CH_x ($x=1,2$) group in the β position of $\text{C}=\text{O}$ group, the near zero temperature dependence of k_{2M3P} in this work confirms that explanation. The pronounced negative temperature dependence of k_{4M2P} and k_{3M2P} is consistent with other ketones already observed containing $-\text{CH}<$ or $-\text{CH}_2-$ group (β , σ or γ position relative to the $\text{C}=\text{O}$ group) not deactivated.

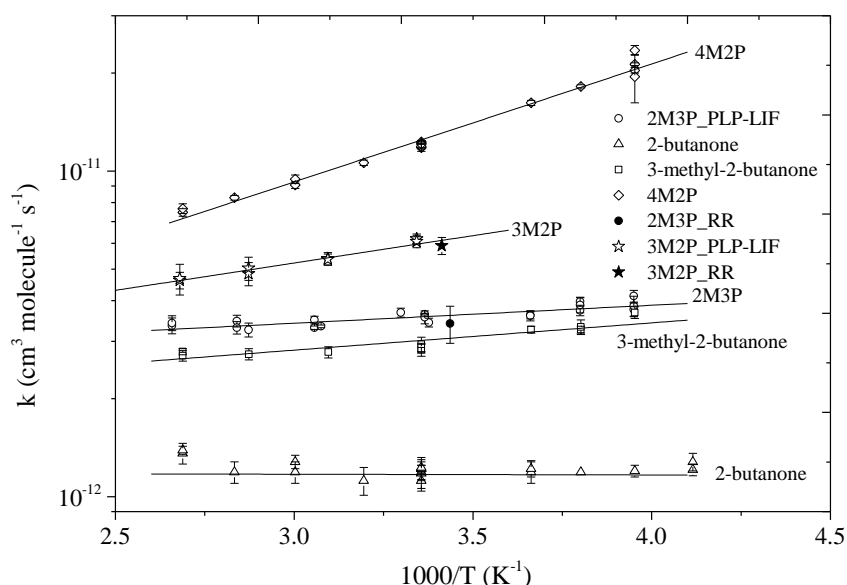
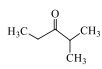


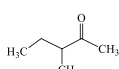
Figure 5-19: Plots of k_{2M3P} , k_{3M2P} , k_{4M2P} , $k_{2\text{-butanone}}$ and $k_{3\text{-methyl-2-butanone}}$ vs $1/T$. The solid line represents the Arrhenius parameter least-squares fit to the individual data points at different temperatures. The uncertainty of each point is 2σ . The temperature dependence data for reaction of OH radical with 4M2P, 3-methyl-2-butanone and 2-butanone are from Le Calvé et al., (1998).

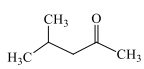
5-4-4- Reaction mechanism of the OH radical + ketones reaction

The previous experimental evidence suggests that ketones react with OH radicals

in a similar way as alkanes via an H-atom abstraction mechanism, resulting by the formation of alkyl radicals (Dagaut et al., 1988; Wallington and Kurylo, 1987). In addition, the estimation method of Atkinson (1987) allows calculating the branching ratios of the H-atoms abstraction from the various $-\text{CH}_3$, $-\text{CH}_2-$ and $>\text{CH}-$ groups for the OH radical + ketone reaction.

e.g. 2M3P  +OH: $-\text{CH}_3$ at 1-position 19.5%, $>\text{CH}-$ at 2-position 52.5%, $-\text{CH}_2-$ at 4-position 18.5%, $-\text{CH}_3$ at 5-position 9.7%;

3M2P  +OH: $-\text{CH}_3$ at 5-position 4.3%, $-\text{CH}_2-$ at 4-position 56.1%, $>\text{CH}-$ at 3-position 32.1%, $-\text{CH}_3-$ at 3-position 5.9%, $-\text{CH}_3$ at 1-position 1.6%;

4M2P  +OH: $-\text{CH}_3$ at 5-position 3.8%, $>\text{CH}-$ at 4-position 90.5%, $-\text{CH}_2-$ at 3-position 5%, $-\text{CH}_3$ at 1-position 0.7%.

As shown in the following pathways (4-5), alkoxy peroxy radical (RO_2) formed after adding O_2 to the alkyl radical ($\text{R}\cdot$). And which would mainly react with NO to form alkoxy radicals ($\text{RO}\cdot$) compared with self-reaction (pathways 6-7). Then $\text{RO}\cdot$ would mainly follow the reactions (Atkinson and Carter, 1991): (a) react with O_2 ; (b) decomposition (c) isomerization via a 6-membered transition state, their expected reaction pathways are shown in Scheme 1-3.

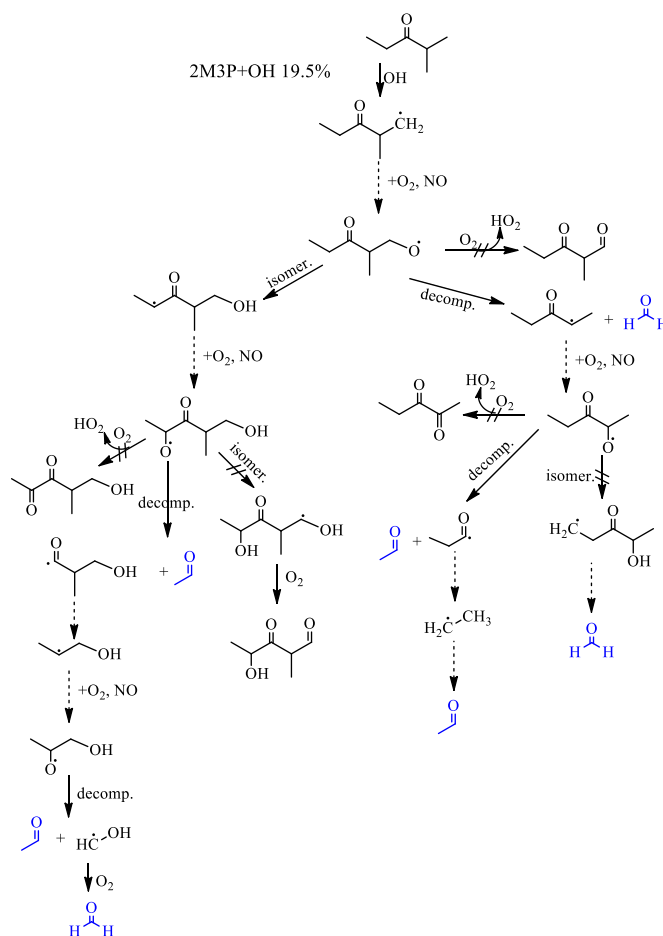


5-4-4-1- 2M3P+OH

As shown in Table 5-5, acetaldehyde and acetone were found to be the main products from the reaction of OH radical with 2M3P, with yields of 104.3 ± 10 and $79.8 \pm 3.0\%$ respectively. The proposed reaction mechanisms for the initial $\text{RO}\cdot$ formed after the H-abstraction from 2M3P are shown in Scheme 5-1(a-d). In addition, because no 2-methyl-pentanedione ($m/z=114$) was detected neither in UHPLC-MS

nor GC-MS nor PTR-ToF-MS, it indicates that the reaction of initial $\text{RO} \cdot$ with O_2 could be of minor importance.

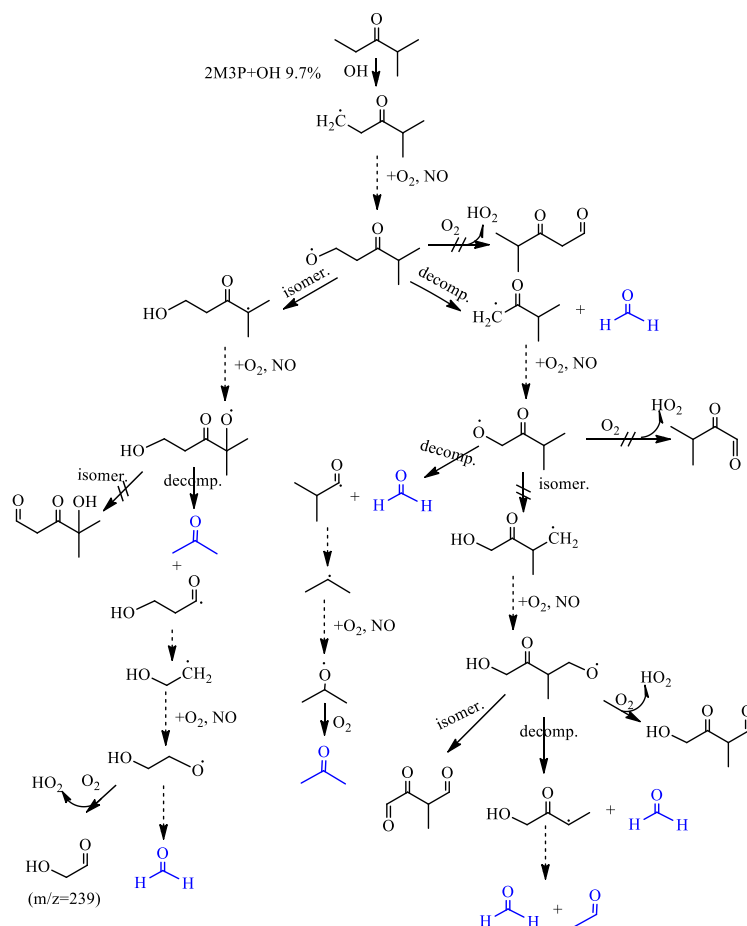
The $\text{CH}_3\text{CH}_2\text{C}(\text{O})\text{CH}(\text{CH}_3)\text{CH}_2\text{O} \cdot$ formed after H-atom abstraction from $-\text{CH}_3$ at 1-position accounts for 19.5% of the overall reaction and can mainly undergo isomerization via a 6-membered transition state and decomposition. As shown in Scheme 5-1(a), the $\text{CH}_3\text{CHO C}(\text{O})\text{CH}(\text{CH}_3)\text{CH}_2\text{OH}$ and $\text{CH}_3\text{CH}_2\text{C}(\text{O})\text{CHO CH}_3$ could be formed from its isomerization and decomposition, respectively. Because the $>\text{CO C}(\text{O})-$ carbon-carbon bond scission is rather faster than $>\text{CO CH}_2-$ carbon-carbon bond scission (Atkinson and Carter, 1991), and the isomerization depends on the position of the $-\text{CH}_3$, $-\text{CH}_2-$ and $>\text{CH}-$ groups relative to the $\text{C}=\text{O}$ group (Atkinson and Aschmann, 1995; Mereau et al., 2003), the decomposition of $\text{CH}_3\text{CHO C}(\text{O})\text{CH}(\text{CH}_3)\text{CH}_2\text{OH}$ and $\text{CH}_3\text{CH}_2\text{C}(\text{O})\text{CHO CH}_3$ radicals dominate to lead one molecule acetaldehyde and two acyl radicals (Scheme 5-1(a)). Considering the experimental acetaldehyde yield, one acyl radical, $\text{CH}_3\text{CH}_2\text{CO} \cdot$; predominantly decompose to lead one more molecule acetaldehyde (Scheme 5-1(a)) (Orlando et al., 2003). The following reaction of another parallel acyl radical, $\text{HOCH}_2\text{CH}(\text{CH}_3)\text{CO} \cdot$; involves the formation of $\text{CH}_3\text{CHO CH}_2\text{OH}$ radical. It assumes that $\geq \text{C}_3$ β -hydroxyalkoxy radicals always decompose rapidly under atmospheric condition (Atkinson and Carter, 1991), one acetaldehyde was expected to be obtained from the decomposition of the $\text{CH}_3\text{CHO CH}_2\text{OH}$ radical (Scheme 5-1(a)). Then the H-atom abstraction from $-\text{CH}_3$ at 1-position account for 39% (19.5×2 %) of the overall acetaldehyde formation.



Scheme 5-1(a): Reaction of OH radical with 2M3P: proposed mechanism leading to the formation of observed reaction products. Compounds in blue represent products observed experimentally. The expected relative importance of the possible RO \cdot reaction pathways are indicated by the arrows: \rightarrow > \nrightarrow ; the intermediary of RO / RO $_2$ \cdot are indicated by \cdots .

The (CH $_3$) $_2$ CHC(O)CH $_2$ CH $_2$ O \cdot formed after H-atom abstraction from -CH $_3$ at 5-position accounts for 9.7% and can mainly undergo isomerization and decomposition meanwhile the isomerization and decomposition are of comparable importance. Then the (CH $_3$) $_2$ CO C(O)CH $_2$ CH $_2$ OH and (CH $_3$) $_2$ CHC(O)CH $_2$ O \cdot formed from its isomerization and decomposition, respectively (Scheme 5-1(b)). Based on the experimental determination of acetone yield, the decomposition of (CH $_3$) $_2$ CO C(O)CH $_2$ CH $_2$ OH and (CH $_3$) $_2$ CHC(O)CH $_2$ O \cdot dominate and lead to one molecule acetone (Scheme 5-1(b)). However, except of the formation of acetone, the decomposition of (CH $_3$) $_2$ CO C(O)CH $_2$ CH $_2$ OH still lead to HOCH $_2$ CH $_2$ CO \cdot radical. As shown in Scheme 5-1(b), the following reaction of HOCH $_2$ CH $_2$ CO \cdot radical

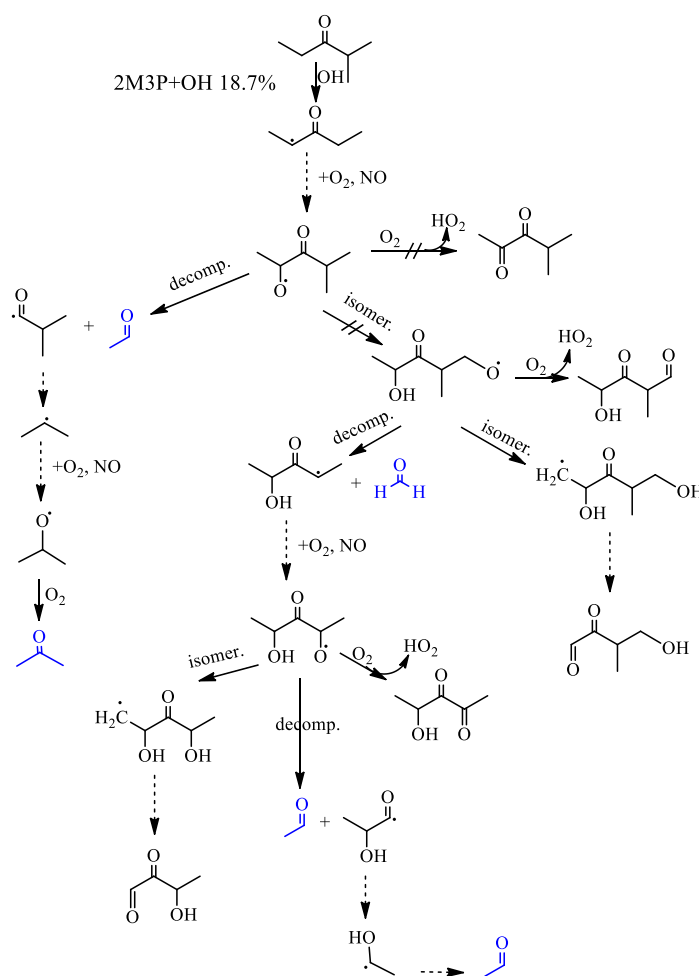
produce $\text{HOCH}_2\text{CH}_2\text{O}\cdot$ radical. While the reaction with O_2 was observed to be predominately for $\text{HOCH}_2\text{CH}_2\text{O}\cdot$ (Niki et al., 1981), the HOCH_2CHO formed from the reaction of $\text{HOCH}_2\text{CH}_2\text{O}\cdot$ with O_2 and which is supposed to be $m/z=239$ in UHPLC-MS (Figure 5-5). Hence the H-atom abstraction from $-\text{CH}_3$ at 5-position account for 9.7% of the overall acetone formation.



Scheme 5-1(b): Reaction of OH radical with 2M3P: proposed mechanism leading to the formation of observed reaction products. Compounds in blue represent products observed experimentally. The expected relative importance of the possible $\text{RO}\cdot$ reaction pathways are indicated by the arrows: $\rightarrow > \nrightarrow$; the intermediary of $\text{RO}\cdot / \text{RO}_2\cdot$ are indicated by \cdots .

The $\text{CH}_3\text{CHO C(O)CH(CH}_3)_2$ radical formed after H-atom abstraction from the $-\text{CH}_2-$ group at 4 position accounts for 18.7% of the overall reaction, which can mainly undergo isomerization and decomposition. The isomerization involves H-atom abstraction from β $-\text{CH}_3$ group and is expected to be minor compared to decomposition (Atkinson and Aschmann, 1995; Mereau et al., 2003). Based on the

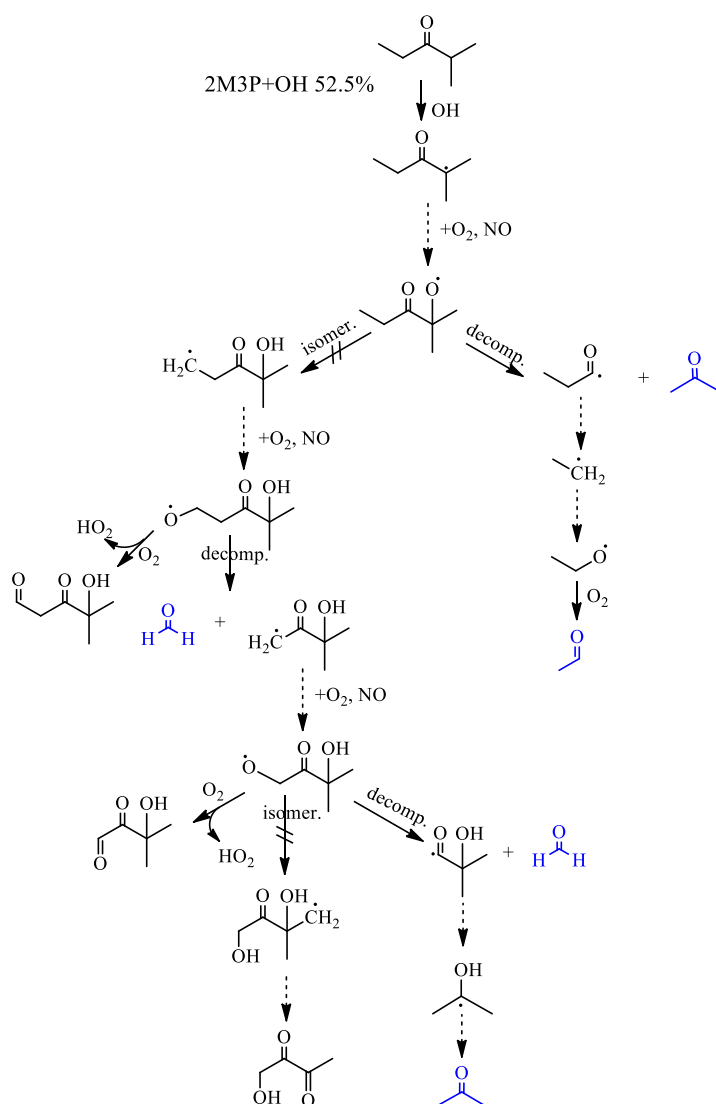
observation of the acetone and acetaldehyde yields, thermal decomposition of $\text{CH}_3\text{CHO C(O)CH(CH}_3)_2$ produce $(\text{CH}_3)_2\text{CHC(O)}\cdot$ plus one molecule acetaldehyde, as shown in Scheme 5-1(c). Then the following reaction of $(\text{CH}_3)_2\text{CHC(O)}\cdot$ produce $\text{CH}_3\text{CHO CH}_3$ radical, which would mainly react with O_2 to lead one molecule acetone (Scheme 5-1(c)) (Orlando et al., 2003). Hence, the H-atom abstraction from $-\text{CH}_2-$ group at 4 position accounts for 18.7% of the overall acetone and acetaldehyde formation, respectively.



Scheme 5-1(c): Reaction of OH radical with 2M3P: proposed mechanism leading to the formation of observed reaction products. Compounds in blue represent products observed experimentally. The expected relative importance of the possible $\text{RO}\cdot$ reaction pathways are indicated by the arrows: $\rightarrow > \rightleftharpoons$; the intermediary of $\text{RO}\cdot$ / $\text{RO}_2\cdot$ are indicated by \cdots .

The $\text{CH}_3\text{CH}_2\text{C(O)CO(CH}_3)_2$ radical formed after H-atom abstraction from $>\text{CH}-$ at 2-position accounts for 52.5% of the overall reaction and cannot react with O_2 ,

leaving decomposition and isomerization as possible pathways (Scheme 5-1(d)). Since the isomerization involves the H-abstraction from the β -CH₃ group, it is expected to be minor compared to decomposition (Atkinson and Aschmann, 1995; Mereau et al., 2003). Then CH₃CH₂C(O)· and one molecule acetone were formed from the decomposition of CH₃CH₂C(O)CO(CH₃)₂. The further fate of CH₃CH₂C(O)· is expected to form one molecule acetaldehyde (Orlando et al., 2003). Hence, the H-atom abstraction from >CH- at 2-position accounts for 52.5% of the overall acetone and acetaldehyde formation, respectively.



Scheme 5-1(d): Reaction of OH radical with 2M3P: proposed mechanism leading to the formation of observed reaction products. Compounds in blue represent products observed experimentally. The expected relative importance of the possible RO· reaction pathways are indicated by the arrows: → > ⇌; the intermediary of RO· / RO₂· are indicated by ⇌.

As shown in Scheme 5-1(a-d), our SAR estimated and experimental determination of acetone and acetaldehyde yields indicate that acetone is formed after the following reaction of H-abstraction from $-\text{CH}_3$ at 5-position, $-\text{CH}_2-$ group at 4 position and $>\text{CH}-$ at 2-position. Acetaldehyde is formed from following reaction of H-abstraction from $-\text{CH}_3$ at 1-position, $-\text{CH}_2-$ group at 4 position and $>\text{CH}-$ at 2-position. The H-abstraction from $>\text{CH}-$ at 2-position accounts for the mostly formation of acetone and acetaldehyde. Furthermore, our measured acetone and acetaldehyde yields of $79.8 \pm 3.0\%$ and $104.3 \pm 10\%$, respectively, are close to the estimated H-atom abstraction branching ratio of 80.9% ($9.7+18.7+52.5\%$) and 110.2% ($39+18.7+52.5\%$).

During the reaction of 2M3P with OH radical, formation of organic nitrate from the reactions of RO_2 radical with NO (Calvert et al., 2011) appears to be less important (Orlando et al., 2003). By taking into account of the experimental determination of formaldehyde, acetone and acetaldehyde yields, the carbon content of the formed products occupies $80.4 \pm 0.7\%$ percent of the carbon content of the consumed 2M3P. The detected HCOOH in FTIR (Figure 5-6) may be formed from secondary chemistry involving reactions of OH radical and HO_2 with HCHO (Tyndall et al., 1998).

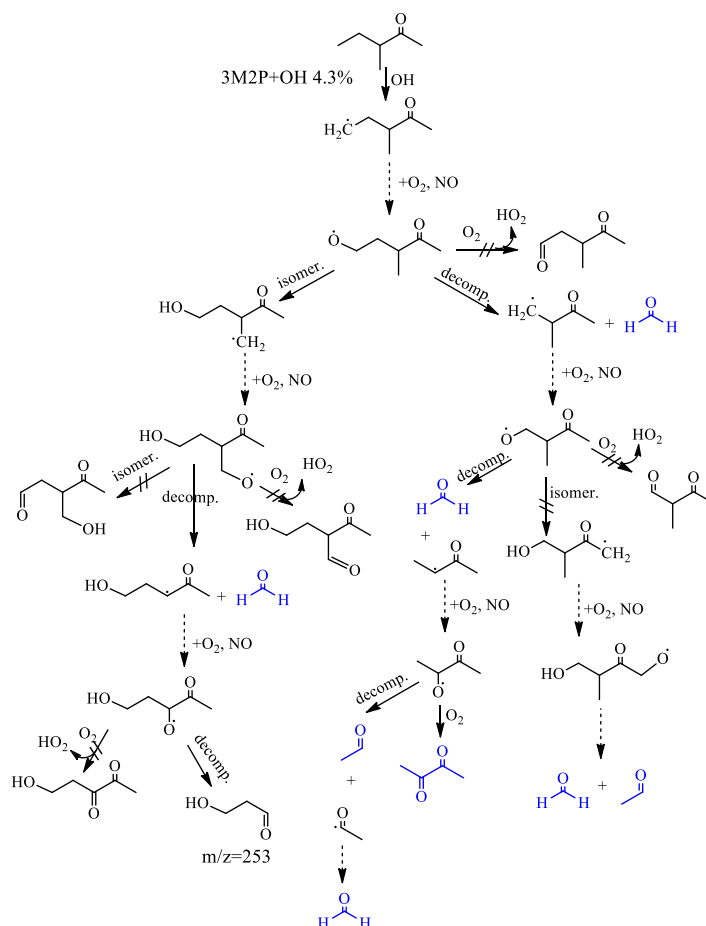
5-4-4-2- 3M2P+OH

As shown in the Table 5-6, acetaldehyde and 2-butanone were found to be the main products from the reaction of OH radical with 3M2P, determined as 109.2 ± 6.1 and $39.8 \pm 1.9\%$ in this work. The 2,3-butanedione was also found to be the minor products of $2.5 \pm 1.8\%$. The possible reaction schemes of the five initial $\text{RO} \cdot$ formed from H-atom abstraction from $-\text{CH}_3$, $-\text{CH}_2-$ and $>\text{CH}-$ groups, are shown in Scheme 5-2(a-d). The relative importance of some $\text{RO} \cdot$ reaction are known from experimental and SAR studies, which have been noted in Scheme 5-2(a-d). While these reaction schemes are complex, the experimental data could help to draw the mechanism. In addition, because no 3-methyl-pentanedione ($m/z=114$) was detected neither in

UHPLC/MS nor GC-MS nor PTR-ToF-MS, it indicates that the reaction of initial $\text{RO} \cdot$ with O_2 could be of minor importance.

Since $\text{CH}_3\text{CH}_2\text{CH}(\text{CH}_3)\text{C}(\text{O})\text{CH}_2\text{O} \cdot$ radical formed after H-abstraction from the $-\text{CH}_3$ at 1-position accounts for only 1.6% of all the reaction, so any 2-butanone and acetaldehyde formation from this branch can only account for minor fraction of the observed products.

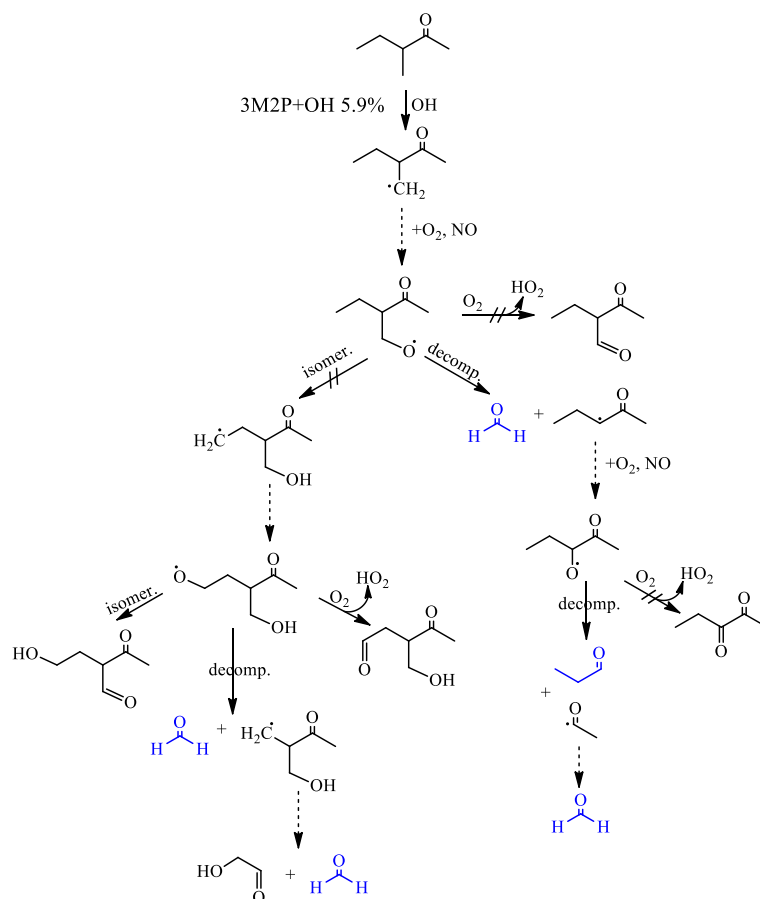
The $\text{CH}_3\text{C}(\text{O})\text{CH}(\text{CH}_3)\text{CH}_2\text{CH}_2\text{O} \cdot$ radical formed after H-atom abstraction from the $-\text{CH}_3$ group at 5 position accounts for 4.3% of the overall reaction, which can mainly undergo isomerization and decomposition. As shown in Scheme 5-2(a), the following reaction of isomerization of $\text{CH}_3\text{C}(\text{O})\text{CH}(\text{CH}_3)\text{CH}_2\text{CH}_2\text{O} \cdot$ involves the formation of $\text{HOCH}_2\text{CH}_2\text{CHO}$, which has been detected in UHPLC-MS as $m/z=253$. In the other way, as shown in Scheme 5-2(a), $\text{CH}_3\text{C}(\text{O})\text{CH}(\text{CH}_3)\text{CH}_2\text{O} \cdot$ formed from the decomposition of $\text{CH}_3\text{C}(\text{O})\text{CH}(\text{CH}_3)\text{CH}_2\text{CH}_2\text{O} \cdot$. Then the following decomposition of $\text{CH}_3\text{C}(\text{O})\text{CH}(\text{CH}_3)\text{CH}_2\text{O} \cdot$ involves the formation of HCHO and $\text{CH}_3\text{C}(\text{O})\text{CHOCH}_3$ radical. As Atkinson and Carter (1991) estimated, $\text{CH}_3\text{C}(\text{O})\text{CHOCH}_3$ would mainly decompose to one molecule acetaldehyde and acyl radical than reacting with O_2 to form 2,3-butanedione (Scheme 5-2(a)). Hence, the H-atom abstraction from the $-\text{CH}_3$ group at 5 position accounts for 4.3% of the overall acetaldehyde formation.



Scheme 5-2(a): Reaction of OH radical with 3M2P: proposed mechanism leading to the formation of observed reaction products. Compounds in blue represent products observed experimentally. The expected relative importance of the possible RO \cdot reaction pathways are indicated by the arrows: \rightarrow > \nrightarrow ; the intermediary of RO \cdot / RO $_2\cdot$ are indicated by \cdots .

The $\text{CH}_3\text{CH}_2\text{CH}(\text{CH}_2\text{O}\cdot)\text{C}(\text{O})\text{CH}_3$ radical formed after H-atom abstraction from the $-\text{CH}_3$ group at 3 position accounts for 5.9% of the overall reaction, which can mainly undergo isomerization and decomposition. Since the isomerization of $\text{CH}_3\text{CH}_2\text{CH}(\text{CH}_2\text{O}\cdot)\text{C}(\text{O})\text{CH}_3$ involves the H-abstraction either from the α $-\text{CH}_3$ group or γ $-\text{CH}_3$ group, the isomerization could be of minor importance and the decomposition dominate the reaction pathway (Atkinson and Aschmann, 1995; Mereau et al., 2003). As shown in Scheme 5-2(b), HCHO and $\text{CH}_3\text{CH}_2\text{CHO}$ $\text{C}(\text{O})\text{CH}_3$ radical were formed from the decomposition of $\text{CH}_3\text{CH}_2\text{CH}(\text{CH}_2\text{O}\cdot)\text{C}(\text{O})\text{CH}_3$. Furthermore, thermochemical calculation (Orlando et al., 2003) indicates that $\text{CH}_3\text{CH}_2\text{CHO}$ $\text{C}(\text{O})\text{CH}_3$ would dominantly decompose to lead

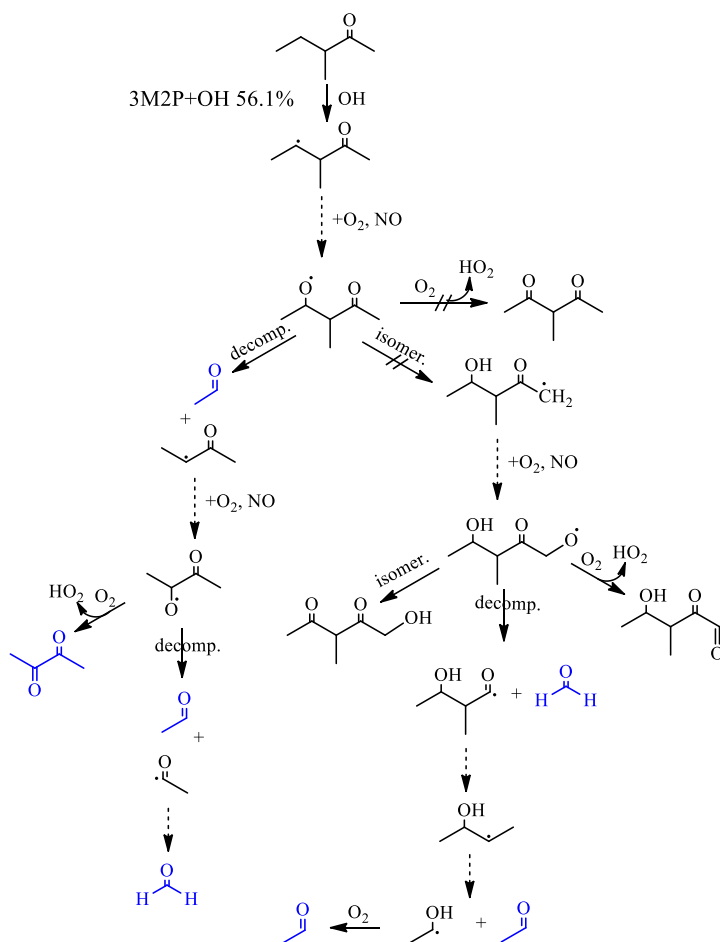
one molecule propanal and $\text{CH}_3\text{C}(\text{O})\cdot$ radical (Scheme 5-2(b)). In addition, the propanal was found in UHPLC-MS as $m/z = 237$ (Figure 5-9) without determination of the yield. Furthermore, the 2,3-pentanedione has not been detected by UHPLC-MS, PTR-ToF-MS and GC-MS in this work.



Scheme 5-2(b): Reaction of OH radical with 3M2P: proposed mechanism leading to the formation of observed reaction products. Compounds in blue represent products observed experimentally. The expected relative importance of the possible $\text{RO}\cdot$ reaction pathways are indicated by the arrows: $\rightarrow > \nrightarrow$; the intermediary of $\text{RO}\cdot$ / $\text{RO}_2\cdot$ are indicated by \cdots .

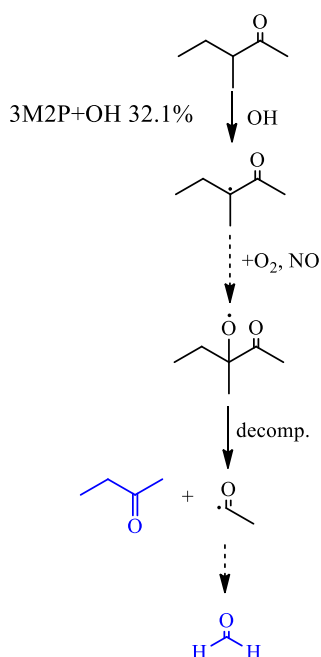
The $\text{CH}_3\text{CHO CH}(\text{CH}_3)\text{C}(\text{O})\text{CH}_3$ radical formed after H-atom abstraction from the $-\text{CH}_2-$ at 4-position accounts for 56.1% of the overall reaction, which can mainly undergo isomerization and decomposition. Since the isomerization of $\text{CH}_3\text{CHO CH}(\text{CH}_3)\text{C}(\text{O})\text{CH}_3$ radical involves the H-abstraction from the α $-\text{CH}_3$ group, the isomerization could be of minor importance (Atkinson and Aschmann, 1995; Mereau et al., 2003). Based on the observed acetaldehyde yield, thermal

decomposition of the $\text{CH}_3\text{CHO}-\text{CH}(\text{CH}_3)\text{C}(\text{O})\text{CH}_3$ radical produce $\text{CH}_3\text{C}(\text{O})\text{CH}-\text{CH}_3$ radical plus one molecule acetaldehyde, as shown in Scheme 5-2(c), is expected to dominate over the alternative decomposition to $\text{CH}_3\text{C}(\text{O})\text{CH}(\text{CH}_3)\text{CHO}$ plus $\text{CH}_3\cdot$ radical. Neglecting of the nitrate formation from the reaction of RO_2+NO (Calvert et al., 2011), the following reaction of $\text{CH}_3\text{C}(\text{O})\text{CH}-\text{CH}_3$ produce $\text{CH}_3\text{C}(\text{O})\text{CHO}-\text{CH}_3$. Thermochemical calculations (Atkinson and Carter, 1991) indicate that decomposition of $\text{CH}_3\text{C}(\text{O})\text{CHO}-\text{CH}_3$ would dominate under atmospheric condition, leading to one more molecule acetaldehyde (Scheme 5-2(c)). In addition, the 2,3-butanedione has also been detected in PTR-ToF-MS to be $2.5\pm1.8\%$. Hence, the H-atom abstraction from the $-\text{CH}_2-$ group at 4-position account for 112.2% of the overall acetaldehyde formation.



Scheme 5-2(c): Reaction of OH radical with 3M2P: proposed mechanism leading to the formation of observed reaction products. Compounds in blue represent products observed experimentally. The expected relative importance of the possible RO \cdot reaction pathways are indicated by the arrows: \rightarrow $>$ \nrightarrow ; the intermediary of RO \cdot / RO $_2\cdot$ are indicated by \rightsquigarrow .

The $\text{CH}_3\text{CH}_2\text{CO}(\text{CH}_3)\text{C}(\text{O})\text{CH}_3$ radical formed after H-atom abstraction from the $>\text{CH}-$ at 3-position accounts for 32.1% of the overall reaction, which can only undergo decomposition. Since $>\text{COC}(\text{O})-$ carbon-carbon bond scission proceed rather than $>\text{COCH}_2-$ carbon-carbon scission (Atkinson and Carter, 1991), as shown in Scheme 5-2(d), the decomposition of $\text{CH}_3\text{CH}_2\text{CO}(\text{CH}_3)\text{C}(\text{O})\text{CH}_3$ radical is expected to predominately lead to one molecule 2-butanone and acyl radical. Hence, the H-atom abstraction from the $>\text{CH}-$ group at 3-position accounts for 32.1% of the overall 2-butanone formation.



Scheme 5-2(d): Reaction of OH radical with 3M2P: proposed mechanism leading to the formation of observed reaction products. Compounds in blue represent products observed experimentally. The expected relative importance of the possible $\text{RO}\cdot$ reaction pathways are indicated by the arrows: $\rightarrow > \nrightarrow$; the intermediary of $\text{RO}\cdot / \text{RO}_2\cdot$ are indicated by \nrightarrow .

Based on the Scheme 5-2(a-d) and the calculated relative importance of the various $\text{RO}\cdot$ pathway, our 2-butanone and acetaldehyde yields indicate that the 2-butanone and acetaldehyde are mainly formed after H-abstraction from $>\text{CH}-$ group at 3-position and $-\text{CH}_2-$ group at 4-position, respectively. Furthermore, our measured 2-butanone and acetaldehyde yields of $39.8 \pm 1.9\%$ and $109.2 \pm 6.1\%$, respectively, are closely to their SAR estimated values: 32.1% and 116.5% ($56.1 \times 2 + 4.3\%$).

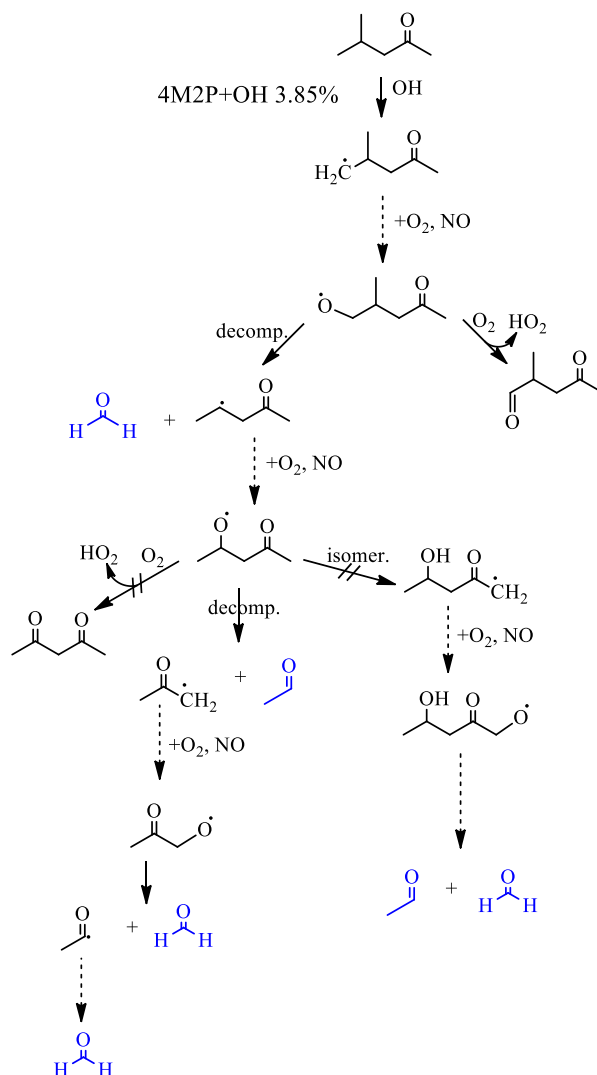
Furthermore, the experimental yield of 2,3-butanedione of $2.5 \pm 1.8\%$ was mainly formed after H-abstraction from $-\text{CH}_2-$ group at 4 position. The propanal with undetermined yield is expected to be produced after the H-abstraction from $-\text{CH}_3$ at 3-position. By taking into account the experimental yields of formaldehyde, 2-butanone, 2,3-butanedione and acetaldehyde, the carbon content of the formed products occupies $70.5 \pm 1.7\%$ percent of the carbon content of the consumed 3M2P.

5-4-4-3- 4M2P + OH

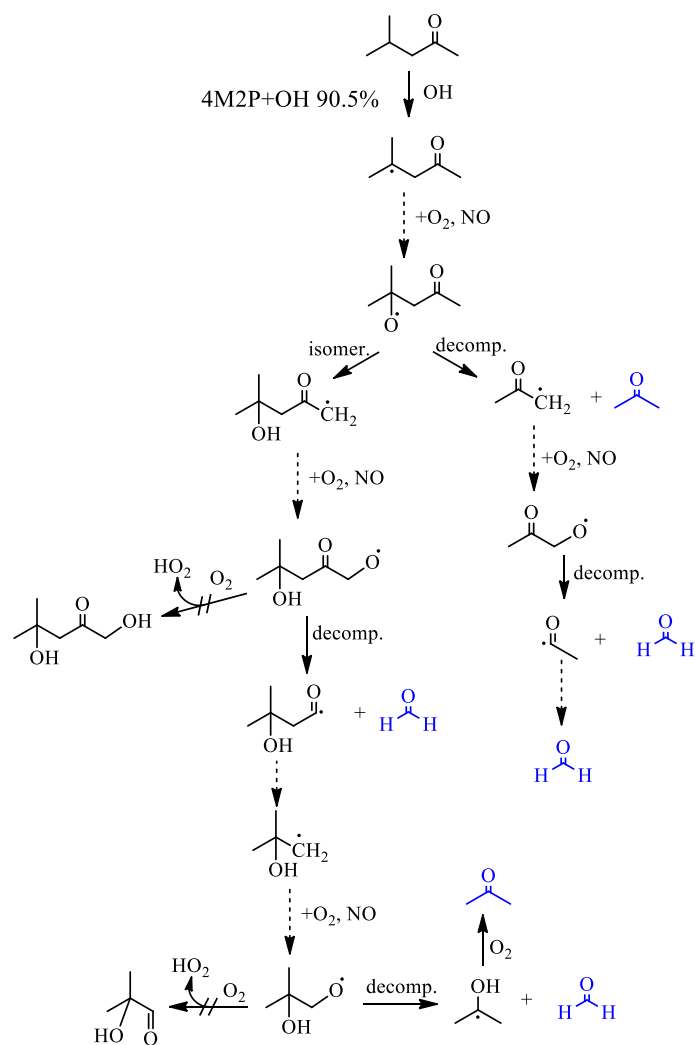
As shown in the Table 5-7, acetone, 2-methylpropanal and HCHO were found to be the main products from the reaction of OH radical with 4M2P, determined as $87.4 \pm 2.2\%$, $10.7 \pm 4.8\%$ and $51.9 \pm 3.5\%$ in this work, respectively. The yield of acetone of $87.4 \pm 2.2\%$ is in reasonable agreement with the yields reported by Cox et al. of 68% (1980) and of 90% (1981) and Atkinson et al., of $78 \pm 6\%$ (1995). Atkinson et al., (1995) also reported the formation of 2-methylpropanal of $7.1 \pm 1.1\%$, which is accordance with this work. Then the possible reaction schemes for the four initially formed alkoxy radicals formed after H-atom abstraction from $-\text{CH}_3$, $-\text{CH}_2-$ and $>\text{CH}-$ groups at different positions, are shown in Schemes 5-3(a-c). The update SAR parameters of Calvert et al., (2011) give the distribution of alkyl radicals to be: $-\text{CH}_3$ at 5-position 3.8%, $>\text{CH}-$ at 4-position 90.5%, $-\text{CH}_2-$ at 3-position 5%, $-\text{CH}_3$ at 1-position 0.7%. Since $\text{CH}_3\text{CH}(\text{CH}_3)\text{CH}_2\text{C}(\text{O})\text{CH}_2\text{O} \cdot$ radical formed after H-abstraction from the $-\text{CH}_3$ at 1-position accounts for only 0.7% of all the reaction, any products formation from this branch can only account for minor fraction of the observed products.

As shown in Scheme 5-3(a), the $\text{CH}_3\text{C}(\text{O})\text{CH}_2\text{CH}(\text{CH}_3)\text{CH}_2\text{O} \cdot$ radical formed after H-abstraction from the $-\text{CH}_3$ at 5-position accounts for 3.8% of all the reaction. As shown in Scheme 5-3(a), any acetone and 2-methylpropanal are not expected to form from the following reaction pathways of $\text{CH}_3\text{C}(\text{O})\text{CH}_2\text{CH}(\text{CH}_3)\text{CH}_2\text{O} \cdot$. The acetaldehyde could be expected to form and has been detected by UHPLC-MS but without quantified the yield in this work. As reported by Atkinson et al., (1995), the

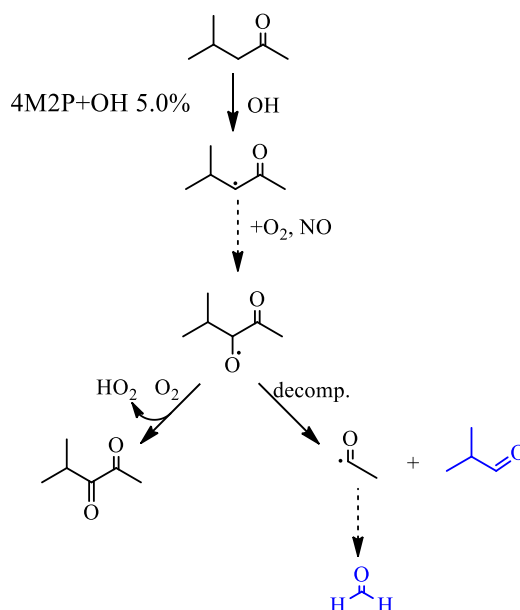
observed acetone and 2-methylpropanal must arise almost totally after H-abstraction from $>\text{CH}-$ and $-\text{CH}_2-$ groups, respectively. And as shown in Scheme 5-3(b) and Scheme 5-3(c), this work perfectly confirms the reaction mechanism for the $\text{CH}_3\text{C}(\text{O})\text{CH}_2\text{CO}(\text{CH}_3)_2$ and $\text{CH}_3\text{C}(\text{O})\text{CHO} \cdot \text{CH}(\text{CH}_3)_2$ radicals drawn by Atkinson et al., (1995).



Scheme 5-3(a): Reaction of OH radical with 4M2P: proposed mechanism leading to the formation of observed reaction products. Compounds in blue represent products observed experimentally. The expected relative importance of the possible RO· reaction pathways are indicated by the arrows: $\rightarrow > \nrightarrow$; The intermediary reaction of RO / RO₂· is indicated by \rightsquigarrow .



Scheme 5-3(b): Reaction of OH radical with 4M2P: proposed mechanism leading to the formation of observed reaction products. Compounds in blue represent products observed experimentally. The expected relative importance of the possible RO· reaction pathways are indicated by the arrows: $\rightarrow > \dashrightarrow$; The intermediary reaction of RO / RO₂· is indicated by \dashrightarrow .



Scheme 5-3(c): Reaction of OH radical with 4M2P: proposed mechanism leading to the formation of observed reaction products. Compounds in blue represent products observed experimentally. The expected relative importance of the possible RO· reaction pathways are indicated by the arrows: $\rightarrow > \nrightarrow$; The intermediary reaction of RO / RO₂· is indicated by \dashrightarrow .

Based on the Scheme 5-3(a-c) and the observed products (acetone and 2-methylpropanal) yield, which indicate that the acetone and 2-methylpropanal must arise almost totally after H-abstraction from $>\text{CH}-$ and $-\text{CH}_2-$ groups, respectively. Furthermore, the detected acetaldehyde using UHPLC-MS mainly formed from the H-abstraction from $-\text{CH}_3$ at 5-position. By taking account of the experimental yields of formaldehyde, acetone and 2-methylpropanal, the carbon content of the formed products occupies $59.5 \pm 3.1\%$ percent of the carbon content of the consumed 4M2P.

5-5- Atmospheric implications

The results summarized above show clearly that different branched structure of ketones have not only markedly different rate constants for reaction with OH radicals but also can form a variety of products. The rate constant data obtained in the present study contribute to a better definition of the tropospheric lifetimes of 2M3P, 3M2P and 4M2P. With a typical tropospheric OH concentration of $2 \times 10^6 \text{ molecule cm}^{-3}$

(Prinn et al., 1995), the following tropospheric lifetimes toward OH reaction ($\tau = \frac{1}{k[\text{OH}]}$) are estimated as: 41 hours, 24 hours and 13 hours for OH radical reaction with 2M3P, 3M2P and 4M2P, respectively. However, photolysis could also contribute significantly to the atmospheric fate of these ketones during the daytime.

As described in the previous section and shown in Scheme 5-1, 5-2 and 5-3, OH radical reactions with 2M3P, 3M2P and 4M2P lead to the formation of HO₂ and RO₂ radicals, which could be converted back to OH in the presence of NO, resulting in a fast cycling of radicals that forms the most important oxidation mechanism in the atmosphere (Davis et al., 2001). In addition, the OH radical initiates reactions with ketones that lead to the major production of ozone in the atmosphere (Dusanter et al., 2008). Furthermore, a high percent of small carbonyl products, e.g. HCHO, acetone, acetaldehyde, 2,3-butanedione, 2-methylpropanal and 2-butanone can be produced from the reaction of OH radical with 2M3P, 3M2P and 4M2P. In polluted environments characterized by high concentration of NO_x (NO+NO₂), like urban area, it is well established that the major products of the destruction of these carbonyl chemicals are OH, RO₂ and HO₂ radicals (Calvert et al., 2011). They are the major atmospheric oxidation agents determining the atmospheric lifetimes of most of the ambient trace gases. As explained in the previous section, CO is also expected to be produced from the OH reaction with the studied ketones. It can indirectly and obviously impact climate by increasing tropospheric ozone and increase the lifetimes of methane and other short-lived greenhouse gases (GHGs) (Prather, 1996).

5-6- Conclusion

The atmospheric fates of 2M3P, 3M2P and 4M2P have been investigated in this work through the measurements of the reaction rate constants with OH radicals and product studies. Both AR and RR methods have been used to determine the rate constants of OH reaction with 2M3P, 3M2P and 4M2P, as 3.49 ± 0.5 (AR+RR), 6.0 ± 0.14 (AR+RR) and 11.02 ± 0.42 (RR), respectively, unit in $10^{-12} \text{ cm}^3 \text{ molecule}^{-1} \text{ s}^{-1}$. Combining with the estimation by SAR method, it is speculated that the difference of

the rate constants between these three studied ketones could be due to the activity of CH_x (x=1,2,3) groups relative to the position of C=O. A new R group rate constant, as $k(\text{sec-C}_4\text{H}_9)=6.3 \times 10^{-12} \text{ cm}^3 \text{ molecule}^{-1} \text{ s}^{-1}$, was obtained in this work. This work also constitutes the first temperature dependence study of 2M3P with OH and shows a slightly temperature dependence.

The reaction of OH radical with 2M3P, 3M2P and 4M2P is believed to proceed via H-abstraction from the CH_x group, giving the following products: HCHO (34.0±6.0%) + acetone (34.0±6.0%) + acetaldehyde (104.3±10%), HCHO (35.4±1.1%) + 2-butanone (39.8±1.9%) + 2,3-butanedione (2.5±1.8%) + acetaldehyde (109.2±6.1%), HCHO (51.9±3.5%) + acetone (87.4±2.2%) + 2-methylpropanal (10.7±4.8%), respectively. The experimental product data of this work provide direct evidence of the destruction mechanism of the OH reaction with 2M3P, 3M2P and 4M2P. However, these formation yield data also indicate that the percentage of OH-abstraction by OH radical from CH_x (-CH₃, -CH₂ and >CH-) depends on the position of CH_x relative to the C=O group. In particular, the isomerization via a 6-membered transition state of alkoxy radicals occurred and could be comparable to the decomposition and the reaction with O₂ in this work. In addition, HO₂ radical were also believed to be formed from the OH reaction with these three studied ketones.

References

- Atkinson, R., Aschmann, S. M., Carter, W. P. L., and Pitts, J. N.: Rate constants for the gas-phase reaction of OH radicals with a series of ketones at 299 ± 2 K, *International Journal of Chemical Kinetics*, 14, 839-847, 10.1002/kin.550140804, 1982.
- Atkinson, R.: A Structure-Activity Relationship for the Estimation of Rate Constants for the Gas-Phase Reactions of OH Radicals with Organic Compounds, *International Journal of Chemical Kinetics*, 19, 799-828, 10.1002/kin.550190903, 1987.
- Atkinson, R., and Carter, W. P. L.: Reactions of Alkoxy Radicals Under Atmospheric Conditions: The Relative Importance of Decomposition Versus Reaction with O₂, *J Atmos Chem*, 13, 195-210, 10.1007/bf00115973, 1991.
- Atkinson, R., and Aschmann, S. M.: Products of the gas-phase OH radical-initiated reactions of 4-methyl-2-pentanone and 2,6-dimethyl-4-heptanone, *International Journal of Chemical Kinetics*, 27, 261-275, 10.1002/kin.550270305, 1995.
- Atkinson, R., Tuazon, E. C., and Aschmann, S. M.: Atmospheric Chemistry of 2-Pentanone and 2-Heptanone, *Environmental Science & Technology*, 34, 623-631, 10.1021/es9909374, 2000.
- Atkinson, R.: Kinetics of the gas-phase reactions of OH radicals with alkanes and cycloalkanes, *Atmos. Chem. Phys.*, 3, 2233-2307, 10.5194/acp-3-2233-2003, 2003.
- Atkinson, R., Baulch, D. L., Cox, R. A., Crowley, J. N., Hampson, R. F., Hynes, R. G., Jenkin, M. E., Rossi, M. J., Troe, J., and Subcommittee, I.: Evaluated kinetic and photochemical data for atmospheric chemistry: Volume II – gas phase reactions of organic species, *Atmos. Chem. Phys.*, 6, 3625-4055, 10.5194/acp-6-3625-2006, 2006.
- Bernard, F.: Etude du devenir atmosphérique de composés organiques volatils biogéniques : réactions avec OH, O₃ et NO₂, 2009.
- Bernard, F., Da ě, V., Mellouki, A., and Sidebottom, H.: Studies of the Gas Phase Reactions of Linalool, 6-Methyl-5-hepten-2-ol and 3-Methyl-1-penten-3-ol with O₃ and OH Radicals, *The Journal of Physical Chemistry A*, 116, 6113-6126, 10.1021/jp211355d, 2012.
- Brauers, T., and Finlayson-Pitts, B. J.: Analysis of relative rate measurements, *International*

- Journal of Chemical Kinetics, 29, 665-672, 10.1002/(SICI)1097-4601(1997)29:9<665::AID-KIN3>3.0.CO;2-S, 1997.
- Calvert, J. G., Mellouki, A., Orlando, J. J., Pilling, M. J., and J., W. T.: The Mechanisms of Atmospheric Oxidation of the Oxygenates, Oxford University Press, New York, 2011.
- Calvert;, J., Mellouki;, A., Orlando;, J., Pilling;, M., and Wallington;, T.: The mechanisms of atmospheric oxidation of the oxygenates, Oxford University Press, Oxford; New York, 2011.
- Calvert;, J. G., Derwent;, R. G., Orlando;, J. J., Tyndall;, G. S., and Wallington, T. J.: Mechanisms of Atmospheric Oxidation of the Alkanes, Oxford University Press, USA, 2008.
- Cox, R. A., Derwent, R. G., and Williams, M. R.: Atmospheric photooxidation reactions. Rates, reactivity, and mechanism for reaction of organic compounds with hydroxyl radicals, Environmental Science & Technology, 14, 57-61, 10.1021/es60161a007, 1980.
- Cox, R. A., Patrick, K. F., and Chant, S. A.: Mechanism of atmospheric photooxidation of organic compounds. Reactions of alkoxy radicals in oxidation of n-butane and simple ketones, Environmental Science & Technology, 15, 587-592, 10.1021/es00087a011, 1981.
- Cuevas, C. A., Notario, A., Martinez, E., and Albaladejo, J.: A kinetic study of the reaction of Cl with a series of linear and ramified ketones as a function of temperature, Physical Chemistry Chemical Physics, 6, 2230-2236, 10.1039/B313587J, 2004.
- Dagaut, P., Wallington, T. J., Liu, R., and Kurylo, M. J.: A kinetic investigation of the gas-phase reactions of hydroxyl radicals with cyclic ketones and diones: mechanistic insights, The Journal of Physical Chemistry, 92, 4375-4377, 10.1021/j100326a026, 1988.
- Davis, A. C., and Francisco, J. S.: Reactivity Trends within Alkoxy Radical Reactions Responsible for Chain Branching, Journal of the American Chemical Society, 133, 18208-18219, 10.1021/ja204806b, 2011.
- Davis, D., Nowak, J. B., Chen, G., Buhr, M., Arimoto, R., Hogan, A., Eisele, F., Mauldin, L., Tanner, D., Shetter, R., Lefer, B., and McMurry, P.: Unexpected high levels of NO observed at South Pole, Geophysical Research Letters, 28, 3625-3628, 10.1029/2000GL012584, 2001.

- Dusanter, S., Vimal, D., and Stevens, P. S.: Technical note: Measuring tropospheric OH and HO₂ by laser-induced fluorescence at low pressure. A comparison of calibration techniques, *Atmos. Chem. Phys.*, 8, 321-340, 10.5194/acp-8-321-2008, 2008.
- Farrugia, L. N., Bejan, I., Smith, S. C., Medeiros, D. J., and Seakins, P. W.: Revised structure activity parameters derived from new rate coefficient determinations for the reactions of chlorine atoms with a series of seven ketones at 290 K and 1 atm, *Chemical Physics Letters*, 640, 87-93, <http://dx.doi.org/10.1016/j.cplett.2015.09.055>, 2015.
- Frank, I., Parrinello, M., and Klamt, A.: Insight into Chemical Reactions from First-Principles Simulations: The Mechanism of the Gas-Phase Reaction of OH Radicals with Ketones, *The Journal of Physical Chemistry A*, 102, 3614-3617, 10.1021/jp980531y, 1998.
- Kwok, E. S. C., and Atkinson, R.: Estimation of hydroxyl radical reaction rate constants for gas-phase organic compounds using a structure-reactivity relationship: An update, *Atmospheric Environment*, 29, 1685-1695, [http://dx.doi.org/10.1016/1352-2310\(95\)00069-B](http://dx.doi.org/10.1016/1352-2310(95)00069-B), 1995.
- Le Calvé S., Hitier, D., Le Bras, G., and Mellouki, A.: Kinetic Studies of OH Reactions with a Series of Ketones, *The Journal of Physical Chemistry A*, 102, 4579-4584, 10.1021/jp980848y, 1998.
- Le Crâne, J.-P., Villenave, E., Hurley, M. D., Wallington, T. J., and Ball, J. C.: Atmospheric Chemistry of Propionaldehyde: Kinetics and Mechanisms of Reactions with OH Radicals and Cl Atoms, UV Spectrum, and Self-Reaction Kinetics of CH₃CH₂C(O)O₂ Radicals at 298 K, *The Journal of Physical Chemistry A*, 109, 11837-11850, 10.1021/jp0519868, 2005.
- Müller, M., Mikoviny, T., Jud, W., D'Anna, B., and Wisthaler, A.: A new software tool for the analysis of high resolution PTR-TOF mass spectra, *Chemometrics and Intelligent Laboratory Systems*, 127, 158-165, <http://dx.doi.org/10.1016/j.chemolab.2013.06.011>, 2013.
- Mellouki, A., Teton, S., and Le Bras, G.: Kinetics of OH radical reactions with a series of ethers, *International Journal of Chemical Kinetics*, 27, 791-805, 10.1002/kin.550270806, 1995.
- Mellouki, A., Wallington, T. J., and Chen, J.: Atmospheric Chemistry of Oxygenated Volatile

- Organic Compounds: Impacts on Air Quality and Climate, Chemical Reviews, 115, 3984-4014, 10.1021/cr500549n, 2015.
- Mereau, R., Rayez, M. T., Caralp, F., and Rayez, J. C.: Isomerisation reactions of alkoxy radicals: theoretical study and structure-activity relationships, Physical Chemistry Chemical Physics, 5, 4828-4833, 10.1039/b307708j, 2003.
- Niki, H., Maker, P. D., Savage, C. M., and Breitenbach, L. P.: An FTIR study of mechanisms for the HO radical initiated oxidation of C₂H₄ in the presence of NO: detection of glycolaldehyde, Chemical Physics Letters, 80, 499-503, [http://dx.doi.org/10.1016/0009-2614\(81\)85065-8](http://dx.doi.org/10.1016/0009-2614(81)85065-8), 1981.
- O'Rji, L. N., and Stone, D. A.: Relative rate constant measurements for the gas-phase reactions of hydroxyl radicals with 4-methyl-2-pentanone, trans-4-octene, and trans-2-heptene, International Journal of Chemical Kinetics, 24, 703-710, 10.1002/kin.550240804, 1992.
- Orlando, J. J., Tyndall, G. S., and Wallington, T. J.: The Atmospheric Chemistry of Alkoxy Radicals, Chemical Reviews, 103, 4657-4690, 10.1021/cr020527p, 2003.
- Prather, M. J.: Time scales in atmospheric chemistry: Theory, GWPs for CH₄ and CO, and runaway growth, Geophysical Research Letters, 23, 2597-2600, 10.1029/96GL02371, 1996.
- Prinn, R. G., Weiss, R. F., Miller, B. R., Huang, J., Alyea, F. N., Cunnold, D. M., Fraser, P. J., Hartley, D. E., and Simmonds, P. G.: Atmospheric Trends and Lifetime of CH₃CCl₃ and Global OH Concentrations, Science, 269, 187-192, 10.1126/science.269.5221.187, 1995.
- Somnitz, H., and Zellner, R.: Theoretical studies of unimolecular reactions of C-2-C-5 alkoxy radicals. Part II. RRKM dynamical calculations, Physical Chemistry Chemical Physics, 2, 1907-1918, 10.1039/b000029i, 2000.
- Tuazon, E. C., Aschmann, S. M., Nguyen, M. V., and Atkinson, R.: H-atom abstraction from selected C-H bonds in 2,3-dimethylpentanal, 1,4-cyclohexadiene, and 1,3,5-cycloheptatriene, International Journal of Chemical Kinetics, 35, 415-426, 10.1002/kin.10143, 2003.
- Tyndall, G. S., Wallington, T. J., and Ball, J. C.: FTIR Product Study of the Reactions CH₃O₂

+ CH₃O₂ and CH₃O₂ + O₃, The Journal of Physical Chemistry A, 102, 2547-2554, 10.1021/jp972784h, 1998.

Wallington, T. J., and Kurylo, M. J.: Flash photolysis resonance fluorescence investigation of the gas-phase reactions of hydroxyl radicals with a series of aliphatic ketones over the temperature range 240-440 K, The Journal of Physical Chemistry, 91, 5050-5054, 10.1021/j100303a033, 1987.

Winer, A. M., Lloyd, A. C., Darnall, K. R., and Pitts, J. N.: Relative rate constants for the reaction of the hydroxyl radical with selected ketones, chloroethenes, and monoterpene hydrocarbons, The Journal of Physical Chemistry, 80, 1635-1639, 10.1021/j100555a024, 1976.

Chapter 6.

**Kinetic and Product studies of Cl atoms Reactions
with a series of branched Ketones**

Chapter 6- Kinetic and Product studies of Cl atoms Reactions with a series of branched Ketones	200
6-1- Introduction.....	201
6-2- Experimental and Material	202
6-2-1- Kinetic measurement	202
6-2-2- Products analysis	204
6-2-3- Chemical.....	204
6-3- Results	204
6-3-1- Rate constant for ketones + Cl atoms using RR method	204
6-3-2- Products formation from the reactions of ketones + Cl atoms	208
6-3-2-1- 2M3P+Cl	208
6-3-2-2- 3M2P+Cl	211
6-3-2-2- 4M2P+Cl	214
6-4- Discussion.....	217
6-4-1- Comparison with literature of the rate coefficients for ketone + Cl reactions	217
6-4-2- Kinetic estimation based on the Structure-Reactivity Relationship (SAR)	218
6-4-3- Reaction mechanism of the reaction of Cl atoms + ketones.....	221
6-4-3-1- 2M3P+Cl	222
6-4-3-2- 3M2P+Cl	230
6-4-3-3- 4M2P+Cl	234
6-4-4- Reaction mechanism comparison between the studied reactions with Cl atoms	238
6-5- Atmospheric implications	239
6-6- Conclusion	241
References.....	243

Chapter 6- Kinetic and Product studies of Cl atoms

Reactions with a series of branched Ketones

Abstract: The relative method with the propane, n-butane, n-hexane and cyclohexane used as references has been used to determine the rate constants for the Cl atom reaction with a series of branched ketones in a 200 L simulation chamber in Orleans, France, at room temperature and ambient pressure. The rate constants obtained (in units of $10^{-10} \text{ cm}^3 \text{ molecule}^{-1} \text{ s}^{-1}$) are: 2M3P (2-methyl-3-pentanone) 1.07 ± 0.26 , 3M2P (3-methyl-2-pentanone) 1.21 ± 0.26 , 4M2P (4-methyl-2-pentanone) 1.35 ± 0.27 . The results are discussed in terms of Cl reactivity trends and combining with published values, a revised Structure Activity Relationship (SAR) parameter and R group reactivity (k_R) of $R(O)R'$ and CH_x ($x=1, 2, 3$) group reactivity (k_{CH_x}) toward Cl atoms is proposed. The product formation from the reaction of the 2M3P, 3M2P and 4M2P with Cl atoms has been investigated by monitoring with PTR-ToF-MS and GC-FID. In the presence of NO, the products and their yields are: acetone ($38.5 \pm 7.7\%$) + acetaldehyde ($77.5 \pm 12.1\%$), 2-butanone ($22.3 \pm 1.5\%$) + acetaldehyde ($75.1 \pm 9.8\%$) + propanal ($13.6 \pm 1.0\%$) and acetone ($25.9 \pm 2.5\%$) + 2-methylpropanal ($23.6 \pm 1.6\%$), for Cl atoms reaction with 2M3P, 3M2P and 4M2P, respectively. In the absence of NO, the products and their yields are: acetone ($39.7 \pm 5.5\%$) + acetaldehyde ($58.2 \pm 5.8\%$), 2-butanone ($18.2 \pm 2.4\%$) + acetaldehyde ($40.3 \pm 1.7\%$) and acetone ($15.1 \pm 0.7\%$) + 2-methylpropanal ($18.2 \pm 0.9\%$), for the reaction of Cl atoms with 2M3P, 3M2P and 4M2P respectively. It indicates that the products formed from studied ketone reactions with Cl atoms in polluted area and clean area are similar. In addition, this work found that the 4M2P, which contains $-CH<$ group in β position relative to $C=O$ group, presents reactivity enough toward Cl_2 to form $CH_3COCH_2C(Cl)(CH_3)_2$ in the condition of $O_2 \gg Cl_2$. Furthermore, the partition ratio of $CH(CH_3)_2CO$ and $CH_3CH_2CO \cdot$ reacting with Cl_2 vs the one reacting with O_2 are estimated to be 3:2.

6-1- Introduction

Ketones play an important role in the chemistry of the polluted atmosphere and which has been described in Chapter 5. The initiated Cl atom degradation is not the main loss process for ketones in the troposphere, but also only recently been identified in the mainland environments such as Colorado, USA, may due to the presence of anthropogenic pollution (Faxon and Allen, 2013; Thornton et al., 2010). Although the global estimation of Cl atoms concentration in the northern hemisphere is orders of magnitude lower than the ambient OH concentration (Arsene et al., 2007), Cl atoms may initiate oxidation of VOCs in a similar manner to that of OH radical (Sulbaek Andersen et al., 2005). In addition, the rate coefficient of reaction of Cl atoms with VOCs are higher, by one order of magnitude or more, compared with OH radical (Calvert; et al., 2011). Hence the reaction of Cl atoms could contribute significantly to the tropospheric degradation of VOCs in areas with high concentration of Cl precursor, e.g. in the MBL.

The reaction of Cl atoms with small and straight-chained ketones have been already the subject of a number of kinetic studies, e.g. acetone, 2-butanone (Calvert; et al., 2011). Only few investigations (Kaiser et al., 2010) have been carried out with large ketones ($>C_5$), giving kinetic and mechanistic data on their atmospheric behavior. Indeed, most of the high ketone studies are focused on the reaction with OH radical. So, the reactivity of OH with numbers of ketones is well correlated by Structure-Activity-Relationship (SAR) whereas similar SAR for Cl reactivity is limited (Farrugia et al., 2015). In the work of Cuevas et al., (2004), they supposed a similar behavior to that of OH + ketone takes place for the reaction of Cl + ketone, which is not confirmed till now. Furthermore, to our best knowledge, the product investigation from the reaction of larger branched ketones with Cl atoms is not well documented.

In light of the importance of ketones and Cl atoms in the troposphere, further considerable efforts are needed to understand the reaction of branched ketones with Cl atoms. The present work deals with three high branched ketones:

2-methyl-3-pentanone (2M3P, $\text{CH}_3\text{CH}_2\text{C}(\text{O})\text{CH}(\text{CH}_3)_2$), 4-methyl-2-pentanone (4M2P, $\text{CH}_3\text{COCH}_2\text{CH}(\text{CH}_3)_2$) and 3-methyl-2-pentanone (3M2P, $\text{CH}_3\text{COCH}(\text{CH}_3)\text{CH}_2\text{CH}_3$), which are widely used as solvents and intermediates for synthesis. In this work, we have studied the 2M3P, 4M2P and 3M2P reactions with Cl atoms and recommended new rate constant values, determined by the relative method. In addition, the products formation from these three reactions have been also investigated:



To our knowledge, this work provides the first determination of the rate constant for reaction 1, and the second for the rate constant of reaction 3. In addition, we report the first product investigation of reaction of 2M3P, 4M2P and 3M2P with Cl atoms in the absence and in the presence of NO. Furthermore, this work aimed also at optimizing the SAR for ketones reaction with Cl atoms. The reported data from this work enable to better understand the atmospheric fate of ketones.

6-2- Experimental and Material

6-2-1- Kinetic measurement

The experiments have been performed using a 200 L atmospheric simulation chamber in ICARE. Cl_2 was introduced into the chamber by streaming zero air (<2% relative humidity) through a calibrated bulb (579 mL), which was then irradiated under 365 nm lamps to generate the Cl atoms source, as:



Studied ketones and reference compounds were measured by a gas chromatograph coupled to a flame ionization detector (GC-FID, Star CP-3800, Varian). DB-1 capillary column (J&W Scientific, 30 m, 0.32 mm, and 5 μm film) was used to perform the chromatographic separation, which was operated at 120 $^\circ\text{C}$.

With relative rate method (RR), the rate constants were determined by following the parallel decays of the ketones and reference compounds from the reaction with Cl atoms and other possible losses (photolysis, leak and sampling):



k_{ketone} ($k_{2\text{M3P}}$, $k_{4\text{M2P}}$, $k_{3\text{M2P}}$) and k_{ref} are the rate constants for the reaction of Cl atoms with ketones (2M3P, 4M2P, 3M2P) and reference compounds, respectively. $k_{\text{L-ketone}}$ and $k_{\text{L-ref}}$ are, respectively, the first order loss of ketones (2M3P, 4M2P, 3M2P) and reference compound, due to photolysis, leak and sampling.

The typical experimental procedures consisted of: (i) Only studied ketones without lamps on for 1 hour to identify the possible wall loss; (ii) Studied ketones with lamps on (different numbers of 356 nm lamps) for 1 hour to check possible photolysis decomposition; (iii) Studied ketones with molecular chlorine (Cl_2) without lamps on for 1 hour to see possible dark reactions. The same tests have been made for the reference compounds. No significant wall losses, dark reactions or photolysis decomposition with 365nm lamps have been observed for the ketones and reference compounds employed.

Assuming that the ketone and reference compounds were only lost by reaction with Cl atoms, it can be shown that:

$$\ln\left(\frac{[\text{ketone}]_0}{[\text{ketone}]_t}\right) = k_{\text{ketone}}/k_{\text{ref}} * \ln\left(\frac{[\text{reference}]_0}{[\text{reference}]_t}\right)$$

where $[\text{ketone}]_0$, $[\text{ketone}]_t$, $[\text{reference}]_0$, and $[\text{reference}]_t$ represent the corresponding concentrations of ketone and reference compounds at initial and reaction time t , respectively. Plotting of $\ln\left(\frac{[\text{ketone}]_0}{[\text{ketone}]_t}\right)$ against $\ln\left(\frac{[\text{reference}]_0}{[\text{reference}]_t}\right)$ will give the slope ($k_{\text{ketone}}/k_{\text{ref}}$), and zero intercept if no complex chemistry occurred.

6-2-2- Products analysis

The products were investigated for the reactions of studied ketones (2M3P, 3M2P and 4M2P) with Cl atoms in the presence of NO and in its absence. Generally, the online sampling of GC-FID (high reactant concentration) and the one of PTR-ToF-MS (IONICON 8000, low reactant concentration) were used to monitor the products. PTR-ToF-MS spectra were analyzed by the PTR-ToF-MS Data Analyzer (Müller et al., 2013).

The offline sampling Ultra High Performance Liquid Chromatograph-Mass Spectrometry (UHPLC/MS, Shimadzu LCMS-2020) was also planned to be used in this work firstly. As usual, carbonyl compounds would be collected on 2,4-dinitro-phenylhydrazine (DNPH)-coated cartridges using one homemade offline auto-sampler. However, we found that the DNPH could be oxidized by the Cl₂ and that could significantly decreased the sampling efficiency. Then, this method was not suitable for the analysis of the reaction of Cl atoms with studied ketones in this work.

6-2-3- Chemical

Cl₂ (99.5% Air liquid), 2M3P (≈97%, Aldrich), 4M2P (99.5%, Aldrich), 3M2P (99%, Aldrich), propane (99.5%, Air liquid), n-butane (99.95%, Air liquid), n-hexane (≥97%, Aldrich) and cyclohexane (≥99.9%, Aldrich). All the liquid compounds in this study were further purified by repeating freeze, pump, thaw cycles and fractional distillation before use.

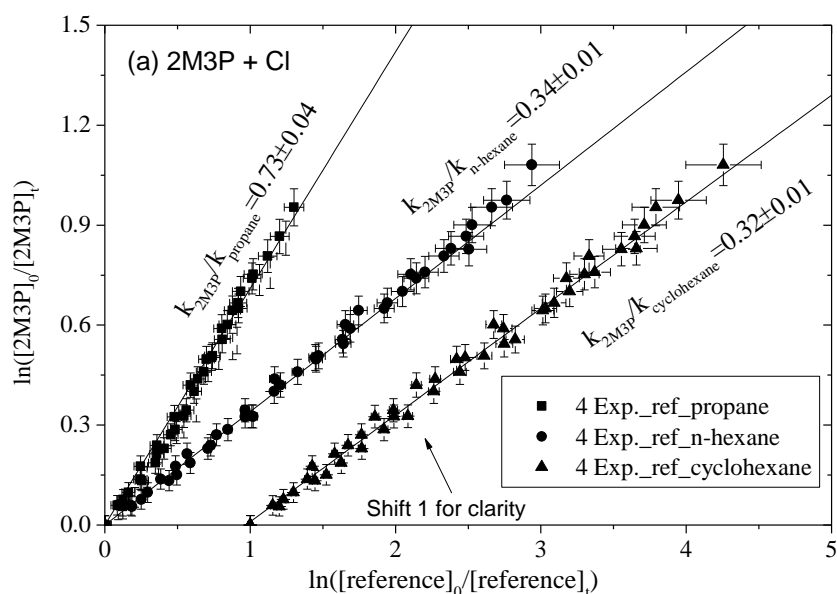
6-3- Results

6-3-1- Rate constant for ketones + Cl atoms using RR method

The rate constants for 2M3P (9.2-27.6 ppm), 4M2P (12.6-28.4 ppm) and 3M2P (4.2-27.9 ppm) have been obtained using the following reference compounds: propane (5.3-28.8 ppm), n-butane (4.9-29.2 ppm), n-hexane (4.9-29.0 ppm) and cyclohexane

(4.5-29.5 ppm). The recommended rate coefficients for the reaction of these compounds with Cl atoms are $k_{(\text{propane}+\text{Cl})}=(1.40\pm0.20)\times10^{-10}$ (Atkinson et al., 2006), $k_{(\text{n-butane}+\text{Cl})}=(2.05\pm0.25)\times10^{-10}$ (Atkinson et al., 2006), $k_{(\text{n-hexane}+\text{Cl})}=(3.15\pm0.40)\times10^{-10}$ (Alwe et al., 2013) and $k_{(\text{cyclohexane}+\text{Cl})}=(3.30\pm0.50)\times10^{-10}$ (Calvert; et al., 2008) at 298 K, respectively (Unit in $\text{cm}^3\text{molecule}^{-1}\text{s}^{-1}$).

The plots of $\ln\frac{[\text{ketone}]_0}{[\text{ketone}]_t}$ against $\ln\frac{[\text{reference}]_0}{[\text{reference}]_t}$ for the reaction of ketone + Cl atoms are shown in Figure 6-1. The calibration for studied ketones and reference compounds were conducted to calculate the errors on both x and y values. Then, $k_{\text{ketone}}/k_{\text{ref}}$ and its uncertainties were obtained using the method and procedure recommended by (Brauers and Finlayson-Pitts, 1997), and reported in Table 6-1. The rate coefficient for the studied ketones (2M3P, 3M2P and 4M2P), k_{ketone} , obtained by combining the rate coefficient values of different reference compounds and their corresponding $k_{\text{ketone}}/k_{\text{ref}}$ are also shown in Table 6-1. It shows that the rate coefficients of individual ketone using different reference compounds are in good agreement. By using the propagation of uncertainty, the errors for k_{ketone} were calculated from the error of $k_{\text{ketone}}/k_{\text{ref}}$ and the error associated with the rate coefficient of reference compounds. The final rate coefficients of studied ketones (2M3P, 4M2P and 3M2P) were obtained from the weighted average of the rate coefficient from each reference, designated by k_{av} in Table 6-1.



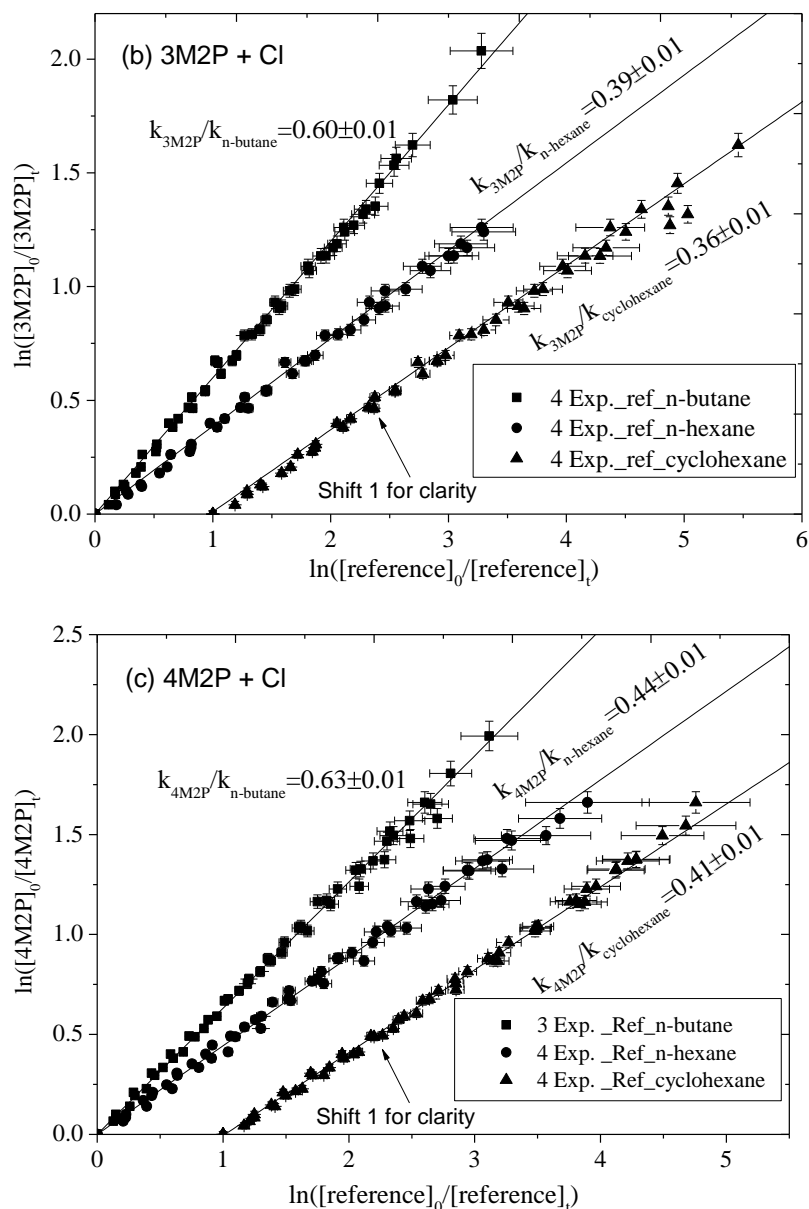
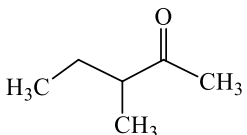
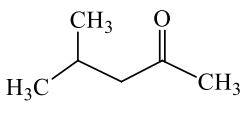
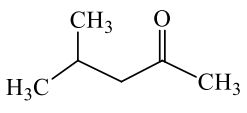


Figure 6-1: Plots of decay of studied ketones: 2M3P (a), 3M2P (b) and 4M2P (c) as a function of the decay of references: n-butane, n-hexane and cyclohexane, in the presence of Cl. 4 Exp. means 4 experiments. Plots obtained from cyclohexane shifted horizontally for clarity.

Table 6-1: Experimental conditions and measured rate constants for ketone+Cl reactions using RR method.

ketone	ref.	exp.	T (K)	$\frac{k_{ketone}}{k_{ref}}$ ^a	k_{ketone} ($10^{-10} \text{ cm}^3 \text{ molecule}^{-1} \text{ s}^{-1}$) ^b	k_{av} ^c
$\text{H}_3\text{C}-\text{CH}_2-\overset{\text{O}}{\parallel}-\text{CH}(\text{CH}_3)_2$	propane	1	292 ± 1	0.78 ± 0.16	1.03 ± 0.21	1.07 ± 0.26
		2		0.74 ± 0.05		
		3		0.73 ± 0.04		
		4		0.73 ± 0.05		

	n-hexane	1		0.34 ± 0.02	1.09 ± 0.19
		2		0.34 ± 0.02	
		3		0.35 ± 0.01	
		4		0.35 ± 0.01	
	cyclohexane	1		0.31 ± 0.02	1.08 ± 0.21
		2		0.34 ± 0.02	
		3		0.33 ± 0.01	
		4		0.33 ± 0.01	
	n-butane	1		0.59 ± 0.02	1.23 ± 0.19
		2		0.60 ± 0.01	
		3		0.61 ± 0.01	
		4		0.59 ± 0.01	
	n-hexane	1		0.37 ± 0.01	1.21 ± 0.20
		2	293 ± 1	0.38 ± 0.01	
		3		0.41 ± 0.01	1.21 ± 0.26
		4		0.38 ± 0.01	
	cyclohexane	1		0.35 ± 0.01	1.19 ± 0.21
		2		0.36 ± 0.01	
		3		0.38 ± 0.01	
		4		0.36 ± 0.01	
	n-butane	1		0.65 ± 0.01	1.29 ± 0.23
		2		0.61 ± 0.01	
		3		0.64 ± 0.01	
		4		0.64 ± 0.01	
	n-hexane	1		0.45 ± 0.01	1.39 ± 0.21
		2		0.42 ± 0.01	
		3	293 ± 1	0.45 ± 0.01	1.35 ± 0.27
		4		0.45 ± 0.01	
	cyclohexane	1		0.41 ± 0.01	1.37 ± 0.23
		2		0.42 ± 0.01	
		3		0.41 ± 0.01	
		4		0.42 ± 0.01	

^a The uncertainties for $k_{\text{ketone}}/k_{\text{ref}}$ were obtained from the least-squares standard deviation of the plot of $\ln \frac{[\text{ketone}]_0}{[\text{ketone}]_t}$ vs $\ln \frac{[\text{reference}]_0}{[\text{reference}]_t}$ which takes into account errors in both abscissa and ordinate scales

^b The uncertainties for k_{ketone} were estimated from the uncertainty of $k_{\text{ketone}}/k_{\text{ref}}$ and the uncertainty of the reference by using the propagation of uncertainty.

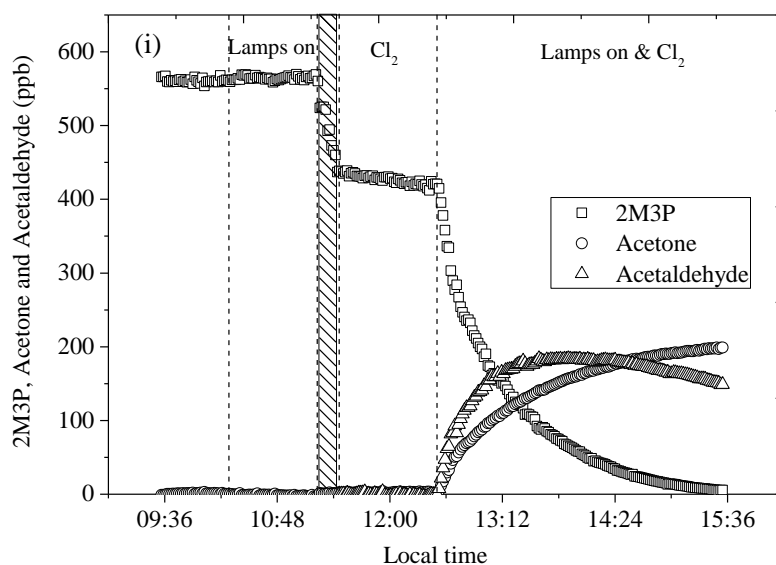
^c Weighted average $k_{\text{av}} = (w_{\text{ref1}}k_{1_ \text{ref1}} + w_{\text{ref2}}k_{1_ \text{ref2}} + \dots) / (w_{\text{ref1}} + w_{\text{ref2}} + \dots)$, where $w_{\text{ref1}} = 1/\sigma_{\text{ref1}}^2$, etc. The error, σ_{av} , was given by: $\sigma_{\text{av}} = (1/\sigma_{\text{ref1}}^2 + 1/\sigma_{\text{ref2}}^2 + \dots)^{-0.5}$ (ref. = reference, exp. = experiment)

6-3-2- Products formation from the reactions of ketones + Cl atoms

A series of irradiated (365 nm) mixtures of Cl_2 -NO (or in the absence of NO)-2M3P/3M2P/4M2P-air were carried out, and the products were monitored by GC-FID and PTR-ToF-MS.

6-3-2-1- 2M3P+Cl

The acetaldehyde and acetone were identified in the reaction of 2M3P with Cl atoms either in the presence or absence of NO, and the observed profiles of 2M3P and the products are shown in the Figure 6-2(i-ii). The amounts of formed products, corrected by their reaction with Cl atoms, are plotted against the consumption of the 2M3P in Figure 6-3(i) and Figure 6-3(ii), for experiments with and without NO, respectively. In conclusion, the least-squares analysis leads to the formation yields given in Table 6-2. For the experiment in the presence of NO, acetaldehyde and acetone were determined to be $77.5 \pm 12.1\%$ and $38.5 \pm 7.7\%$, respectively. For the experiment in the absence of NO, acetaldehyde and acetone were determined to be $58.2 \pm 5.8\%$ and $39.7 \pm 5.5\%$, respectively.



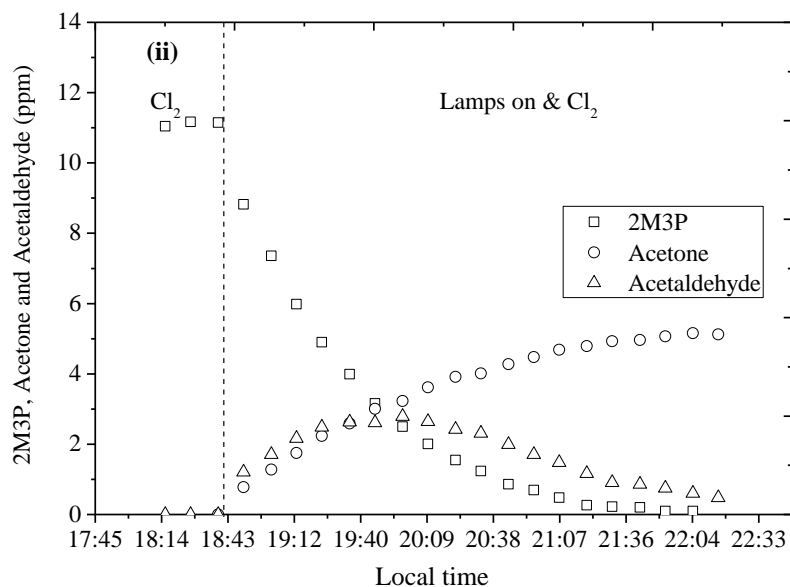
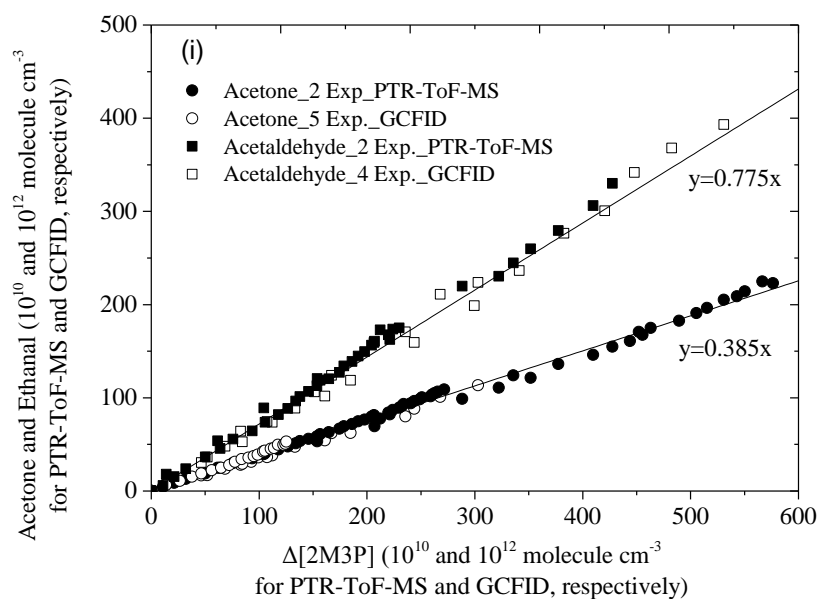


Figure 6-2(i-ii): Time-concentration profiles of 2M3P and the reaction products during its reaction with Cl atoms in the presence of NO (i) and in the absence of NO (ii). Note: the pattern part in (i) shows the Cl₂ was introduced with high flow of air and hence 2M3P was diluted.



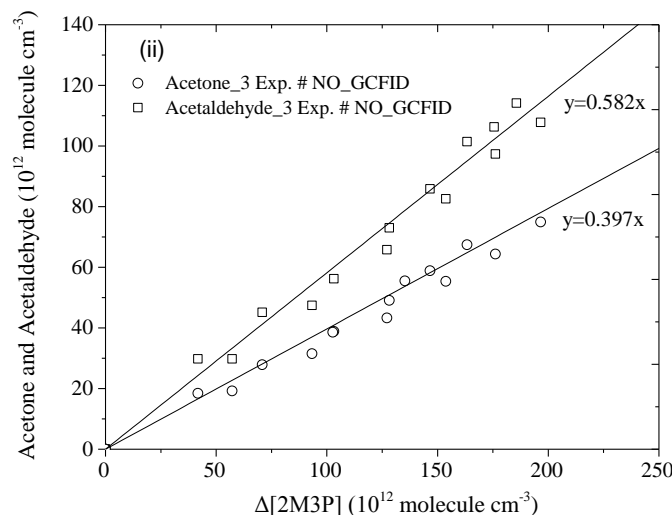


Figure 6-3(i-ii): Plots of the amounts of formed acetone and acetaldehyde, corrected by their reaction with the Cl atoms, against the amounts of consumed 2M3P with Cl atoms in the presence of NO (i) and in the absence of NO (ii). (Exp. & NO = experiment in the presence of NO; Exp. # NO = experiment in the absence of NO.)

Table 6-2: Experimental conditions and products formation yields for the reaction of 2M3P with Cl atoms under ambient temperature (298 ± 2 K) and pressure.

Exp.	[ketone] ₀ (ppb)	[NO] ₀ (ppm)	Ethanal ^a (%)	Acetone ^a (%)	Technique/ Carbon budget (%)
1	12742	39.6	78.7 \pm 2.6	38.5 \pm 1.8	GCFID
2	4642	19.8	77.3 \pm 7.3	34.8 \pm 2.5	GCFID
3	9300	59.1	73.6 \pm 5.9	37.7 \pm 3.1	GCFID
4	27059	43.0	77.8 \pm 5.0	38.3 \pm 5.7	GCFID
5	5948	11.9		41.4 \pm 1.8	GCFID
6	420	1.5	80.4 \pm 5.0	39.3 \pm 1.8	PTR-ToF-MS
7	194	2.5	77.1 \pm 2.2	39.6 \pm 0.9	PTR-ToF-MS
8	11151	NaN	55.7 \pm 4.5	38.3 \pm 3.2	GCFID
9	8699	NaN	60.8 \pm 3.6	40.2 \pm 3.1	GCFID
10	6018	NaN		40.5 \pm 3.2	GCFID
Av&NO^{b,d}			77.5\pm12.1	38.5\pm7.7	44.8\pm1.2
Av#NO^{c,d}			58.2\pm5.8	39.7\pm5.5	39.0\pm1.9

^a product yield (%) = $\frac{y}{x} \times 100 = \frac{[\text{formed products}]}{[\text{consumed 2M3P}]} \times 100$ (products: acetaldehyde=Ethanal,

acetone);

^b Av&NO = Average of experiments in the presence of NO;

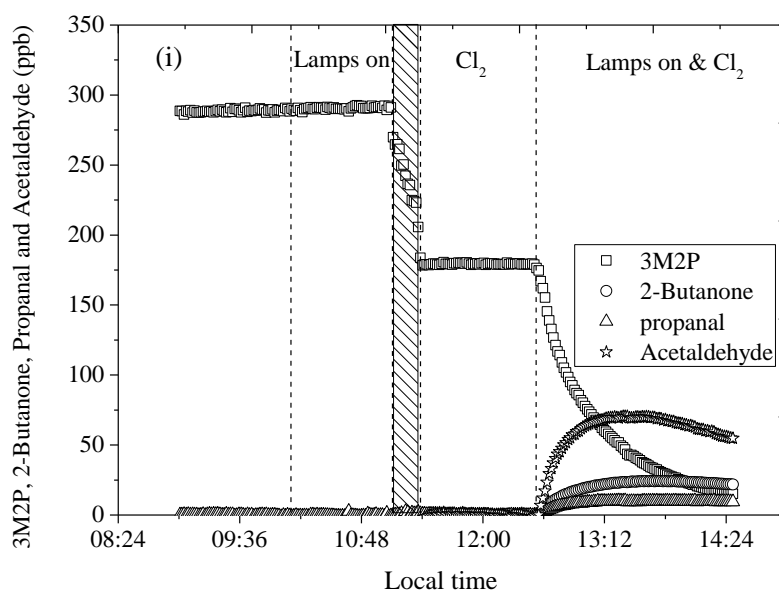
^c Av#NO = Average of experiments in the absence of NO;

^d Indicated errors are 1σ standard deviations combined with estimated overall uncertainties of instruments and statistic errors of repeat experiments.

(NaN=without NO)

6-3-2-2- 3M2P+Cl

The acetaldehyde and 2-butanone were identified in the reaction of 3M2P with Cl atoms in the presence and in the absence of NO and the observed profiles are shown in the Figure 6-4 (i-ii). The amounts of the products corrected for their reaction with Cl atoms, are plotted against the consumption of the 3M2P in Figure 6-5(i) and Figure 6-5(ii). In conclusion, the least-squares analysis leading to the formation yields are given in Table 6-3. For the reaction of 3M2P+Cl in the presence of NO, acetaldehyde, 2-butanone and propanal were determined to be $75.1 \pm 9.8\%$, $22.3 \pm 1.5\%$ and $13.6 \pm 1.0\%$, respectively. For the reaction of 3M2P+Cl in the absence of NO, acetaldehyde and 2-butanone were determined to be $40.3 \pm 1.7\%$ and $18.2 \pm 2.4\%$, respectively.



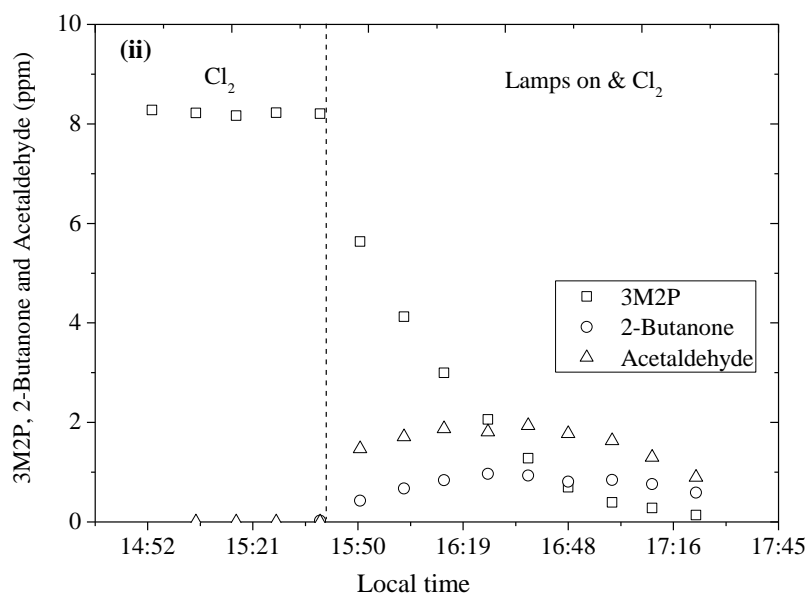
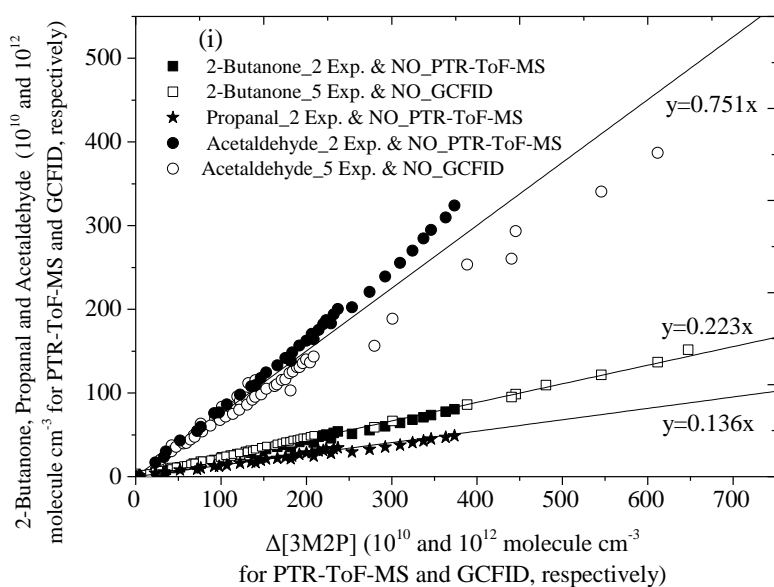


Figure 6-4(i-ii): Time-concentration profiles of 3M2P and the reaction products during its reaction with Cl atoms in the presence of NO (i) and in the absence of NO (ii). Note: the pattern part in (i) shows the Cl_2 was introduced with high flow of air and hence 3M2P was diluted.



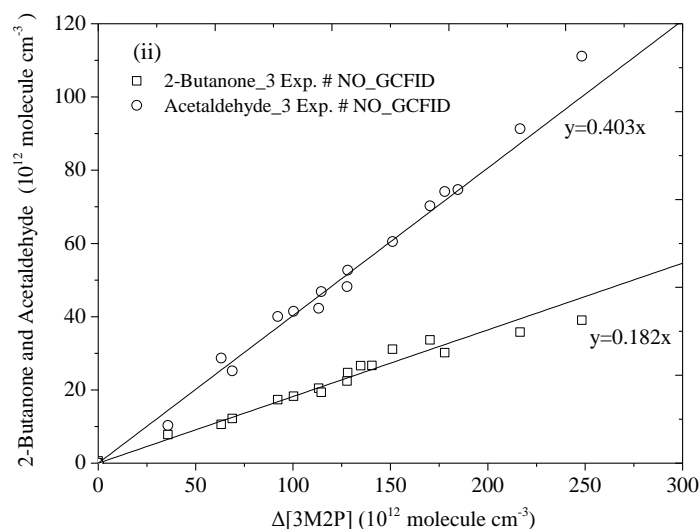


Figure 6-5(i-ii): Plots of the amounts of formed 2-butanone, propanal and acetaldehyde, corrected for their reaction with the Cl atoms, against the amounts of consumed 3M2P with Cl atoms in the presence of NO (i) and in the absence of NO (ii). (Exp. & NO = experiment in the presence of NO; Exp. # NO = experiment in the absence of NO)

Table 6-3: Experiment conditions and products formation yields for the reaction of 3M2P with Cl atoms under ambient temperature (299 ± 1) and pressure.

Exp.	[ketone] ₀ (ppb)	[NO] ₀ (ppm)	Ethanal ^a (%)	2-Butanone ^a (%)	Propanal ^a (%)	Technique/ Carbon budget (%)
1	176	54.5	84.1 ± 2.2	22.6 ± 0.6	14.3 ± 0.4	PTR-ToF-MS
2	234	33.3	87.0 ± 2.6	21.6 ± 0.7	12.9 ± 0.4	PTR-ToF-MS
3	6900	151.4	81.8 ± 2.8	21.7 ± 0.7		GCFID
4	22600	120.1	67.1 ± 2.7	22.0 ± 0.7		GCFID
5	6000	23.9	76.5 ± 2.3	22.7 ± 0.6		GCFID
6	28700	121.4	61.4 ± 0.6	22.3 ± 0.1		GCFID
7	10700	10.7	67.7 ± 1.4	23.6 ± 0.4		GCFID
8	8200	NaN	40.0 ± 1.3	20.8 ± 0.7		GCFID
9	6000	NaN	38.9 ± 1.0	17.8 ± 0.6		GCFID
10	10100	NaN	42.2 ± 1.6	16.0 ± 0.2		GCFID
Av&NO^{b,d}			75.1 ± 9.8	22.3 ± 1.5	13.6 ± 1.0	46.7 ± 2.6
Av#NO^{c,d}			40.3 ± 1.7	18.2 ± 2.4		32.1 ± 1.4

^a product yield (%) = $\frac{y}{x} * 100 = \frac{[\text{formed products}]}{[\text{consumed 3M2P}]} * 100$ (products: acetaldehyde =

ethanal, 2-butanone and propanal = propionaldehyde);

^b average of experiments in the presence of NO = Av&NO;

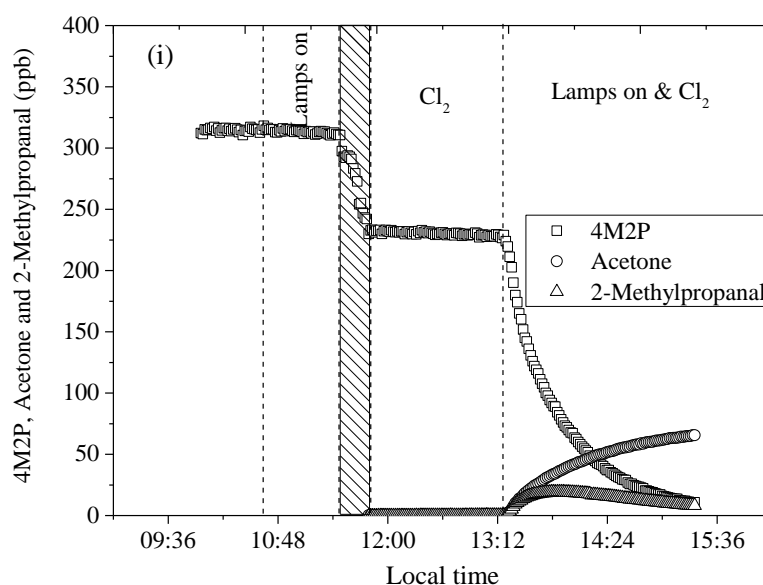
^c average of experiments in the absence of NO = Av#NO

^d Indicated errors are 1σ standard deviations combined with estimated overall uncertainties of instruments and statistic errors of repeat experiments.

(NaN=without NO, GCFID did not identify propanal because of the detection limit)

6-3-2-2- 4M2P+Cl

The acetone and 2-methylpropanal were identified in the reaction of 4M2P with Cl atoms both in the presence and in the absence of NO, and the observed profiles of the 4M2P and products are shown in the Figure 6-6(i) and Figure 6-6(ii), respectively. The amounts of formed products, corrected for their reaction with Cl atoms, are plotted against the consumption of the 4M2P in Figure 6-7(i-ii) for the two series of experiments. In conclusion, the least-squares analysis leads to the formation yields given in Table 6-4. For the experiment of 4M2P reaction with NO, acetone and 2-methylpropanal were determined to be $25.9 \pm 2.5\%$ and $23.6 \pm 1.6\%$, respectively. For the experiment of 4M2P reaction without NO, acetone and 2-methylpropanal were determined to be $18.2 \pm 0.9\%$ and $15.1 \pm 0.7\%$, respectively.



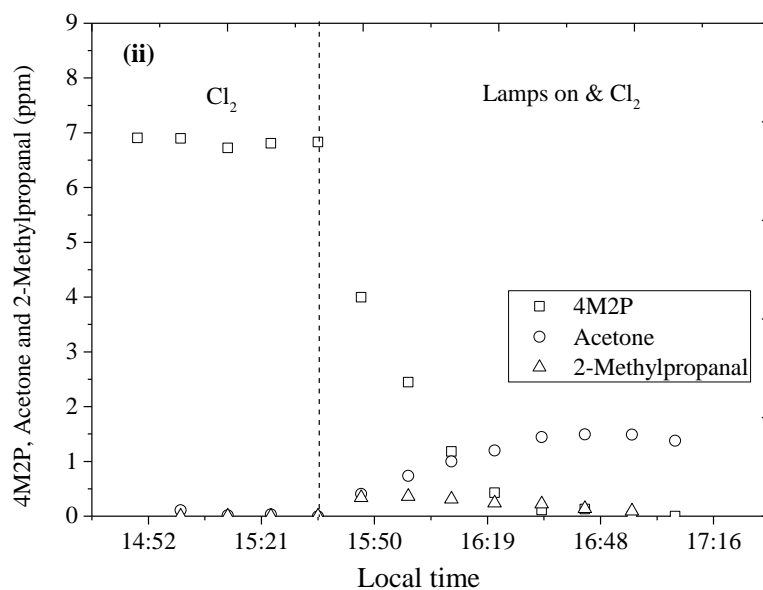
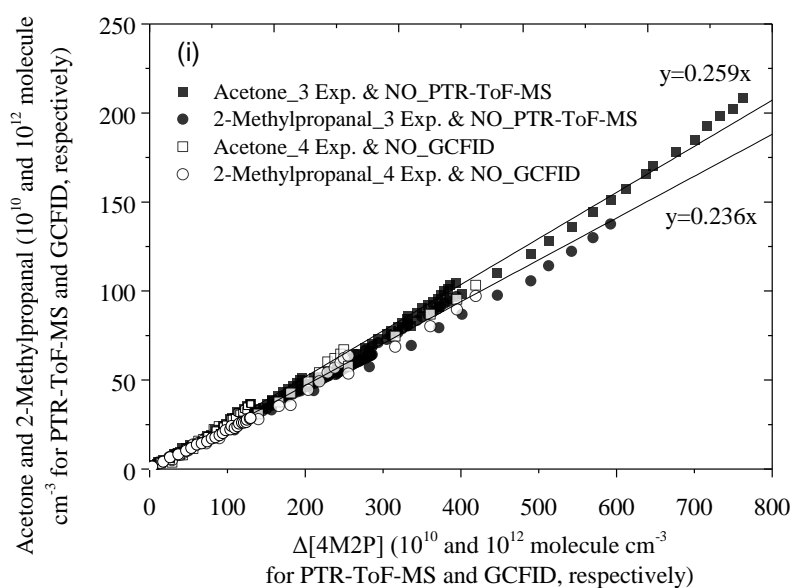


Figure 6-6(i-ii): Time-concentration profiles of 4M2P and the reaction products during its reaction with Cl atoms in the presence of NO (i) and in the absence of NO (ii). Note: the pattern part in (i) shows the Cl_2 was introduced with high flow of air and hence 4M2P was diluted.



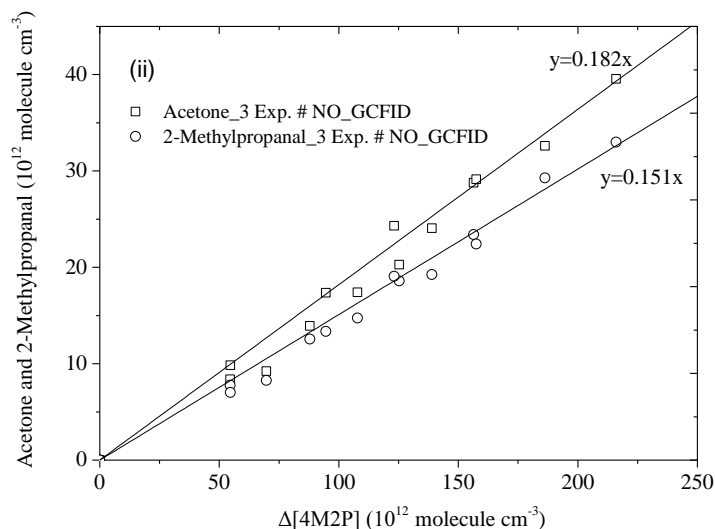


Figure 6-7(i-ii): Plots of the amounts of formed acetone and 2-methylpropanal, corrected for their reaction with Cl atoms, against the amounts of consumed 4M2P with Cl atoms in the presence of NO (i) and in the absence of NO (ii). (Exp. & NO = experiment in the presence of NO; Exp. # NO = experiment in the absence of NO)

Table 6-4: Experiment conditions and products formation yields for the reaction of 4M2P with Cl atoms under ambient temperature (299 ± 1 K) and pressure.

Exp.	[ketone] ₀ (ppb)	[NO] ₀ (ppm)	Acetone ^a (%)	2-Methylpropanal ^a (%)	Technique/ Carbon budget (%)
1	508	66.6	27.3 \pm 0.3	23.0 \pm 0.9	PTR-ToF-MS
2	131	47.7	25.8 \pm 2.3	22.5 \pm 0.9	PTR-ToF-MS
3	224	59.9	26.9 \pm 0.4	24.8 \pm 0.4	PTR-ToF-MS
4	11300	137.9	25.5 \pm 0.3	26.5 \pm 0.4	GCFID
5	4500	80.1	24.4 \pm 0.5	23.4 \pm 0.6	GCFID
6	20300	129.7	24.3 \pm 0.5	23.6 \pm 0.4	GCFID
7	6600	11.5	27.1 \pm 0.4	21.5 \pm 0.2	GCFID
8	11200	NaN	18.0 \pm 0.4	15.6 \pm 0.2	GCFID
9	6800	NaN	17.5 \pm 0.5	14.3 \pm 0.1	GCFID
10	6600	NaN	19.1 \pm 0.6	15.5 \pm 0.3	GCFID
Av&NO^{b,d}			25.9\pm2.5	23.6\pm1.6	28.7\pm1.1
Av#NO^{c,d}			18.2\pm0.9	15.1\pm0.7	19.2\pm0.8

^a product yield (%) = $\frac{y}{x} * 100 = \frac{[\text{formed products}]}{[\text{consumed 4M2P}]} * 100$ (products: acetone,

2-methylpropanal);

^b Average of experiments in the presence of NO = Av&NO;

^c Average of experiments in the absence of NO = Av#NO

^d Indicated errors are 1 σ standard deviations combined with estimated overall uncertainties of instruments and statistic errors of repeat experiments.

(NaN=without NO)

6-4- Discussion

6-4-1- Comparison with literature of the rate coefficients for ketone + Cl reactions

There are several studies on the rate coefficient determination of 4M2P and 3M2P reaction with Cl atoms, but there are no reports for 2M3P. Table 6-5 includes the rate coefficients determined in this work and the literature.

To our best knowledge, this work presents the first report about the rate coefficient of the reaction of 2M3P with Cl atoms (k_{2M3P}).

The reported k_{4M2P} in this work is in good agreement with those reported from other RR method studies (Farrugia et al., 2015; Kaiser and Wallington, 2007). However some small discrepancies exist between the rate coefficients obtained by the flash photolysis based studies (Notario et al., 2000; Cuevas et al., 2004) and this work for k_{4M2P} . Taketani et al., (2006) and Kaiser and Wallington (2007) comment that the regeneration of the Cl atoms in the PLP-RF (pulsed laser photolysis-resonance fluorescence) would be the most probable process to underestimate the rate coefficient, which happened because of the high concentration of molecular chlorine and formed alkyl radicals during the reaction of ketones with Cl atoms. The reported k_{3M2P} in this work is in fair agreement with the only report from Farrugia et al., (2015).

Table 6-5: Summary of the rate coefficients for the reaction of Cl atoms with the studied ketones (2M3P, 3M2P and 4M2P) obtained in this work and in previous studies.

ketone	$k_{SAR} (10^{-10} \text{ cm}^3 \text{ molecule}^{-1} \text{ s}^{-1})$	$k (10^{-10} \text{ cm}^3 \text{ molecule}^{-1} \text{ s}^{-1})$	Technique	reference
2M3P	0.84 ^a 1.14 ^b 0.97 ^c	1.07 ± 0.26	RR-GCFID	This work*
4M2P	1.25 ^a 1.16 ^b 1.27 ^c	0.97 ± 0.12 0.85 ± 0.04 1.28 ± 0.01 1.10 ± 0.05	PLP-RF PLP-RF RR-GCFID RR-GCFID	Notario et al., 2000 Cuevas et al., 2004 Kaiser and Wallington. 2007 Farrugia et al., 2015

3M2P		1.35 ±0.27	RR-GCFID	This work*
	1.23 ^a	0.94 ±0.10	RR-FTIR	Farrugia et al., 2015
	1.44 ^b			
	1.23 ^c	1.21 ±0.26	RR-GCFID	This work*

^a Value calculated using structure activity relationship (SAR) following the parameters: $k_{\text{prim}}=2.84$, $k_{\text{sec}}=8.95$, $k_{\text{tert}}=6.48$ (units in $10^{-11} \text{ cm}^3 \text{ molecule}^{-1} \text{ s}^{-1}$). $F_{(-\text{CH}_3)}=1.00$, $F_{(-\text{CH}_2-)}=F_{(-\text{CH}-)}=F_{(>\text{C}<)}=0.8$, $F_{(>\text{CO})}=0.037$, $F_{(-\text{CH}_2\text{C}(\text{O})\text{R})}=1.17$ from Calvert et al., (2008).

^b Value calculated using SAR with revised $F_{(>\text{CO})}=0.342$, $F_{(-\text{CH}_2\text{C}(\text{O})\text{R})}=0.563$ from Farrugia et al., (2015). Other parameters are the same of those in ^a.

^c Value calculated using SAR with revised $k_{\text{prim}}=3.32$, $k_{\text{sec}}=8.34$ and $k_{\text{tert}}=6.09$ (units in $10^{-11} \text{ cm}^3 \text{ molecule}^{-1} \text{ s}^{-1}$) from Aschmann and Atkinson (1995). Other parameters are the same of those in ^a.

6-4-2- Kinetic estimation based on the Structure-Reactivity Relationship (SAR)

By analogy with ketone reaction with OH radical, the reaction of ketone with Cl atoms can also be calculated using three different SAR methods:

i. SAR1: the initial SAR1 estimation of the rate coefficient of the ketone reaction with Cl atoms was proposed by Calvert et al., (2011) with the following parameters: $k_{\text{prim}}=2.84$, $k_{\text{sec}}=8.95$, $k_{\text{tert}}=6.48$ (units in $10^{-11} \text{ cm}^3 \text{ molecule}^{-1} \text{ s}^{-1}$). $F_{(-\text{CH}_3)}=1.00$, $F_{(-\text{CH}_2-)}=F_{(-\text{CH}-)}=F_{(>\text{C}<)}=0.8$, $F_{(>\text{CO})}=0.037$, $F_{(-\text{CH}_2\text{C}(\text{O})\text{R})}=1.17$. Recently, Farrugia et al., (2015) revised the $F_{(>\text{CO})}$ and $F_{(-\text{CH}_2\text{C}(\text{O})\text{R})}$ factors by 0.342 and 0.563, respectively, to take into account the branching of methyl-ketones. The rate coefficients of the studied ketones (2M3P, 4M2P and 3M2P) reaction with Cl atoms were calculated using these two types of parameters given above and the results are displayed in Table 6-5. It shows some slight differences between the calculated values and the experimental ones (maxi $\approx 20\%$). Indeed, the uncertainty of the k_{prim} , k_{sec} , k_{tert} could mainly contribute to the errors in SAR1 calculation. That is the reason why, the SAR1 for alkanes reactions with Cl at 298 K have been revised by Aschmann and Atkinson (1995) with values for k_{prim} , k_{sec} and k_{tert} of 3.32, 8.34 and 6.09 $\times 10^{-11} \text{ cm}^3 \text{ molecule}^{-1} \text{ s}^{-1}$, respectively. Then, $k_{2\text{M3P}}$, $k_{3\text{M2P}}$, $k_{4\text{M2P}}$ were also calculated using these

parameters and the group substituent factors ($F_{(-CH_3)}$, $F_{(-CH_2-)}=F_{(-CH<)}=F(>C<)$, $F_{(>CO)}$, $F_{(-CH_2C(O)R)}$) from Calvert et al., (2011). These new SAR1 calculated rate coefficients values are in excellent agreement with the experimental ones ($< 7\%$). These SAR1 parameters also give accurate predictions for 2-pentanone, 3-methyl-2-butanone, 2-hexanone and 5-methyl-2-hexanone with 1.28, 0.57, 1.75 and 1.35, respectively, in good agreement with the experimental values of 1.11, 0.52, 1.93 and 1.34 $\times 10^{-10}$ cm^3 molecule $^{-1}$ s $^{-1}$.

ii. SAR2: described as k_{R_group} (RC(O)R') additivity method. By analogy with the ketones reactions with OH radical, the rate coefficients of the ketones reaction with Cl atoms can be calculated assuming that the group rate constants of CH_3 and R groups on the either side of the $\text{C}=\text{O}$ in $\text{CH}_3\text{C}(\text{O})\text{R}$ are independent and additive. Thus $k_{(\text{CH}_3\text{C}(\text{O})\text{R})}=k_{(\text{CH}_3)}+k_{(\text{R})}$ and $k_{(\text{CH}_3)} = k_{(\text{acetone}+\text{Cl})}/2=0.01 \times 10^{-10}$ cm^3 molecule $^{-1}$ s $^{-1}$. Then, the groups rate constants at 298 K are given in Table 6-6 as: $k_{(\text{n-C}_2\text{H}_5)}= 0.39$ from n-butanone (Atkinson et al., 2006), $k_{(\text{n-C}_3\text{H}_7)}=1.10$ from 2-pentanone (Taketani et al., 2006;Kaiser and Wallington, 2007;Takahashi et al., 2007;Farrugia et al., 2015), $k_{(\text{iso-C}_3\text{H}_7)}=0.64$ from 3-methyl-2-butanone (Notario et al., 2000;Cuevas et al., 2004;Kaiser and Wallington, 2007;Farrugia et al., 2015), $k_{(\text{n-C}_4\text{H}_9)}=1.92$ from 2-hexanone (Taketani et al., 2006;Takahashi et al., 2007), $k_{(\text{sec-C}_4\text{H}_9)}=0.98$ from 3-methyl-2-pentanone ((Farrugia et al., 2015) and this work), $k_{(\text{iso-C}_4\text{H}_9)}=1.26$ from 4-methyl-2-pentanone ((Kaiser and Wallington, 2007;Farrugia et al., 2015) and this work), $k_{(\text{tert-C}_4\text{H}_9)}=0.47$ from 3,3-dimethyl-2-butanone (Farrugia et al., 2015), $k_{(\text{iso-C}_5\text{H}_{11})}=1.33$ from 5-methyl-2-hexanone (Notario et al., 2000;Cuevas et al., 2004). Using these group rate constants, the rate coefficients of 2M3P, 3-hexanone reaction with Cl atoms are estimated to be 1.03 and 0.78, respectively, which are closely to the experiments values 1.07 ± 0.26 (this work) and 0.79 (Calvert et al., 2011), units in 10^{-10} cm^3 molecule $^{-1}$ s $^{-1}$.

Table 6-6: Reactivity of alkyl group R or R' in ketones (RC(O)R') for the reaction of ketone + Cl atoms at 298 K.

alkyl group R	k_R	ketone	$k_{\text{ketone}} \pm \sigma$	Reference
CH ₃ -	0.01	acetone	0.021 \pm 0.003	Atkinson et al., 2006
n-C ₂ H ₅ -	0.39	n-butanone	0.4 \pm 0.06	Atkinson et al., 2006
n-C ₃ H ₇ -	1.10	2-pentanone	1.11 \pm 0.10	Taketani et al., 2006
			1.23 \pm 0.13	Takahashi et al., 2007
			1.16 \pm 0.10	Kaiser and Wallington, 2007
			1.08 \pm 0.05	Farrugia et al., 2015
			1.11^a	
iso-C ₃ H ₇ -	0.64	3-methyl-2-butanone	0.71 \pm 0.09	Notario et al., 2000
			0.62 \pm 0.05	Kaiser and Wallington, 2007
			0.68 \pm 0.06	Farrugia et al., 2015
			0.52^a	
n-C ₄ H ₉ -	1.31	2-hexanone	0.65 \pm 0.06	Albaladejo et al., 2003
			0.65 \pm 0.04	Cuevas et al., 2004
			1.88 \pm 0.15	Taketani et al., 2006
			2.08 \pm 0.32	Takahashi et al., 2007
			1.32^a	
sec-C ₄ H ₉ -	0.98 ^b	3-methyl-2-pentanone	0.94 \pm 0.10	Farrugia et al., 2015
			1.21 \pm 0.21	This work*
			0.99^a	
iso-C ₄ H ₉ -	1.26 ^b	4-methyl-2-pentanone	1.28 \pm 0.01	Kaiser and Wallington, 2007
			1.1 \pm 0.05	Farrugia et al., 2015
			1.34 \pm 0.21	This work*
			1.27^a	
tert-C ₄ H ₉ -	0.47	3,3-dimethyl-2-butanone	0.48 \pm 0.05	Farrugia et al., 2015
iso-C ₅ H ₁₁ -	1.33	5-methyl-2-hexanone	1.06 \pm 0.14	Notario et al., 2000
			1.48 \pm 0.10	Cuevas et al., 2004
			1.34^a	

units of k_R and k in $10^{-10} \text{ cm}^3 \text{ molecule}^{-1} \text{ s}^{-1}$

^a Weighted average from the equation of $(w_1k_1 + w_2k_2 + \dots) / (w_1 + w_2 + \dots)$, where $w_1 = 1/\sigma^2$, etc.

^b values were calculated using the values from this work

iii. SAR3: described as $k_{(\text{CH}_x)}$ additivity method. CH_x (x=1, 2,3) group rate coefficients are determined corresponding to their position relative to C=O in ketones, like $k_{2\text{-butanone}} = k_{(\text{CH}_3)\alpha} + k_{(\text{CH}_2)\alpha} + k_{(\text{CH}_3)\beta}$. Thus, the k_{CH_x} (x=1, 2,3) are estimated in Table 6-7 and calculated as: $k_{(\text{CH}_3)\alpha} = 0.011$ from acetone (Atkinson et al., 2006), $k_{(\text{CH}_3)\beta} = 0.157$ from 3,3 dimethyl-2-butanone (Farrugia et al., 2015), $k_{(\text{CH}_2)\alpha} = 0.233$ from

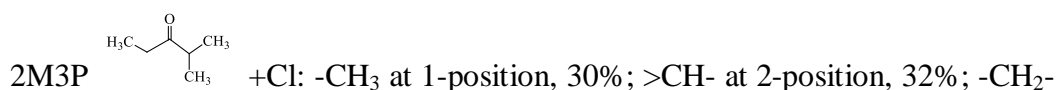
2-butanone (Atkinson et al., 2006), $k_{(\text{CH}_2)\beta}=0.859$ from 2-pentanone (Taketani et al., 2006;Takahashi et al., 2007;Kaiser and Wallington, 2007;Farrugia et al., 2015), $k_{(\text{CH}_2)\gamma}=0.206$ from 2-hexanone (Taketani et al., 2006;Takahashi et al., 2007;Albaladejo et al., 2003), $k_{(\text{CH})\alpha}=0.330$ from 3-methyl-2-butanone (Notario et al., 2000;Cuevas et al., 2004;Kaiser and Wallington, 2007;Farrugia et al., 2015), $k_{(\text{CH})\beta}=1.020$ from 4M2P ((Kaiser and Wallington, 2007;Farrugia et al., 2015) and this work), $k_{(\text{CH})\gamma}=0.226$ from 5-methyl-2-hexanone (Notario et al., 2000;Cuevas et al., 2004). The CH_x ($x=1, 2, 3$) groups in δ position and beyond, and also CH_3 in γ position, are considered not to be influenced by $\text{C}=\text{O}$, so the $k_{(\text{CH}_x)}$ in these positions are taken from the SAR calculation for alkanes. In addition, the rate coefficients of 2M3P, 3M2P and 4M2P are estimated to be 1.04, 1.36 and 1.27, respectively, using these $k_{(\text{CH}_x)}$ parameters and they are found to be in full agreement with the experimental values, 1.07, 1.21 and 1.35, respectively, units in $10^{-10} \text{ cm}^3 \text{ molecule}^{-1} \text{ s}^{-1}$.

Table 6-7: CH_x ($x=1, 2, 3$) group rate constants (k_{CH_x} ($x=1, 2, 3$), units are $10^{-10} \text{ cm}^3 \text{ molecule}^{-1} \text{ s}^{-1}$) for ketones reaction with Cl atoms at 298 K.

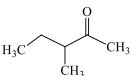
CH_x group	a-position	β -position	γ -position	$>\delta$ -position
$-\text{CH}_3$	0.011	0.157	0.002	0.002
$-\text{CH}_2-$	0.233	0.859	0.206	0.014
$-\text{CH}-$	0.330	1.020	0.226	0.024

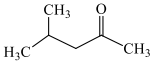
6-4-3- Reaction mechanism of the reaction of Cl atoms + ketones

The previous experimental evidence (Calvert et al., 2011) suggests that ketones react with Cl atoms in a similar way as OH radical mainly via an H-atom abstraction mechanism, resulting by alkyl radicals formation. As reported by Atkinson et al., (1995), the SAR allows the calculation of branching ratios corresponding to H-atoms abstraction from the various $-\text{CH}_3$, $-\text{CH}_2-$ and $>\text{CH}-$ groups. e.g.

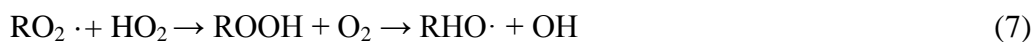
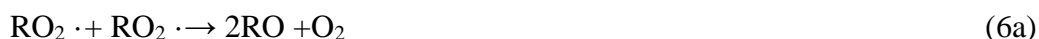


at 4-position, 23%; -CH₃ at 5-position, 15%;

3M2P  +Cl: -CH₃ at 5-position, 0.2%; -CH₂- at 4-position, 63%; >CH- at 3-position, 24%; -CH₃- at 3-position, 12%; -CH₃ at 1-position, 0.8%;

4M2P  +Cl: -CH₃ at 5-position, 0.3%; >CH- at 4-position, 80%; -CH₂- at 3-position, 18%; -CH₃ at 1-position, 0.8%.

After adding O₂, the alkyl peroxy radical (RO₂·) is expected to be formed (pathway 4) from the alkyl radical (R·). Then, in the presence of NO, RO₂ radical would mainly react with NO to form alkoxy radical (RO·, pathway 5). The RO radical could follow the reactions: (a) reaction with O₂; (b) decomposition; (c) isomerization via a 6-membered transition state. In the absence of NO, RO₂ could either proceed by a self-reaction (pathway 6) or react with HO₂ radical (pathway 7).



6-4-3-1- 2M3P+Cl

The experiments in the presence of NO Acetaldehyde and acetone were found to be the main products from the reaction of Cl atoms with 2M3P, with yields of 77.5±12.1% and 38.5±7.7%, respectively (Table 6-2). In addition, the m/z 31.01 and 62.03 were also identified as the products in PTR-ToF-MS analysis. Herein, m/z 31.01 and 62.03 were supposed to be HCHO·H⁺ and CH₃NO₂·H⁺, respectively. With the PTR-ToF-MS, conversion of ion rate (cps) to concentration (ppb) is based on the primary ion rate and PTR drift tube conditions. In this work, the PTR drift tube conditions were constant. To compare the m/z 31.01 formation between 2M3P/3M2P/4M2P reactions with Cl atoms, as shown in Figure 6-8, the linear-least square analysis of products' signal intensity (cps) as function of the consumed 2M3P

signal intensity (m/z 101.09) was performed. As shown in Figure 6-8, the formation yield of m/z 31.01 was estimated to be 9.0% and the one of CH_3NO_2 (m/z 62.03) showed a continuous increase with the consumed 2M3P, which indicates that CH_3NO_2 was not a primary product from the reaction of 2M3P with Cl atoms. In addition, CH_3NO_2 is expected to be formed from CH_3 radical reaction with NO_2 .

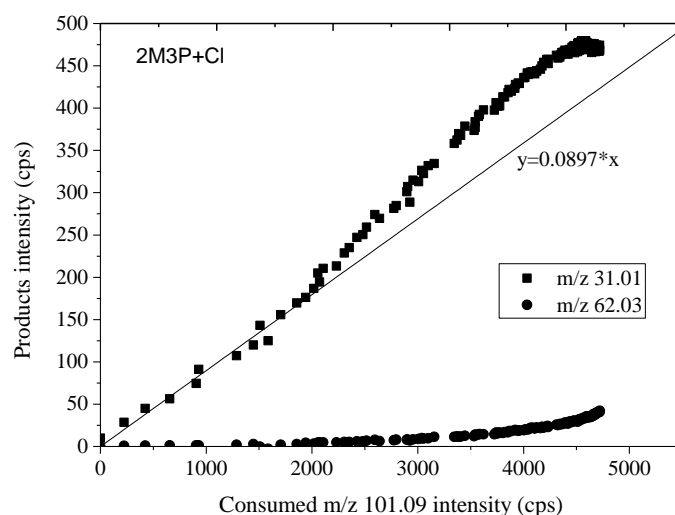
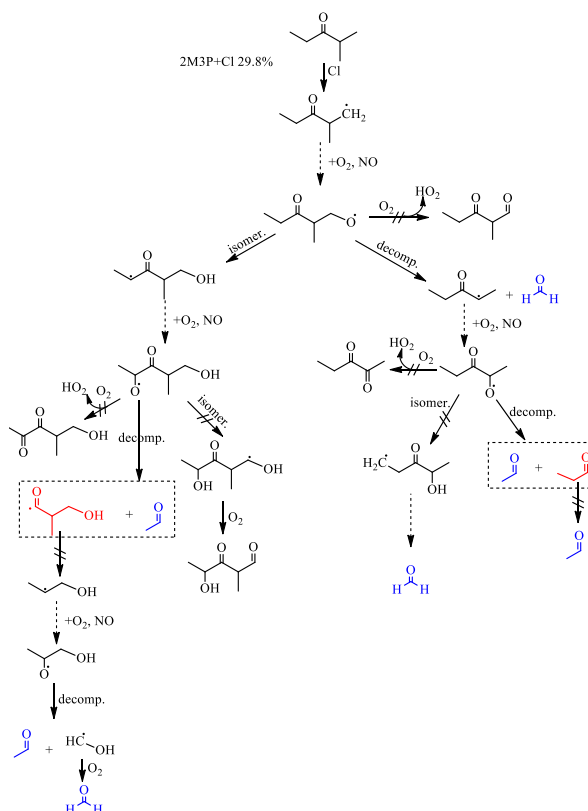


Figure 6-8: Products' intensity (cps) vs the intensity of consumed 2M3P in the reaction of 2M3P with Cl. m/z 31.01 and 62.03 were associated to $\text{HCHO}\cdot\text{H}^+$ and $\text{CH}_3\text{NO}_2\cdot\text{H}^+$, respectively.

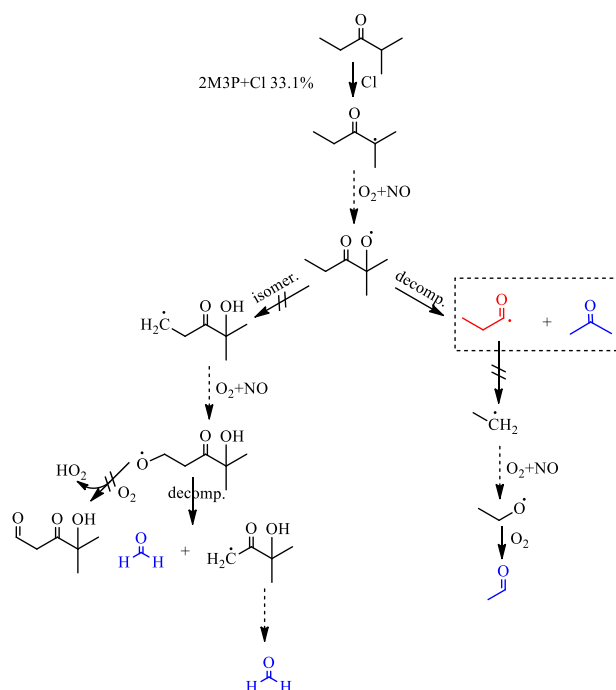
The Scheme 6-1a shows the $\text{CH}_3\text{CH}_2\text{C}(\text{O})\text{CH}(\text{CH}_3)\text{CH}_2\text{O}$ formed after H-atom abstraction from $-\text{CH}_3$ at 1-position, which may react with O_2 or isomerize via 6-members transition state or decompose. However, since the mass m/z 115.06 (methyl pentanedione) was identified using the PTR-ToF-MS, its reaction with O_2 is expected to be less important in this work. The decomposition and isomerization of $\text{CH}_3\text{CH}_2\text{C}(\text{O})\text{CH}(\text{CH}_3)\text{CH}_2\text{O}$ could be of comparable importance, which could give $\text{CH}_3\text{CH}_2\text{C}(\text{O})\text{CH}_2\cdot$ and $\text{CH}_3\text{CH}_2\text{C}(\text{O})\text{CH}(\text{CH}_3)\text{CH}_2\text{OH}\cdot$ radicals. Then, their following reaction are expected to form $\text{CH}_3\text{CH}_2\text{C}(\text{O})\text{CHO}$ and $\text{CH}_3\text{CHOC}(\text{O})\text{CH}(\text{CH}_3)\text{CH}_2\text{OH}$ radicals. Since Atkinson et al., (1991) have reported that $>\text{CO}-\text{C}(\text{O})-$ carbon-carbon bond scission is rather faster than $>\text{CO}-\text{CH}_2-$ carbon-carbon bond scission, the decomposition of $\text{CH}_3\text{CH}_2\text{C}(\text{O})\text{CHO}$ and $\text{CH}_3\text{CHO}-\text{C}(\text{O})\text{CH}(\text{CH}_3)\text{CH}_2\text{OH}$ radicals would dominate and generate one molecule acetaldehyde and acetyl radical.

Kaiser et al., investigated the reaction of Cl atoms with 3-pentanone/butanone either in N_2 or O_2 , when 500 ppm O_2 presented in the reaction of Cl+3-pentanone/butanone, the maximum 95%/56% of $CH_3C(O)Cl$ formed, however there is no $CH_3C(O)Cl$ formed when the reaction of Cl+3-pentanone/butanone happened in the absence of O_2 (Kaiser et al., 2009, 2010). By analogy with $CH_3C(O)$ radical, the acetyl radicals (Scheme 6-1a in red) would mainly react with Cl_2 and form $CH_3C(O)Cl$ and $CH_2(OH)CH(CH_3)C(O)Cl$. As shown in Scheme 6-1a, just one molecule of acetaldehyde could be formed from the following reaction of H-abstraction from CH_3 group at 1- position and account for 29.8% of overall acetaldehyde formation. However, two molecules of acetaldehyde could be formed if it hypothesizes that $CH_2(OH)CH(CH_3)C(O)$ and $CH_3C(O)$ mainly react with O_2 (Scheme 6-1a, following reaction of acetyl radicals in red). Hence, H-abstraction from $-CH_3$ group at 1-position accounts for 59.6% of the overall acetaldehyde formation.



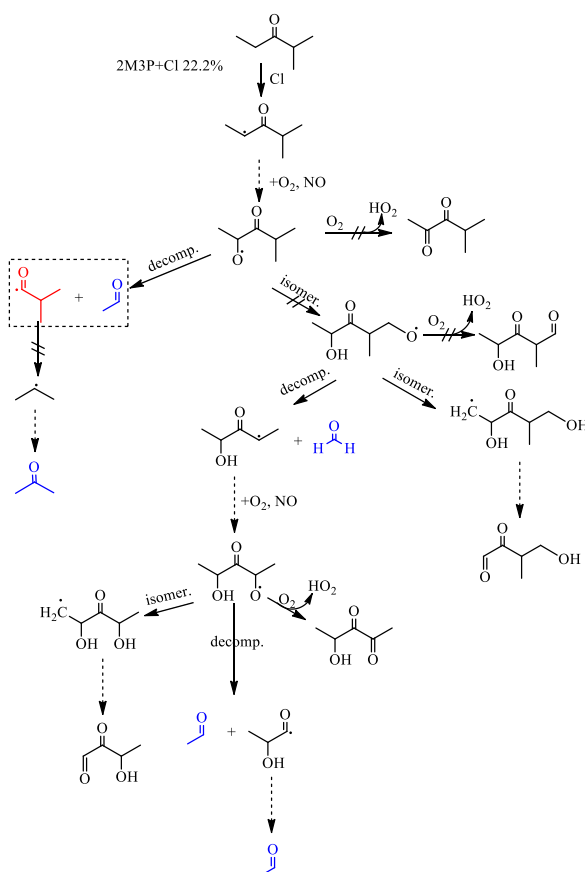
Scheme 6-1a: Reaction of Cl atoms with 2M3P in the presence of NO: proposed mechanism leading to the formation of observed reaction products (in blue). Compounds in red represent intermediate products which mainly react with Cl_2 . The expected relative importance of the possible RO reaction pathways are indicated by the arrows: $\rightarrow > \nrightarrow$; the intermediary of RO / RO_2 are indicated by \cdots .

The Scheme 6-1b shows the $\text{CH}_3\text{CH}_2\text{C}(\text{O})\text{CO}(\text{CH}_3)_2$ formed after H-atom abstraction from -CH at 2-position, which would proceed by isomerization via a 6-members transition state and decomposition. As described in the previous section, the $>\text{CO C}(\text{O})\cdot$ carbon-carbon bond scission is rather faster than $>\text{CO CH}_2\cdot$ carbon-carbon bond scission (Atkinson and Carter, 1991), and the isomerization rates depend on the position of the $-\text{CH}_x$ groups relative to the $\text{C}=\text{O}$ group (Aschmann and Atkinson, 1995; Mereau et al., 2003). Then, the decomposition could be dominant for $\text{CH}_3\text{CH}_2\text{C}(\text{O})\text{CHO}(\text{CH}_3)_2$ and would give one molecule of acetone and acetyl radical. Since the acetyl radical was expected mainly to react with Cl_2 (Kaiser et al., 2010), as shown in Scheme 6-1b, the H-atom abstraction from -CH at 2-position account for 33.1% of the overall acetone formation. However, one molecule of acetaldehyde could be formed if it hypothesizes that $\text{CH}_3\text{CH}_2\text{C}(\text{O})\cdot$ mainly reacts with O_2 (following reaction of Scheme 6-1b in red). And hence, H-abstraction from -CH group at 2-position accounts for 33.1% of the overall acetaldehyde and 33.1% of the overall acetone formed.



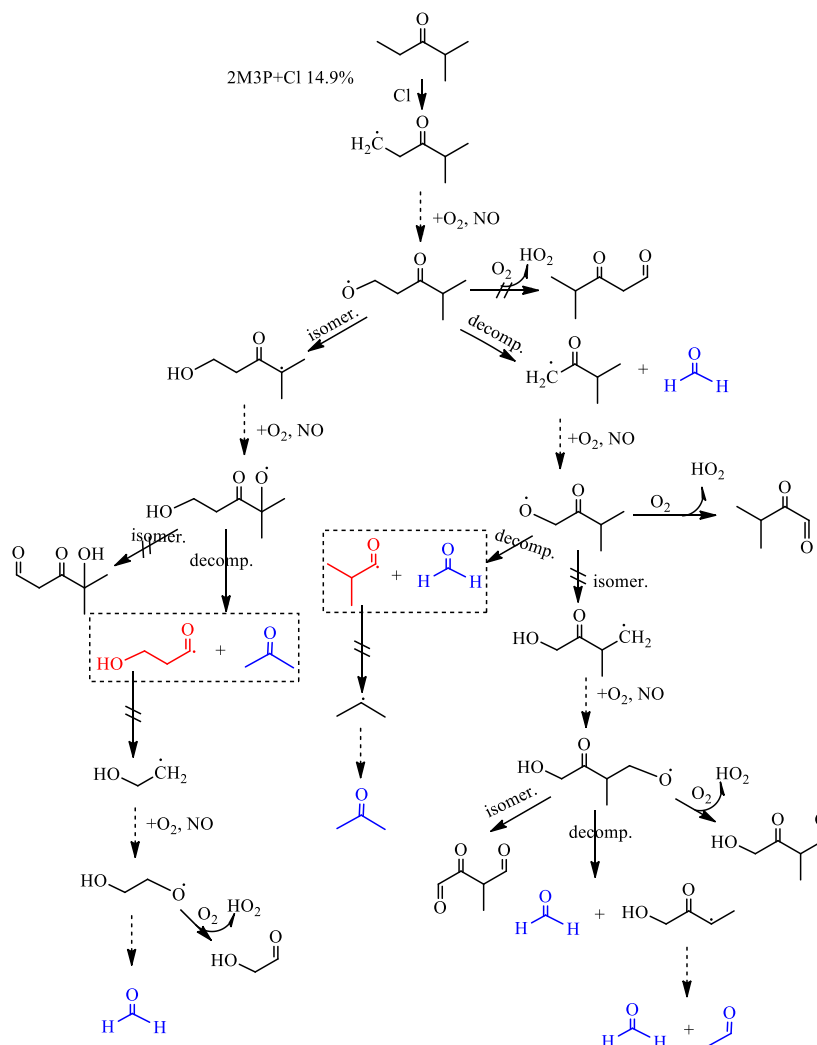
Scheme 6-1b: Reaction of Cl atoms with 2M3P in the presence of NO: proposed mechanism leading to the formation of observed reaction products (in blue). Compounds in red represent intermediate products which mainly react with Cl_2 . The expected relative importance of the possible $\text{RO}\cdot$ reaction pathways are indicated by the arrows: $\rightarrow > \nrightarrow$; the intermediaries of $\text{RO}\cdot$ / $\text{RO}_2\cdot$ are indicated by \cdots .

The Scheme 6-1c shows the $\text{CH}_3\text{CHO C}(\text{O})\text{CH}(\text{CH}_3)_2$ formed after H-atom abstraction from $-\text{CH}_2$ at 4-position. Since the isomerization via 6-members transition state (H-abstraction from $-\text{CH}_3$ is supposed to be slow in SAR) and the reaction with O_2 (no m/z 115.06 was identified in PTR-ToF-MS) are expected less important, $\text{CH}_3\text{CHO C}(\text{O})\text{CH}(\text{CH}_3)_2$ would mainly decompose to one molecule of acetaldehyde and $\text{CH}(\text{CH}_3)_2\text{CO}$. If it hypothesis that $\text{CH}(\text{CH}_3)_2\text{CO}$ would mainly react with Cl_2 to form $\text{CH}(\text{CH}_3)_2\text{COCl}$ than reacts with O_2 , the H-atom abstraction from $-\text{CH}_2$ at 4-position accounts for 22.2% of the overall acetaldehyde formation. However, as shown in Scheme 6-1c, one molecule of acetone could be formed if it hypothesizes that $\text{CH}(\text{CH}_3)_2\text{CO}$ mainly reacts with O_2 . And hence, H-abstraction from $-\text{CH}_2$ group at 4-position accounts for 22.2% of the overall acetaldehyde and 22.2% of acetone formed.



Scheme 6-1c: Reaction of Cl atoms with 2M3P in the presence of NO: proposed mechanism leading to the formation of observed reaction products (in blue). Compounds in red represent intermediate products which mainly react with Cl_2 . The expected relative importance of the possible $\text{RO} \cdot$ reaction pathways are indicated by the arrows: $\rightarrow > \Rightarrow$; the intermediary of $\text{RO} \cdot / \text{RO}_2 \cdot$ are indicated by \leadsto .

The Scheme 6-1d shows the $\text{CH}_2\text{O}-\text{CH}_2\text{C}(\text{O})\text{CH}(\text{CH}_3)_2$ formed after H-atom abstraction from $-\text{CH}_3$ at 5-position, which could decompose, isomerize, or react with O_2 . The decomposition and isomerization could be of comparable importance and $(\text{CH}_3)_2\text{CHC}(\text{O})\text{CH}_2\text{O}\cdot$ and $(\text{CH}_3)_2\text{CO}-\text{C}(\text{O})\text{CH}_2\text{CH}_2\text{OH}$ could be formed, respectively. As explained in the former section, for the $>\text{CO}-\text{C}(\text{O})\cdot$ radical the decomposition is more expected than the isomerization and the reaction with O_2 . Hence, $(\text{CH}_3)_2\text{CHC}(\text{O})\text{CH}_2\text{O}$ and $(\text{CH}_3)_2\text{CO}-\text{C}(\text{O})\text{CH}_2\text{CH}_2\text{OH}$ could produce the formaldehyde plus acetyl radical, and acetone plus acetyl radical, respectively. Since acetyl radical would mainly react with Cl_2 (Kaiser et al., 2010), the H-atom abstraction from $-\text{CH}_3$ at 5-position account for 7% of the overall acetone formation. However, as shown in Scheme 6-1d, one more molecule of acetone could be formed if it hypothesizes that $\text{CH}(\text{CH}_3)_2\text{CO}$ mainly reacts with O_2 . Hence, H-atom abstraction from $-\text{CH}_3$ group at 5-position accounts for 14.9% of the overall acetone formed.



Scheme 6-1d: Reaction of Cl atoms with 2M3P in the presence of NO: proposed mechanism leading to the formation of observed reaction products (in blue). Compounds in red represent intermediate products which mainly react with Cl_2 . The expected relative importance of the possible $\text{RO} \cdot$ reaction pathways are indicated by the arrows: $\rightarrow > \nrightarrow$; the intermediary of $\text{RO} \cdot / \text{RO}_2 \cdot$ are indicated by \cdots .

Based on the Scheme 6-1(a-d), the formation yields of acetone and acetaldehyde were estimated to be 40.1% (33.1%+7%) and 52% (29.8%+22.2%), respectively, with the hypothesis that the acetyl radicals ($\text{CH}_3\text{CH}_2\text{CO} \cdot$ and $\text{CH}(\text{CH}_3)_2\text{CO} \cdot$) mainly react with Cl_2 . However, formation yields of acetone and acetaldehyde were estimated to be 70.2% (33.1%+22.2+14.9%) and 114.9% ($29.8 \times 2 = 59.8 + 33.1 + 22.2$), respectively, if it hypothesizes that the acetyl radicals ($\text{CH}_3\text{CH}_2\text{CO} \cdot$ and $\text{CH}(\text{CH}_3)_2\text{CO} \cdot$) mainly react with O_2 . Furthermore, our measured yields of acetone and acetaldehyde are $38.5 \pm 7.7\%$ and $77.5 \pm 12.1\%$, respectively. It indicates that the

experimental yield of acetone ($38.5 \pm 7.7\%$) is closely to its estimated yield (40.1%) if $\text{CH}(\text{CH}_3)_2\text{CO}$ mainly (100%) reacts with Cl_2 . However, the experimental acetaldehyde's yield ($77.5 \pm 12.1\%$) is different than estimated values. It indicates that only part of the $\text{CH}_3\text{CH}_2\text{CO} \cdot$ would react with Cl_2 . Combining the experimental and estimated acetaldehyde's yield, the partition ratio of $\text{CH}_3\text{CH}_2\text{CO} \cdot$ reactivity toward to Cl_2 vs $\text{CH}_3\text{CH}_2\text{CO} \cdot$ reactivity toward O_2 is estimated to be 3:2 $[(1 - \frac{77.5-52}{114.9-52}) : (\frac{77.5-52}{114.9-52})]$. The reactions of acetyl radical with Cl_2 then appear to be important. As the mass m/z 135 (chloro-2-methyl-3-pentanone) was not detected by PTR-ToF-MS, it indicates that the $\text{R} \cdot$ (from H-abstraction from 2M3P) radical would not react with Cl_2 . By taking into account the experimental yields of acetone and acetaldehyde, the carbon content of the formed products occupies $44.8 \pm 1.2\%$ percent of the carbon content of the consumed 2M3P. It also supposes that the small products, e.g. CO and HCHO, account for large percent carbon content of the consumed 2M3P.

The experiments in the absence of NO As shown in the Table 6-2, acetaldehyde and acetone were found to be the main products from the reaction of Cl atom with 2M3P in the absence of NO, with yields of $58.2 \pm 5.8\%$ and $39.7 \pm 5.5\%$, respectively, in this work.

After the H-abstraction from the CH_x group and the reaction with O_2 , the alkyl peroxy (RO_2) radicals would be formed. The self-reaction of RO_2 radical could follow the pathways 6a and 6b to give RO radical and aldehyde plus alcohol. Some authors (Tyndall et al., 1998) have suggested that the branching fraction k_{6a}/k_6 could be equal to 35-45%. However, if the HO_2 concentration is sufficiently high, the RO_2 radicals would react almost exclusively with HO_2 , which would mainly produce RO radical (pathway 7). Finally, the similar formation yield of acetone and acetaldehyde between the reaction in the presence and in the absence of NO could suggest that the RO_2 radical mainly proceed by reaction pathways 6b or 7 to form RO radical in this work.

6-4-3-2- 3M2P+Cl

The experiments in the presence of NO As shown in the Table 6-3, acetaldehyde, 2-butanone and propanal were found to be the main products from the reaction of Cl atoms with 3M2P, with yields determined as $75.1 \pm 9.8\%$, $22.3 \pm 1.5\%$ and $13.6 \pm 1.0\%$, respectively. In addition, the masses m/z 31.01, 62.03 and 115.06 were also identified by PTR-ToF-MS and could be associated to $\text{HCHO} \cdot \text{H}^+$, $\text{CH}_3\text{NO}_2 \cdot \text{H}^+$ and $\text{CH}_3\text{C}(\text{O})\text{CH}(\text{CH}_3)\text{C}(\text{O})\text{CH}_3 \cdot \text{H}^+$ (3-methyl-2,4-pentanedione and H^+ cluster ion), respectively. However, 3-methyl-2,4-pentanedione was expected to be formed from the reaction of $\text{CH}_3\text{CH}(\text{O} \cdot)\text{CH}(\text{CH}_3)\text{C}(\text{O})\text{CH}_3$ radical with O_2 , which was induced from the H-abstraction from the $-\text{CH}_2$ group at 4 position of 3M2P. By analogy to 2M3P+Cl reaction, the hypothesized formation yields of m/z 31.01 and 115.06 were estimated to be 7.6% and 5.4%, respectively, calculating from the linear-least square analysis of their signal intensity (Figure 6-9). As shown in Figure 6-9, same result as 2M3+Cl reaction, CH_3NO_2 was not a primary product from the reaction of 3M2P with Cl atoms, but was expected to be formed from $\text{CH}_3 \cdot$ radical reaction with NO_2 .

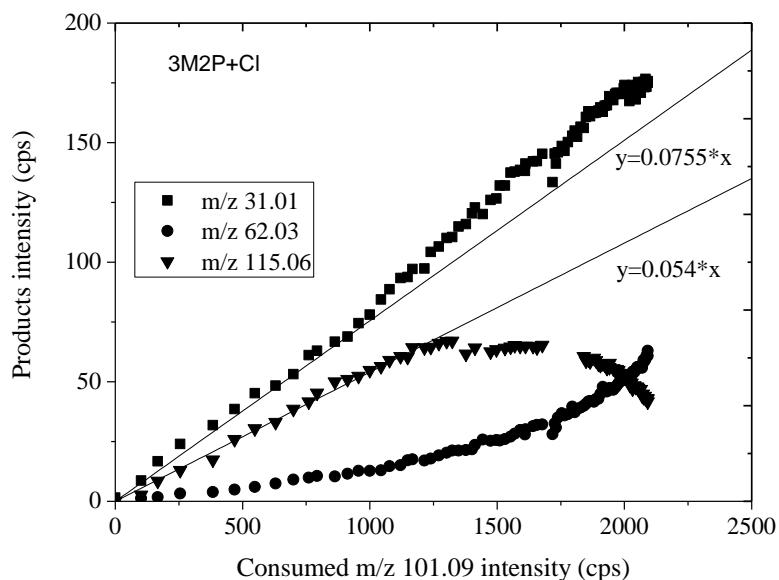
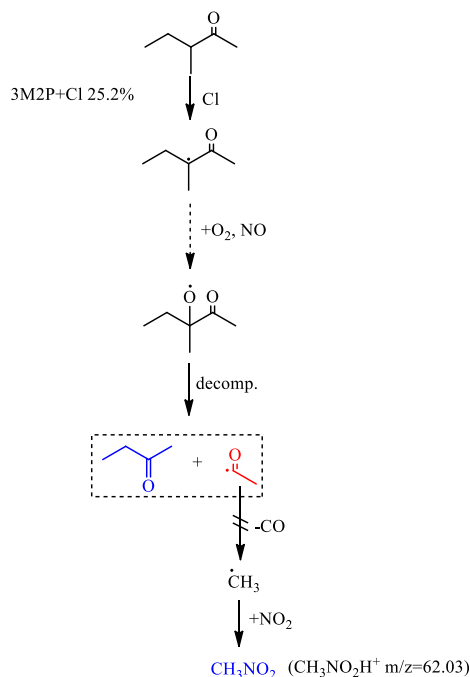


Figure 6-9: Products' intensity (cps) vs the intensity of consumed 3M2P in the reaction of 3M2P with C Masses m/z 31.01, 62.03 and 115.06 detected by PTR-ToF-MS were attributed to $\text{HCHO} \cdot \text{H}^+$, $\text{CH}_3\text{NO}_2 \cdot \text{H}^+$ and $\text{CH}_3\text{C}(\text{O})\text{CH}(\text{CH}_3)\text{C}(\text{O})\text{CH}_3 \cdot \text{H}^+$, respectively.

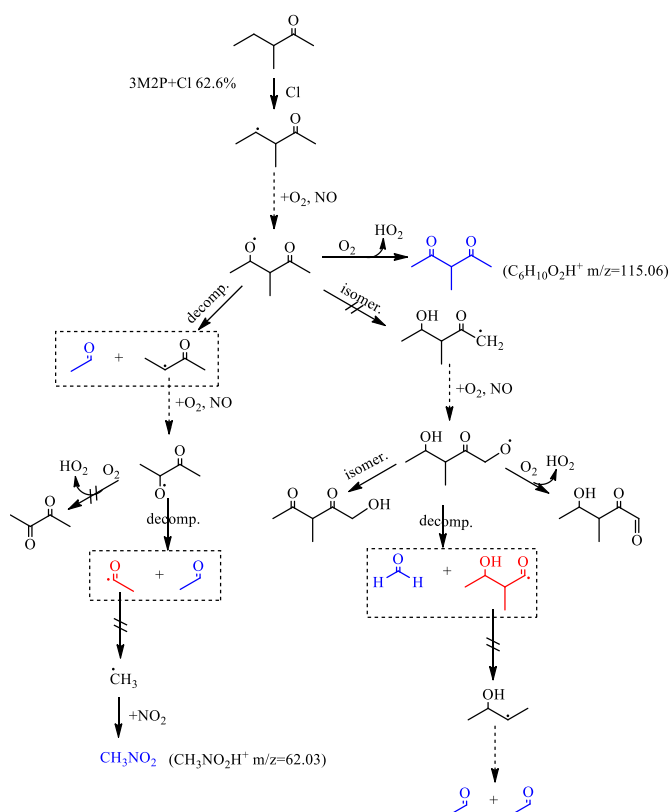
231

Scheme 6-2b shown the $\text{CH}_3\text{CH}_2\text{CH}(\text{CH}_3)(\text{O})\cdot\text{C}(\text{O})\text{CH}_3$ radical formed after H-atom abstraction from $-\text{CH}$ at 3-position, which could only proceed by decomposition. After, the decomposition of $\text{CH}_3\text{CH}_2\text{CH}(\text{CH}_3)(\text{O})\cdot\text{C}(\text{O})\text{CH}_3$ radical would form the 2-butanone and acetyl radical. Hence, the H-atom abstraction from $-\text{CH}$ at 3-position accounts for 25.2% of the overall 2-butanone formation.



Scheme 6-2b: Reaction of Cl atoms with 3M2P in the presence of NO: proposed mechanism leading to the formation of observed reaction products (in blue). Compounds in red represent intermediate products which mainly react with Cl₂. The expected relative importance of the possible RO· reaction pathways are indicated by the arrows: $\rightarrow > \nrightarrow$; The intermediary of RO / RO₂· are indicated by \rightarrow .

The Scheme 6-2c show the $\text{CH}_3\text{CH}(\text{O})\cdot\text{CH}(\text{CH}_3)\text{C}(\text{O})\text{CH}_3$ radical formed after H-atom abstraction from $-\text{CH}_2$ at 4-position, which could proceed by decomposition, isomerization and reaction with O₂. As described in the previous sections, mass m/z 115.06 ($\text{CH}_3\text{CH}(\text{O})\cdot\text{CH}(\text{CH}_3)\text{C}(\text{O})\text{CH}_3\cdot\text{H}^+$ cluster) was detected by PTR-ToF-MS which could be mainly formed from the reaction of $\text{CH}_3\text{CH}(\text{O})\cdot\text{CH}(\text{CH}_3)\text{C}(\text{O})\text{CH}_3$ radical with O₂. Since the isomerization rates depend on the position of the $-\text{CH}_x$ groups relative to the $>\text{CO}$ group (Atkinson and Aschmann, 1995; Mereau et al., 2003), the isomerization of $\text{CH}_3\text{CH}(\text{O})\cdot\text{CH}(\text{CH}_3)\text{C}(\text{O})\text{CH}_3$ radical involves H-abstraction from $\alpha\text{-CH}_3$ and could be of minor importance. Then, the decomposition of



Scheme 6-2c: Reaction of Cl atoms with 3M2P in the presence of NO: proposed mechanism leading to the formation of observed reaction products (in blue). Compounds in red represent intermediate products which mainly react with Cl₂. The expected relative importance of the possible RO· reaction pathways are indicated by the arrows: → > ⇝; The intermediary of RO / RO₂· are indicated by ⇝.

Based on the Scheme 6-2(a-c) and the relative importance of the various alkoxy radical pathways, our measured of 2-butanone, acetaldehyde and propanal yields indicate that the 2-butanone, acetaldehyde and propanal are mainly formed after

H-abstraction from >CH- group at 3-position, -CH₂- group at 4-position and -CH₃ group at 3-position, respectively. Our measured of 2-butanone and propanal yields of $22.3 \pm 1.5\%$ and $13.6 \pm 1.0\%$, respectively, are closely to the estimated values, 25.2% and 11.3%. In addition, this work estimates the yield of 3-methyl-2,4-pentanedione to be $\approx 25\%$. By taking into account experimental yields of 2-butanone, propanal, acetaldehyde and 3-methyl-2,4-pentanedione, the carbon content of the formed products occupies 72% percent of the carbon content of the consumed 3M2P. Hence, the undetermined formation yield of small products, e.g. CO, HCHO, and the possible organochloride could account for $\approx 25\%$ of consumed 3M2P.

The experiments in the absence of NO As shown in the Table 6-3, acetaldehyde and 2-butanone were found to be the main products from the reaction of Cl atoms with 3M2P in the absence of NO, with values of $40.3 \pm 1.7\%$ and $18.2 \pm 2.4\%$, respectively.

As seen for the experiments in the presence of NO, the H-abstraction from -CH₃ group at 1 and 5 position is of minor importance comparatively to the overall products formation from the reaction of 3M2P with Cl atoms. The self-reaction of RO₂ radical (60%, pathway 6a) would mainly generate the RO radical (Tyndall et al., 1998), but they also could be mostly be formed from the pathway 7 if the HO₂ concentration is sufficiently high. This work found the same products from the 3M2P reaction with Cl atoms in the absence or in the presence of, but with less products formation yields. It indicates that the RO₂ radical mainly produces RO radical through self-reaction or reaction with HO₂.

6-4-3-3- 4M2P+Cl

The experiments in the presence of NO As shown in the Table 6-4, acetone and 2-methylpropanal were found to be the main products from the reaction of Cl atoms with 4M2P, with yields of $25.9 \pm 2.5\%$ and $23.6 \pm 1.6\%$, respectively. In addition, the masses *m/z* 31.01, 62.03, 115.06 and 135.01 were also identified as products with

PTR-ToF-MS and could be associated to $\text{HCHO}\cdot\text{H}^+$, $\text{CH}_3\text{NO}_2\cdot\text{H}^+$, $(\text{CH}_3)_2\text{CHC}(\text{O})\text{C}(\text{O})\text{CH}_3\cdot\text{H}^+$ (4-methyl-2,3-pentanedione and H^+ cluster) and $(\text{CH}_3)_2\text{CClCH}_2\text{C}(\text{O})\text{CH}_3\cdot\text{H}^+$ respectively. The hypothesized yield of masses m/z 31.01 and m/z 115.06 were determined to be 21.9% and 10.0%, respectively (Figure 6-10), calculated from the linear-least square analysis of their intensity (cps). In addition, as shown in Figure 6-10, both masses m/z 62.03 and m/z 135.01 are continuously increasing with the consumed 4M2P.

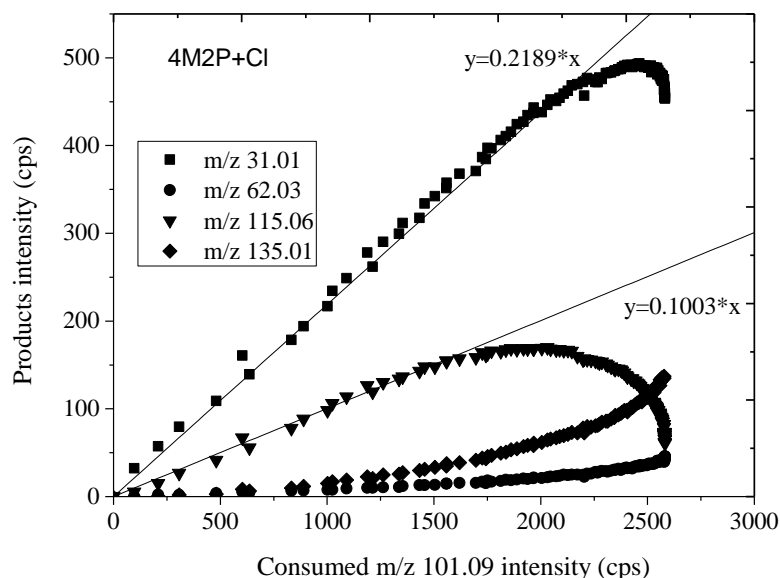
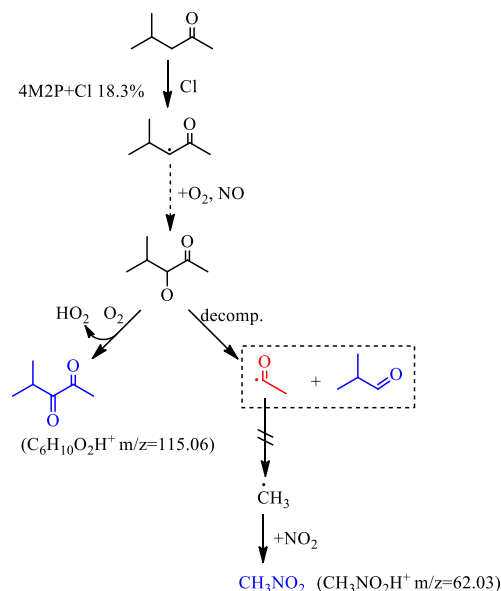


Figure 6-10: Products' intensity (cps) vs the intensity of consumed 4M2P in the reaction of 4M2P with Cl. Masses m/z 31.01, 62.03, 115.06 and 135.01 were associated to $\text{HCHO}\cdot\text{H}^+$, $\text{CH}_3\text{NO}_2\cdot\text{H}^+$, $\text{CH}_3\text{C}(\text{O})\text{CH}(\text{CH}_3)\text{C}(\text{O})\text{CH}_3\cdot\text{H}^+$ and $(\text{CH}_3)_2\text{CClCH}_2\text{C}(\text{O})\text{CH}_3\cdot\text{H}^+$ respectively, using PTR-ToF-MS.

Based on the SAR calculation, the H-abstraction from $-\text{CH}_3$ group at 1 and 5 position accounts for 0.82% and 0.27% of the overall reaction, respectively. It indicates that any product formed from these two reactions could only account for minor fraction of the overall products formation.

The Scheme 6-3a shows the $(\text{CH}_3)_2\text{CHCHO C}(\text{O})\text{CH}_3$ formed after H-atom abstraction from $-\text{CH}_2$ at 3-position, which could proceed by both decomposition and reaction with O_2 . Then, one acetyl radical and 2-methylpropanal would be formed from the decomposition of $(\text{CH}_3)_2\text{CHCHO C}(\text{O})\text{CH}_3$. In the other way, the 4-methyl-2,3-pentanedione could be formed from the reaction of

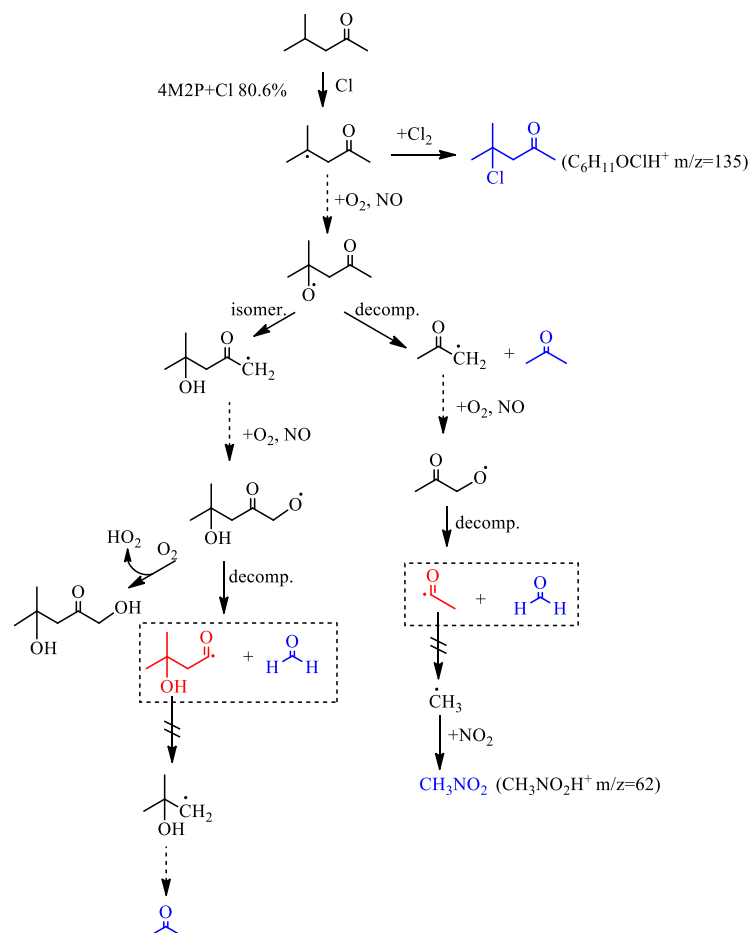
$(\text{CH}_3)_2\text{CHCHO C}(\text{O})\text{CH}_3$ with O_2 , since whose cluster with H^+ was identified at the mass m/z 115.06 with the PTR-ToF-MS. Hence, the H-atom abstraction from $-\text{CH}_2$ at 3-position accounts for 18.3% of the overall 2-methylpropanal formation.



Scheme 6-3a: Reaction of Cl atoms with 4M2P in the presence of NO: proposed mechanism leading to the formation of observed reaction products (in blue). Compounds in red represent intermediate products which mainly react with Cl_2 . The expected relative importance of the possible $\text{RO} \cdot$ reaction pathways are indicated by the arrows: $\rightarrow > \nrightarrow$; The intermediary of $\text{RO} \cdot / \text{RO}_2 \cdot$ are indicated by \cdots .

The Scheme 6-3b shows the $(\text{CH}_3)_2\text{C CH}_2\text{C}(\text{O})\text{CH}_3$ formed after H-atom abstraction from $-\text{CH}$ at 4-position, which cannot react with O_2 , leading to the decomposition and isomerization as possible pathways. Atkinson et al., (1995) have measured the reaction of 4M2P with OH radical and suggested that the decomposition of $(\text{CH}_3)_2\text{CO CH}_2\text{C}(\text{O})\text{CH}_3$ radical could be the dominant pathway to give a $\text{CH}_3\text{C}(\text{O})\text{CH}_2$ radical and one molecule of acetone. In this work, it is supposed that most of $(\text{CH}_3)_2\text{CO CH}_2\text{C}(\text{O})\text{CH}_3$ radical would decompose to one molecule of acetone and $\text{CH}_3\text{C}(\text{O})\text{CH}_2$ radical. Since the mass m/z 135.01 was identified with the PTR-ToF-MS, it indicates that $(\text{CH}_3)_2\text{C CH}_2\text{C}(\text{O})\text{CH}_3$ could also react with Cl_2 to form $(\text{CH}_3)_2\text{CClCH}_2\text{C}(\text{O})\text{CH}_3$. However, the mass m/z 135.01 ($(\text{CH}_3)_2\text{CClCH}_2\text{C}(\text{O})\text{CH}_3 \cdot \text{H}^+$) was not identified both from the reaction of Cl with 2M3P and 3M2P. As discussed by Kaiser et al., (2009), the α position of the $\text{C}=\text{O}$

group is significantly deactivated toward Cl_2 reaction while the β position retains a more normal Cl_2 reactivity relative to that observed for alkyl radicals. This work found that only the $-\dot{\text{C}} <$ radical in β position to $\text{C}=\text{O}$ group has enough activity to react with Cl_2 .



Scheme 6-3b: Reaction of Cl atoms with 4M2P in the presence of NO: proposed mechanism leading to the formation of observed reaction products (in blue). Compounds in red represent intermediate products which mainly react with Cl_2 . The expected relative importance of the possible $\text{RO} \cdot$ reaction pathways are indicated by the arrows: $\rightarrow > \Rightarrow$; The intermediary of $\text{RO} / \text{RO}_2 \cdot$ are indicated by \cdots .

Based on the Scheme 6-3(a-b) and the calculated relative importance of the various alkoxy radical pathways, our measured acetone and 2-methylpropanal yields indicate that they are mainly formed after H-abstraction from $-\text{CH}_2-$ group at 3-position and $>\text{CH}-$ group at 4-position, respectively. In addition, the measured 2-methylpropanal yield of $23.6 \pm 1.6\%$ is close to the estimated 2-methylpropanal yield of 18.3% . Taking into account the formed 4-methyl-2,3-pentanedione, the SAR

underestimates the partition ratio of H-abstraction from $-\text{CH}_2-$ group. Furthermore, our measured acetone yield of $25.9 \pm 2.5\%$ was independently lower than the estimated acetone 80.6%, which could be explained by the reaction of $(\text{CH}_3)_2\text{C}-\text{CH}_2\text{C}(\text{O})\text{CH}_3$ with Cl_2 to form $(\text{CH}_3)_2\text{CClCH}_2\text{C}(\text{O})\text{CH}_3$ (whose cluster with H^+ is m/z 135 using PTR-ToF-MS). Considering the experimental yields of acetone and 2-methylpropanal, the carbon content of the detected products occupies $28.7 \pm 1.1\%$ percent of the carbon content of the consumed 4M2P.

The experiments in the absence of NO As shown in the Table 6-4, acetone and 2-methylpropanal were found to be the products of the reaction of Cl atoms with 4M2P in the absence of NO, determined as $18.2 \pm 0.9\%$ and $15.1 \pm 0.7\%$, respectively, and detected by GC-FID in this work.

As for the experiment in the presence of NO, the H-abstraction from $-\text{CH}_3$ group at 1 and 5 position is of minor importance comparatively to any products formation from the reaction of 4M2P with Cl atoms. And the acetone and 2-methylpropanal are expected to be mainly formed after H-abstraction from $-\text{CH}_2-$ group at 3-position and $>\text{CH}-$ group at 4-position, respectively. Tyndall et al., (1998) have reported that the k_{6a}/k_6 ratio could be around 60% to give RO radical, and 92% of the reaction of RO_2 radical with HO_2 would follow pathway 7 to give RO radical (Tyndall et al., 2001). It could explain that the reaction of 4M2P with Cl atoms in the absence of NO has the same products as the reaction in the presence of NO but with less formation yield.

6-4-4- Reaction mechanism comparison between the studied reactions with Cl atoms

As discussed in the previous section, the mass m/z 115.06 (PTR-ToF-MS) was identified as a product of the reaction of Cl atoms with 3M2P and 4M2P, but not detected in the 2M3P reaction with Cl atoms. In addition, the estimated formation (using the PTR-ToF-MS intensity cps) corresponding to the mass m/z 115.06 from

4M2P+Cl (10.3%) is higher than the one from 3M2P+Cl (5.4%). It could be explained by the trend of reactivity of CH_x group depending on their position relative to the C=O group, which was also confirmed in the kinetic study combining the SAR calculation.

Furthermore, the mass m/z 135.01 ($((\text{CH}_3)_2\text{CHC}(\text{O})\text{C}(\text{O})\text{CH}_3\cdot\text{H}^+$ cluster detected by PTR-ToF-MS) was detected in the reaction of 4M2P+Cl but it was not the case in the reaction of 2M3P/3M2P+Cl. During the reaction of 4M2P+Cl, the mass m/z 135.01 was expected to be formed from $(\text{CH}_3)_2\text{C}\cdot\text{CH}_2\text{C}(\text{O})\text{CH}_3$ radical reaction with Cl₂. Kaiser et al., (2009) have investigated the products and mechanism of the reaction of Cl with butanone in N₂/O₂ without NO. In their study, addition of O₂ in the butanone reaction with Cl/Cl₂ in N₂ causes 3-chlorobutanone yield to decrease from 76% in N₂ to 2% in O₂, and the 4-chlorobutanone also decreases but by a much smaller amount: 22.5% with N₂ to 18.5% in O₂. They concluded that the α position to C=O group is significantly deactivated toward Cl₂ reaction while the β position retains a more normal Cl₂ reactivity relative to that observed for alkyl radicals. This was confirmed later in the reaction of 3-pentanone with Cl atoms (Kaiser et al., 2010). Because the mass m/z 135.01 was identified in reaction of 4M2P+Cl without detection in the reaction of 2M3P/3M2P+Cl, this work suggests that only the -CH₂ group in β position to C=O presents enough reactivity toward Cl₂ in the condition of O₂>>Cl₂. However, more studies are needed to confirm it.

6-5- Atmospheric implications

This work shows clearly that ketones with different branched structures do not present a large difference between their rate constants for reactions with Cl atoms. In addition, the rate constant data obtained in this work contribute to a better definition of the tropospheric lifetimes of 2M3P, 3M2P and 4M2P. With a typical average global tropospheric Cl concentration of 1×10^4 atoms cm⁻³ (Wingenter et al., 1996), the following tropospheric lifetimes toward Cl atoms reaction ($\tau=1/k[\text{Cl}]$) are estimated as: 264 hours, 230 hours and 207 hours for 2M3P, 3M2P and 4M2P shown in table,

respectively. However, photolysis and reaction with OH radical could also contribute significantly to the atmospheric fate of these ketones during the day time. Indeed, the consumption of ketones by Cl atoms becomes more important in areas (marine area) with substantially high concentrations than the global concentration, which is about of $0.3-1 \times 10^5$ atoms cm^{-3} (Pszenny et al., 1993).

Table 6-8: Estimated atmospheric chemical lifetimes τ for the reactions of studied ketones with OH and Cl atoms.

Ketone	τ (hours)	
	τ_{OH}	τ_{Cl}
2M3P	41	265
3M2P	24	230
4M2P	13	207

The concentration of OH and Cl atoms used in the calculations are 2×10^6 molecule cm^{-3} , 1.0×10^4 molecule cm^{-3} , respectively. Rate coefficients of OH radical reaction: this work. Rate coefficient of Cl atoms reaction: this work.

From the products and mechanism analysis, this work indicates that the reaction of 2M3P/3M2P/4M2P with Cl atoms could contribute significantly to the formation of OVOC: acetaldehyde, acetone, propanal, 2-butanone and 2-methylpropanal in the atmosphere either in the presence of NO (polluted air like urban area) or in the absence of NO (clean air like remote area). Their photolysis, reaction with OH radical and reaction with NO_3 radical would be the important source of SOA, HO_2 and OH radical. In addition, the reaction of 2M3P/3M2P/4M2P with Cl atoms would also produce significant amount of HO_2 and OH radical, which are the most important trace gases in the troposphere (Davis et al., 2001). Furthermore, a quantity of CO is also expected to be produced from the Cl atoms reaction with 2M3P/3M2P/4M2P. Since CO is a relatively long-lived substance in the atmosphere, it can indirectly obviously impacts climate by increasing the lifetimes of methane and other short-lived greenhouse gases (GHGs) and increasing tropospheric ozone, as well as eventually oxidizing to CO_2 (Prather, 1996). In addition, the reaction of CO with OH radical also leads to impact on oxidation of SO_2 to sulfate (Shindell et al., 2006). And

sulfate has been recognized as an important precursor of SOA in the atmosphere.

6-6- Conclusion

To date, the atmospheric fates of 2M3P, 3M2P and 4M2P, the kinetic and products studies of their reaction with Cl atoms have been conducted in this work. With the relative method, the rate constants of Cl atoms with 2M3P, 3M2P and 4M2P were determined to be: 1.07 ± 0.26 , 1.21 ± 0.26 and 1.35 ± 0.27 , respectively (unit in $10^{-10} \text{ cm}^3 \text{ molecule}^{-1} \text{ s}^{-1}$). It confirms the slight deactivating effect of the C=O group to the CH_x group in the α position (Notario et al., 2000). By comparing the SAR results using the different calculation parameters, revised SAR calculation parameters are recommended: $k_{\text{prim}}=3.32$, $k_{\text{sec}}=8.34$ and $k_{\text{tert}}=6.09$ (units in $10^{-11} \text{ cm}^3 \text{ molecule}^{-1} \text{ s}^{-1}$), $F(-\text{CH}_3)=1.00$, $F(-\text{CH}_2-)=F(-\text{CH}<)=F(>\text{C}<)=0.8$, $F(>\text{CO})=0.037$, $F(-\text{CH}_2\text{C}(\text{O})\text{R})=1.17$, for the reaction of ketones with Cl atoms. Then, by combining the rate constants of acetone, n-butanone, 2-pentanone, 3-methyl-2-butanone, 2-hexanone, 3M2P, 4M2P, 3,3-dimethyl-2-butanone and 5-methyl-2-hexanone reaction with Cl atoms, the $k_{\text{R}}(\text{RC}(\text{O})\text{R}')$ are also recommended to estimate the reaction rate constants of other ketones with Cl atoms. Furthermore, the rate constants of acetone, 3,3-dimethyl-2-butanone, 2-butanone, 2-pentanone, 2-hexanone, 3-methyl-2-butanone, 4M2P, 5-methyl-2-hexanone reaction with Cl atoms were also utilized to determine the CH_x (x=1, 2,3) group rate coefficients ($k_{(\text{CH}_x)}$), which could be also used to estimate the other ketones reaction with Cl atoms.

The reaction of Cl atoms with saturated ketones is believed to proceed via H-abstraction from the CH_x group, which give the following products yields: acetone ($38.5 \pm 7.7\%$) + acetaldehyde ($77.5 \pm 12.1\%$), 2-butanone ($22.3 \pm 1.5\%$) + acetaldehyde ($75.1 \pm 9.8\%$) + propanal ($13.6 \pm 1.0\%$) and acetone ($25.9 \pm 2.5\%$) + 2-methylpropanal ($23.6 \pm 1.6\%$), respectively, for Cl atoms reaction with 2M3P, 3M2P and 4M2P in the presence of NO. Then, for the reaction of Cl atoms with 2M3P, 3M2P and 4M2P in the absence of NO, the same products were also found with the following yields: acetone ($39.7 \pm 5.5\%$) + acetaldehyde ($58.2 \pm 5.8\%$), 2-butanone ($18.2 \pm 2.4\%$) +

acetaldehyde ($40.3 \pm 1.7\%$) and acetone ($15.1 \pm 0.7\%$) + 2-methylpropanal ($18.2 \pm 0.9\%$), respectively. It indicates that the final products of ketones reaction with Cl atoms could be similar in clean and polluted areas.

Cl atoms are less specific in the sites of abstraction than OH, as discussed in the previously kinetic study. However, the activity of the different sites in ketone toward Cl still presents discrepancy. Because the mass m/z 135.01 ($((\text{CH}_3)_2\text{CHC}(\text{O})\text{C}(\text{O})\text{CH}_3 \cdot \text{H}^+$ cluster detected by PTR-ToF-MS) was identified in reaction of 4M2P+Cl without detection in the reaction of 2M3P/3M2P+Cl, this work suggests that only the $\cdot\text{C}$ group in β position to $\text{C}=\text{O}$ presents enough reactivity toward Cl_2 in the condition of $\text{O}_2 \gg \text{Cl}_2$. In the reaction of 2M3P with Cl atoms, this work also found that the partition ratio of $\text{CH}(\text{CH}_3)_2\text{CO} \cdot$ reactivity toward to Cl_2 vs $\text{CH}_3\text{CH}_2\text{CO} \cdot$ reactivity toward to O_2 is estimated to be 3:2. Furthermore, the possible mechanism pathways of the 2M3P, 3M2P and 4M2P reaction with Cl atoms in the presence of NO and in the absence of NO have been proposed in this work.

References

- Albaladejo, J., Notario, A., Cuevas, C. A., Jiménez, E., Cabañas, B., and Martínez, E.: Gas-phase chemistry of atmospheric Cl atoms: a PLP-RF kinetic study with a series of ketones, *Atmospheric Environment*, **37**, 455-463, [http://dx.doi.org/10.1016/S1352-2310\(02\)00921-4](http://dx.doi.org/10.1016/S1352-2310(02)00921-4), 2003.
- Alwe, H. D., Walawalkar, M., Sharma, A., Pushpa, K. K., Dhanya, S., and Naik, P. D.: Rate Coefficients for the Gas-Phase Reactions of Chlorine Atoms with Cyclic Ethers at 298 K, *International Journal of Chemical Kinetics*, **45**, 295-305, 10.1002/kin.20765, 2013.
- Arsene, C., Bougiatioti, A., Kanakidou, M., Bonsang, B., and Mihalopoulos, N.: Tropospheric OH and Cl levels deduced from non-methane hydrocarbon measurements in a marine site, *Atmospheric Chemistry and Physics*, **7**, 4661-4673, 2007.
- Aschmann, S. M., and Atkinson, R.: RATE CONSTANTS FOR THE GAS-PHASE REACTIONS OF ALKANES WITH CL ATOMS AT 296+/-2 K, *International Journal of Chemical Kinetics*, **27**, 613-622, 10.1002/kin.550270611, 1995.
- Atkinson, R., and Carter, W. P. L.: REACTIONS OF ALKOXY RADICALS UNDER ATMOSPHERIC CONDITIONS - THE RELATIVE IMPORTANCE OF DECOMPOSITION VERSUS REACTION WITH O-2, *J Atmos Chem*, **13**, 195-210, 10.1007/bf00115973, 1991.
- Atkinson, R., and Aschmann, S. M.: Products of the gas-phase OH radical-initiated reactions of 4-methyl-2-pentanone and 2,6-dimethyl-4-heptanone, *International Journal of Chemical Kinetics*, **27**, 261-275, 10.1002/kin.550270305, 1995.
- Atkinson, R., Baulch, D. L., Cox, R. A., Crowley, J. N., Hampson, R. F., Hynes, R. G., Jenkin, M. E., Rossi, M. J., Troe, J., and Subcommittee, I.: Evaluated kinetic and photochemical data for atmospheric chemistry: Volume II – gas phase reactions of organic species, *Atmos. Chem. Phys.*, **6**, 3625-4055, 10.5194/acp-6-3625-2006, 2006.
- Brauers, T., and Finlayson-Pitts, B. J.: Analysis of relative rate measurements, *International Journal of Chemical Kinetics*, **29**, 665-672, 10.1002/(SICI)1097-4601(1997)29:9<665::AID-KIN3>3.0.CO;2-S, 1997.
- Calvert, J. G., Derwent, R. G., Orlando, J. J., Tyndall, G. S., and J., W. T.: Mechanisms of

- Atmospheric Oxidation of the Alkanes, Oxford University Press, New York, 2008.
- Calvert, J. G., Mellouki, A., Orlando, J. J., Pilling, M. J., and J., W. T.: The Mechanisms of Atmospheric Oxidation of the Oxygenates, Oxford University Press, New York, 2011.
- Calvert;, J., Mellouki;, A., Orlando;, J., Pilling;, M., and Wallington;, T.: The mechanisms of atmospheric oxidation of the oxygenates, Oxford University Press, Oxford; New York, 2011.
- Calvert;, J. G., Derwent;, R. G., Orlando;, J. J., Tyndall;, G. S., and Wallington, T. J.: Mechanisms of Atmospheric Oxidation of the Alkanes, Oxford University Press, USA, 2008.
- Cuevas, C. A., Notario, A., Martinez, E., and Albaladejo, J.: A kinetic study of the reaction of Cl with a series of linear and ramified ketones as a function of temperature, Physical Chemistry Chemical Physics, 6, 2230-2236, 10.1039/B313587J, 2004.
- Davis, D., Nowak, J. B., Chen, G., Buhr, M., Arimoto, R., Hogan, A., Eisele, F., Mauldin, L., Tanner, D., Shetter, R., Lefer, B., and McMurry, P.: Unexpected high levels of NO observed at South Pole, Geophysical Research Letters, 28, 3625-3628, 10.1029/2000GL012584, 2001.
- Farrugia, L. N., Bejan, I., Smith, S. C., Medeiros, D. J., and Seakins, P. W.: Revised structure activity parameters derived from new rate coefficient determinations for the reactions of chlorine atoms with a series of seven ketones at 290 K and 1 atm, Chemical Physics Letters, 640, 87-93, <http://dx.doi.org/10.1016/j.cplett.2015.09.055>, 2015.
- Faxon, C. B., and Allen, D. T.: Chlorine chemistry in urban atmospheres: a review, Environmental Chemistry, 10, 221-233, <http://dx.doi.org/10.1071/EN13026>, 2013.
- Kaiser, E. W., and Wallington, T. J.: Rate Constants for the Reaction of Cl with a Series of C4 to C6 Ketones Using the Relative Rate Method, The Journal of Physical Chemistry A, 111, 10667-10670, 10.1021/jp075088i, 2007.
- Kaiser, E. W., Wallington, T. J., and Hurley, M. D.: Products and Mechanism of the Reaction of Cl with Butanone in N2/O2 Diluent at 297–526 K, The Journal of Physical Chemistry A, 113, 2424-2437, 10.1021/jp809169h, 2009.
- Kaiser, E. W., Wallington, T. J., and Hurley, M. D.: Products and Mechanism of the Reaction of Chlorine Atoms with 3-Pentanone in 700–950 Torr of N2/O2 Diluent at 297–515 K,

- The Journal of Physical Chemistry A, 114, 343-354, 10.1021/jp9083663, 2010.
- Müller, M., Mikoviny, T., Jud, W., D'Anna, B., and Wisthaler, A.: A new software tool for the analysis of high resolution PTR-TOF mass spectra, *Chemometrics and Intelligent Laboratory Systems*, 127, 158-165, <http://dx.doi.org/10.1016/j.chemolab.2013.06.011>, 2013.
- Mereau, R., Rayez, M. T., Caralp, F., and Rayez, J. C.: Isomerisation reactions of alkoxy radicals: theoretical study and structure-activity relationships, *Physical Chemistry Chemical Physics*, 5, 4828-4833, 10.1039/b307708j, 2003.
- Notario, A., Mellouki, A., and Le Bras, G.: Rate constants for the gas-phase reactions of chlorine atoms with a series of ketones, *International Journal of Chemical Kinetics*, 32, 62-66, 10.1002/(SICI)1097-4601(2000)32:1<62::AID-JCK7>3.0.CO;2-3, 2000.
- Prather, M. J.: Time scales in atmospheric chemistry: Theory, GWPs for CH₄ and CO, and runaway growth, *Geophysical Research Letters*, 23, 2597-2600, 10.1029/96GL02371, 1996.
- Pszenny, A. A. P., Keene, W. C., Jacob, D. J., Fan, S., Maben, J. R., Zetwo, M. P., Springer-Young, M., and Galloway, J. N.: Evidence of inorganic chlorine gases other than hydrogen chloride in marine surface air, *Geophysical Research Letters*, 20, 699-702, 10.1029/93GL00047, 1993.
- Shindell, D. T., Faluvegi, G., Stevenson, D. S., Krol, M. C., Emmons, L. K., Lamarque, J. F., Páron, G., Dentener, F. J., Ellingsen, K., Schultz, M. G., Wild, O., Amann, M., Atherton, C. S., Bergmann, D. J., Bey, I., Butler, T., Cofala, J., Collins, W. J., Derwent, R. G., Doherty, R. M., Drevet, J., Eskes, H. J., Fiore, A. M., Gauss, M., Hauglustaine, D. A., Horowitz, L. W., Isaksen, I. S. A., Lawrence, M. G., Montanaro, V., Müller, J. F., Pitari, G., Prather, M. J., Pyle, J. A., Rast, S., Rodriguez, J. M., Sanderson, M. G., Savage, N. H., Strahan, S. E., Sudo, K., Szopa, S., Unger, N., van Noije, T. P. C., and Zeng, G.: Multimodel simulations of carbon monoxide: Comparison with observations and projected near-future changes, *Journal of Geophysical Research: Atmospheres*, 111, n/a-n/a, 10.1029/2006JD007100, 2006.
- Sulbaek Andersen, M. P., Nielsen, O. J., Wallington, T. J., Hurley, M. D., and DeMore, W. B.: Atmospheric Chemistry of CF₃OCF₂CF₂H and CF₃OC(CF₃)₂H: Reaction with Cl

- Atoms and OH Radicals, Degradation Mechanism, Global Warming Potentials, and Empirical Relationship between $k(\text{OH})$ and $k(\text{Cl})$ for Organic Compounds, *The Journal of Physical Chemistry A*, 109, 3926-3934, 10.1021/jp044635m, 2005.
- Takahashi, K., Iwasaki, E., Matsumi, Y., and Wallington, T. J.: Pulsed Laser Photolysis Vacuum UV Laser-Induced Fluorescence Kinetic Study of the Gas-Phase Reactions of $\text{Cl}(2\text{P}_{3/2})$ Atoms with C3–C6 Ketones, *The Journal of Physical Chemistry A*, 111, 1271-1276, 10.1021/jp066410c, 2007.
- Taketani, F., Matsumi, Y., Wallington, T. J., and Hurley, M. D.: Kinetics of the gas phase reactions of chlorine atoms with a series of ketones, *Chemical Physics Letters*, 431, 257-260, 10.1016/j.cplett.2006.09.101, 2006.
- Thornton, J. A., Kercher, J. P., Riedel, T. P., Wagner, N. L., Cozic, J., Holloway, J. S., Dube, W. P., Wolfe, G. M., Quinn, P. K., Middlebrook, A. M., Alexander, B., and Brown, S. S.: A large atomic chlorine source inferred from mid-continental reactive nitrogen chemistry, *Nature*, 464, 271-274, 10.1038/nature08905, 2010.
- Tyndall, G. S., Wallington, T. J., and Ball, J. C.: FTIR Product Study of the Reactions $\text{CH}_3\text{O}_2 + \text{CH}_3\text{O}_2$ and $\text{CH}_3\text{O}_2 + \text{O}_3$, *The Journal of Physical Chemistry A*, 102, 2547-2554, 10.1021/jp972784h, 1998.
- Tyndall, G. S., Cox, R. A., Granier, C., Lesclaux, R., Moortgat, G. K., Pilling, M. J., Ravishankara, A. R., and Wallington, T. J.: Atmospheric chemistry of small organic peroxy radicals, *Journal of Geophysical Research: Atmospheres*, 106, 12157-12182, 10.1029/2000JD900746, 2001.
- Wingenter, O. W., Kubo, M. K., Blake, N. J., Smith, T. W., Blake, D. R., and Rowland, F. S.: Hydrocarbon and halocarbon measurements as photochemical and dynamical indicators of atmospheric hydroxyl, atomic chlorine, and vertical mixing obtained during Lagrangian flights, *Journal of Geophysical Research: Atmospheres*, 101, 4331-4340, 10.1029/95JD02457, 1996.

Chapter 7.

Conclusions and Perspectives

Chapter 7- Conclusions and Perspectives	248
References	252

Chapter 7- Conclusions and Perspectives

This final section will highlight the original contributions of this work and go through some recommendations and potential studies that could be a follow up of the work presented in this thesis. Several aspects of atmospheric chemistry have been investigated, including the ozonolysis of alkenes and OVOC (Chapter 3), photolysis of a ketone and its perfluorinated analogue (Chapter 4), the reaction of OH radical (Chapter 5) and Cl atom (Chapter 6) with three ketones. This work has employed four different simulation chambers (90 m³ outdoor simulation chamber-HELIOS, 7.3 m³ indoor simulation chamber-CSA, 3.4 m³ moveable simulation chamber-Moving Chamber and 200 L indoor simulation chamber) and several analytical techniques (including GC-FID, GC-MS, UHPLC-MS, FTIR, PTR-TOF-MS, SMPS-CPC, HCHO monitor, spectroradiometer). We have also used complementary experimental techniques such as pulsed laser photolysis-laser induced fluorescence (PLP-LIF) and UV-Visible absorption cell. These techniques and analytical tools have been described in Chapter 2. More precisely, kinetic and product branching ratios have been investigated and reported for the first time in HELIOS. All these investigations, their outcomes, and future recommendations are to be individually discussed here.

The first achievement to be highlighted in this summary is the successful characterization of a ICARE large outdoor simulation chamber - HELIOS. Successful experiments of the ozonolysis of isoprene, methacrolein (MACR) and methyl vinyl ketone (MVK) under ambient temperature and pressure (Chapter 3) confirmed the suitability of HELIOS for investigations under dark conditions. Isoprene is arguably the most abundant emitted non-methane hydrocarbon (NMHC) into the atmosphere, with estimates around 500-750 Tg y⁻¹ (Guenther et al., 2006; Zimmerman et al., 1988). MACR and MVK, account for a combined molar yield of >50% from the oxidation of isoprene, were the major constituents of first-generation carbonyl products in the oxidation of isoprene. In addition, MACR and MVK might also be released directly from the anthropogenic sources (Biesenthal and Shepson, 1997). Hence, more than

320 Tg y⁻¹ of MACR and MVK were estimated to be present in the atmosphere (Chen et al., 2008). Using HELIOS, the rate constants of O₃ reaction with isoprene was determined to be $k = (9.3 \pm 0.7)$ and $k = (11.3 \pm 1.7) \times 10^{-18} \text{ cm}^3 \text{ molecule}^{-1} \text{ s}^{-1}$ at 285 ± 2 K and 294 ± 2 K, respectively; MACR: $k = (7.1 \pm 0.6) \times 10^{-19} \text{ cm}^3 \text{ molecule}^{-1} \text{ s}^{-1}$ at 284.9 ± 0.9 K; MVK: $k = (4.5 \pm 0.1) \times 10^{-18} \text{ cm}^3 \text{ molecule}^{-1} \text{ s}^{-1}$ at 288.0 ± 1.8 K. The rate constant values determined in HELIOS matched well with the IUPAC recommendations. The OH radical and some stable products (HCHO, CO, HCOOH) formation yield produced from the ozonolysis of isoprene, MACR and MVK were also determined. In addition, in excess of isoprene and absence of cyclohexane, the SOA yield was $Y_{\text{SOA}} \approx 3.5 \pm 2.5 \%$, higher than that obtained during the experiments conducted in excess of ozone in both, without and with cyclohexane added in the ozonolysis of isoprene, $Y_{\text{SOA}} \approx 1.0 \pm 0.2 \%$ and $< 1\%$, respectively. Future work includes the study of the fate of the Criegee Intermediates (CI), formed from the ozonolysis of isoprene, either in HELIOS or a horizontal long-flow tube (3 m) and detected using home-made CIMS (Kukui et al., 2009). The chemistry of CIs is thought to play a central role in controlling the budgets of many tropospheric species including OH, organic acids, and SOA and play a pivotal role in shaping the composition of the Earth's lower atmosphere (Welz et al., 2014).

Furthermore, successful experiments of the photolysis of the perfluoro-ketone and its non-fluorinated analogue using natural irradiation confirmed the suitability of HELIOS to conduct photolysis studies in almost real atmospheric conditions (chapter 4). Perfluoro-2-methyl-3-pentanone (PF-2M3P) is an advanced heat transfer fluid with high dielectric strength and widely used in the industry, and 2-methyl-3-pentanone (2M3P) is the “parent” of PF-2M3P. The photolysis is expected to be their important decomposition pathway in the atmosphere as also encountered for numerous carbonyl compounds (Mu and Mellouki, 2000). Using HELIOS, the photolysis rates of PF-2M3P and 2M3P were determined to be $J = (1.1\text{-}3.8)$ and $J = (1.9\text{-}3.4) \times 10^{-6} \text{ s}^{-1}$ under the conditions used in this work. The photolysis rate of PF-2M3P obtained in this work is in good agreement with the literatures (D'Anna et

al., 2005; Taniguchi et al., 2003). By analogy to other (perfluoro)-ketone, the photolysis mechanism of PF-2M3P and 2M3P are proposed. Some different reaction pathways happened in the photolysis of 2M3P compared with PF-2M3P, and which need more investigation in experiment and modeling. The ozonolysis experiments of PF-2M3P and 2M3P indicate that both of them do not react with O₃, thus this process is negligible in the atmosphere.

Another achievement contribution to be noted is measurement of the rate coefficients and SAR improvement obtained for OH radical and Cl atom reactions with a series of branched ketones. Ketones play an important role in the chemistry of the atmosphere. They could be either emitted as primary pollutants from partial oxidation of hydrocarbons fuels, plant emission and escape from the factory or arise as secondary pollutants from the oxidation of VOCs (Mellouki et al., 2015). Given the limited number of reports on the chemistry of larger branched ketones, Chapter 5 and Chapter 6 aimed at addressing this and investigated further these compounds and their kinetics with OH radical and Cl atoms using 200L simulation chamber in Orleans, France. The current work dealt with three high branched ketones: 2M3P, 3-methyl-2-pentanone (3M2P) and 4-methyl-2-pentanone (4M2P) which are widely used as solvents or as intermediates for syntheses in the industry. As discussed in Chapter 5, the rate constants of OH radical reaction with 2M3P, 3M2P, 4M2P were determined to be $k = (3.5 \pm 0.5)$, (6.0 ± 0.2) and (11.0 ± 0.4) , respectively, unit in $10^{-12} \text{ cm}^3 \text{ molecule}^{-1} \text{ s}^{-1}$. In addition, the temperature dependence of 2M3P and 3M2P reaction with OH radical was also determined using PLP-LIF. As discussed in Chapter 6, the rate constants of Cl atom reaction with the 2M3P, 3M2P, 4M2P were determined to be $k = (1.07 \pm 0.26)$, (1.21 ± 0.26) , (1.35 ± 0.27) , respectively, unit in $10^{-10} \text{ cm}^3 \text{ molecule}^{-1} \text{ s}^{-1}$. The reactivity trends of -CH_x (1, 2, 3) in ketone toward OH radical and Cl atom obtained were similar to those previously reported by (Le Calvé et al., 1998) and stress the importance of obtaining such SARs. Furthermore, the products formation yields from the reaction of OH radical and Cl atom with studied ketones were also investigated using 7.3 m³ and 200 L simulation chamber. Hence, the

reaction mechanisms of OH radical and Cl atom reaction with studied ketones were proposed using experimental values and SAR simulation. In particular, from the products and mechanism analysis, this work indicates that the reaction of studied ketones with OH radical and Cl atom could contribute significantly to the removal of these OVOCs in the atmosphere either in the presence of NO (polluted air like urban area) or in the absence of NO (clean air like remote area). The photolysis, reaction with OH radical of these OVOC would be the important source of SOA, HO₂ and OH radical. In addition, the reaction of studied ketones with OH radical and Cl atom would also produce significant amounts of HO₂ and OH radicals. Future proposed work includes the study of photolysis of 2M3P, 3M2P, 4M2P and OH generation, which could be investigated either in HELIOS using natural irradiation or in the 7.3 m³ CSA using artificial lamps. The photolysis rate and mechanism should be considered in the future work.

References

- Biesenthal, T. A., and Shepson, P. B.: Observations of anthropogenic inputs of the isoprene oxidation products methyl vinyl ketone and methacrolein to the atmosphere, *Geophysical Research Letters*, 24, 1375-1378, 10.1029/97GL01337, 1997.
- Chen, Z. M., Wang, H. L., Zhu, L. H., Wang, C. X., Jie, C. Y., and Hua, W.: Aqueous-phase ozonolysis of methacrolein and methyl vinyl ketone: a potentially important source of atmospheric aqueous oxidants, *Atmospheric Chemistry and Physics*, 8, 2255-2265, 2008.
- D'Anna, B., Sellevåg, S. R., Wirtz, K., and Nielsen, C. J.: Photolysis Study of Perfluoro-2-methyl-3-pentanone under Natural Sunlight Conditions, *Environmental Science & Technology*, 39, 8708-8711, 10.1021/es048088u, 2005.
- Guenther, A., Karl, T., Harley, P., Wiedinmyer, C., Palmer, P. I., and Geron, C.: Estimates of global terrestrial isoprene emissions using MEGAN (Model of Emissions of Gases and Aerosols from Nature), *Atmos. Chem. Phys.*, 6, 3181-3210, 10.5194/acp-6-3181-2006, 2006.
- Kukui, A., Ancellet, G., and Le Bras, G.: Chemical ionisation mass spectrometer for measurements of OH and Peroxy radical concentrations in moderately polluted atmospheres, *Journal of Atmospheric Chemistry*, 61, 133-154, 10.1007/s10874-009-9130-9, 2009.
- Le Calvé S., Hitier, D., Le Bras, G., and Mellouki, A.: Kinetic Studies of OH Reactions with a Series of Ketones, *The Journal of Physical Chemistry A*, 102, 4579-4584, 10.1021/jp980848y, 1998.
- Mellouki, A., Wallington, T. J., and Chen, J.: Atmospheric Chemistry of Oxygenated Volatile Organic Compounds: Impacts on Air Quality and Climate, *Chemical reviews*, 115, 3984-4014, 10.1021/cr500549n, 2015.
- Mu, Y. J., and Mellouki, A.: The near-UV absorption cross sections for several ketones, *Journal of Photochemistry and Photobiology a-Chemistry*, 134, 31-36, 2000.
- Taniguchi, N., Wallington, T. J., Hurley, M. D., Guschin, A. G., Molina, L. T., and Molina, M. J.: Atmospheric Chemistry of C₂F₅C(O)CF(CF₃)₂: Photolysis and Reaction with Cl

Atoms, OH Radicals, and Ozone, *The Journal of Physical Chemistry A*, 107, 2674-2679, 10.1021/jp0220332, 2003.

Welz, O., Eskola, A. J., Sheps, L., Rotavera, B., Savee, J. D., Scheer, A. M., Osborn, D. L., Lowe, D., Murray Booth, A., Xiao, P., Anwar, H. K. M., Percival, C. J., Shallcross, D. E., and Taatjes, C. A.: Rate coefficients of C(1) and C(2) Criegee intermediate reactions with formic and acetic Acid near the collision limit: direct kinetics measurements and atmospheric implications, *Angewandte Chemie*, 53, 4547-4550, 10.1002/anie.201400964, 2014.

Zimmerman, P. R., Greenberg, J. P., and Westberg, C. E.: Measurements of atmospheric hydrocarbons and biogenic emission fluxes in the Amazon Boundary layer, *Journal of Geophysical Research: Atmospheres*, 93, 1407-1416, 10.1029/JD093iD02p01407, 1988.

Acknowledges

This work could never been performed without the collaboration friendship, guidance and support of many people in and outside ERA group in ICARE.

First and foremost, big thanks go to my supervisor and mentor Abdelwahid MELLOUKI for his constant support and dedication throughout my studies. I have learnt so much from your mentorship, guidance and willingness to support my endeavours professionally, out of scientific curiosity and in for my future career, and I am appreciating for all your patience and attention during these past four years. In addition, many thanks to V éronique DAELE for her friendly guidance during my time in ICARE. Her great assistance in my researches and life make everything goes easy and push me continually forward.

I came to ICARE with a limited experimental background and could not thank Mathieu CAZAUNAU enough for teaching me the rope. I really benefit a lot from co-working with him in the big simulation chamber (80 m³), he deserves the tutor in the first year of my studying in ICARE. In addition, I would like to thank very much to research engineers in ICARE, Mahmoud IDIR, Benoit GROSSELIN, Roland BENOIT, the guys with professional knowledge and rich experience. They show and taught me varied of the technique skills, like PLP-LIF, GC-MS, UHPLC-MS and API-Tof-MS, I thank their patience and tolerance of my ignorance.

From the bottom of my heart, I am really appreciating my brother Jinhe WANG for his introduction, without him, I do not even have the chance to start thesis in ICARE. Actually, Prof. Jianmin CHEN acted as a bridge between me and ICARE before I came to ICARE, I thanks his introduction and assistance. Dawei HU and Hui CHEN, you are also like brothers to me and you were both so kind enough to teach me some technique skills in the lab, e.g. PTR-Tof-MS and SMPS.

The work here is not mine alone and required the excellent and tireless efforts of many people during the lab studies, Stephanie DE PERSIS, Li ZHOU, Antonia ZOGKA, Warda AIT-HELAL, Joris LEGLISE, Thibault DESBOIS, thanks to them for making this thesis possible. Outside of the work place, I also thank Ravishankara AR. and Steven S. BROWN for their support of the CRDS for measuring NO₃ radical. And thanks Valery CATOIRE for his support of SPIRIT for measuring CO. In

addition, many thanks to the exchange master students between Fudan University and Shandong University and Orleans University to ICARE, especially Ashley VIANA, Min CAI, Lei LIU and Tong ZHAO, for their efforts in the data analysis and MCM simulation.

Furthermore, I am very happy to meet so many people in the lab and outside, Yuri Bedjanian, Alexandre KUKUI, Manolis N. ROMANIAS, Julien MORIN, Vanessa BROCCHI, Song ZHAO, Lin HE, Ouchen IBRAHIM. The communication with them expanded my knowledge. Also, thanks to the China Scholarship Council (CSC) for funding my PhD.

My family, immediate and extended, you have supported my interests and curiosity for so long and it really is impossible to communicate what wonderful people you are. My parents have always supported me to pursue what I decided even they do not understand what I am doing. Thank you for your love. And I have a great thanks to my sisters and brother; they have done and are doing my job to take care of my old parents. I can feel the heart of my family even I am 10 thousand km away. Finally, Xinying LIU- my wife, confident and collaborator - you constantly inspire me to excel. We fall in love for nine years and then we married last year, during the whole time, you always support me and give me the power to overcome obstacles to focus my interesting. Thank you for becoming part of this endeavour and seeing this moment!

Annex I: Uncertainty analysis.....	257
1- Linear least-squares fitting.....	257
2- Uncertainty analysis of Rate constant	258
2-1- Uncertainty analysis of decay rate k' (s^{-1}).....	258
2-2- Uncertainty analysis of Rate constant (AR method)	259
2-3- Uncertainty analysis of Rate constant (RR method)	260
2-4- Uncertainty analysis of product formation yield.....	261
Annex II: IR absorption cross sections.....	262
References.....	272

Annex I: Uncertainty analysis

The uncertainty can be expressed in a number of ways, which may be defined either by the absolute error Δx or relative error $(\Delta x)/x$. Generally, the uncertainty is quantified in terms of the standard deviation (SD), σ , the positive square root of variance, σ^2 . If the statistical probability distribution of the variable is known or can be assumed, it is possible to derive confidence limits to describe the region within which the true value of the variable may be found. For example, the 95% confidence limits for a one-dimensional variable belonging to a normal distribution are approximately $\pm 1\sigma$ from the average value x , which means that $x \pm \sigma$ will cover the true value in roughly 95% of cases. The assessment of uncertainties is important for the determination of appropriate design margins and for understanding how those uncertainties can be reduced.

1- Linear least-squares fitting

Representation of the relationship between x (independent) and y (dependent) variables by a linear least-squares fitting is a routine process in scientific, eg. decay rate (s^{-1}) is obtained from the linear least-squares fitting of $\ln(C_0/C_t)$ vs time interval (s), formation yield is obtained from the linear least-squares fitting of products formation concentration vs the consumed reactant concentration. Often the result parameters of a linear least-squares fitting, slope and y-intercept, can be related to fundamental physical quantities. It is therefore very important that the parameters accurately represent the data collected, and that uncertainties in the parameters are estimated and applied correctly.

Brauers and Finlayson-Pitts et al. (1997) has discussed the linear least-squares fitting of X_t and Y_t without forcing to zero has a number of variations, they indicated the 5 most common cases as:

Case 1: Case 1: X_t is the independent variable and all Y_t points have unit weight.

Case 2: X_t is the independent variable, Y_t has error $\delta_{Y(t)}$ and is weighted to the linear least-square fitting by $w_{(t)} = (1/\delta_{Y(t)})^2$

Case 3: Y_t is the independent variable and all X_t points have unit weight.

Case 4: Y_t is the independent variable, X_t has error $\delta_{X(t)}$ and is weighted to the linear least-square fitting by $w_{(t)} = (1/\delta_{X(t)})^2$

Case 5: X_t and Y_t have error $\delta_{X(t)}$ and $\delta_{Y(t)}$, respectively. Then, the linear least-square fitting which takes into account errors in both X_t and Y_t , and the weight assigned to each point is $w_{(t)} = 1 / (\delta_{Y(t)}^2 + b^2 \delta_{X(t)}^2)$

In order to assess whether there is any systematic bias in the calculated slopes associated with these 1-5 *Cases*, Brauers and Finlayson-Pitts et al. (1997) created a program based on DOSBOX to exam each type of least-square fitting (1-5 *Cases* above). Finally, their preferred method is that of Case 5 above, in which errors in both X_t and Y_t are taken into account. This gives a better estimate of the true value of the slope and intercept than a simple regression analysis which does not take into account uncertainties in both X_t and Y_t or only takes into account uncertainties in one of them. Brauers and Finlayson-Pitts et al. (1997) also found that the distribution around the expected value of Case 5 is narrower than Case 1-4, so that the frequency of “outliers” should be diminished.

In this work, **the program created by Brauers and Finlayson-Pitts et al. (1997) was used to perform the least-square fitting** by taking account of the errors in both X_t and Y_t , which given a more believable slope, SD of slope, intercept and SD of intercept.

2- Uncertainty analysis of Rate constant

2-1- Uncertainty analysis of decay rate k' (s^{-1})

In a typical experiment, a reaction mixture containing compound A and radical R is prepared ($A + R \rightarrow \text{products}$). During the reaction, the concentration of A decrease from the initial concentration $[A]_0$ to $[A]_t$ as a function of time t . Then the loss rate of

A as k_A' , can be calculated by least-square fitting of $\ln\left(\frac{[A]_0}{[A]_t}\right)$ as a function time t . It is therefore the errors in $\ln\left(\frac{[A]_0}{[A]_t}\right)$ and t are needed.

(i) If $Y_t = \ln\left(\frac{[A]_0}{[A]_t}\right)$, the **uncertainty in Y_t** at time t , $\delta_{Y(t)}$ can be obtained by equation:

$$\delta_{Y(t)} = \frac{\delta_A}{[A]_0} \left[1 + \frac{[A]_0^2}{[A]_t^2} \right]^2$$

where δ_A is the random error on measurement of $[A]$, was estimated by repeated injections of A (calibration). From this procedure, the $\delta_A = \text{SD } (\sigma)$ was calculated from the least-square fitting of concentration (calculated from the liquid volume, random error was estimate to be 5%) vs the instrument signal.

(ii) **uncertainty of time** did not expected.

Finally, k_A' and SD (σ) of k_A' were calculated by least-square fitting of $\ln\left(\frac{[A]_0}{[A]_t}\right)$ vs t using the program of Brauers and Finlayson-Pitts et al. (1997).

2-2- Uncertainty analysis of Rate constant (AR method)

For example isoprene reaction with O_3 , the loss of isoprene due to either its reaction with O_3 or the dilution (leakage and air consumption by the instruments):



Under the condition where $[O_3] \gg [\text{isoprene}]_0$, then

$$-\frac{d\ln([VOC])}{dt} = k_{\text{iso}}' = k_{\text{loss}}' + k_{\text{iso}}'[O_3]_0$$

Where the pseudo-first order rate constant, k_{iso} ($\text{s}^{-1} \text{ cm}^3 \text{ molecule}^{-1}$), was calculated from the linear fitting of $(k_{\text{iso}}' - k_{\text{loss}}')$ vs the initial concentration of O_3 , $[O_3]_0$.

(i) the **uncertainty of $(k_{\text{iso}}' - k_{\text{loss}}')$** was obtained from the errors of k_{iso}' and k_{loss}' using the standard methods of uncertainty propagation. For a general function, $f = ax - by$, with two independent variables, x and y , the uncertainty in f , Δf , can be

approximated as:

$$\Delta f = \sqrt{a^2 * \Delta x^2 + b^2 * \Delta y^2}$$

Where Δx and Δy are the uncertainty of x and y , respectively. In this work, the SD (1σ) were used as the errors of k_{iso} ' and k_{loss} ', which was calculated from the linear least-square fitting described from the Section 2-1-.

(ii) the **uncertainty of $[O_3]_0$** was estimated by repeated injections of A (calibration) and has explained in Section 2-1-.

Finally, rate constant k_{iso} ($s^{-1} \text{ cm}^3 \text{ molecule}^{-1}$), was calculated from the linear fitting of (k_{iso} ' - k_{loss} ') vs the $[O_3]_0$ by taking both errors.

2-3- Uncertainty analysis of Rate constant (RR method)

For example 2M3P reaction with OH radical, when propane was used as the reference, in a mixture in which both 2M3P and propane were removed by OH radical:



By following the simultaneous decrease in both 2M3P and propane, the rate constant ratio $v_{ratio} = \frac{k_{2M3P}}{k_{\text{propane}}}$ can be obtained.

Generally, the equation to obtain the rate constant ratio $\frac{k_{VOC}}{k_{\text{reference}}}$ was showing as follow:

$$\left\{ \ln\left(\frac{[VOC]_0}{[VOC]_t}\right) - k'_{\text{loss}} * t \right\} = \frac{k_{VOC}}{k_{\text{reference}}} * \left\{ \ln\left(\frac{[reference]_0}{[reference]_t}\right) - k'_{\text{loss}} * t \right\}$$

(i) In this work, the loss of 2M3P and propane without OH radical did not identified, so $v_{ratio} = \frac{k_{2M3P}}{k_{\text{propane}}}$ and its SD (σ_{ratio}) were calculated from the linear least-square fitting of $\ln\left(\frac{[isoprene]_0}{[isoprene]_t}\right)$ vs $\ln\left(\frac{[propane]_0}{[propane]_t}\right)$. Indeed, the errors (1σ) of $\ln\left(\frac{[isoprene]_0}{[isoprene]_t}\right)$ and $\ln\left(\frac{[propane]_0}{[propane]_t}\right)$ were calculated following the method described in

Section 2-1-.

(ii) Then the k_{2M3P} was calculated from the equation: $k_{2M3P} = k_{\text{propane}} * v_{\text{ratio}}$. For a general function, $f = x*y$, with two independent variables, x and y , the uncertainty in f , Δf , can be approximated as:

$$\Delta f = |f| \sqrt{\left(\frac{\Delta x}{\mu_x}\right)^2 + \left(\frac{\Delta y}{\mu_y}\right)^2}$$

Where Δx and Δy are the uncertainty of x and y , respectively. And the μ_x and μ_y are the average value of x and y , respectively. In this work, the SD (1σ) of v_{ratio} has been calculated in (i), and the k_{propane} is 20% extracted from Calvert et al. (2011) and IUPAC (2006).

(ii) Finally, **the average of k_{2M3P} , k_{av}** , from the different repeated experiment using different references was calculated using the weighted average equation as:

$k_{\text{av}} = (w_{\text{ref1}}k_{\text{ref1}} + w_{\text{ref2}}k_{\text{ref2}} + \dots) / (w_{\text{ref1}} + w_{\text{ref2}} + \dots)$, where $w_{\text{ref1}} = 1/\sigma_{\text{ref1}}$, etc.

The uncertainty, σ_{av} , is given by: $\sigma_{\text{av}} = (1/\sigma_{\text{ref1}} + 1/\sigma_{\text{ref2}} + \dots)^{-0.5}$

2-4- Uncertainty analysis of product formation yield

Normally, the product formation yield and its uncertainty (1σ) were calculated from the linear-least square fitting of product concentration $[\text{product}]_t$ vs the consumed reactant concentration $[\text{consumed reactant}]$ using the program of Brauers and Finlayson-Pitts et al. (1997). The uncertainty of $[\text{product}]$ and $[\text{consumed reactant}]$ were estimated by repeated injection of the compound (calibration) (see Section 2-1-).

The **final product formation yield and its uncertainty from different experiments** were calculated using **weighted average** explained in Section 2-3-.

Annex II: IR absorption cross sections

IR absorption cross sections σ (10^{-20} cm² molecule⁻¹) of perfluoro-2-methyl-3-pentanone (PF-2M3P), 2-methyl-3-pentanone (2M3P) measured in this work.

Wavenumber (cm-1)	σ		Wavenumber (cm-1)	σ		Wavenumber (cm-1)	σ	
	PF-2M3P	2M3P		PF-2M3P	2M3P		PF-2M3P	2M3P
715.5-749.5	0.00	N/A	1221.5	0.75	0.00	1823.5	0.02	0.00
750.5	0.02	0.00	1222.5	0.79	0.00	1824.5	0.02	0.00
751.5	0.03	0.00	1223.5	0.83	0.00	1825.5	0.02	0.00
752.5	0.03	0.00	1224.5	0.87	0.00	1826.5	0.02	0.00
753.5	0.04	0.00	1225.5	0.92	0.00	1827.5	0.02	0.00
754.5	0.05	0.00	1226.5	0.97	0.00	1828.5	0.02	0.00
755.5	0.07	0.00	1227.5	1.04	0.00	1829.5	0.02	0.00
756.5	0.08	0.00	1228.5	1.15	0.00	1830.5	0.02	0.00
757.5	0.09	0.00	1229.5	1.23	0.00	1831.5	0.02	0.00
758.5	0.10	0.00	1230.5	1.29	0.00	1832.5	0.02	0.00
759.5	0.10	0.00	1231.5	1.30	0.00	1833.5	0.01	0.00
760.5	0.11	0.00	1232.5	1.29	0.00	1834.5	0.01	0.00
761.5	0.10	0.00	1233.5	1.26	0.00	1835.5	0.01	0.00
762.5	0.09	0.00	1234.5	1.21	0.00	1836.5	0.01	0.00
763.5	0.08	0.00	1235.5	1.14	0.00	1837.5	0.02	0.00
764.5	0.07	0.00	1236.5	1.09	0.00	1838.5	0.01	0.00
765.5	0.06	0.00	1237.5	1.09	0.00	1839.5	0.01	0.00
766.5	0.05	0.00	1238.5	1.13	0.00	1840.5	0.01	0.00
767.5	0.03	0.00	1239.5	1.21	0.00	1841.5	0.01	0.00
768.5	0.03	0.00	1240.5	1.31	0.00	1842.5	0.02	0.00
769.5	0.02	0.00	1241.5	1.46	0.00	1843.5	0.02	0.00
770.5	0.02	0.00	1242.5	1.54	0.00	1844.5	0.01	0.00
771.5	0.02	0.00	1243.5	1.58	0.00	1845.5	0.02	0.00
772.5	0.02	0.00	1244.5	1.59	0.00	1846.5	0.01	0.00
773.5	0.01	0.00	1245.5	1.56	0.00	1847.5	0.01	0.00
774.5	0.01	0.00	1246.5	1.52	0.00	1848.5	0.02	0.00
775.5	0.01	0.00	1247.5	1.47	0.00	1849.5	0.01	0.00
776.5	0.01	0.00	1248.5	1.42	0.00	1850.5-2727.5	0.00	0.00
777.5	0.01	0.00	1249.5	1.39	0.00	2728.5	0.00	0.00
778.5	0.01	0.00	1250.5	1.38	0.00	2729.5	0.00	0.00
779.5	0.01	0.00	1251.5	1.39	0.00	2730.5	0.00	0.00
780.5	0.02	0.00	1252.5	1.41	0.00	2731.5	0.00	0.00
781.5	0.01	0.00	1253.5	1.45	0.00	2732.5	0.00	0.00
782.5	0.01	0.00	1254.5	1.50	0.00	2733.5	0.00	0.00

783.5	0.01	0.00	1255.5	1.58	0.00	2734.5	0.00	0.00
784.5	0.01	0.00	1256.5	1.63	0.00	2735.5	0.00	0.00
785.5	0.01	0.00	1257.5	1.70	0.00	2736.5	0.00	0.00
786.5	0.02	0.00	1258.5	1.77	0.00	2737.5	0.00	0.00
787.5	0.02	0.00	1259.5	1.83	0.00	2738.5	0.00	0.00
788.5	0.02	0.00	1260.5	1.87	0.00	2739.5	0.00	0.00
789.5	0.01	0.00	1261.5	1.89	0.00	2740.5	0.00	0.00
790.5	0.01	0.00	1262.5	1.92	0.00	2741.5	0.00	0.00
791.5	0.02	0.00	1263.5	1.93	0.00	2742.5	0.00	0.00
792.5	0.02	0.00	1264.5	1.93	0.00	2743.5	0.00	0.00
793.5	0.02	0.00	1265.5	1.94	0.00	2744.5	0.00	0.00
794.5	0.02	0.00	1266.5	1.95	0.00	2745.5	0.00	0.00
795.5	0.02	0.00	1267.5	1.95	0.00	2746.5	0.00	0.00
796.5	0.02	0.00	1268.5	1.96	0.00	2747.5	0.00	0.00
797.5	0.02	0.00	1269.5	1.93	0.00	2748.5	0.00	0.00
798.5	0.02	0.00	1270.5	1.87	0.00	2749.5	0.00	0.00
799.5	0.02	0.00	1271.5	1.72	0.00	2750.5	0.00	0.00
800.5	0.02	0.00	1272.5	1.48	0.00	2751.5	0.00	0.00
801.5	0.03	0.00	1273.5	1.25	0.00	2752.5	0.00	0.00
802.5	0.03	0.00	1274.5	1.06	0.00	2753.5	0.00	0.00
803.5	0.03	0.00	1275.5	0.91	0.00	2754.5	0.00	0.00
804.5	0.04	0.00	1276.5	0.79	0.00	2755.5	0.00	0.00
805.5	0.05	0.00	1277.5	0.70	0.00	2756.5	0.00	0.00
806.5	0.07	0.00	1278.5	0.62	0.00	2757.5	0.00	0.00
807.5	0.09	0.00	1279.5	0.57	0.00	2758.5	0.00	0.00
808.5	0.11	0.00	1280.5	0.52	0.00	2759.5	0.00	0.00
809.5	0.14	0.00	1281.5	0.49	0.00	2760.5	0.00	0.00
810.5	0.19	0.00	1282.5	0.46	0.00	2761.5	0.00	0.00
811.5	0.22	0.00	1283.5	0.45	0.00	2762.5	0.00	0.00
812.5	0.24	0.00	1284.5	0.44	0.00	2763.5	0.00	0.00
813.5	0.25	0.00	1285.5	0.45	0.00	2764.5	0.00	0.00
814.5	0.25	0.00	1286.5	0.45	0.01	2765.5	0.00	0.00
815.5	0.24	0.00	1287.5	0.46	0.01	2766.5	0.00	0.00
816.5	0.23	0.00	1288.5	0.47	0.01	2767.5	0.00	0.00
817.5	0.20	0.00	1289.5	0.49	0.00	2768.5	0.00	0.00
818.5	0.17	0.00	1290.5	0.51	0.01	2769.5	0.00	0.00
819.5	0.14	0.00	1291.5	0.53	0.01	2770.5	0.00	0.00
820.5	0.11	0.00	1292.5	0.57	0.01	2771.5	0.00	0.00
821.5	0.09	0.00	1293.5	0.61	0.01	2772.5	0.00	0.00
822.5	0.07	0.00	1294.5	0.67	0.01	2773.5	0.00	0.00
823.5	0.05	0.00	1295.5	0.79	0.01	2774.5	0.00	0.00
824.5	0.04	0.00	1296.5	0.90	0.01	2775.5	0.00	0.00
825.5	0.04	0.00	1297.5	1.03	0.01	2776.5	0.00	0.00
826.5	0.03	0.00	1298.5	1.17	0.01	2777.5	0.00	0.00

827.5	0.03	0.00	1299.5	1.32	0.01	2778.5	0.00	0.00
828.5	0.03	0.00	1300.5	1.46	0.01	2779.5	0.00	0.00
829.5	0.03	0.00	1301.5	1.58	0.01	2780.5	0.00	0.00
830.5	0.03	0.00	1302.5	1.66	0.01	2781.5	0.00	0.00
831.5	0.03	0.00	1303.5	1.72	0.01	2782.5	0.00	0.00
832.5	0.04	0.00	1304.5	1.75	0.01	2783.5	0.00	0.00
833.5	0.04	0.00	1305.5	1.74	0.01	2784.5	0.00	0.00
834.5	0.05	0.00	1306.5	1.69	0.01	2785.5	0.00	0.00
835.5	0.06	0.00	1307.5	1.62	0.01	2786.5	0.00	0.00
836.5	0.08	0.00	1308.5	1.50	0.01	2787.5	0.00	0.00
837.5	0.11	0.00	1309.5	1.24	0.01	2788.5	0.00	0.00
838.5	0.14	0.00	1310.5	1.06	0.01	2789.5	0.00	0.00
839.5	0.17	0.00	1311.5	0.88	0.01	2790.5	0.00	0.00
840.5	0.20	0.00	1312.5	0.72	0.01	2791.5	0.00	0.00
841.5	0.23	0.00	1313.5	0.58	0.01	2792.5	0.00	0.00
842.5	0.24	0.00	1314.5	0.47	0.01	2793.5	0.00	0.00
843.5	0.25	0.00	1315.5	0.39	0.01	2794.5	0.00	0.00
844.5	0.25	0.00	1316.5	0.34	0.01	2795.5	0.00	0.00
845.5	0.23	0.00	1317.5	0.31	0.01	2796.5	0.00	0.00
846.5	0.20	0.00	1318.5	0.28	0.01	2797.5	0.00	0.00
847.5	0.17	0.00	1319.5	0.27	0.01	2798.5	0.00	0.00
848.5	0.14	0.00	1320.5	0.25	0.01	2799.5	0.00	0.00
849.5	0.10	0.00	1321.5	0.24	0.01	2800.5	0.00	0.00
850.5	0.06	0.00	1322.5	0.23	0.01	2801.5	0.00	0.00
851.5	0.05	0.00	1323.5	0.23	0.01	2802.5	0.00	0.00
852.5	0.04	0.00	1324.5	0.22	0.01	2803.5	0.00	0.00
853.5	0.04	0.00	1325.5	0.22	0.01	2804.5	0.00	0.00
854.5	0.03	0.00	1326.5	0.22	0.01	2805.5	0.00	0.00
855.5	0.03	0.00	1327.5	0.22	0.02	2806.5	0.00	0.00
856.5	0.03	0.00	1328.5	0.22	0.02	2807.5	0.00	0.00
857.5	0.03	0.00	1329.5	0.22	0.02	2808.5	0.00	0.00
858.5	0.02	0.00	1330.5	0.22	0.02	2809.5	0.00	0.00
859.5	0.02	0.00	1331.5	0.21	0.02	2810.5	0.00	0.00
860.5	0.02	0.00	1332.5	0.21	0.02	2811.5	0.00	0.01
861.5	0.02	0.00	1333.5	0.20	0.02	2812.5	0.00	0.01
862.5	0.02	0.00	1334.5	0.19	0.02	2813.5	0.00	0.01
863.5	0.02	0.00	1335.5	0.18	0.02	2814.5	0.00	0.01
864.5	0.02	0.00	1336.5	0.17	0.03	2815.5	0.00	0.01
865.5	0.02	0.00	1337.5	0.15	0.03	2816.5	0.00	0.01
866.5	0.02	0.00	1338.5	0.15	0.03	2817.5	0.00	0.01
867.5	0.02	0.00	1339.5	0.14	0.03	2818.5	0.00	0.01
868.5	0.02	0.00	1340.5	0.14	0.03	2819.5	0.00	0.01
869.5	0.02	0.00	1341.5	0.12	0.03	2820.5	0.00	0.01
870.5-940.5	0.00	0.00	1342.5	0.12	0.04	2821.5	0.00	0.01

941.5	0.00	0.01	1343.5	0.11	0.04	2822.5	0.00	0.01
942.5	0.00	0.01	1344.5	0.10	0.04	2823.5	0.00	0.01
943.5	0.00	0.01	1345.5	0.10	0.04	2824.5	0.00	0.01
944.5	0.00	0.01	1346.5	0.09	0.04	2825.5	0.00	0.01
945.5	0.00	0.01	1347.5	0.09	0.05	2826.5	0.00	0.01
946.5	0.00	0.01	1348.5	0.08	0.05	2827.5	0.00	0.01
947.5	0.00	0.01	1349.5	0.08	0.05	2828.5	0.00	0.01
948.5	0.00	0.02	1350.5	0.08	0.05	2829.5	0.00	0.01
949.5	0.00	0.02	1351.5	0.08	0.05	2830.5	0.00	0.01
950.5	0.00	0.02	1352.5	0.08	0.05	2831.5	0.00	0.01
951.5	0.01	0.02	1353.5	0.09	0.05	2832.5	0.00	0.01
952.5	0.01	0.02	1354.5	0.09	0.05	2833.5	0.00	0.01
953.5	0.01	0.02	1355.5	0.10	0.05	2834.5	0.00	0.01
954.5	0.01	0.02	1356.5	0.11	0.05	2835.5	0.00	0.01
955.5	0.01	0.02	1357.5	0.11	0.05	2836.5	0.00	0.01
956.5	0.01	0.02	1358.5	0.12	0.05	2837.5	0.00	0.01
957.5	0.01	0.02	1359.5	0.13	0.05	2838.5	0.00	0.01
958.5	0.01	0.03	1360.5	0.13	0.05	2839.5	0.00	0.01
959.5	0.02	0.03	1361.5	0.14	0.05	2840.5	0.00	0.01
960.5	0.02	0.03	1362.5	0.14	0.06	2841.5	0.00	0.01
961.5	0.02	0.03	1363.5	0.14	0.05	2842.5	0.00	0.01
962.5	0.02	0.03	1364.5	0.13	0.05	2843.5	0.00	0.01
963.5	0.02	0.03	1365.5	0.12	0.05	2844.5	0.00	0.01
964.5	0.03	0.03	1366.5	0.11	0.05	2845.5	0.00	0.01
965.5	0.03	0.04	1367.5	0.10	0.05	2846.5	0.00	0.01
966.5	0.04	0.04	1368.5	0.09	0.05	2847.5	0.00	0.01
967.5	0.04	0.04	1369.5	0.08	0.05	2848.5	0.00	0.01
968.5	0.05	0.04	1370.5	0.07	0.05	2849.5	0.00	0.01
969.5	0.06	0.04	1371.5	0.06	0.05	2850.5	0.00	0.01
970.5	0.07	0.05	1372.5	0.05	0.05	2851.5	0.00	0.01
971.5	0.09	0.05	1373.5	0.05	0.05	2852.5	0.00	0.01
972.5	0.10	0.05	1374.5	0.05	0.05	2853.5	0.00	0.01
973.5	0.11	0.05	1375.5	0.05	0.05	2854.5	0.00	0.01
974.5	0.12	0.05	1376.5	0.04	0.05	2855.5	0.00	0.01
975.5	0.13	0.05	1377.5	0.04	0.06	2856.5	0.00	0.01
976.5	0.14	0.05	1378.5	0.04	0.06	2857.5	0.00	0.01
977.5	0.16	0.05	1379.5	0.04	0.06	2858.5	0.00	0.01
978.5	0.17	0.05	1380.5	0.04	0.06	2859.5	0.00	0.01
979.5	0.19	0.05	1381.5	0.03	0.07	2860.5	0.00	0.01
980.5	0.22	0.06	1382.5	0.03	0.06	2861.5	0.00	0.01
981.5	0.24	0.05	1383.5	0.03	0.07	2862.5	0.00	0.01
982.5	0.27	0.05	1384.5	0.03	0.07	2863.5	0.00	0.02
983.5	0.29	0.05	1385.5	0.03	0.07	2864.5	0.00	0.02
984.5	0.31	0.05	1386.5	0.03	0.07	2865.5	0.00	0.02

985.5	0.32	0.05	1387.5	0.03	0.07	2866.5	0.00	0.02
986.5	0.31	0.05	1388.5	0.03	0.07	2867.5	0.00	0.02
987.5	0.30	0.04	1389.5	0.03	0.06	2868.5	0.00	0.02
988.5	0.27	0.04	1390.5	0.03	0.06	2869.5	0.00	0.03
989.5	0.24	0.04	1391.5	0.03	0.06	2870.5	0.00	0.03
990.5	0.20	0.03	1392.5	0.03	0.06	2871.5	0.00	0.03
991.5	0.17	0.03	1393.5	0.03	0.05	2872.5	0.00	0.04
992.5	0.14	0.03	1394.5	0.02	0.06	2873.5	0.00	0.04
993.5	0.11	0.03	1395.5	0.03	0.05	2874.5	0.00	0.05
994.5	0.10	0.02	1396.5	0.03	0.05	2875.5	0.00	0.05
995.5	0.08	0.02	1397.5	0.03	0.04	2876.5	0.00	0.06
996.5	0.08	0.02	1398.5	0.03	0.03	2877.5	0.00	0.06
997.5	0.07	0.02	1399.5	0.02	0.03	2878.5	0.00	0.07
998.5	0.07	0.02	1400.5	0.00	0.03	2879.5	0.00	0.07
999.5	0.07	0.01	1401.5	0.00	0.02	2880.5	0.00	0.08
1000.5	0.06	0.01	1402.5	0.00	0.02	2881.5	0.00	0.08
1001.5	0.06	0.01	1403.5	0.00	0.02	2882.5	0.00	0.09
1002.5	0.06	0.01	1404.5	0.00	0.02	2883.5	0.00	0.09
1003.5	0.06	0.01	1405.5	0.00	0.02	2884.5	0.00	0.09
1004.5	0.05	0.02	1406.5	0.00	0.02	2885.5	0.00	0.10
1005.5	0.05	0.02	1407.5	0.00	0.02	2886.5	0.00	0.10
1006.5	0.05	0.02	1408.5	0.00	0.02	2887.5	0.00	0.10
1007.5	0.05	0.02	1409.5	0.00	0.02	2888.5	0.00	0.10
1008.5	0.04	0.02	1410.5	0.00	0.02	2889.5	0.00	0.10
1009.5	0.04	0.02	1411.5	0.00	0.02	2890.5	0.00	0.11
1010.5	0.04	0.03	1412.5	0.00	0.02	2891.5	0.00	0.11
1011.5	0.05	0.03	1413.5	0.00	0.02	2892.5	0.00	0.11
1012.5	0.05	0.04	1414.5	0.00	0.02	2893.5	0.00	0.11
1013.5	0.06	0.04	1415.5	0.00	0.02	2894.5	0.00	0.11
1014.5	0.07	0.04	1416.5	0.00	0.03	2895.5	0.00	0.11
1015.5	0.08	0.04	1417.5	0.00	0.02	2896.5	0.00	0.11
1016.5	0.09	0.04	1418.5	0.00	0.02	2897.5	0.00	0.11
1017.5	0.12	0.05	1419.5	0.00	0.03	2898.5	0.00	0.11
1018.5	0.15	0.05	1420.5	0.00	0.03	2899.5	0.00	0.11
1019.5	0.18	0.05	1421.5	0.00	0.03	2900.5	0.00	0.11
1020.5	0.22	0.05	1422.5	0.00	0.03	2901.5	0.00	0.11
1021.5	0.26	0.05	1423.5	0.00	0.03	2902.5	0.00	0.10
1022.5	0.29	0.05	1424.5	0.00	0.03	2903.5	0.00	0.10
1023.5	0.32	0.05	1425.5	0.00	0.02	2904.5	0.00	0.10
1024.5	0.33	0.05	1426.5	0.00	0.02	2905.5	0.00	0.10
1025.5	0.33	0.05	1427.5	0.00	0.02	2906.5	0.00	0.10
1026.5	0.31	0.05	1428.5	0.00	0.02	2907.5	0.00	0.11
1027.5	0.28	0.05	1429.5	0.00	0.02	2908.5	0.00	0.11
1028.5	0.24	0.05	1430.5	0.00	0.02	2909.5	0.00	0.11

1029.5	0.20	0.04	1431.5	0.00	0.02	2910.5	0.00	0.11
1030.5	0.16	0.04	1432.5	0.00	0.02	2911.5	0.00	0.11
1031.5	0.13	0.04	1433.5	0.00	0.02	2912.5	0.00	0.11
1032.5	0.11	0.03	1434.5	0.00	0.03	2913.5	0.00	0.11
1033.5	0.10	0.03	1435.5	0.00	0.01	2914.5	0.00	0.11
1034.5	0.10	0.03	1436.5	0.00	0.02	2915.5	0.00	0.11
1035.5	0.10	0.02	1437.5	0.00	0.03	2916.5	0.00	0.10
1036.5	0.10	0.02	1438.5	0.00	0.03	2917.5	0.00	0.10
1037.5	0.10	0.02	1439.5	0.00	0.03	2918.5	0.00	0.10
1038.5	0.10	0.02	1440.5	0.00	0.02	2919.5	0.00	0.10
1039.5	0.09	0.02	1441.5	0.00	0.03	2920.5	0.00	0.10
1040.5	0.08	0.01	1442.5	0.00	0.03	2921.5	0.00	0.10
1041.5	0.06	0.01	1443.5	0.00	0.03	2922.5	0.00	0.10
1042.5	0.05	0.01	1444.5	0.00	0.03	2923.5	0.00	0.10
1043.5	0.04	0.01	1445.5	0.00	0.03	2924.5	0.00	0.10
1044.5	0.03	0.01	1446.5	0.00	0.03	2925.5	0.00	0.10
1045.5	0.03	0.01	1447.5	0.00	0.04	2926.5	0.00	0.09
1046.5	0.03	0.01	1448.5	0.00	0.04	2927.5	0.00	0.09
1047.5	0.03	0.01	1449.5	0.00	0.04	2928.5	0.00	0.09
1048.5	0.03	0.01	1450.5	0.00	0.04	2929.5	0.00	0.09
1049.5	0.02	0.01	1451.5	0.00	0.04	2930.5	0.00	0.09
1050.5	0.00	0.01	1452.5	0.00	0.05	2931.5	0.00	0.09
1051.5	0.00	0.01	1453.5	0.00	0.05	2932.5	0.00	0.09
1052.5	0.00	0.01	1454.5	0.00	0.06	2933.5	0.00	0.09
1053.5	0.00	0.01	1455.5	0.00	0.06	2934.5	0.00	0.09
1054.5	0.00	0.01	1456.5	0.00	0.05	2935.5	0.00	0.10
1055.5	0.00	0.01	1457.5	0.00	0.07	2936.5	0.00	0.10
1056.5	0.00	0.01	1458.5	0.00	0.07	2937.5	0.00	0.10
1057.5	0.00	0.01	1459.5	0.00	0.07	2938.5	0.00	0.11
1058.5	0.00	0.01	1460.5	0.00	0.07	2939.5	0.00	0.12
1059.5	0.00	0.01	1461.5	0.00	0.08	2940.5	0.00	0.12
1060.5	0.00	0.01	1462.5	0.00	0.08	2941.5	0.00	0.13
1061.5	0.00	0.01	1463.5	0.00	0.08	2942.5	0.00	0.14
1062.5	0.00	0.01	1464.5	0.00	0.09	2943.5	0.00	0.14
1063.5	0.00	0.01	1465.5	0.00	0.09	2944.5	0.00	0.15
1064.5	0.00	0.01	1466.5	0.00	0.10	2945.5	0.00	0.15
1065.5	0.00	0.01	1467.5	0.00	0.10	2946.5	0.00	0.15
1066.5	0.00	0.01	1468.5	0.00	0.10	2947.5	0.00	0.14
1067.5	0.00	0.01	1469.5	0.00	0.10	2948.5	0.00	0.15
1068.5	0.00	0.01	1470.5	0.00	0.10	2949.5	0.00	0.15
1069.5	0.00	0.01	1471.5	0.00	0.10	2950.5	0.00	0.15
1070.5	0.00	0.01	1472.5	0.00	0.10	2951.5	0.00	0.15
1071.5	0.00	0.01	1473.5	0.00	0.10	2952.5	0.00	0.14
1072.5	0.00	0.01	1474.5	0.00	0.10	2953.5	0.00	0.14

1073.5	0.00	0.01	1475.5	0.00	0.09	2954.5	0.00	0.14
1074.5	0.00	0.01	1476.5	0.00	0.08	2955.5	0.00	0.14
1075.5	0.00	0.01	1477.5	0.00	0.07	2956.5	0.00	0.14
1076.5	0.00	0.01	1478.5	0.00	0.07	2957.5	0.00	0.14
1077.5	0.00	0.01	1479.5	0.00	0.07	2958.5	0.00	0.14
1078.5	0.00	0.01	1480.5	0.00	0.07	2959.5	0.00	0.13
1079.5	0.00	0.01	1481.5	0.00	0.07	2960.5	0.00	0.13
1080.5	0.00	0.01	1482.5	0.00	0.06	2961.5	0.00	0.13
1081.5	0.00	0.01	1483.5	0.00	0.05	2962.5	0.00	0.14
1082.5	0.00	0.02	1484.5	0.00	0.04	2963.5	0.00	0.14
1083.5	0.00	0.02	1485.5	0.00	0.04	2964.5	0.00	0.15
1084.5	0.00	0.02	1486.5	0.00	0.04	2965.5	0.00	0.16
1085.5	0.00	0.02	1487.5	0.00	0.04	2966.5	0.00	0.17
1086.5	0.00	0.03	1488.5	0.00	0.04	2967.5	0.00	0.19
1087.5	0.00	0.03	1489.5	0.00	0.03	2968.5	0.00	0.22
1088.5	0.00	0.03	1490.5	0.00	0.02	2969.5	0.00	0.23
1089.5	0.00	0.04	1491.5	0.00	0.02	2970.5	0.00	0.25
1090.5	0.00	0.05	1492.5	0.00	0.02	2971.5	0.00	0.26
1091.5	0.00	0.05	1493.5	0.00	0.01	2972.5	0.00	0.27
1092.5	0.00	0.06	1494.5	0.00	0.01	2973.5	0.00	0.28
1093.5	0.00	0.07	1495.5	0.00	0.01	2974.5	0.00	0.29
1094.5	0.00	0.08	1496.5	0.00	0.01	2975.5	0.00	0.30
1095.5	0.00	0.08	1497.5	0.00	0.01	2976.5	0.00	0.31
1096.5	0.00	0.09	1498.5	0.00	0.01	2977.5	0.00	0.32
1097.5	0.00	0.09	1499.5	0.00	0.01	2978.5	0.00	0.33
1098.5	0.00	0.09	1500.5-1700.5	0.00	0.00	2979.5	0.00	0.33
1099.5	0.00	0.10	1701.5	0.00	0.03	2980.5	0.00	0.33
1100.5	0.00	0.10	1702.5	0.00	0.03	2981.5	0.00	0.33
1101.5	0.03	0.10	1703.5	0.00	0.03	2982.5	0.00	0.33
1102.5	0.03	0.10	1704.5	0.00	0.04	2983.5	0.00	0.33
1103.5	0.03	0.10	1705.5	0.00	0.04	2984.5	0.00	0.31
1104.5	0.03	0.10	1706.5	0.00	0.04	2985.5	0.00	0.30
1105.5	0.03	0.11	1707.5	0.00	0.04	2986.5	0.00	0.29
1106.5	0.03	0.11	1708.5	0.00	0.05	2987.5	0.00	0.27
1107.5	0.04	0.11	1709.5	0.00	0.06	2988.5	0.00	0.25
1108.5	0.04	0.10	1710.5	0.00	0.06	2989.5	0.00	0.23
1109.5	0.04	0.10	1711.5	0.00	0.07	2990.5	0.00	0.21
1110.5	0.04	0.09	1712.5	0.00	0.08	2991.5	0.00	0.20
1111.5	0.04	0.08	1713.5	0.00	0.10	2992.5	0.00	0.18
1112.5	0.04	0.08	1714.5	0.00	0.11	2993.5	0.00	0.17
1113.5	0.04	0.07	1715.5	0.00	0.12	2994.5	0.00	0.16
1114.5	0.04	0.07	1716.5	0.00	0.12	2995.5	0.00	0.14
1115.5	0.05	0.06	1717.5	0.00	0.14	2996.5	0.00	0.12
1116.5	0.05	0.06	1718.5	0.00	0.16	2997.5	0.00	0.11

1117.5	0.05	0.05	1719.5	0.00	0.17	2998.5	0.00	0.10
1118.5	0.05	0.05	1720.5	0.00	0.19	2999.5	0.00	0.09
1119.5	0.05	0.05	1721.5	0.00	0.20	3000.5	0.00	0.08
1120.5	0.06	0.04	1722.5	0.00	0.21	3001.5	0.00	0.07
1121.5	0.07	0.04	1723.5	0.00	0.22	3002.5	0.00	0.06
1122.5	0.07	0.04	1724.5	0.00	0.23	3003.5	0.00	0.06
1123.5	0.08	0.04	1725.5	0.00	0.25	3004.5	0.00	0.05
1124.5	0.09	0.03	1726.5	0.00	0.26	3005.5	0.00	0.05
1125.5	0.10	0.03	1727.5	0.00	0.27	3006.5	0.00	0.04
1126.5	0.12	0.03	1728.5	0.00	0.28	3007.5	0.00	0.04
1127.5	0.14	0.03	1729.5	0.00	0.29	3008.5	0.00	0.03
1128.5	0.17	0.03	1730.5	0.00	0.29	3009.5	0.00	0.03
1129.5	0.20	0.03	1731.5	0.00	0.29	3010.5	0.00	0.02
1130.5	0.24	0.03	1732.5	0.00	0.29	3011.5	0.00	0.02
1131.5	0.28	0.02	1733.5	0.00	0.28	3012.5	0.00	0.02
1132.5	0.32	0.02	1734.5	0.00	0.28	3013.5	0.00	0.02
1133.5	0.38	0.02	1735.5	0.00	0.27	3014.5	0.00	0.02
1134.5	0.41	0.02	1736.5	0.00	0.26	3015.5	0.00	0.02
1135.5	0.42	0.02	1737.5	0.00	0.25	3016.5	0.00	0.01
1136.5	0.42	0.02	1738.5	0.00	0.23	3017.5	0.00	0.01
1137.5	0.40	0.02	1739.5	0.00	0.22	3018.5	0.00	0.01
1138.5	0.38	0.02	1740.5	0.00	0.20	3019.5	0.00	0.01
1139.5	0.34	0.02	1741.5	0.00	0.19	3020.5	0.00	0.01
1140.5	0.29	0.02	1742.5	0.00	0.18	3021.5	0.00	0.01
1141.5	0.25	0.02	1743.5	0.00	0.16	3022.5	0.00	0.01
1142.5	0.20	0.01	1744.5	0.00	0.14	3023.5	0.00	0.01
1143.5	0.17	0.01	1745.5	0.00	0.13	3024.5	0.00	0.01
1144.5	0.15	0.01	1746.5	0.00	0.12	3025.5	0.00	0.01
1145.5	0.13	0.01	1747.5	0.00	0.11	3026.5	0.00	0.01
1146.5	0.12	0.01	1748.5	0.00	0.10	3027.5	0.00	0.01
1147.5	0.11	0.01	1749.5	0.00	0.08	3028.5	0.00	0.01
1148.5	0.11	0.01	1750.5	0.00	0.07	3029.5	0.00	0.01
1149.5	0.11	0.01	1751.5	0.02	0.07	3030.5	0.00	0.01
1150.5	0.11	0.01	1752.5	0.03	0.06	3031.5	0.00	0.01
1151.5	0.11	0.01	1753.5	0.02	0.05	3032.5	0.00	0.01
1152.5	0.11	0.01	1754.5	0.02	0.04	3033.5	0.00	0.01
1153.5	0.12	0.01	1755.5	0.02	0.03	3034.5	0.00	0.01
1154.5	0.12	0.01	1756.5	0.02	0.03	3035.5	0.00	0.00
1155.5	0.13	0.01	1757.5	0.02	0.03	3036.5	0.00	0.00
1156.5	0.15	0.01	1758.5	0.02	0.03	3037.5	0.00	0.00
1157.5	0.16	0.01	1759.5	0.02	0.02	3038.5	0.00	0.00
1158.5	0.18	0.01	1760.5	0.02	0.02	3039.5	0.00	0.00
1159.5	0.21	0.01	1761.5	0.02	0.02	3040.5	0.00	0.00
1160.5	0.25	0.01	1762.5	0.02	0.02	3041.5	0.00	0.00

1161.5	0.28	0.01	1763.5	0.03	0.02	3042.5	0.00	0.00
1162.5	0.32	0.01	1764.5	0.03	0.01	3043.5	0.00	0.00
1163.5	0.36	0.01	1765.5	0.03	0.02	3044.5	0.00	0.00
1164.5	0.41	0.01	1766.5	0.03	0.02	3045.5	0.00	0.00
1165.5	0.45	0.01	1767.5	0.04	0.01	3046.5	0.00	0.00
1166.5	0.50	0.01	1768.5	0.04	0.01	3047.5	0.00	0.00
1167.5	0.55	0.01	1769.5	0.05	0.01	3048.5	0.00	0.00
1168.5	0.60	0.01	1770.5	0.05	0.00	3049.5	0.00	0.00
1169.5	0.64	0.01	1771.5	0.06	0.00	3050.5	0.00	0.00
1170.5	0.69	0.01	1772.5	0.07	0.00	3051.5	0.00	0.00
1171.5	0.74	0.02	1773.5	0.09	0.00	3052.5	0.00	0.00
1172.5	0.78	0.02	1774.5	0.11	0.00	3053.5	0.00	0.00
1173.5	0.82	0.02	1775.5	0.13	0.00	3054.5	0.00	0.00
1174.5	0.85	0.02	1776.5	0.15	0.00	3055.5	0.00	0.00
1175.5	0.86	0.02	1777.5	0.18	0.00	3056.5	0.00	0.00
1176.5	0.86	0.02	1778.5	0.21	0.00	3057.5	0.00	0.00
1177.5	0.83	0.02	1779.5	0.24	0.00	3058.5	0.00	0.00
1178.5	0.75	0.02	1780.5	0.27	0.00	3059.5	0.00	0.00
1179.5	0.64	0.02	1781.5	0.31	0.00	3060.5	0.00	0.00
1180.5	0.55	0.02	1782.5	0.32	0.00	3061.5	0.00	0.00
1181.5	0.48	0.02	1783.5	0.32	0.00	3062.5	0.00	0.00
1182.5	0.43	0.02	1784.5	0.33	0.00	3063.5	0.00	0.00
1183.5	0.38	0.02	1785.5	0.32	0.00	3064.5	0.00	0.00
1184.5	0.35	0.02	1786.5	0.31	0.00	3065.5	0.00	0.00
1185.5	0.34	0.02	1787.5	0.28	0.00	3066.5	0.00	0.00
1186.5	0.36	0.02	1788.5	0.25	0.00	3067.5	0.00	0.00
1187.5	0.40	0.02	1789.5	0.22	0.00	3068.5	0.00	0.00
1188.5	0.44	0.02	1790.5	0.19	0.00	3069.5	0.00	0.00
1189.5	0.47	0.02	1791.5	0.16	0.00	3070.5	0.00	0.00
1190.5	0.50	0.02	1792.5	0.14	0.00	3071.5	0.00	0.00
1191.5	0.50	0.02	1793.5	0.10	0.00	3072.5	0.00	0.00
1192.5	0.50	0.01	1794.5	0.08	0.00	3073.5	0.00	0.00
1193.5	0.48	0.01	1795.5	0.07	0.00	3074.5	0.00	0.00
1194.5	0.46	0.01	1796.5	0.06	0.00	3075.5	0.00	0.00
1195.5	0.43	0.01	1797.5	0.04	0.00	3076.5	0.00	0.00
1196.5	0.40	0.01	1798.5	0.04	0.00	3077.5	0.00	0.00
1197.5	0.38	0.01	1799.5	0.04	0.00	3078.5	0.00	0.00
1198.5	0.36	0.01	1800.5	0.04	0.00	3079.5	0.00	0.00
1199.5	0.35	0.01	1801.5	0.03	0.00	3080.5	0.00	0.00
1200.5	0.35	0.01	1802.5	0.03	0.00	3081.5	0.00	0.00
1201.5	0.36	0.01	1803.5	0.03	0.00	3082.5	0.00	0.00
1202.5	0.37	0.01	1804.5	0.02	0.00	3083.5	0.00	0.00
1203.5	0.37	0.01	1805.5	0.02	0.00	3084.5	0.00	0.00
1204.5	0.38	0.01	1806.5	0.02	0.00	3085.5	0.00	0.00

1205.5	0.37	0.01	1807.5	0.02	0.00	3086.5	0.00	0.00
1206.5	0.36	0.01	1808.5	0.02	0.00	3087.5	0.00	0.00
1207.5	0.35	0.01	1809.5	0.02	0.00	3088.5	0.00	0.00
1208.5	0.34	0.01	1810.5	0.02	0.00	3089.5	0.00	0.00
1209.5	0.33	0.00	1811.5	0.02	0.00	3090.5	0.00	0.00
1210.5	0.32	0.00	1812.5	0.02	0.00	3091.5	0.00	0.00
1211.5	0.32	0.00	1813.5	0.02	0.00	3092.5	0.00	0.00
1212.5	0.34	0.00	1814.5	0.02	0.00	3093.5	0.00	0.00
1213.5	0.36	0.00	1815.5	0.02	0.00	3094.5	0.00	0.00
1214.5	0.40	0.00	1816.5	0.02	0.00	3095.5	0.00	0.00
1215.5	0.45	0.00	1817.5	0.02	0.00	3096.5	0.00	0.00
1216.5	0.49	0.00	1818.5	0.02	0.00	3097.5	0.00	0.00
1217.5	0.55	0.00	1819.5	0.02	0.00	3098.5	0.00	0.00
1218.5	0.60	0.00	1820.5	0.02	0.00	3099.5	0.00	0.00
1219.5	0.66	0.00	1821.5	0.02	0.00	3100.5	0.00	0.00
1220.5	0.71	0.00	1822.5	0.02	0.00			

References

- Atkinson, R., Baulch, D. L., Cox, R. A., Crowley, J. N., Hampson, R. F., Hynes, R. G., Jenkin, M. E., Rossi, M. J., Troe, J., and Subcommittee, I.: Evaluated kinetic and photochemical data for atmospheric chemistry: Volume II – gas phase reactions of organic species, *Atmos. Chem. Phys.*, 6, 3625-4055, 10.5194/acp-6-3625-2006, 2006.
- Brauers, T., and Finlayson-Pitts, B. J.: Analysis of relative rate measurements, *International Journal of Chemical Kinetics*, 29, 665-672, 10.1002/(SICI)1097-4601(1997)29:9<665::AID-KIN3>3.0.CO;2-S, 1997.
- J. G. Calvert, A. Mellouki, J. J. Orlando, M. J. Pilling, and Wallington, T. J.: *The Mechanisms of Atmospheric Oxidation of the Oxygenates*, Oxford University Press, New York, 2011.

Dégradation atmosphérique des COV: Isoprène et ses produits d'ozonolyse, une perfluoro-cétone et des cétones à longue chaîne

Les composés organiques volatils (COV) constituent des polluants gazeux qui sont émis par des activités humaines et biogéniques. Ils ont une influence majeure sur la chimie de la troposphère qui influe sur la santé humaine, la qualité de l'air et le changement climatique mondial. Dans ce projet, la nouvelle chambre de simulation atmosphérique extérieure - HELIOS au CNRS-ICARE (Orléans, France) est une chambre 90 m³ Teflon-FEP qui permet la cinétique et les études mécaniques de l'ozonolyse de l'isoprène, de la méthacroleïne et de la méthylvinylcétone sous la condition sombre et la photolyse du perfluoro- (PF-2M3P) et non fluorée 2-méthyl-3-pentanone (2M3P) dans des conditions d'irradiation naturelles. De plus, la photolyse de PF-2M3P a également été réalisée dans une chambre mobile de 3,4 m³. Pour analyser la photolyse de PF-2M3P et 2M3P, leurs sections transversales d'absorption ont été mesurées par une cellule d'absorption associée à un spectrophotomètre UV-visible.

Deux autres chambres de simulation : la chambre intérieure de 7,3 m³-CSA et la chambre intérieure de 200 L au CNRS-ICARE (Orléans, France) permettent des études cinétiques et mécaniques des réactions OH et Cl avec trois cétones à longue chaîne : 2M3P, 3M2P (3 -méthyl-2-pentanone) et 4M2P (4-méthyl-2-pentanone). En outre, Photolyse à Laser Pulsé – Fluorescence Induite par Laser (PLP-LIF) a été utilisé pour mesurer la première dépendance à la température des constantes de vitesse pour les réactions de OH avec 2M3P et 3M2P. Une large gamme et des outils analytiques complémentaires ont été utilisés dans le présent travail, y compris la spectroscopie infrarouge à transformée de Fourier (FTIR), le spectromètre de masse de chromatographie en phase gazeuse (GC-MS), Réaction du transfert de protons- Temps de vol- Spectromètre de masse (PTR-ToF- MS), Spectromètre de masse de chromatographe liquide ultra haute vitesse (UHPLC-MS) pour la mesure de COV / OVOC, Scanning Mobility Particle Sizer-Condensation Particle Counter (SMPS-CPC) pour la mesure de la distribution de taille de SOA.

Mots clés : Composés organiques volatils, chambre de simulation, ozonolyse, photolyse, radical OH, atome Cl

Atmospheric degradation of VOCs: Isoprene and its ozonolysis products, a perfluoro-ketone and long chain ketones

Volatile organic compounds (VOCs) constitute a major gas pollutants emitted from both human and biogenic activities. They have a major influence on the chemistry of the troposphere impacting human health, air quality and global climate change. In the present work, the newly built outdoor atmospheric simulation chamber-HELIOS at CNRS-ICARE (Orléans, France) is a 90 m³ Teflon-FEP chamber, that allows the kinetics and mechanistic investigations of ozonolysis of isoprene, methacrolein and methyl vinyl ketone under dark condition and photolysis of perfluoro- (PF-2M3P) and non-fluorinated 2-methyl-3-pentanone (2M3P) under natural irradiation conditions. In addition, the photolysis of PF-2M3P was also conducted in one 3.4 m³ moveable chamber. In order to determine the photolysis rate of PF-2M3P and 2M3P, their absorption cross sections were measured using an absorption cell coupled with one UV-visible spectrophotometer.

In addition, two other simulation chambers : the 7.3 m³ indoor chamber-CSA and 200 L indoor chamber at CNRS-ICARE (Orléans, France) allow kinetics and mechanistic investigations of OH and Cl reactions with three long chain ketones: 2M3P, 3M2P (3-methyl-2-pentanone) and 4M2P (4-methyl-2-pentanone). In addition, a pulsed laser photolysis-laser induced fluorescence (PLP-LIF) system was used to measure the first temperature dependence of the rate constants for the reactions of OH with 2M3P and 3M2P. A wide range and complementary analytical tools have been used to conduct the present work including Fourier Transform Infrared Spectroscopy (FTIR), Gas Chromatograph-Mass spectrometer (GC-MS), Proton Transfer Reaction-Time of Flight-Mass Spectrometer (PTR-ToF-MS), Ultra High speed Liquid Chromatograph-Mass Spectrometer (UHPLC-MS) for measuring VOC/OVOC, Scanning Mobility Particle Sizer-Condensation Particle Counter (SMPS-CPC) for measuring size distribution of SOA.

Keywords: Volatile organic compounds, simulation chamber, ozonolysis, photolysis, OH radical, Cl atom,

